Using Pulse R-Factors to Estimate Structural Response to Earthquake Ground Motions

Isabel Cuesta and Mark A. Aschheim
Department of Civil and Environmental Engineering
University of Illinois at Urbana-Champaign

January 25, 2001

Copyright 2001
Board of Trustees at the University of Illinois
All Rights Reserved

Acknowledgments

Various individuals and organizations have been supportive in academic and financial matters, and we sincerely appreciate their assistance.

Financial support provided by a fellowship from the Spanish Ministry of Education and Culture (1995-1999) and a research assistantship from the University of Illinois (1999-2000) to the first author is gratefully acknowledged. In addition, this work was supported in part by the Earthquake Engineering Research Centers Program of the National Science Foundation under Award Number EEC-9701785.

We are grateful to professors Daniel P. Abrams, Douglas A. Foutch, William J. Hall, Youssef M. A. Hashash, and A. S. Veletsos for their critical feedback and suggestions, which have enriched this work. We are also thankful to Edgar Black, who has been especially helpful at many points throughout this research effort.

Contents

1 **Introduction and Background** **1**

1.1 Statement of the Problem 1

1.2 Historical Perspective: Evolution of Strength Reduction Factors 3

1.2.1 History of Code Strength Reduction Factors 3

1.2.2 History of R-Factor Models 6

1.2.3 Response of SDOF Systems to Pulses and Ground Motions 12

1.3 Objectives and Scope 15

1.3.1 Objectives 15

1.3.2 Scope and Limitations 15

1.4 Organization 16

2 **Record Segment Identification in Earthquake Records** **17**

2.1 Introduction 17

2.2 Peak Response of SDOF Systems to Ground Motions 18

2.2.1 Identification of Peak Response Occurrence Time of SDOF Systems Subjected to Ground Motions 18

2.2.2 Response to Ground Motion Recorded Segments 21

2.2.2.1 Isoductile Strength Parameter 23

2.2.2.2 Strength Reduction Factor 27

2.2.3 Limitations 27

2.3 Summary 31

3 Isoductile Strengths and Strength Reduction Factors of Elasto-plastic SDOF Systems Subjected to Simple Pulse Waveforms 32

3.1 Introduction 32

3.2 Methodology 33

3.2.1 Pulse Waveforms 34

3.2.2 Periods 36

3.2.3 Displacement Ductility 36

3.3 Analytical Results 38

3.3.1 Isoductile Strength Spectra 38

3.3.1.1 General features 38

3.3.1.2 Short period systems 43

3.3.1.3 Long period systems 43

3.3.2 Strength Reduction Factors 45

3.4 Applicability of the Newmark and Hall Observations 48

3.5 Summary 51

4 Estimating Isoductile SDOF Response Spectra Using Pulse R-factors 53

4.1 Introduction 53

4.2 Methodology 57

4.2.1 Systems 57
4.2.2 Ground Motions 58
4.2.3 Pulse Waveforms 58
4.2.4 Isoductile Strength Spectra 60
4.2.5 Error Measures 62
4.3 Results 67
4.3.1 The Best Pulses 67
4.3.2 Simplification No. 1 - Identifying a Subset of Best Pulses 71
4.3.3 Simplification No. 2 – Identifying Characteristic Periods for the Best Pulses 77
4.3.4 Near-Fault Ground Motions 78
4.4 Summary 83

5 Comparisons of Inelastic Response Spectra Determined Using Conventional and Pulse R-Factors 85
5.1 Introduction 85
5.2 Framework of Study 87
5.3 Analytical Results 89
5.3.1 Error Measures 94
5.3.2 Findings 99
5.4 Summary 104

6 Estimating the Response of Multistory Buildings Using Pulse R-Factors 105
6.1 Introduction 105
6.2 Equivalent SDOF Modeling of Multistory Buildings 106

6.3 Methodology Using the Pulse R-Factors 108
  6.3.1 Estimating Peak Displacement Using the Pulse R-Factors 109
  6.3.2 Estimating Interstory Drift Index Using the Pulse R-Factors 110
6.4 Peak Roof Displacement and IDI Estimates for 4- and 12-Story Frames 112
  6.4.1 Characteristic of the Frames 112
  6.4.2 Peak Displacement Estimates 115
    6.4.2.1 Example of Peak Displacement Estimation 115
    6.4.2.2 Numerical Results 117
    6.4.2.3 Analysis of Results 124
  6.4.3 IDI Estimates 131
    6.4.3.1 Numerical Results 134
    6.4.3.2 Analysis of Results 139
6.5 Inelastic Response of the Flexible-4 Building 140
  6.5.1 Scaling the acceleration records. 141
  6.5.2 Peak displacement estimates 142
  6.5.3 IDI estimates 149
6.6 Summary 156

7 Conclusions and Future Research **159**
7.1 Conclusions 159
7.2 Future Research 166

A Description of the 24 Simple Pulse Waveforms **168**

List of Tables

1.1 Parameters R^* and T^* for the Riddell, Hidalgo, and Cruz R-factor model [22] 9

1.2 Parameters a and b for the Nassar and Krawinkler R-factor model [23] 10

1.3 Abstract of previous work 13

2.1 Properties of recorded ground motions and their identifiers 19

2.2 Time parameters for peak response to each ground motion 21

3.1 Description and classification of acceleration pulses 35

4.1 Index number of the acceleration pulses $^+$ 59

4.2 Ground motion-pulse match classification $^+$ 68

4.3 Characteristic pulse periods, T_p 75

4.4 Average errors $AE^s = E^s_{*,d}(i,\hat{j})$ using (a) qua(2) for μ = 4 and 8, and qua(3) for μ = 2, (b) qua(2) (i =31) for all ductilities, and (c) qua(3) (i =13) for all ductilities . 75

4.5 Normalized errors $NE^a_{gm,*}(i,\hat{j})$ at $T_p = T_1^*$ and $T_p = T_g$, using (a) qua(2) for all ductilities, (b) qua(3) for all ductilities, (c) qua(2) for $\mu = 4$ and 8, and qua(3) for $\mu = 2$. Overall errors OE^a, for short duration (SD), long duration (LD), forward directive (FD), and all ground motions 76

5.1 Periods (in s) 99

5.2 Errors $NE^{a}_{gm,*}$ and OE^{a} using the pulses and 6 R-factor models. The pulse R-factors are calculated with T_p equal to T_1^*, T_2^*, and T_g. The errors are computed for elasto-plastic SDOF systems having 5% damping 101

5.4 Average errors AE^{s} for the six types of hysteresis SDOF systems using 6 R-factor models and the pulses with $T_p = T_1^*$, T_2^*, and T_g 102

6.1 Characteristics of the buildings for the 1st mode of vibration 113

6.2 Characteristics of the buildings for the 2nd mode of vibration 113

6.3 Mode shapes and modal interstory drift indices of the 4-story buildings for the first and second mode of vibration 113

6.4 Mode shapes and modal interstory drift indices of the 12-story buildings for the first and second mode of vibration 115

6.5 Peak roof displacements for Flexible-4 (cm) 119

6.7 Peak roof displacements for Rigid-4 (cm) 120

6.8 Peak roof displacements for Flexible-12 (cm) 120

6.9 Peak roof displacements for Rigid-12 (cm) 121

6.10 Estimate peak roof displacement/Drain peak roof displacement ratio for Flexible-4 . 121

6.11 Estimate peak roof displacement/Drain peak roof displacement ratio for Rigid-4 . . 122

6.12 Estimate peak roof displacement/Drain peak roof displacement ratio for Flexible-12 122

6.13 Estimate peak roof displacement/Drain peak roof displacement ratio for Rigid-12 . 123

6.14 Results for all cases 129

6.15 Results for nonlinear cases 130

6.16 Mean and standard deviation of the IDI ratios, $IDI^{s}/IDI_{DRAIN-2DX}$, $s = a, b, c$ for each building averaged for all stories and ground motions 137

6.17 Mean and standard deviation of the IDI ratios, $IDI^s/IDI_{DRAIN-2DX}$, $s = a, b, c$, over all buildings, stories, and ground motions 138

6.18 Acceleration scale factor, χ 143

6.19 Estimate peak roof displacement/Drain peak roof displacement ratio for Flexible-4, over all ground motion records and stories 149

6.20 Mean and standard deviation of the ratios $IDI^a/IDI_{DRAIN-2DX}$ over all ground motions and ductility values 153

6.21 Mean and standard deviation of the ratios $IDI^b/IDI_{DRAIN-2DX}$ over all ground motions and ductility values 153

6.22 Mean and standard deviation of the ratios $IDI^c/IDI_{DRAIN-2DX}$ for all ground motions and ductility values 153

A.1 Quadratric family 169

A.2 Sinusoidal family 170

A.3 Triangular trh family 170

A.4 Triangular trl family 170

A.5 Rectangular family 170

A.6 Triangular tr0 family 171

List of Figures

1.1 Strength reduction factors versus period (T) prescribed by 4 codes for design of reinforced concrete structural wall buildings 2

1.2 Strength-displacement curves for an elastic and inelastic SDOF system 5

2.1 Yield strength-displacement cycles of elasto-plastic systems 19

2.2 Pulse containing $a_{g,max}$ and $v_{g,max}$ for each ground motion in the range $(t_1 - t_2)_{cycle}$ from Table 2.2 22

2.3 Strength response spectra for systems subjected to the records, η_r, and to the pulses, η_p, for the pulses defined in Fig. 2.1 for the Short Duration motions 24

2.4 Strength response spectra for systems subjected to the records, η_r, and to the pulses, η_p, for the pulses defined in Fig. 2.1 for the Long Duration motions 25

2.5 Strength response spectra for systems subjected to the records, η_r, and to the pulses, η_p, for the pulses defined in Fig. 2.1 for the Forward Directive motions 26

2.6 R-factor response spectra for systems subjected to the Short Duration motions, R_r, and to the pulses, R_p 28

2.7 R-factor response spectra for systems subjected to the Long Duration motions, R_r, and to the pulses, R_p 29

2.8 R-factor response spectra for systems subjected to the Forward Directive motions, R_r, and to the pulses, R_p 30

3.1 Acceleration time history of a pulse 34

3.2 Comparison of elastic strength, (a) η vs. T/t_d, and (b) η vs. T/T_p, for the quadratic family 37

3.3 Strength parameter, η, vs. T/T_p of systems with $\mu = 1$, 2, 4, and 8. Forced and overall responses to gradual loading pulses 39

3.4 Strength parameter, η, vs. T/T_p of systems with $\mu = 1$, 2, 4, and 8. Forced and overall responses to shock loading pulses 40

3.5 Overall response of systems with $\mu = 1$, 2, 4, and 8 subjected to quadratic pulses, (a) Strength parameter, η, vs. T/T_p; (b) R-factors vs. T/T_p 42

3.6 R-factor vs. T/T_p of systems with $\mu = 1$, 2, 4, and 8. Forced and overall responses to gradual loading pulses 46

3.7 R-factor vs. T/T_p of systems with $\mu = 1$, 2, 4, and 8. Forced and overall responses to gradual loading pulses 47

3.8 R-factor vs. ductility μ: (a) Forced and overall responses of systems having $T/t_d = 0.01$, (b) Forced response of systems having $T/t_d = 8$, (c) Overall response of systems having $T/t_d = 8$, and (d) Forced and overall responses of systems having $T/t_d = 100$ 49

4.1 Comparison for NR94NWHL.360 record among the strength response spectra to the record, η_r, the overall response to the pulse qua(2), η_p, and the ratio of the elastic response spectrum to the record to the R-factor of the same pulse, $\eta_e/R_p(T_p = 0.75\,s)$. (a) Systems having $\mu = 2$, (b) Systems having $\mu = 4$, and (c) Systems having $\mu = 8$ 55

4.2 Normalized acceleration, velocity, and displacement time histories of the qua(2), qua(3), and sin(5) pulses 56

4.3 Isoductile strength response spectra for (a) overall response to qua(2), (b) forced response to qua(3), and (c) forced response to sin(5) 61

4.4 R-factor response spectra for (a) overall response to qua(2), (b) forced response to qua(3), and (c) forced response to sin(5) 61

4.5 Errors $E^s_{6,d}(13, j)$ vs. the characteristic period of the pulse, T_p, in the estimate of the response to CH85LLEO.010 record with the R-factor of the forced response to the qua(3) pulse 64

4.6 Minimum error, $E^a_{gm,*}(i, \hat{j})$, for: (a) the estimate of LP89CORR.090 ($gm = 4$), and (b) for the estimate of LN92LUCN.250 ($gm = 11$) records using 24 pulses in forced and overall response. Numbers 1, 7, 13, 17, and 21 correspond to the quadratic family of pulses 65

4.7 Average error, $AE^a = E^a_{*,*}(i, j)$, for the estimate of all the records using 24 pulses in forced and overall response with $T_p = T_g$. Numbers 1, 7, 13, 17, and 21 correspond to the quadratic family of pulses 66

4.8 R-factor response spectra to the LN92LUCN.250 record and the equal energy rule R-factor, $R = \sqrt{2\mu - 1}$ 69

4.9 Isoductile strength response spectra to short duration records, η_y, and their estimates $\hat{\eta}_y$, with their best pulses at $T_p = \hat{T}_o$ given by E^a_o (see Table 4.2) 72

4.10 Isoductile strength response spectra to long duration records, η_y, and their estimates $\hat{\eta}_y$, with their best pulses at $T_p = \hat{T}_o$ given by E^a_o (see Table 4.2) 73

4.11 Isoductile strength response spectra to forward directive records, η_y, and their estimates $\hat{\eta}_y$, with their best pulses at $T_p = \hat{T}_o$ given by E^a_o (see Table 4.2) 74

4.12 Isoductile strength response spectra to short duration records, η_y, and their estimates $\hat{\eta}_y$, with the qua(2) pulse at $T_p = T_g$ (see Table 4.3) 80

4.13 Isoductile strength response spectra to long duration records, η_y, and their estimates $\hat{\eta}_y$, with the qua(2) pulse for all records except MX85SCT1.270, for which the sin(5) pulse was used, at $T_p = T_g$ (see Table 4.3) 81

4.14 Isoductile strength response spectra to forward directive records, η_y, and their estimates $\hat{\eta}_y$, with the qua(2) pulse at $T_p = T_g$ (see Table 4.3) 82

5.1 Normalized acceleration, velocity, and displacement time histories of the qua(2) and sin(5) pulses 88

5.2 R-factor response spectra to the qua(2) pulse 91

5.3 R-factor response spectra to the sin(5) pulse 92

5.4 R-factor vs. ductility μ for short period systems $T/t_d = 0.005$; (a) to the qua(2) pulse, (b) to the sin(5) pulse 93

5.5 Estimated R-factor response spectra for the 1940 N-S component of El Centro earthquake (IV40ELCN.180 record, $T_g = 0.65$ s) 95

5.6 Graphical determination of the period T_2^* for the CH85VALP.070 record 97

5.7 Graphical determination of the period T_2^* for the sin(5) pulse 98

6.1 First and second mode shapes for the 4- and 12-story buildings 114

6.2 Ductility values associated with the first mode for the 4-story buildings subjected to the IV40ELCN.180 record ($T_g = 0.65$ s, $\alpha = 10\%$, $\beta = 5\%$) 117

6.3 Peak roof displacement comparisons for the Flexible-4 building 125

6.4 Peak roof displacement comparisons for the Flexible-4 building 126

6.5 Peak roof displacement comparisons for the Flexible-12 building 127

6.6 Peak roof displacement comparisons for the Rigid-12 building 128

6.7 Ratio $IDI^a/IDI_{DRAIN-2DX}$ for Flexible-4 building subjected to each ground motion 133

6.8 Mean ratio $IDI^s/IDI_{DRAIN-2DX}$, $s = a, b, c$, per story for Flexible-4 building over all records 134

6.9 Mean ratio $IDI^s/IDI_{DRAIN-2DX}$, $s = a, b, c$, per story for Rigid-4 building over all records 135

6.10 Mean ratio $IDI^s/IDI_{DRAIN-2DX}$, $s = a, b, c$, per story for Flexible-12 building over all records 135

6.11 Mean ratio $IDI^s/IDI_{DRAIN-2DX}$, $s = a, b, c$, per story for Rigid-12 building over all records 136

6.12 Mean and standard deviation of the IDI ratios, for each building and IDI model over all stories and ground motions 137

6.13 Mean and standard deviation of the IDI ratios for each IDI model, over all buildings, stories, and ground motions 138

6.14 Peak roof displacement comparisons for the Flexible-4 building, $\mu \sim 2$ 145

6.15 Peak roof displacement comparisons for the Flexible-4 building, $\mu \sim 4$ 146

6.16 Peak roof displacement comparisons for the Flexible-4 building, $\mu \sim 8$ 147

6.17 Mean and standard deviations for the peak roof displacement ratio over all ductility value 148

6.18 Ratio $IDI^a/IDI_{DRAIN-2DX}$ for Flexible-4 building subjected to each ground motion scaled, over all ductility value using Eq. 6.9 150

6.19 Ratio $IDI^b/IDI_{DRAIN-2DX}$ for Flexible-4 building subjected to each scaled ground motion, over all ductility values using Eq. 6.10 151

6.20 Ratio $IDI^c/IDI_{DRAIN-2DX}$ for Flexible-4 building subjected to each scaled ground motion, over all ductility values using Eq. 6.11 152

6.21 Mean ratios $IDI^s/IDI_{DRAIN-2DX}$, $s = a, b, c$ for Flexible-4 building, for each story, over all scaled ground motions and ductility values 154

6.22 Mean and standard deviation of the IDI ratios, $IDI^s/IDI_{DRAIN-2DX}$, $s = a, b, c$ for Flexible-4 building, over all scaled ground motions, stories, and ductility values . . . 155

A.1 Normalized acceleration, velocity, and displacement time histories of the quadratic family of pulses 171

A.2 Normalized acceleration, velocity, and displacement time histories of the sinusoidal family of pulses 172

A.3 Normalized acceleration, velocity, and displacement time histories of the triangular families of pulses trh and trl, having rise times, t_r, equal to 1/2 and 1 times the duration of the first incursion 172

A.4 Normalized acceleration, velocity, and displacement time histories of the rectangular family of pulses 173

A.5 Normalized acceleration, velocity, and displacement time histories of the triangular family of pulses having rise time, t_r, equal to 0 times the duration of the first incursion173

B.1 Ratio $IDI^a/IDI_{DRAIN-2DX}$ for Flexible-4 building subjected to each ground motion using Eq. 6.9 175

B.2 Ratio $IDI^a/IDI_{DRAIN-2DX}$ for Rigid-4 building subjected to each ground motion using Eq. 6.9 176

B.3 Ratio $IDI^a/IDI_{DRAIN-2DX}$ for Flexible-12 building subjected to each ground motion using Eq. 6.9 177

B.4 Ratio $IDI^a/IDI_{DRAIN-2DX}$ for Rigid-12 building subjected to each ground motion using Eq. 6.9 178

B.5 Ratio $IDI^b/IDI_{DRAIN-2DX}$ for Flexible-4 building subjected to each ground motion using Eq. 6.10 179

B.6 Ratio $IDI^b/IDI_{DRAIN-2DX}$ for Rigid-4 building subjected to each ground motion using Eq. 6.10 180

B.7 Ratio $IDI^b/IDI_{DRAIN-2DX}$ for Flexible-12 building subjected to each ground motion using Eq. 6.10 181

B.8 Ratio $IDI^b/IDI_{DRAIN-2DX}$ for Rigid-12 building subjected to each ground motion using Eq. 6.10 182

B.9 Ratio $IDI^c/IDI_{DRAIN-2DX}$ for Flexible-4 building subjected to each ground motion using Eq. 6.11 183

B.10 Ratio $IDI^c/IDI_{DRAIN-2DX}$ for Rigid-4 building subjected to each ground motion using Eq. 6.11 184

B.11 Ratio $IDI^c/IDI_{DRAIN-2DX}$ for Flexible-12 building subjected to each ground motion using Eq. 6.11 185

B.12 Ratio $IDI^c/IDI_{DRAIN-2DX}$ for Rigid-12 building subjected to each ground motion using Eq. 6.11 186

B.13 Ratio $IDI^a/IDI_{DRAIN-2DX}$ for Flexible-4 building subjected to each ground motion scaled to get $\mu \sim 2$, using Eq. 6.9 187

B.14 Ratio $IDI^a/IDI_{DRAIN-2DX}$ for Flexible-4 building subjected to each ground motion scaled to get $\mu \sim 4$, using Eq. 6.9 188

B.15 Ratio $IDI^a/IDI_{DRAIN-2DX}$ for Flexible-4 building subjected to each ground motion scaled to get $\mu \sim 8$, using Eq. 6.9 189

B.16 Ratio $IDI^b/IDI_{DRAIN-2DX}$ for Flexible-4 building subjected to each ground motion scaled to get $\mu \sim 2$ using Eq. 6.10 190

B.17 Ratio $IDI^b/IDI_{DRAIN-2DX}$ for Flexible-4 building subjected to each ground motion scaled to get $\mu \sim 4$ using Eq. 6.10 191

B.18 Ratio $IDI^b/IDI_{DRAIN-2DX}$ for Flexible-4 building subjected to each ground motion scaled to get $\mu \sim 8$ using Eq. 6.10 192

B.19 Ratio $IDI^c/IDI_{DRAIN-2DX}$ for Flexible-4 building subjected to each ground motion scaled to get $\mu \sim 2$ using Eq. 6.11 193

B.20 Ratio $IDI^c/IDI_{DRAIN-2DX}$ for Flexible-4 building subjected to each ground motion scaled to get $\mu \sim 4$ using Eq. 6.11 194

B.21 Ratio $IDI^c/IDI_{DRAIN-2DX}$ for Flexible-4 building subjected to each ground motion scaled to get $\mu \sim 8$ using Eq. 6.11 195

List of Symbols

a, b, c	Coefficients used in Eq. 1.11.
a_g	Pulse acceleration.
A	Coefficient used in Eq. 4.1.
$a_{g,max}$	Peak ground acceleration.
AE^s	Average error ($s = a, b, c$).
d	Ductility index number.
d_g	Pulse displacement.
$d_{g,max}$	Peak ground displacement.
D	Dead load.
$D(T)$	Elastic displacement response spectrum.
E	Horizontal and vertical earthquake-induced forces.
E_k	Kinetic energy.
E_s	Strain energy.
E^s	Error measures ($s = a, b, c$).

E_o^s	Reference error using the optimal pulse.
g	Gravity acceleration.
gm	Ground motion index.
i	Pulse index number.
I_m	Impulse magnitude.
IDI^a	Interstory drift index using Eq. 6.9.
IDI^b	Interstory drift index using Eq. 6.10.
IDI^c	Interstory drift index using Eq. 6.11.
IDI^i	Estimated interstory drift index for the story i.
$IDI_{DRAIN-2DX}$	Interstory drift index using DRAIN-2DX program.
$IDI^i(\phi_j)$	Modal interstory drift index for story i, defined as the interstory drift index calculated for the assumed deformed mode shape $\{\phi_j\}$.
j	Pulse characteristic period index number.
K	Coefficient used by SEAOC in 1959 [1].
L_{eq}	Earthquake excitation factor.
m	Mass of the system.
M	Diagonal mass matrix of a MDOF system.
$max(u_{el}^{sdof})$	Maximum elastic displacement of the equivalent SDOF system.
M_{eq}	Mass of the equivalent SDOF system.
M_L	Richter magnitude.

M_t	Total mass of a MDOF system.
M_W	Moment magnitude.
n_p	Number of periods.
N	Number of points for a geometric distribution.
NE^s	Normalized error $(s = a, b, c)$.
OE^s	Overall error $(s = a, b, c)$.
qua	Quadratic family of pulses.
Q_E	Effect of horizontal seismic forces.
r	Geometric ratio used in Eq. 3.1.
rec	Rectangular family of pulses.
R	Strength reduction factor.
R_d	Ductility factor (NEHRP provisions).
R_p	Strength reduction factor of a system subjected to a pulse.
R_R	Redundancy factor.
R_s	Strength factor.
R^{sdof}	Equivalent SDOF R-factor.
R_β	Damping factor.
R_μ	Ductility factor.
R_ω	Reduction factor (SEAOC Bluebook).
R^*	Parameter used in Eq. 1.10.

s	= a, b, c defines the three error measures given by Eqs. 4.4, 4.5, and 4.6, respectively.
sin	Sinusoidal family of pulses.
S_a	Elastic pseudo-acceleration.
S_v	Elastic psedo-velocity.
S_{DS}	Design spectral response acceleration at short periods.
t	Time.
t_d	Pulse duration.
t_r	Rise time.
trh	Triangular family of pulses, having $t_r = 1/2$ the duration of the first incursion.
$tr0$	Triangular family of pulses, having $t_r = 0$ the duration of the first incursion.
$tr1$	Triangular family of pulses, having $t_r = 1$ the duration of the first incursion.
t_1	Time of maximum positive displacement of a SDOF system.
$min\,(t_1)$	Minimum t_1 for all systems subjected to a ground motion.
t_2	Time of maximum negative displacement.
$max\,(t_2)$	Maximum t_2 for all systems subjected to a ground motion.
T	Natural period of a system.
T_a	Limiting period used in Eqs. 1.9 and 1.13.
T_a', T_b	Limiting periods used in Eq. 1.9.
T_c	Limiting periods used in Eq. 1.13.
T_g	Characteristic period of the ground motion.

T_p	Characteristic pulse period.
T_s	Period used in the NEHRP Guidelines [2].
T_G	Predominant period of the ground motion used in Eq. 1.12.
$\hat{T}_o$	Optimal period for the optimal pulse of each ground motion.
T_1, T_2	First and second periods of vibration.
T_1^*	Optimal period for the qua(2) and qua(3) pulses of each ground motion for elasto-plastic systems having $\beta = 5\%$.
T_2^*	Limiting period defined in Eq. 5.7.
T^*	Parameter used in Eq. 1.10.
u	Relative displacement.
u_d	Design displacement.
u_e	Elastic displacement.
u_e^{sdof}	Equivalent SDOF elastic displacement.
$u_{g,o}$	Instantaneous change in ground displacement.
u_m	Maximum ultimate displacement.
u_{uj}^{mdof}	Peak roof displacement given by Eq. 6.7 for the mode of vibration j.
$u_{u,DRAIN-2DX}^{mdof}$	Peak roof displacement obtained with DRAIN-2DX.
$u_{u,vidic}^{mdof}$	Estimated peak roof displacement using Vidic R-factor model.
$u_{u,pul(T_g)}^{mdof}$	Estimated peak roof displacement using the pulse R-factor model, having $T_p = T_1^*$.
$u_{u,pul(T_1^*)}^{mdof}$	Estimated peak roof displacement using Ordaz R-factor model, having $T_p = T_g$.

$u_{u,record}^{mdof}$	Estimated peak roof displacement using the ground motion R-factor.
u_y	Yield displacement.
u_y^{mdof}	MDOF yield displacement.
u_y^{sdof}	Equivalent SDOF yield displacement.
u_1,$u_1^{'}$	Peak positive displacements.
u_2	Peak negative displacement.
v_g	Pulse velocity.
$v_{g,max}$	Peak ground velocity.
V_d	Design strength.
V_e	Strength required for elastic response.
V_m	Ultimate strength.
V_y	Yield strength.
V_y^{mdof}	Yield strength of a MDOF system.
W_t	Total weight of a MDOF system.
$\ddot{y}_o$	Instantaneous change in ground acceleration.
α	Post-yield stiffness.
α_e	Effective modal mass coefficient.
β	Damping ratio.
η	Strength parameter.
η_e	Elastic strength parameter of a system subjected to a ground motion.

η_e^{sdof}	Equivalent SDOF elastic strength parameter.
η_p	Strength parameter of a system subjected to a simple pulse.
η_r	Strength parameter of a system subjected to a ground motion.
η_y	Yield strength parameter.
η_y^{mdof}	MDOF yield strength parameter.
η_y^{sdof}	Equivalent SDOF yield strength parameter.
$\hat{\eta}_y$	Estimated yield strength parameter.
κ	Ratio T/t_d.
μ	Ductility demand of a system.
ξ	Coefficient used in Eq. 1.14.
ρ	Redundancy factor (NEHRP provisions).
$\phi_{ea}, \phi_{ev}, \phi_{ed}$	Amplification factors used in Eq. 1.9.
$\{\phi\}$	Deformed shape vector or mode of vibration.
$\{\phi_1\}, \{\phi_2\}$	First and second modes of vibration.
Φ	Site coefficient used in Eq. 1.12.
ω	Circular frequency of a system.
Ω_o	Overstrength factor (NEHRP provisions).

List of Abbreviations

FD	Forward directive records.
g.m.	Ground motion.
IDI	Interstory drift index.
LD	Long duration records.
MDOF	Multi-degree-of-freedom.
R/C	Reinforced concrete.
SD	Short duration records.
SDOF	Single-degree-of-freedom.

Chapter 1

Introduction and Background

1.1 Statement of the Problem

Codes for the seismic design of buildings and bridges worldwide usually obtain the lateral design force by dividing the strength required for elastic response by a reduction factor that accounts for the inelastic behavior of the structure, overstrength of the structure, and other factors that are considered to be important. Improving the techniques used for estimating the lateral strength required for structures subjected to earthquake ground motions, as well as improving the conceptual foundations of these techniques would be of value. For example, fig. 1.1 shows the reduction factors used in the United States [2], Mexico, Japan, and European [3] nations for reinfored concrete (R/C) structural wall buildings of regular configuration, having fundamental period T, and located on rock sites [4]. While the reduction factor is period-dependent in the European and Mexican codes, in the United States and Japan, the reduction factor is invariant with period.

Codes in the United States designate different values of the reduction factor for different framing systems, reflecting perceptions of their ductility capacity, likely overstrength, and performance in past earthquakes. The advent of performance-based seismic design introduces a need for accuracy in estimating the peak displacement of the structure and the damage associated with its response.

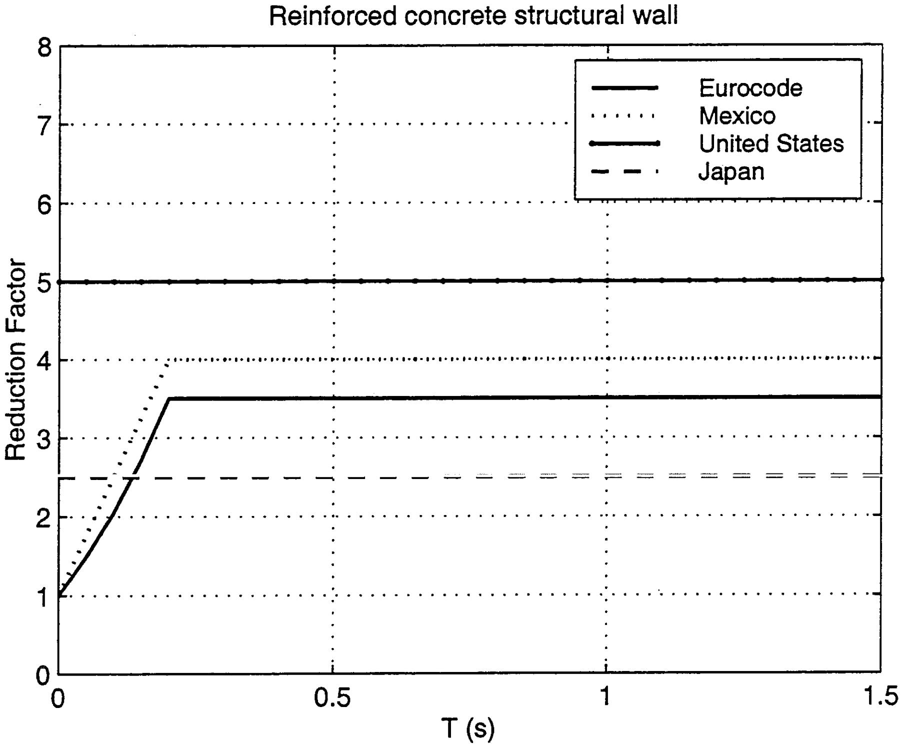

Figure 1.1: Strength reduction factors versus period (T) prescribed by 4 codes for design of reinforced concrete structural wall buildings

Not only are the ground motions subject to variability, but the reduction factors also vary relative to the ground motions. Increasing attention to both safety and economic consequences underscores the need to improve the reduction factors used in the design of buildings and bridges [4].

Although the reduction factor depends on the material overstrength, design overstrength, and redundancy characteristics of the structural system, as described in the Commentary of the *NEHRP Provisions* [2], the present work focuses only on the strength reduction factor (R-factor), defined as the ratio of the strength required for the system to remain elastic when responding to a given ground motion and the strength required for the system to develop a specified degree of a non-linear behavior, with the degree of nonlinearity indexed by the ductility of the system.

A better understanding of the inlastic behavior of systems under complex ground motions may develop when the characteristics of inelastic response to simple ground motions is understood. The simpler ground motions have been called elementary forces, explosive-type loads, pulse-type forces [5], pulse excitations or pulse force [6], or impulsive loads [7] in the literature. These names refer to forces or accelerations that contain a single impulse of arbitrary form.

This work shows that inelastic response of structures is affected similarly by simple pulses and earthquake ground motions. These similarities allow a new approach to be developed to estimate R-factors for systems with varied load-deformation and hysteretic characteristics to earthquake ground motions using the R-factors for systems subjected to simple pulses. The approach makes use of the observation that R-factors for systems responding to simple pulses are similar to those obtained for earthquake ground motion records.

1.2 Historical Perspective: Evolution of Strength Reduction Factors

1.2.1 History of Code Strength Reduction Factors

The Structural Engineers Association of California (SEAOC) in 1959 [1] made an attempt to account for non-linear behavior in the design of structures in the design provisions prepared for the Uniform Building Code. In these provisons the elastic base shear force was multiplied by a coefficient K equal to 1.33 for bearing wall buildings, 0.80 for dual systems, 0.67 for moment-resisting frames, and 1.00 for framing systems not classified among the other categories.

The K factor expresses the same concept as the R-factor in the sense of reducing the design strength. When the K factor is used, the design strength is multiplied by the K factor; the R-factor is applied as a divisor to the elastic strength. Hence, the R-factor is defined as the ratio of the force that an elastic system would develop under a given ground motion to the force that this system would develop if the system had non-linear inelastic behavior.

The first time that the R-factor terminology was introduced in the United States was in ATC-3-06, 1978 [8]. At that time, a committee was formed to determine values of these factors. The committee based its decision on "the inherent toughness, amount of damping when undergoing inelastic response, and observed past performance of various types of framing systems." A footnote to the table of R-factors states "these factors should be periodically reviewed as additional experience and research information are obtained."

Further research has been conducted since the publication of ATC-3-06 (e.g. [9, 10, 11, 12, 13]). ATC-34 [14] identified several intrinsic properties that should affect the strength reduction factor.

Researchers at the University of California in the mid-1980's [15, 16] proposed the R-factor should be composed of three separate factors, as described in ATC-19 [4], having the following relationship:

$$R = R_s \cdot R_\mu \cdot R_\beta \tag{1.1}$$

where: R_s = strength factor, R_μ = ductility factor, and R_β = damping factor, which was set to 1.0.

Others (Freeman [17], ATC-19 [4], and ATC-34 [14]) have considered the R-factor of a system to be the product of three factors:

$$R = R_s \cdot R_\mu \cdot R_R \tag{1.2}$$

where R_s = strength factor, R_μ = ductility factor, and R_R = redundancy factor. In this formulation, the redundancy factor, R_R, is associated with the number of plastic hinges that develop before collapse [18]. Failure occurs when all vertical lines of seismic framing of a redundant, ductile, seismic framing system have failed. If a structure should collapse when the first hinge initiates, the system is considered to lack redundancy, resulting in $R_R = 1$.

The strength factor, R_s, is the ratio of the maximum ultimate strength, V_m, and the design strength, V_d, as shown in Fig. 1.2. Nonlinear analysis is used to establish the ultimate strength, V_m, of a system.

Finally, the ductility factor, R_μ, is the ratio of the strength required for elastic response to the

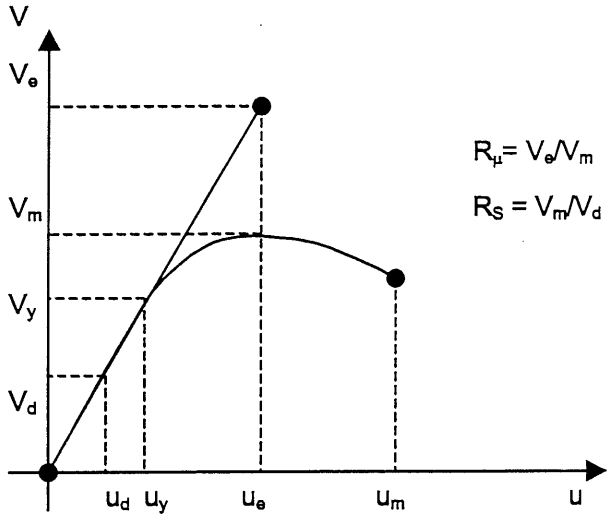

Figure 1.2: Strength-displacement curves for an elastic and inelastic SDOF system

ground motion, V_e, to the ultimate strength, V_m. Hence,

$$R = R_s \cdot R_\mu \cdot R_R = \frac{V_m}{V_d} \cdot \frac{V_e}{V_m} \cdot R_R \tag{1.3}$$

Information about these three components of the R-factor can be found in ATC-19 [4].

The *NEHRP Provisions* [2] also takes into account these three components. The R-factor in this document is the product of the first two components, the overstrength factor, R_s, and the ductility factor, R_μ, which are termed R_d and Ω_o, respectively. The Ω_o factor considers the system, material, and design overstrength of the structure. The redundancy factor, R_R, is considered in the combination of loads using the factor ρ:

$$E = \rho \cdot Q_E \pm 0.2 \cdot S_{DS} \cdot D \tag{1.4}$$

where E = horizontal and vertical earthquake-induced forces, Q_E = effect of horizontal seismic forces, D = dead load, S_{DS} = design spectral response acceleration at short periods, and ρ = redundancy factor.

The parameter ρ varies with the seismic design category, and ranges from 1 for redundant systems to 1.5 for non-redundant systems. This penalizes non-redundant systems by increasing the design force level.

The 1988 *SEAOC* "Blue Book" [19] uses a similar procedure, based on working stress design. In the *Blue Book*, the elastic forces are reduced by a factor called R_w, while in the *NEHRP provisions,* the elastic forces are reduced by R for design at the ultimate strength level.

The foregoing analytical study considers the response of SDOF oscillators. For the elasto-plastic SDOF oscillators, the ultimate strength and the design strength are equal to the yield strength V_y. For this case, the factor $R_s = 1$. Since the oscillator has only one degree of freedom, the oscillator is a non-redundant system, and $R_R = 1$. Therefore, the R-factor given by Eq. 1.2 or 1.3 is simplified to $R = R_\mu$. The ductility reduction factor R_μ in the previous discussion is from now on called the strength reduction factor, and is simply called the R-factor for convenience. The R-factor relates the strength required for elastic response to the yield strength associated with a specified displacement ductility response.

1.2.2 History of R-Factor Models

Much has been published on the strength reduction factor in the literature. Several physically-based idealizations have been used to gain insight into the R-factors determined for ground motion records [20]. These physical idealizations were developed in analytical studies of undamped systems subjected to a small number of pulses. The original observations for short, intermediate, and long period systems are described in this section, along with six models developed over the last three decades by Newmark and Hall [21], Riddell, Hidalgo, and Cruz [22], Nassar and Krawinkler [23], Miranda [24], Vidic, Fajfar, and Fischinger [25], and Ordaz and Pérez-Rocha [26].

The original observations for short, intermediate, and long period systems are as follows [20]:

1. *Short period systems*:

    - *Instantaneous change in ground acceleration.* For short period systems subjected to acceleration pulses having one incursion and those having discontinuous acceleration, the

R-factor was estimated as follows [20]. The external force associated with an instantaneous change in ground acceleration, $\ddot{y}_o$, is considered to produce work in deforming the system through the maximum displacementat, u_m, given by $-m\ddot{y}_o u_m$, where m is the mass of the system. The external work done is set equal to the work done in deforming the elasto-plastic system, resulting in:

$$R = \frac{2\mu - 1}{\mu} \tag{1.5}$$

- *Preservation of the force.* For short period systems subjected to continuous acceleration functions [20] and for systems with periods less than an empirical limit of 0.0303 s subjected to ground motions [7, 27], any reduction in strength would result in very large ductility demands. Hence, the yield strength must equal the strength required for elastic response, or

$$R = 1 \quad for\ all\ \mu \tag{1.6}$$

Thus, for very short period systems the excitation is received as a quasi-static loading. Even modest reductions in strength result in displacements that are very large compared with the yield displacement.

2. *Intermediate period systems*:

- *Instantaneous change in ground velocity.* It is considered that an instantaneous change in ground velocity causes a change in the kinetic energy of the system, independent of the load-deformation relation. The work done in driving the elasto-plastic system to its maximum displacement is equal to this change in kinetic energy. Equating the work done on an elasto-plastic system and the change in kinetic energy results in:

$$R = \sqrt{2\mu - 1} \tag{1.7}$$

This is termed the "equal energy rule" and was said to be applicable to intermediate period systems (having periods between 0.125 to 0.5 s subjected to earthquake ground motions) [7, 27]. However, this rule is found to be valid only for certain pulses (Section 3.4) and many of the R-factor models that followed do not conform to this idealization.

3. *Long period systems*:

   - *Instantaneous change in ground displacement.* For an instantaneous change in ground displacement, $-u_{g,o}$, the maximum deformation of a long period system, $u_{g,o}$, is independent of the load-deformation relation. This is known as the "equal displacement rule," for which the R-factor is given by:

     $$R = \mu \tag{1.8}$$

     This rule was said to be applicable for periods larger than approximately 0.5 s [7, 27]. For very long period systems, the maximum displacements of elastic and inelastic systems are equal, and equal the ground displacement.

The six R-factor models considered in detail in this study (Newmark and Hall [21], Riddell, Hidalgo, and Cruz [22], Nassar and Krawinkler [23], Miranda [24], Vidic, Fajfar, and Fischinger [25], and Ordaz and Pérez-Rocha [26]) are summarized in the following:

1. *Newmark and Hall* [21] developed strength reduction factors for elasto-plastic SDOF systems with damping β = 0.5, 1, 2, 3, 5, 7, 10, and 20% of critical damping based on three ground motions and pulse excitations, for ductilities $\mu \leq 10$. The strength reduction factor is given

Table 1.1: Parameters R^* and T^* for the Riddell, Hidalgo, and Cruz R-factor model [22]

Parameter	$\mu = 2$	$\mu = 3$	$\mu = 4$	$\mu = 5$	$\mu = 6$	$\mu = 7$	$\mu = 8$
R^*	2.0	3.0	4.0	5.0	5.6	6.2	6.8
T^*	0.1	0.2	0.3	0.4	0.4	0.4	0.4

as a function of the ductility and period of the system:

$$R = \begin{cases} 1 & 0 \leq T < \frac{T_a}{10} \\ \sqrt{2\mu - 1}\left(\frac{T_a}{4T}\right)^{-2.513 log\left(\sqrt{2\mu-1}\right)} & \frac{T_a}{10} \leq T < \frac{T_a}{4} \\ \sqrt{2\mu - 1} & \frac{T_a}{4} \leq T < T_a^{'} \\ \mu\frac{T}{T_a} & T_a^{'} \leq T < T_a \\ \mu & T_a \leq T < T_b \\ \mu & T_b \leq T < 10 \end{cases} \tag{1.9}$$

where:

- $T_a = 2\pi\frac{\phi_{ev} v_{g,max}}{\phi_{ea} a_{g,max}}$, $T_a^{'} = T_a\frac{\mu}{\sqrt{2\mu-1}}$, and $T_b = 2\pi\frac{\phi_{ed} d_{g,max}}{\phi_{ev} v_{g,max}}$ are the delimiting periods
- $d_{g,max}$, $v_{g,max}$, and $a_{g,max}$ are the peak ground displacement, velocity, and acceleration, respectively,
- ϕ_{ed}, ϕ_{ev}, and ϕ_{ea} are amplification factors applied to $d_{g,max}$, $v_{g,max}$, and $a_{g,max}$, respectively, to determine ordinates of the elastic spectrum in the displacement, velocity, and acceleration regions, with $\phi_{ed} = 2.73 - 0.45 ln\beta$, $\phi_{ev} = 3.38 - 0.67 ln\beta$, and $\phi_{ea} = 4.38 - 1.04 ln\beta$.

2. *Riddell, Hidalgo, and Cruz* [22] used 4 sets of ground motions to develop approximate mean strength reduction factors for elasto-plastic systems having $\beta = 5\%$ and $\mu \leq 10$. They recommended:

$$R = \begin{cases} 1 + \frac{R^*-1}{T^*}T & \frac{T}{T^*} \leq 1 \\ R^* & \frac{T}{T^*} > 1 \end{cases} \tag{1.10}$$

where R* and T* depend on the ductility of the system, as shown in Table 1.1.

Table 1.2: Parameters a and b for the Nassar and Krawinkler R-factor model [23]

α	a	b
0.00	1.00	0.42
0.02	1.00	0.37
0.10	0.80	0.29

3. *Nassar and Krawinkler* [23] analyzed the inelastic response of elasto-plastic, bilinear, and stiffness-degrading systems having $\beta = 5\%$ and $\mu \leq 8$, using 15 ground motions recorded in the western United States on alluvium and rock sites. Strength reduction factors were calculated as the mean of the ratios of elastic to inelastic isoductile strengths. Based on analytical considerations, strength reduction factors were assumed to have the functional form

$$R = [c(\mu - 1) + 1]^{\frac{1}{c}} \tag{1.11}$$

with the parameter c given by: $c(T, \alpha) = \frac{T^a}{1+T^a} + \frac{b}{T}$. These functions were fit to the computed means to obtain values of the parameters a and b, given in Table 1.2, as functions of the post-yield stiffness, α.

4. *Miranda* [24] considered 124 ground motions divided in rock, alluvium, and soft soil categories, for bilinear systems having $\alpha = 3\%$, $\beta = 5\%$, and $\mu \leq 6$. Mean strength reduction factors were approximated by the function:

$$R = 1 + \frac{\mu - 1}{\Phi} \geq 1 \tag{1.12}$$

where the coefficient Φ depends on the soil condition as follows:

(a) For rock sites $\Phi = 1 + \frac{1}{10T - \mu T} - \frac{1}{2T} exp\left[-\frac{2}{3}\left(lnT - \frac{3}{5}\right)^2\right]$

(b) For alluvium sites $\Phi = 1 + \frac{1}{12T - \mu T} - \frac{2}{5T} exp\left[-2\left(lnT - \frac{1}{5}\right)^2\right]$

(c) For soft soil sites $\Phi = 1 + \frac{T_G}{3T} - \frac{3T_G}{4T} exp\left[-3\left(ln\frac{T}{T_G} - \frac{1}{4}\right)^2\right]$

For soft soil sites, T_G a "predominant period of the ground motion" is used in the expression for Φ. Miranda defined this period T_g to be the period at which the maximum relative velocity occurs for an elastic system having $\beta = 5\%$.

5. Vidic, Fajfar, and Fischinger [28, 25] developed strength reduction factor relations based on the response of bilinear and stiffness degrading (Q-model) systems to records from California, Montenegro, Chile, and Mexico City. The post-yield stiffness was 10% of the initial stiffness, $\mu \leq 10$, and viscous damping either was constant (proportional to the mass) or was proportional to the instantaneous stiffness. The proposed R-factor relations for bilinear systems and 5% mass-proportional damping are given by the following bilinear relation:

$$R = \begin{cases} 1.35\,(\mu-1)^{0.95}\frac{T}{T_c} & \frac{T}{T_c} \leq 1 \\ 1.35\,(\mu-1)^{0.95}+1 & \frac{T}{T_c} > 1 \end{cases} \tag{1.13}$$

   where:

   - $T_c = 0.75\mu^{0.2}T_a$
   - $T_a = 2\pi\frac{\phi_{ev}v_{g,max}}{\phi_{ea}a_{g,max}}$
   - $a_{g,max}$ and $v_{g,max}$ are the peak ground acceleration and velocity, respectively
   - ϕ_{ea} is the acceleration amplification factor (= 2.5)
   - ϕ_{ev} = is the velocity amplification factor equal to 2.0, 1.8, 2.6, and 2.8 for Standard, U.S.A., Chilean and the soft soils of Mexico City records, respectively, for 5% damping. In the present study, $\phi_{ev} = 1.8$ is used for the ground motions recorded in the U.S.A., $\phi_{ev} = 2.6$ is used for the ground motions recorded in Chile, $\phi_{ev} = 2.8$ is used for the soft soil Mexico City record, and $\phi_{ev} = 2.0$ is used for the other records.

6. *Ordaz and Pérez-Rocha* [26] used 445 ground motions from the Guerrero and Mexico City Accelerographic Arrays with elasto-plastic systems having $\beta = 5\%$ and $\mu = 1.5$, 2, 4, and 8. They recommended:

$$R = 1 + (\mu - 1)\left(\frac{D(T)}{d_{g,max}}\right)^{\xi(\mu)} \tag{1.14}$$

where $d_{g,max}$ = peak ground displacement, $D(T)$ = elastic displacement response spectrum computed for the damping considered, and$\xi(\mu) = 0.388(\mu - 1)^{0.173}$. The formula applies for a wide variety of site conditions (implicit in $D(T)$), and for damping ratios between 2 and 10%.

These and other researchers (e.g. [29, 24, 23, 26, 22, 25, 21]) have studied the inelastic response of systems with different damping ratios, stiffness degradation, and ductilities using various numbers of ground motions records. Some have determined R-factors recommendations based on statistical analysis of the computed results, obtaining mean strength reduction factors which are dependent on the period and the ductility of the structure. For example, a structure having a specific period and strength associated with with a specific ductility response may require $R_\mu = 6.4$ for one record and $R_\mu = 3.8$ for another record resulting in a mean R-factor $R_\mu = 5.1$. Therefore, $R_\mu = 5.1$ would result in a very conservative design if the first record shakes the structure, and in a non-conservative design that could potentially result in failure if the second record shakes the structure. Hence, R_μ is a characteristic of the structure in relation to the ground motion.

1.2.3 Response of SDOF Systems to Pulses and Ground Motions

Several researchers have considered the effect of various pulses on the response of SDOF systems [5, 6, 7, 30, 31, 20, 32, 33]. These pulses have been described as elementary forces, explosive-type loads, pulse-type forces [5], pulse excitations or pulse forces [6], and impulsive loads [7] in the literature. As summarized in Table 1.3, an early study on undamped elastic response to simple pulses was by Jacobsen and Eyre [5], elasto-plastic inelastic response was considered by Biggs [33], and a more thorough treatment of inelastic response was presented by Veletsos [34, 20, 31, 30, 32]. As shown in Table 1.3, these studies considered a limited variety of pulses [33, 20, 30, 32] or emphasized elastic response [5, 20].

Researchers have long been aware of similarities in the response of single-degree-of-freedom (SDOF) systems to ground motions and to pulse-type excitations (e.g. [30, 20, 31, 32]). Investigators recently have used pulses to represent near fault ground motions [35, 36, 37, 38, 39, 40]. Other

Table 1.3: Abstract of previous work

Researchers	Pulses	Load -deformation response	Damping (% of critical)
Jacobsen & Ayre[5]	More than 30 pulses: ½ cycle sine pulses, triangular pulses, exponential pulses, skewed-versed sine pulses, step pulses, pulses with rest period.	Elastic SDOF systems	0
Biggs[33]	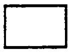 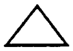 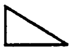 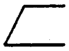	Elastic and Elasto-Plastic SDOF systems	0
Veletsos & Newmark[20]	Around 30 pulses: ½ cycle vel. pulses, displ. pulses with partial recovery, ½ cycle displ. pulse, full-cycle disp. pulses, ½ cycle accel. pulses	Elastic SDOF systems	0, 5, 10, 20, 50, 100
	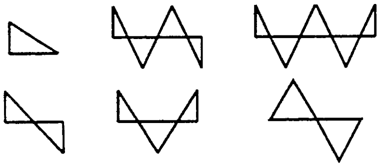	Elasto-Plastic SDOF systems	0, 10
Veletsos[30]	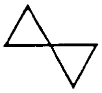 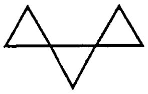	5 different nonlinear SDOF systems, Elasto-Plastic 1,2,3 DOF systems	0
Veletsos & Vann[32]	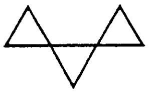	Elasto-Plastic 1,2,3,5 DOF systems	0

investigators have studied large numbers of ground motions to determine mean or approximate strength reduction factors to obtain the strengths associated with constant ductility demands (e.g. [11, 24, 23, 26, 27]).

Observation of computed response indicates that only a few cycles of ground motion cause yielding in many of the systems of practical interest [41]. These cycles describe a pulse of irregular form over a short interval of the ground motion and of sufficient intensity to cause yielding in a given structure [20, 31, 34, 42]. The equal displacement, equal energy, and equal acceleration rules were established first for pulses and were then applied to ground motions based on similarities between pulses and ground motions [30, 20, 31, 32, 43, 44]. Thus, it should not be surprising that the R-factors determined for pulses resemble those determined for ground motions. Even though the response of a system subjected to a ground motion and a simple pulse are different, it may be noticed that the R-factor obtained for a ground motion is very similar to the R-factor obtained for a particular pulse. The following three conditions are satisfied for R-factors of elasto-plastic systems under ground motions and simple pulses:

1. $R = 1$ for the elastic response ($\mu = 1$) for all periods.
2. $R = \mu$ for long period systems.
3. $R = 1$ independent of the ductility for very short period systems. Ground motions and several of the pulses explored in this thesis follow this rule.

Sewell [45] found that the damaging characteristics of numerous ground motions can be separated into two distinct components: (1) an elastic contribution, given by the elastic pseudo-acceleration spectrum, and (2) a strength reduction factor, R, applied to the elastic spectrum to determine the strengths of nonlinear oscillators that result in constant ductility responses. A systematic dependence of R-factors on earthquake magnitude and distance could not be identified, nor could a systematic dependence of R-factors on record duration be identified. Thus, one may conclude that R-factors of ground motions are not dependent on the ground motion waveform to the extent that the ground motion waveform may vary systematically with earthquake magnitude and distance and the duration of the record. Therefore, inelastic response can be considered in the present study of R-factors applicable to elastic spectra for ground motions selected without particular regard as to the source magnitude, epicentral distance, or record duration.

1.3 Objectives and Scope

1.3.1 Objectives

The main objectives of this study are:

1. To understand the inelastic response of SDOF systems subjected to simple pulses.
2. To develop an understanding of the strength reduction factors associated with various pulse shapes.
3. To develop and refine the observation that pulse R-factors may be used in conjunction with elastic response spectra to estimate the inelastic spectra associated with earthquake ground motions.
4. To identify the applicability and limitations of using pulse R-factors to estimate inelastic response spectra with regard to the duration and frequency content of the ground motions and the presence or absence of near-fault forward directivity features.
5. To understand the applicability of using pulse R-factors to estimate peak displacements and interstory drift indices of regular multistory buildings subjected to earthquake ground motions.

1.3.2 Scope and Limitations

The results of this study are strictly valid only for the 15 ground motions, 24 pulses, and the range of periods considered, although it is believed that the basic findings are more generally applicable.

Parameters that may affect the design and response of more complex structures (e.g. bridges and buildings), such as redundancy and overstrength, are not explicitly addressed in this study. The applications to MDOF systems that are considered assume structural behavior dominated by flexural deformations in the plane of the frame. Effects of torsional behavior and vertical ground motions effects were not considered.

1.4 Organization

This report is organized as follows: Chapter 2 introduces the concept of identifying the cycles contained in the ground motions that cause SDOF systems to reach their peak responses, and compares peak responses to these cycles with peak responses computed using the complete ground motion records. Chapter 3 focuses on the inelastic response of elasto-plastic SDOF oscillators subjected to 24 simple pulse waveforms. The strengths and corresponding strength reduction factors required for constant ductility responses are discussed, as are the concepts of equal energy, equal displacement, and preservation of force. Chapter 4 presents the technique for estimating inelastic response spectra for elasto-plastic SDOF systems subjected to strong ground motions. Chapter 5 compares the isoductile response spectra generated using pulse R-factors with those determined using the $R - \mu - T$ relations recommended by other investigators, for elasto-plastic, bilinear, and stiffness-degrading oscillators. Chapter 6 introduces the use of pulse R-factors for estimating the peak response of MDOF systems subjected to ground motion excitations. Estimates of peak roof displacements and interstory drift indices obtained using pulse R-factors and other $R - \mu - T$ relations are compared with the peak values determined by nonlinear dynamic analysis of the MDOF systems. Chapter 7 presents conclusions and recommendations for future research.

Chapter 2

Record Segment Identification in Earthquake Records

2.1 Introduction

Observations of computed response indicate that only a few cycles of ground motion cause yielding in many simple systems of practical interest [41]. These cycles describe a pulse of irregular form over a short interval of the ground motion record and of sufficient intensity to cause yielding in a given structure [34, 20, 31].

Bonelli [42] pointed out that the main non-linear incursions are closely related to long pulses in the records, and identified the acceleration pulses of six ground motions that reproduced the inelastic response of a 10-story reinforced concrete structural wall building. According to Bonelli, there are certain segments consisting of portions of the complete acceleration history of the record that produce the maximum inelastic responses. The problem is that, in general, the occurrence time of the maximum displacements as well as the pulse shape are not known *a priori*.

In the same year, Bozorgnia and Mahin [37] indicated that inelastic demands in near-source records are due to long period pulses contained within the records, and that idealized pulses may be used to approximate the inelastic response due to the entire record.

In this chapter, the determination of the portions of complete accelerograms that produce maximum inelastic deformation is undertaken and results are presented graphically. Comparisons between the response of systems to whole ground motion records and to pulses within the records are also presented.

2.2 Peak Response of SDOF Systems to Ground Motions

This section identifies: (1) the occurrence time of maximum displacements of SDOF elasto-plastic systems having various periods and ductility demands subjected to 15 ground motions, (2) the record segments that produce the peak displacements, and (3) comparisons between the responses of the systems subjected to the complete ground motions and subjected to the record segments within the record that produce maximum displacements.

2.2.1 Identification of Peak Response Occurrence Time of SDOF Systems Subjected to Ground Motions

In order to identify the occurrence time of the maximum inelastic responses, elasto-plastic SDOF systems with 5% of critical damping are studied when subjected to 15 ground motions. These recorded ground motions were selected from those used in FEMA-307 [46]. Three categories of motions were defined: Short Duration (SD), Long Duration (LD), and Forward Directive (FD). Five records were selected for each category (Table 2.1). Associated with each record is an identifier name, an identifier number, the origin of the record and date, the peak ground acceleration relative to the acceleration of gravity, magnitude, and characteristic period, T_g, which ranges from 0.2 to 2 s over the 15 records.

During the ground motion actions, the SDOF oscillators reach a peak displacement that may involve inelastic response or just elastic response. This peak may be either in the first or third

Table 2.1: Properties of recorded ground motions and their identifiers

	Identifier	No.	Earthquake Date*	$\frac{a_{g,max}}{g}$	Magnitude	T_g (s)
SD	WN87MWLN.090	1	Whittier Narrows 1/8/87	0.175	$M_L = 5.9$	0.20
SD	BB92CIVC.360	2	Bigg Bear 28/6/92	0.544	$M_L = 6.5$	0.40
SD	SP88GUKA.360	3	Spitak 7/12/88	0.207	$M_W = 6.8$	0.55
SD	LP89CORR.090	4	Loma Prieta 17/10/99	0.478	$M_W = 6.9$	0.85
SD	NR94CENT.360	5	Northridge 17/1/94	0.221	$M_W = 6.7$	1.00
LD	CH85LLEO.010	6	Central Chile 3/3/85	0.711	$M_L = 7.8$	0.30
LD	CH85VALP.070	7	Central Chile 3/3/85	0.176	$M_L = 7.8$	0.55
LD	IV40ELCN.180	8	Imperial Valley 18/5/40	0.348	$M_L = 6.3$	0.65
LD	LN92JOSH.360	9	Landers 28/6/92	0.274	$M_W = 7.4$	1.30
LD	MX85SCT1.270	10	Michoacan 19/9/85	0.171	$M_W = 8.0$- 8.1	2.00
FD	LN92LUCN.250	11	Landers 29/6/92	0.733	$M_W = 7.4$	0.20
FD	LP89SARA.360	12	Loma Prieta 17/10/89	0.504	$M_W = 6.9$	0.40
FD	NR94NWHL.360	13	Northridge 17/1/94	0.589	$M_W = 6.7$	0.80
FD	NR94SYLH.090	14	Northridge 17/1/94	0.604	$M_W = 6.7$	0.90
FD	KO95TTRI.360	15	Hyogo-Ken Nambu 17/1/95	0.617	$M_W = 6.9$	1.40

* day/month/year

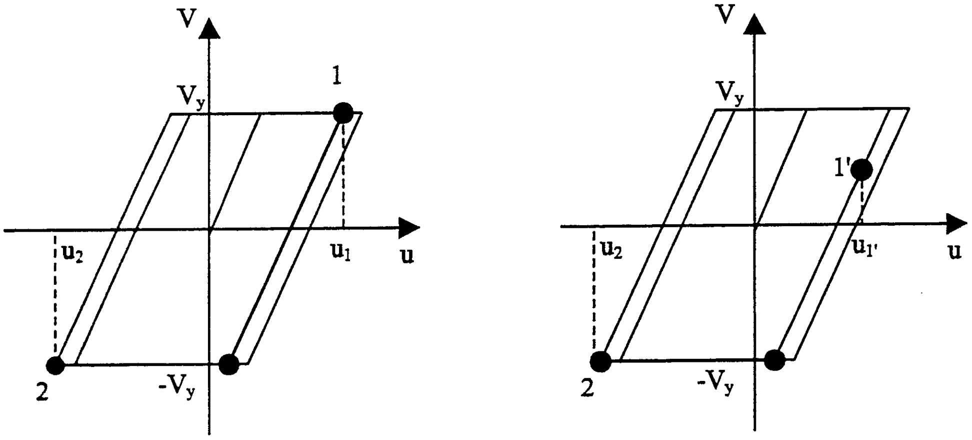

COMPLETE ½ CYCLE

INCOMPLETE ½ CYCLE

Figure 2.1: Yield strength-displacement cycles of elasto-plastic systems

quadrant; the discussion below assumes the peak displacement is in the third quadrant. The motion preceding the peak displacement u_2 in Fig. 2.1 begins at u_1 in the case of a "complete" 1/2 cycle (yield strength V_y is reached), or u_1' in the case of an "incomplete" 1/2 cycle (yield strength is not reached). The displacements u_1 and u_2 occur at times t_1 and t_2, respectively. The "complete 1/2 cycle" of Fig. 2.1 refers to the cycle that starts by unloading from a yield condition (u_1, V_y) and finishes at the maximum negative displacement $(u_2, -V_y)$ without any reversals in the middle of the cycle. The "incomplete 1/2 cycle" refers to the cycle that starts at a point $1'$ of maximum displacement without yielding and finishes at $(u_2, -V_y)$, without any reversals between u_1' and u_2.

A set of 150 systems was studied for each ground motion, consisting of 15 periods ranging from 0.04 to 3 s and 10 strengths ranging from 0.1 to 2 times the product of the mass, m, and peak ground acceleration, $a_{g,max}$. Response time histories were generated using the computer program NONSPEC [47]. For each of the systems with non-linear behavior, the 1/2 cycle (complete or incomplete) that contained the peak displacement (positive or negative) was identified together with the initial time t_1 and final time t_2, corresponding to the displacements u_1(or u_1') and u_2. It was observed that the interval of time from t_1 to t_2 was very similar for all systems for each particular ground motion. During this segment of time, the displacement of most of the systems that reached yield strength went from the prior peak value u_1(or u_1') to the peak value u_2 without any reversal.

Table 2.2 shows the times at which the peak ground acceleration, $a_{g,max}$, and peak ground velocity, $v_{g,max}$, of each ground motion record are reached. The table also shows the minimum time, $min\,(t_1)$, and maximum time, $max\,(t_2)$, among all the t_1 and t_2 values obtained for all systems that have complete or incomplete 1/2 cycles, where multiple $min\,(t_1) - max\,(t_2)$ ranges are shown, each describes the interval over which most of the 150 oscillators reached their peak displacements. It so happens that records having only one interva of time have the peak ground acceleration and peak ground velocity reached within that interval, while records having two intervals of time have the peak ground acceleration reached in one interval and the peak ground velocity reached in the other interval. Of all the durations of ground motion considered (in some cases larger than one

Table 2.2: Time parameters for peak response to each ground motion

Ground motion	$t(a_{g,max})$ (s)	$t(v_{g,max})$ (s)	$min\,(t_1) - \; max\,(t_2)$ (s)	$(t_1 - \; t_2)_{cycle}$ (s)
WN87MWLN.090	4.12	4.08	3.98-4.22	3.80-4.40
BB92CIVC.360	5.10	5.05	5.02-5.5	4.80-5.72
SP88GUKA.360	10.48	10.49	10.34-11.12	10.12-11.32
LP89CORR.090	4.04	3.96	3.84-4.62	3.60-4.80
NR94CENT.360	8.92	9.80	8.7-9.38, 9.54-10.68	8.50-10.92
CH85LLEO.010	43.34	41.43	43.5-44.22, 41.3-42.28	41.12-44.40
CH85VALP.070	26.62	29.30	26.4-26.9, 28.54-29.5	26.20-29.72
IV40ELCN.180	2.12	2.16	1.78-2.5	1.50-2.72
LN92JOSH.360	25.98	27.48	25.56-26.42, 26.68-27.72	25.32-27.92
MX85SCT1.270	58.08	58.44	58.48-60.1	57.8-60.32
LN92LUCN.250	10.37	10.39	10.38-13.02	10.12-13.20
LP89SARA.360	7.34	6.28	6.24-8.18	6.00-8.40
NR94NWHL.360	4.32	5.34	4.04-5.16, 5.32-6.14	3.80-6.32
NR94SYLH.090	4.08	6.48	3.86-5.48, 6.14-7.7	3.60-7.92
KO95TTRI.360	5.83	6.28	5.29-6.69	5.12-6.92

minute), only a small interval of time, with duration less than 4 seconds, is really significant for the oscillators considered. The meaning of the last column in Table 2.2 is described in Section 2.2.2.

2.2.2 Response to Ground Motion Recorded Segments

The maximum displacements of the structures that occur in the intervals of time $min\,(t_1) - max\,(t_2)$ identified in Table 2.2 are the ones of interest for the design of structures. Perhaps, if the main cycle that produces the maximum inelastic responses is known, it may be a suitable substitute for the ground motion for design purposes.

The identification of the timing of these record segments resulted in the values $min\,(t_1)$ and $max\,(t_2)$ in Table 2.2. Considering that the cycles were calculated only for systems having strengths ranging from 0.1 up to $2m \cdot a_{g,max}$ and periods from 0.04 to 3.0 s, a margin of roughly 0.2 s was considered in identifying the limits of $min\,(t_1)$ and $max\,(t_2)$ to take into account systems with smaller or larger strengths; therefore, the time segment of the record with interval ($min\,(t_1) - 0.2$ s, $max\,(t_2) + 0.2$ s) is set to be $(t_1 - \; t_2)_{cycle}$ in Table 2.2. Fig. 2.2 plots the record segment of each

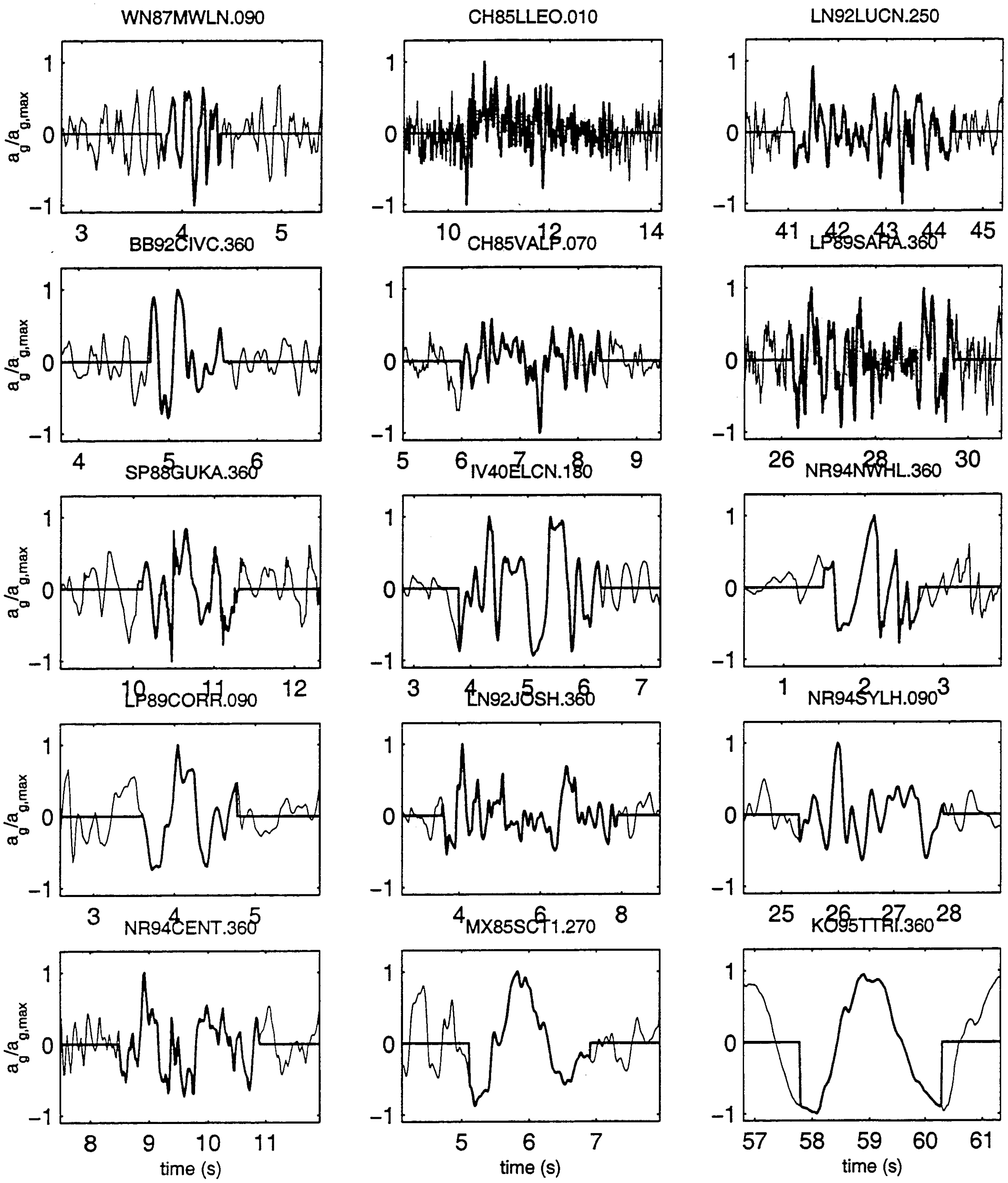

Figure 2.2: Pulse containing $a_{g,max}$ and $v_{g,max}$ for each ground motion in the range $(t_1 - t_2)_{cycle}$ from Table 2.2

ground motion record which is contained in the interval $(t_1 - t_2)_{cycle}$. Comparisons between the responses of the systems to the records and to the record segments comprised in $(t_1 - t_2)_{cycle}$ are presented in this section in terms of the strengths and reduction factors.

2.2.2.1 Isoductile Strength Parameter

The inelastic response spectra for systems having periods from 0.04 to 3 s and strengths to result in ductility demands equal to 1, 2, 4, and 8 subjected to the ground motions and to the pulses were calculated using the computer program PCNSPEC [48], a modified version of NONSPEC [47]. For a given period, the strength-ductility relation is not necessarily monotonic since the same ductility may result for different strengths; the largest strength required to achieve the specified ductility was retained in cases where different strengths result in the same ductility.

Figures 2.3 to 2.5 compare the response spectra of elasto-plastic systems having ductility demands of 1, 2, 4, and 8 for the SD, LD, and FD records (Table 2.1).The spectra plot the dimensionless strength parameter, η, defined as the ratio

$$\eta(\mu, T) = \frac{V_y(\mu, T)}{m \cdot a_{g,max}} \tag{2.1}$$

where:

- $\eta(\mu, T)$ = strength parameter of a system with ductility μ and natural period T
- $V_y(\mu, T)$ = yield strength of a system with ductility μ and natural period T
- m = mass of the system
- $a_{g,max}$ = peak ground acceleration

For each record, two strength spectra are plotted. The strengths required for constant ductility responses to the record, η_r, and the isoductile strengths η_p for the pulse of each record over the

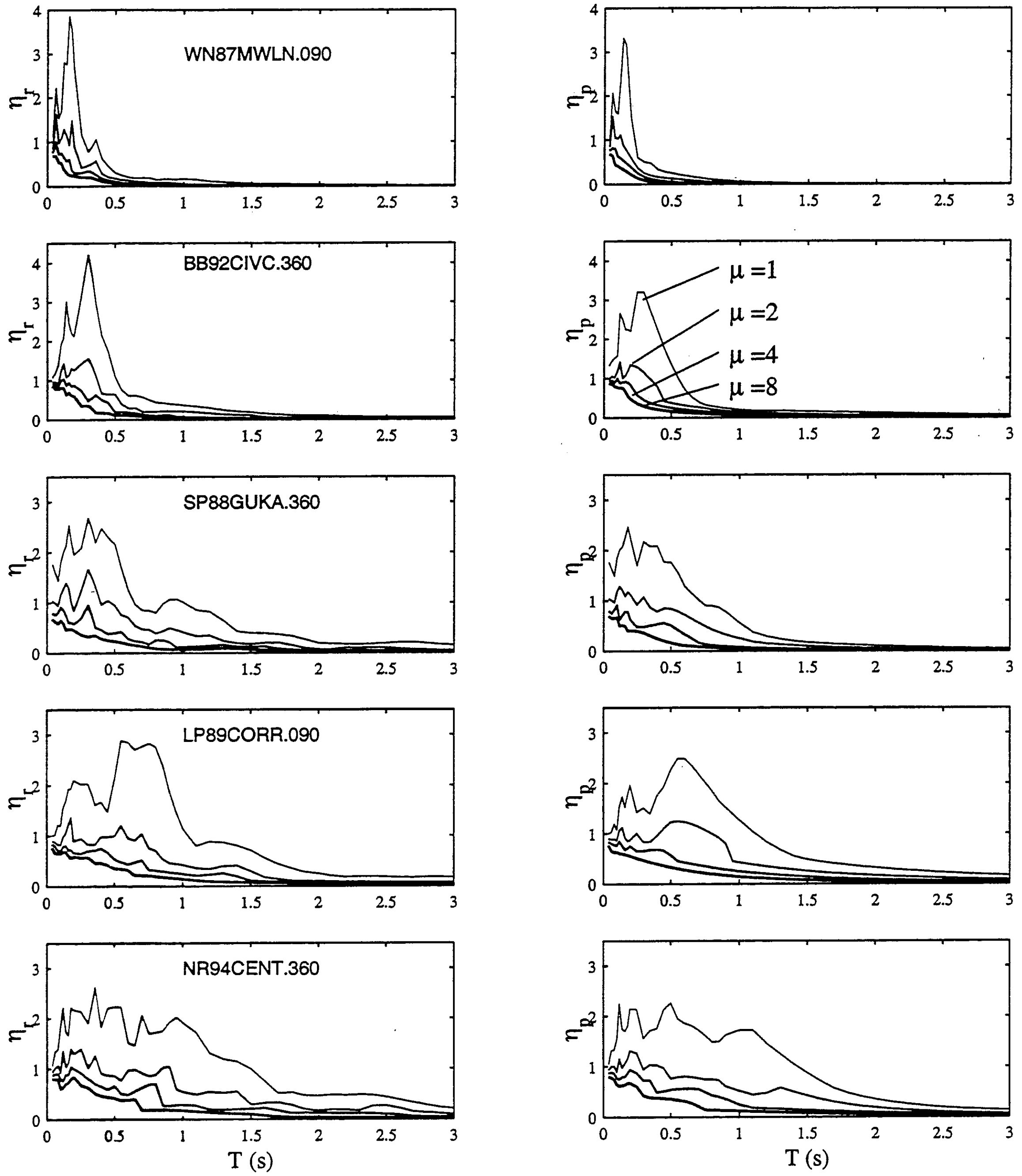

Figure 2.3: Strength response spectra for systems subjected to the records, η_r, and to the pulses, η_p, for the pulses defined in Fig. 2.1 for the Short Duration motions

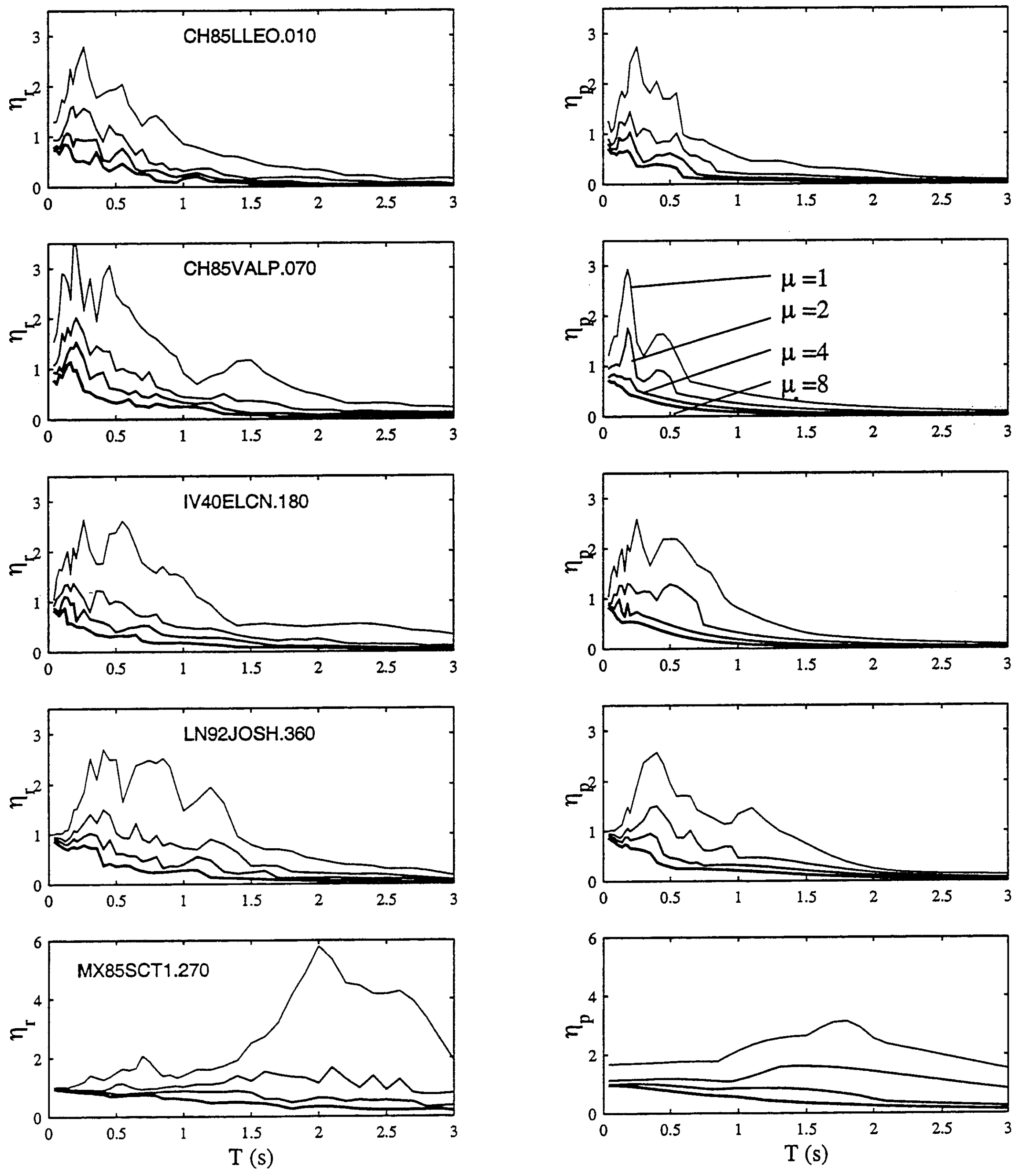

Figure 2.4: Strength response spectra for systems subjected to the records, η_r, and to the pulses, η_p, for the pulses defined in Fig. 2.1 for the Long Duration motions

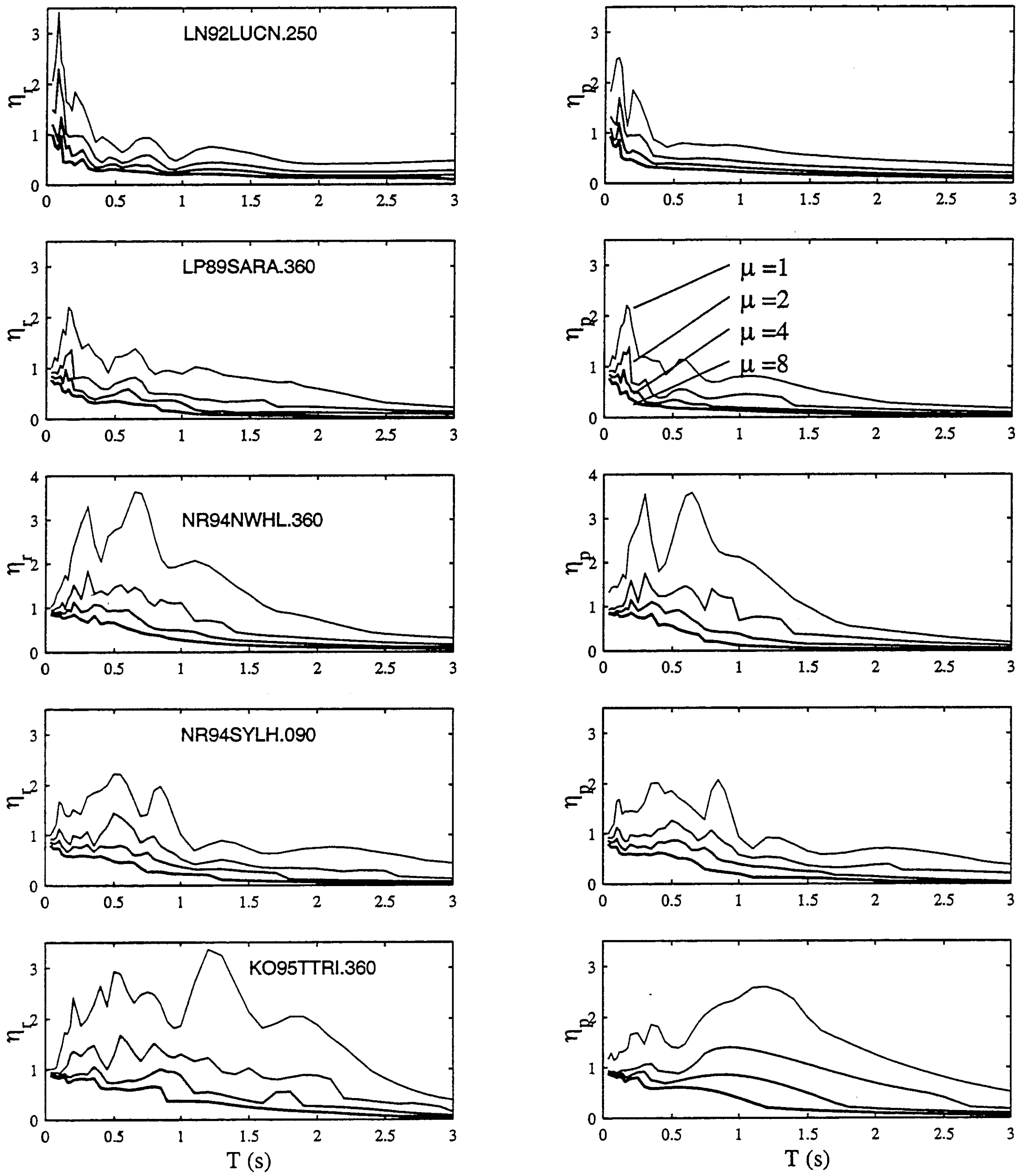

Figure 2.5: Strength response spectra for systems subjected to the records, η_r, and to the pulses, η_p, for the pulses defined in Fig. 2.1 for the Forward Directive motions

interval $(t_1 - t_2)_{cycle}$ are shown in Fig. 2.1. Focusing on the elastic strength response, in some cases, $\eta_r(\mu = 1, T)$ is very similar to $\eta_p(\mu = 1, T)$ (e.g. NR94CENT.360 and NR94SYLH.360 records) and in other cases, is very different (e.g. MX85SCT1.270 and KO95TTRI.360 records). Considering the inelastic strength responses, for $\mu = 2$, 4, and 8, similar trends can be found between η_r and η_p in the short and long period ranges of the spectra. In the intermediate period range, the differences are larger.

2.2.2.2 Strength Reduction Factor

The strength reduction factor, or R-factor, is given by the ratio

$$R(\mu, T) = \frac{V_y(\mu = 1, T)}{V_y(\mu, T)} \tag{2.2}$$

where:

- $V_y(\mu = 1, T)$ = strength required for elastic response of a system having natural period T
- $V_y(\mu, T)$ = yield strength of a system having ductility μ and natural period T

Figures 2.6 to 2.8 present values of R_r, the R-factor spectra for the systems subjected to the SD, LD, and FD records, respectively, and values of R_p, the R-factor spectra for the systems subjected to the pulses ranging $(t_1 - t_2)_{cycle}$ in Fig. 2.1. It can be observed that, for short period systems, the R_r and R_p factors are fairly similar, while for intermediate and long period systems the R-factors are quite different, especially for $\mu = 8$; in general, the strength reduction factors generated by the pulses are smaller than those computed for by the complete records.

2.2.3 Limitations

In this chapter, many of the systems studied reached yielding in one or two cycles of the ground motion. However:

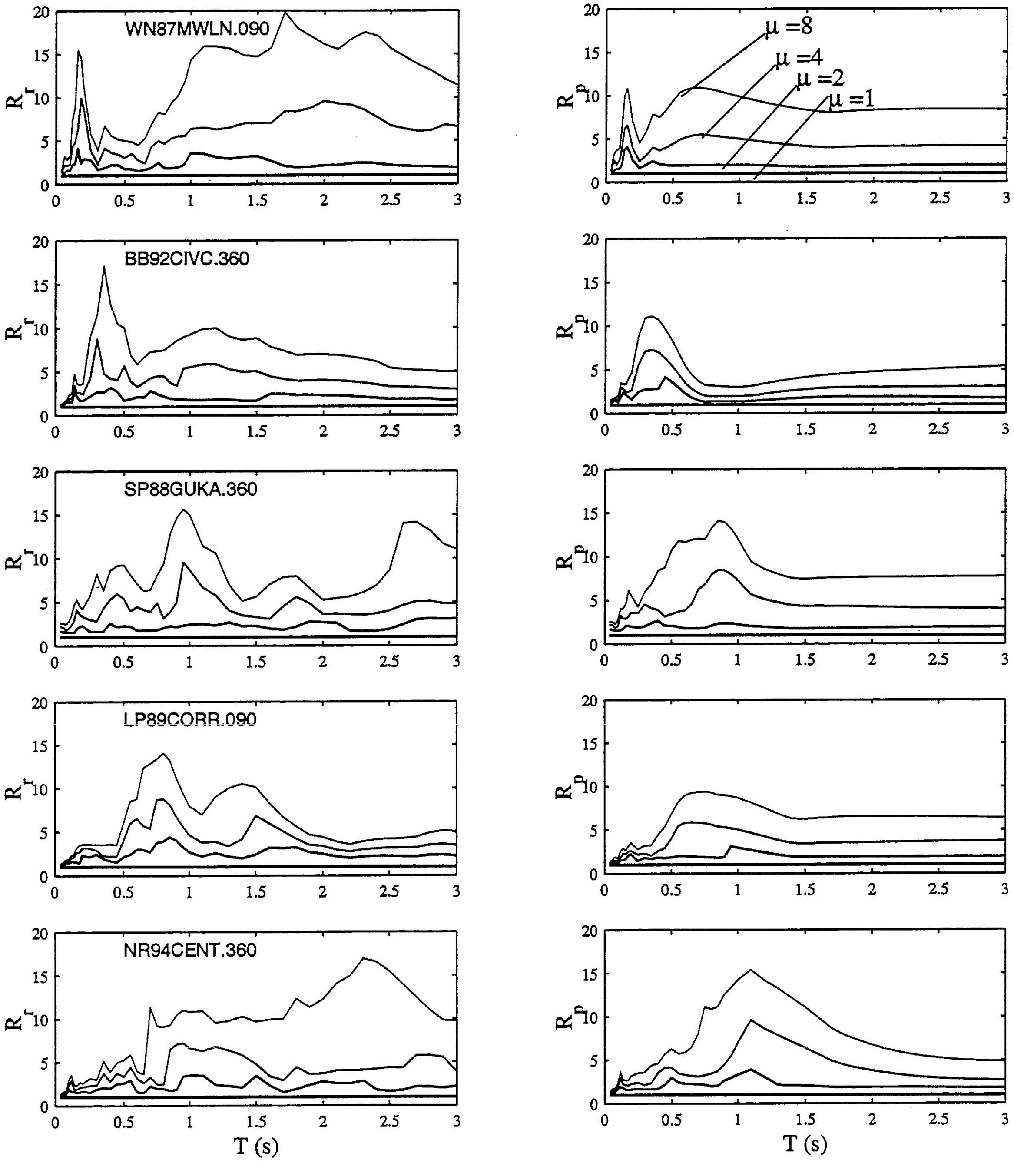

Figure 2.6: R-factor response spectra for systems subjected to the Short Duration motions, R_r, and to the pulses, R_p

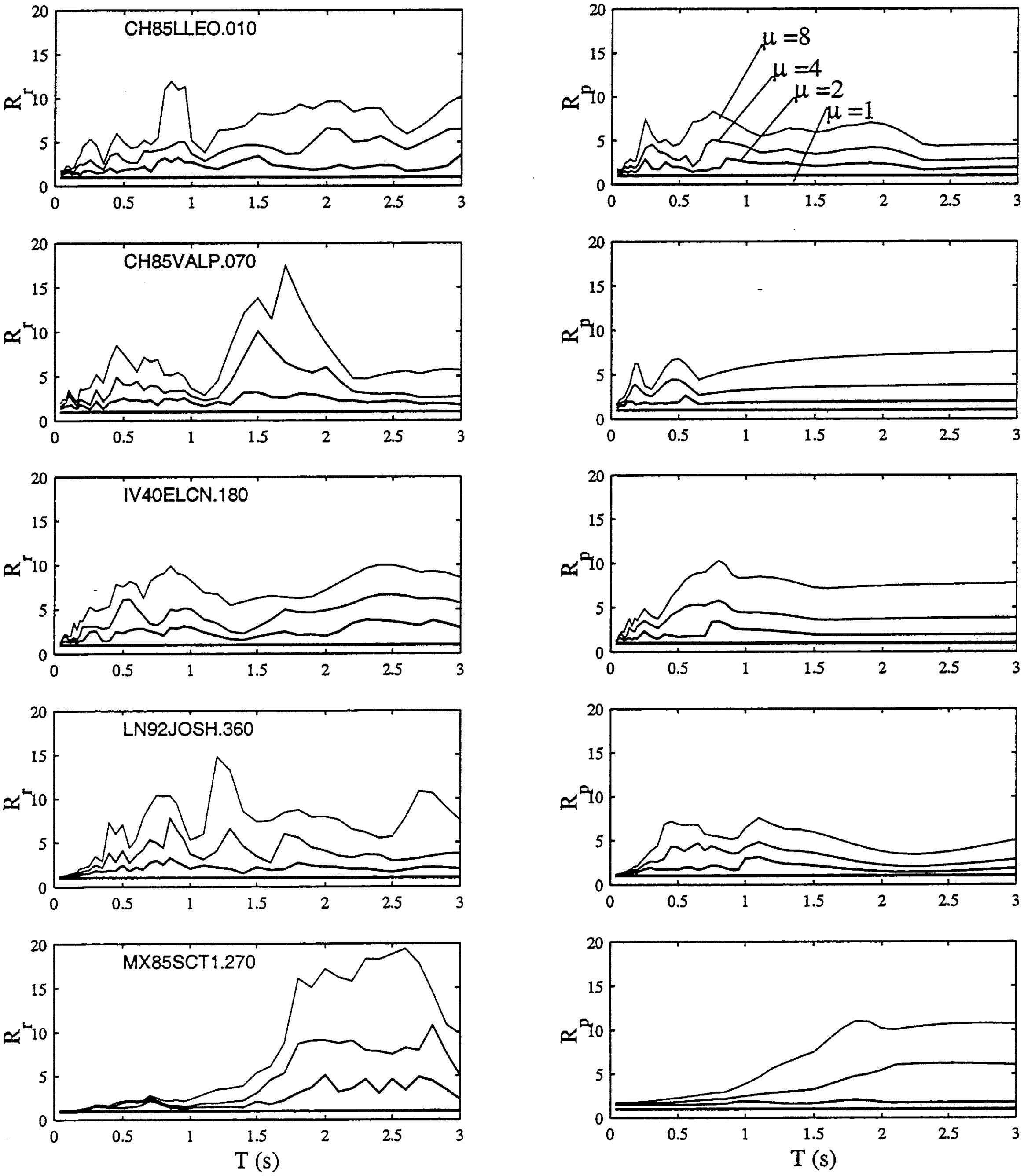

Figure 2.7: R-factor response spectra for systems subjected to the Long Duration motions, R_r, and to the pulses, R_p

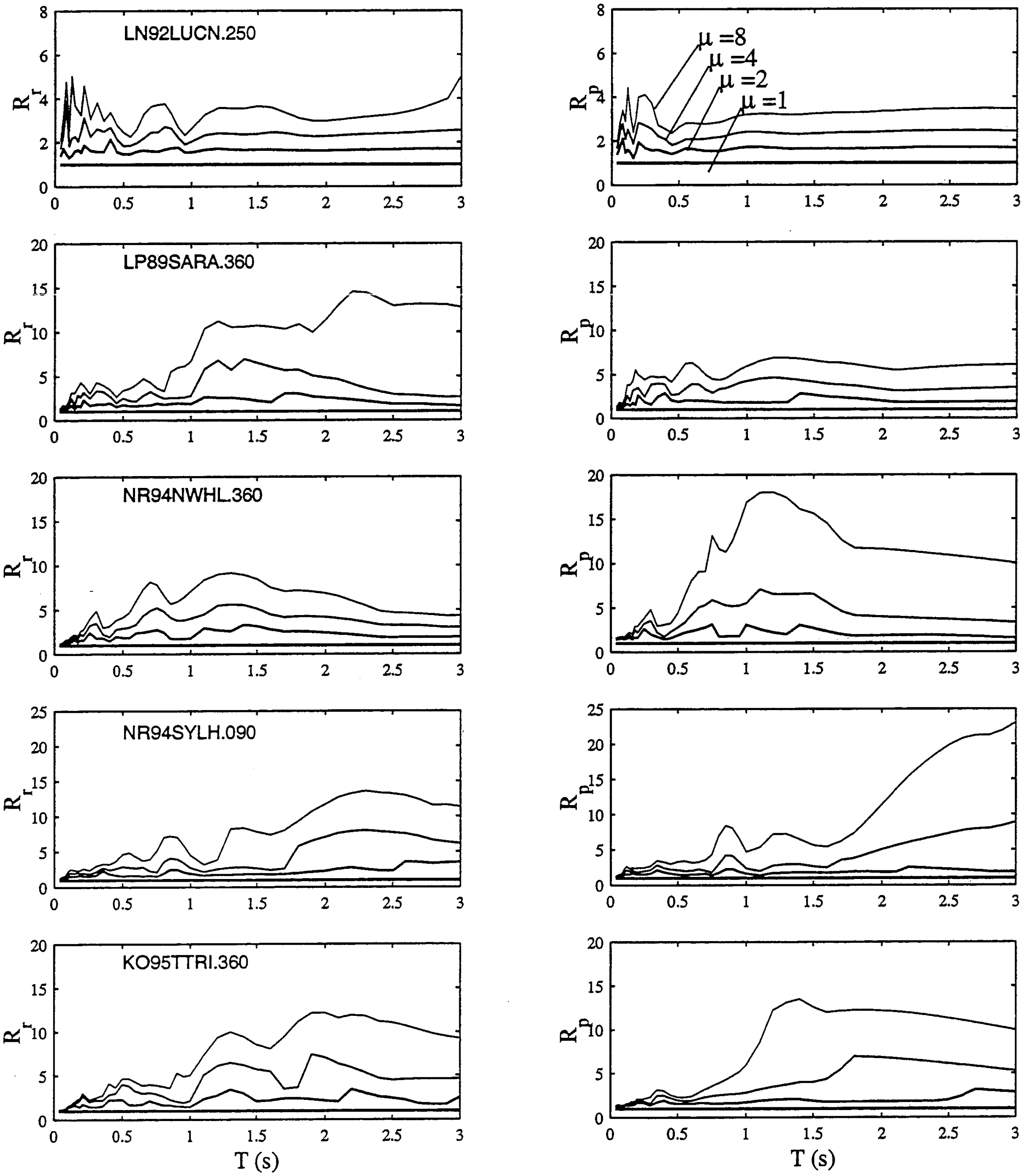

Figure 2.8: R-factor response spectra for systems subjected to the Forward Directive motions, R_r, and to the pulses, R_p

- Not all of the systems reach the peak ductility response within the same interval of the motion.
- Systems with different characteristics may reach the peak ductility response in different intervals, and these intervals are not known *a priori.*
- The shape and duration of the intervals are erratic, irregular, and unpredictable over their entire set of records, even though for a given record nearly all systems reached their peak ductility in a narrow segment of the ground motion record.

2.3 Summary

Only a few cycles of ground motion cause yielding in many of the systems studied. These cycles define a segment of the ground motions characterized by its short duration and irregular shape, and produce peak ductility demands at consistent times that can not be predicted *a priori.* The pulses often are a poor substitute for the records since the associated elastic and isoductile strength spectra differ. Compared to the strength response spectra, the R-factors of the pulses are better approximations to the R-factors of the records. Since the occurrence times and pulse shapes are not known *a priori*, the use of simple pulse shapes to determine R-factors that may be applicable to the elastic response spectra determined for the complete ground motion record is explored in Chapters 3 to 6.

Chapter 3

Isoductile Strengths and Strength Reduction Factors of Elasto-plastic SDOF Systems Subjected to Simple Pulse Waveforms

3.1 Introduction

To better understand inelastic response to complicated waveforms such as the ground motions generated by earthquakes leads one to consider, as a starting point, the inelastic demands generated by simpler motions. In this chapter, the inelastic response of elasto-plastic SDOF oscillators subjected to 24 simple pulse waveforms is studied. The waveforms contain linear, quadratic, sinusoidal, and triangular acceleration components that repeat for not more than several cycles. Similarities and differences in oscillator response characteristics are presented and organized by a characteristic period. Strengths and corresponding strength reduction factors required for constant ductility responses are discussed. Response data are compared with expectations based on the concepts of equal energy, equal displacement, and preservation of force. Limitations on the applicability of the equal energy concept are identified.

The effect of various pulses on the response of SDOF systems [33, 6, 7, 5, 20, 31, 30, 32] has been considered by several researchers. These pulses have been described as elementary forces, explosive-type loads, pulse-type forces [5], pulse excitations or pulse forces [6], and impulsive loads [7] in the literature. As summarized in Table 1.3, an early study on undamped elastic response to simple pulses was by Jacobsen and Ayre [5], elasto-plastic inelastic response was considered by Biggs [33], and a more thorough treatment of inelastic response was presented by Veletsos [34, 20, 31, 30, 32]. As shown in Table 1.3, these studies considered a limited variety of pulses [33, 20, 30, 32] or emphasized elastic response [5, 20]. The present study considers the nonlinear response of elasto-plastic oscillators subjected to a broader set of 24 pulses. Strengths to achieve displacement ductilities, μ, equal to 1, 2, 4, and 8 were computed for SDOF oscillators having viscous damping equal to 5% of critical damping. Similarities and differences in the required strengths and corresponding strength reduction factors are discussed. The applicability of the equal displacement rule [34] and rules based on preservation of energy [49, 34] and force to the data set are identified. Chapter 4 identifies a subset of these pulses whose R-factors resemble those obtained from recorded ground motions, allowing the pulse R-factors to be used in conjunction with site specific elastic response spectra to obtain estimated inelastic response spectra.

3.2 Methodology

This parametric study addresses the response of elasto-plastic oscillators having viscous damping equal to 5% of critical damping, for the following conditions:

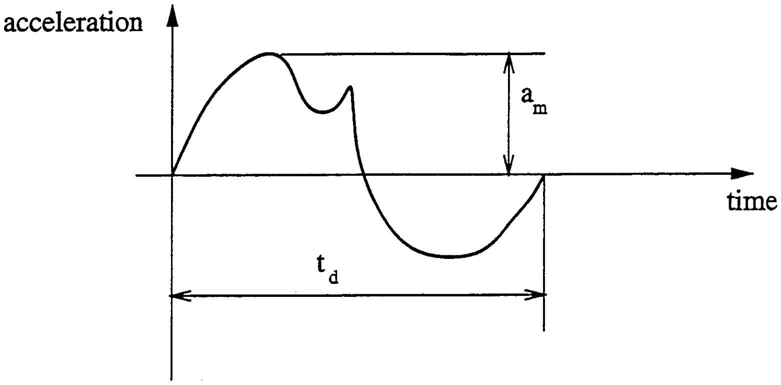

Figure 3.1: Acceleration time history of a pulse

3.2.1 Pulse Waveforms

Twenty-four acceleration pulses were used, defined by their shape and duration. The pulses (shown in Table 3.1) are classified according to four criteria:

1. *Pulse shape.* Six pulse shapes were defined, using quadratic (qua), sinusoidal (sin), rectangular (rec), and triangular (tr0, trh, trl) components. The triangular pulse families are named according to the rise time of the first incursion; tr0, trh, and trl have rise time, t_r, equal to 0, 1/2, and 1 times the duration of the first incursion, respectively.

2. *Number of incursions.* The trace of the acceleration waveform may alternate between positive and negative accelerations. A pulse having only positive acceleration is said to have one incursion. A pulse having two incursions has acceleration in one direction followed by a reversal in the opposite direction, and so on.

3. *Final pulse velocity.* If the integral of the pulse acceleration is zero, the pulse is said to be "balanced" (the motion has zero final velocity). "Unbalanced" pulses have non-zero velocity for $t \geq t_d$, where t_d is the duration of the pulse (Fig. 3.1).

4. *Initial acceleration.* "Shock" loading refers to pulses with non-zero initial acceleration; "gradual" loading refers to those with zero initial acceleration. The qua, sin, trh, and trl families apply loading gradually; the rec and tr0 families are shock pulses (the use of the phrase "shock loading" in this thesis has no direct relation to the effects of blast loading on structures).

Table 3.1: Description and classification of acceleration pulses

		WAVEFORM FAMILY					
		rec	tr0	qua	sin	trh	tr1
		SHOCK LOADING		GRADUAL LOADING			
NUMBER OF INCURSIONS	1	* 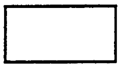 $T_p/t_d=2$	* 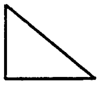 4	* 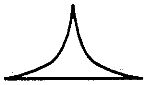 2	* 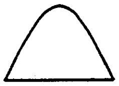 2	* 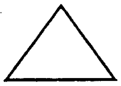 2	* 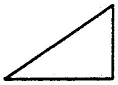 2
	2	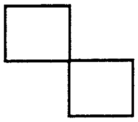 $T_p/t_d=1$	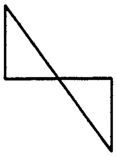 2	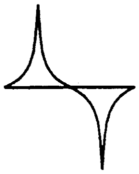 1	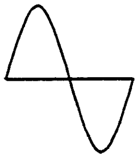 1	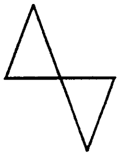 1	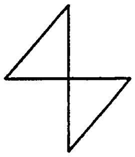 1
	3	* 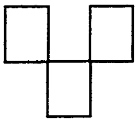 $T_p/t_d=2/3$	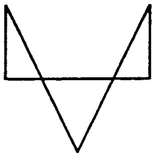 1	* 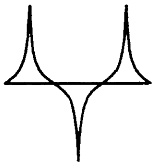 2/3	* 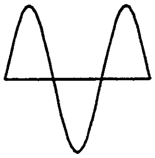 2/3	—	—
	4	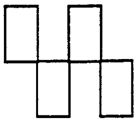 $T_p/t_d=1/2$	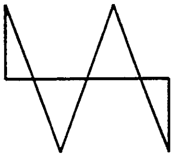 2/3	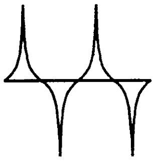 1/2	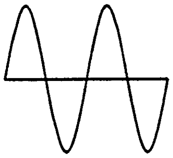 1/2	—	—
	5	* 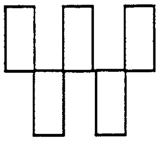 $T_p/t_d=2/5$	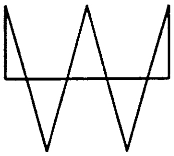 1/2	* 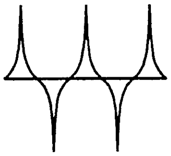 2/5	* 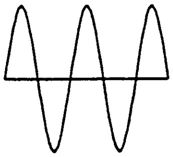 2/5	—	—

* pulse has non-zero final velocity.

The pulses are identified according to the convention family_name(number_of_incursions). For example, qua(2) refers to a quadratic pulse with 2 incursions, and tr0(5) is a triangular pulse, having five incursions, with $t_r = 0$. Appendix A shows the equations defining the acceleration histories of the 24 pulses used in this study and the figures of the acceleration, velocity, and displacement time histories of each pulse versus the dimensionless time parameter t/t_d.

3.2.2 Periods

One-hundred and seven periods, T, were considered. The first 100 values were distributed geometrically to provide greater resolution in the short period range. The geometric ratio, r, of a set of N points is given by:

$$r = exp\left\{\frac{ln(\kappa_N) - ln(\kappa_1)}{N-1}\right\} \tag{3.1}$$

where $\kappa = T/t_d$, κ_1 and κ_N are the first and the N^{th} values of κ, respectively. Intermediate values κ_i are given by $\kappa_i = r^{i-1}\kappa_N$. The first 100 periods were defined by $\kappa_1 = 0.01$ and $\kappa_N = \kappa_{100} = 15$. These are supplemented by 7 additional periods corresponding to κ = 20, 25, 30, 40, 60, 80, and 100. Accordingly, the duration of the pulse is constrained to $t_d \in [0.01T, 100T]$, where T is the natural period of vibration of the system calculated using the initial stiffness.

3.2.3 Displacement Ductility

Strengths required for each SDOF oscillator to achieve specified ductilities (hereinafter referred to as isoductile strengths) were computed for displacement ductilities μ = 1, 2, 4, and 8 as shown in Section 2.2.2.1. Isoductile strengths were computed for two cases. "Forced response" refers to cases in which the specified ductility demand is reached during the pulse excitation ($0 < t/t_d \leq 1$), while "overall response" refers to cases in which the specified ductility demand occurs at any time during or after the excitation ($0 < t/t_d \leq \infty$), following the terminology of Ref. [6].

A consistent basis was desired for interpreting the isoductile strength data. The pulse duration,

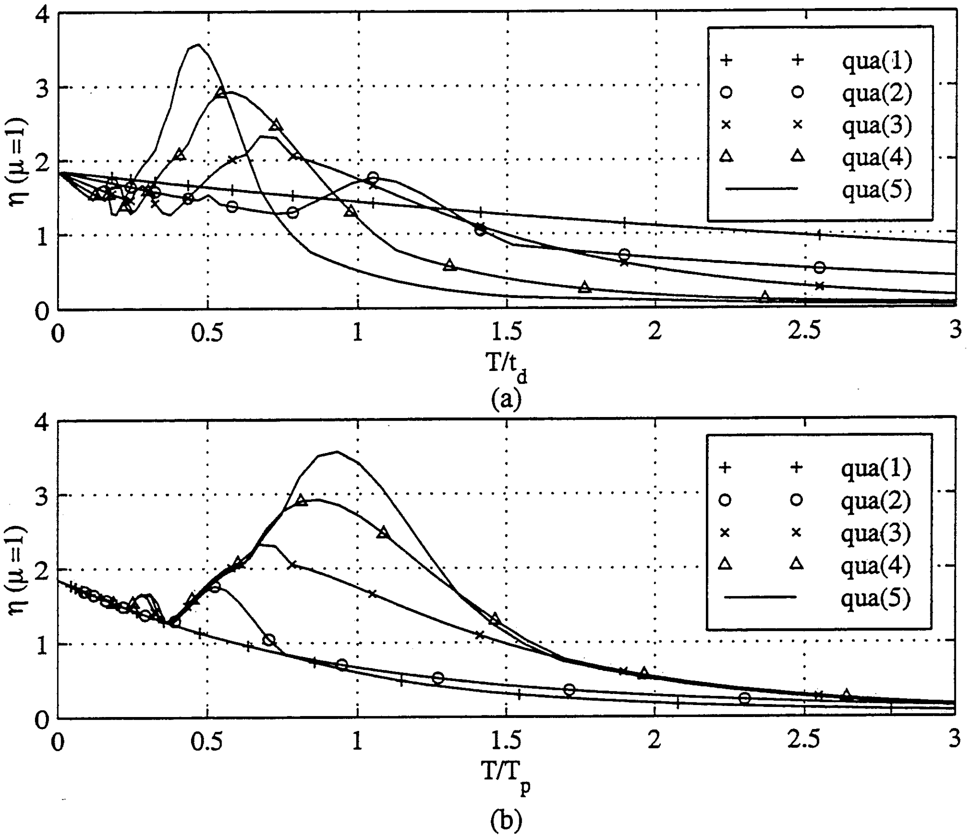

Figure 3.2: Comparison of elastic strength, (a) η vs. T/t_d, and (b) η vs. T/T_p, for the quadratic family

t_d, did not organize the data well, because the pulses had varied numbers of incursions. Instead, it was found that the data were better organized with respect to a parameter termed the characteristic period, T_p. For the families sin, qua, rec, trh, and tr1, the duration of the pulse having a complete cycle (2 incursions) defines the characteristic period ($T_p = t_d$). A different convention is used for the tr0 family, for which T_p was set equal to the duration of the pulse having 3 incursions. The characteristic period is the same for all pulses of the same family. For example, T_p equals the duration of the pulse sin(2). The pulse sin(1) has half a cycle, and $T_p = 2t_d$ for this pulse. This procedure, when applied to all pulses, results in the ratios T_p/t_d shown in Table 3.1.

The isoductile strengths for systems with $\mu = 1$ subjected to the qua pulse family are plotted in Fig. 3.2. The strengths have little consistency when plotted against t/t_d, but similarities are apparent when plotted against T/T_p. The curves show similar trends for small and large period ratios T/T_p; these trends are also present for larger ductilities. While the characteristic period was useful for organizing the results, the response spectra were so varied that it was not possible to define the notions of short, intermediate, and long period systems using consistent numerical limits for the set of 24 pulses.

3.3 Analytical Results

The strengths and strength reduction factors associated with the computed isoductile response data are presented in this section.

3.3.1 Isoductile Strength Spectra

3.3.1.1 General features

Figures 3.3 and 3.4 plot the dimensionless strength parameter η given in Eq. 2.1 vs. T/T_p for the gradual and shock pulses, respectively, for $\mu = 1$, 2, 4, and 8. Overall and forced responses are plotted with different line types in the figures. It can be observed that:

- The largest strengths are required for elastic behavior. As ductility increases, strength curves become smoother and decrease in magnitude. The largest reduction in strength is in the vicinity of $T = T_p$, for all 24 pulses. Large reductions also occur for short period systems ($T/T_p < 0.5$) subjected to shock pulses. For any pulse, the strength reduction tends to be larger for an increase in ductility from 1 to 2 than for increases from 2 to 4 or from 4 to 8.

- The "forced" isoductile strengths are equal to the "overall" isoductile strengths for many values of T/T_p. For some intervals of T/T_p, the forced strengths are smaller than the overall strengths. For $\mu = 1$, the point of divergence is $T/T_p = 1$ for the qua, sin, trh, and rec families and for the trl(2) pulse. For the trl(1) pulse, forced and overall responses differ for all T/T_p (the differences are too small to be seen in much of Fig. 3.3). The point of divergence for the tr0 family occurs at values of $T < T_p$ that depend on the number of incursions.

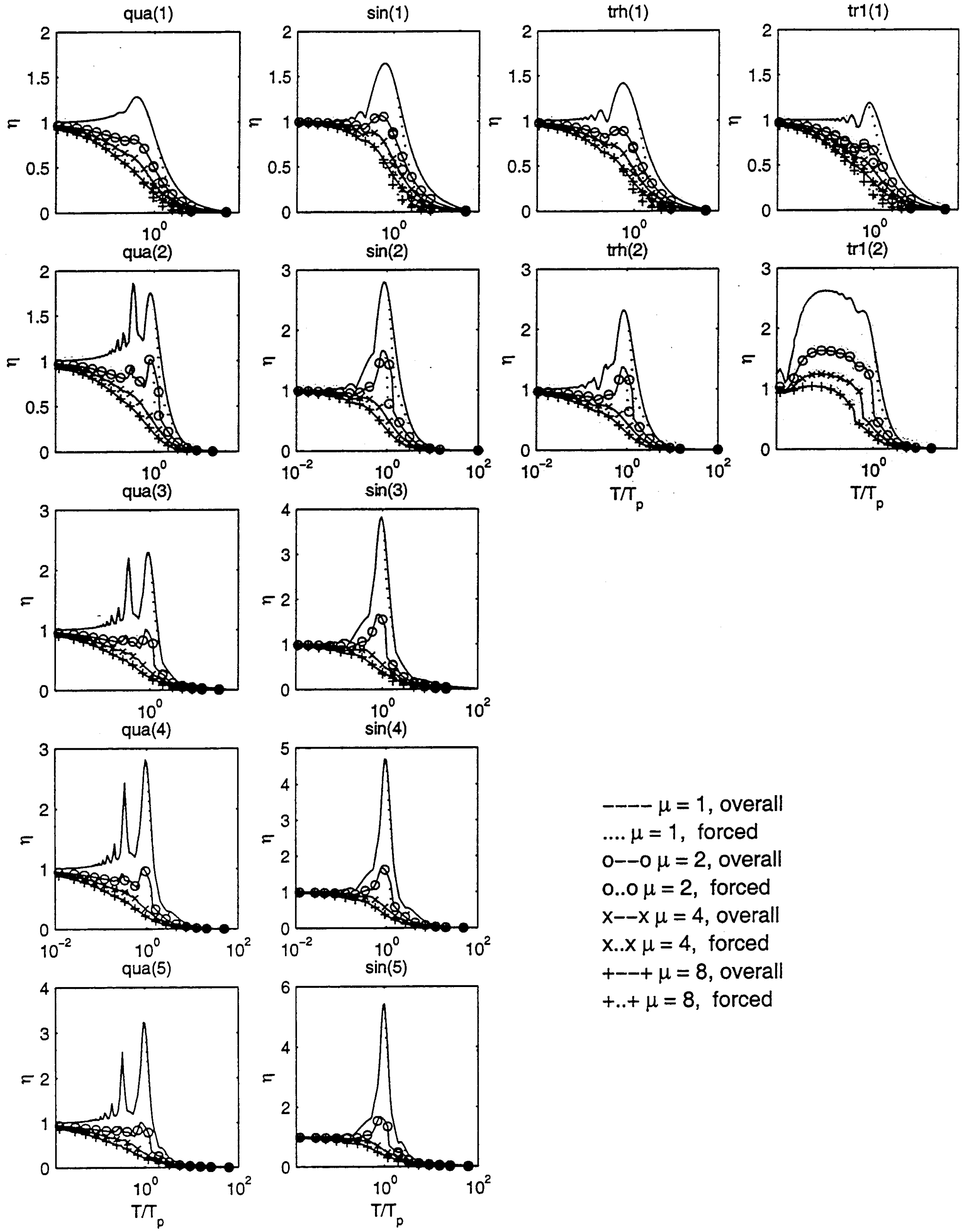

Figure 3.3: Strength parameter, η, vs. T/T_p of systems with $\mu = 1$, 2, 4, and 8. Forced and overall responses to gradual loading pulses

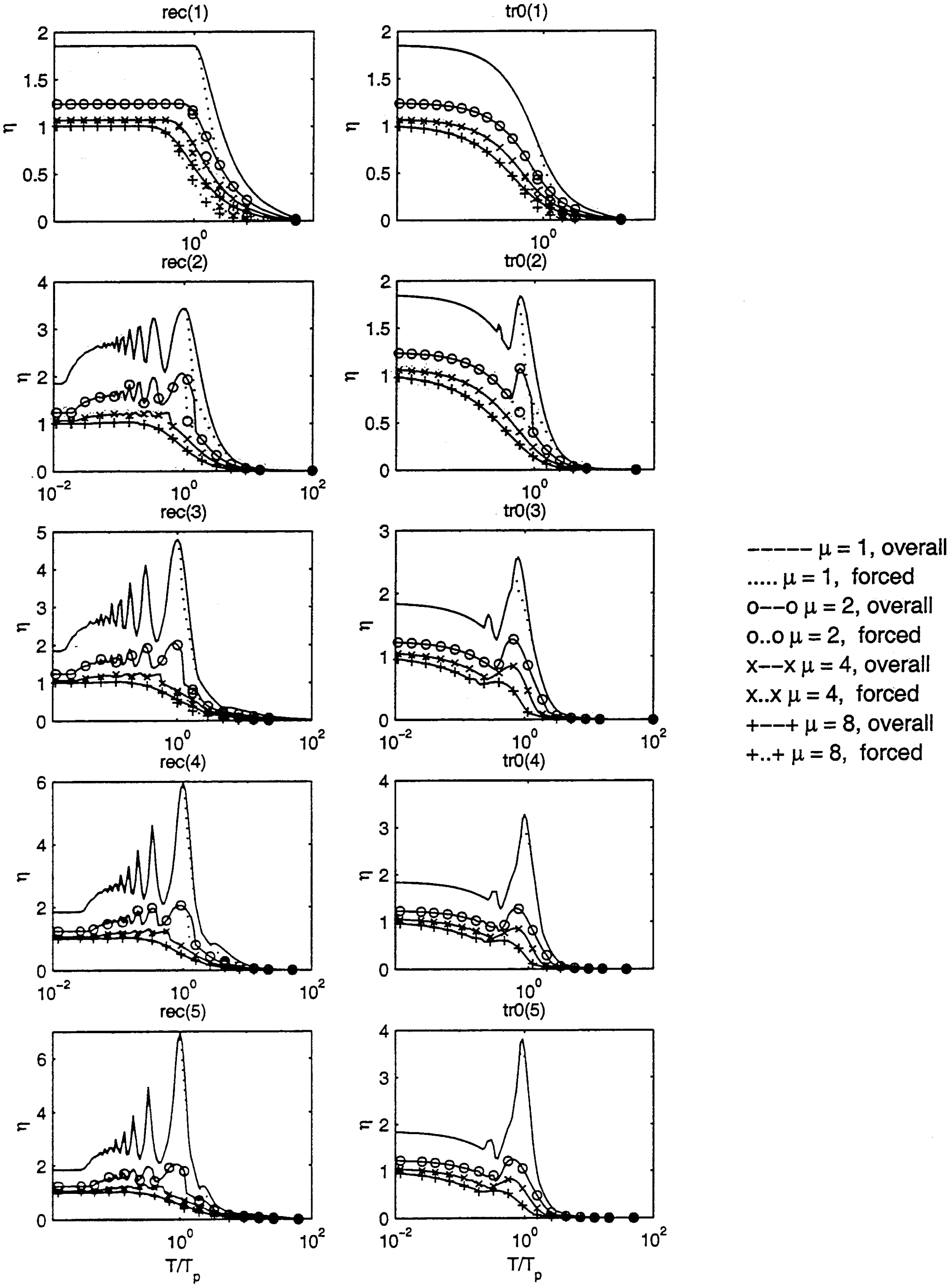

Figure 3.4: Strength parameter, η, vs. T/T_p of systems with μ = 1, 2, 4, and 8. Forced and overall responses to shock loading pulses

- The largest differences in magnitude between forced and overall strength spectra are found for $\mu = 1$, particularly for pulses with one incursion. The greater the ductility, the lesser is the difference.

- Peak spectral isoductile strengths occur at the same value of T/T_p in 94 out of 96 cases (24 pulses x 4 ductility values = 96 cases); the exceptions are trl(1) and tr0(3) for $\mu = 1$. The largest isoductile strengths for overall responses equaled those for forced responses in 81 of the 96 cases.

Strength spectra for each pulse family have distinct signatures that identify and differentiate each other. The largest differences in the strength spectra are found for $T/T_p < 1$. In this region the shape of the pulse is important and determines the behavior of the systems. Peak isoductile strengths are located in the region of $0 < T/T_p \leq 1$. Peak isoductile strengths for $\mu \geq 4$ occur for $T/T_p \approx 0$ for all pulses except the rec family and trl(2). The tr0(1) and tr0(2) pulses are the only pulses for which peak isoductile strengths occur for $T/T_p \approx 0$ for $\mu \geq 1$. As can be seen in Fig. 3.2b, as the number of incursions increases, the value of T/T_p at which the peak isoductile strengths occurs tends to unity for $\mu = 1$.

The number of incursions for a given family of pulses has a significant effect on the required elastic strength, especially in the region near $T/T_p = 1$. The larger the number of incursions, the higher is the strength necessary for elastic response (see Fig. 3.5a), due to the development of resonance. The elastic spectra increase as the number of incursions increases, and the spectra often have similar shapes, with peaks and troughs occurring at nearly the same periods. However, the number of incursions has little effect on the isoductile strengths for $\mu \geq 2$ (Fig. 3.5a). The peak spectral isoductile strengths shift to lower periods as the number of incursions of the pulse decreases and as the ductility increases.

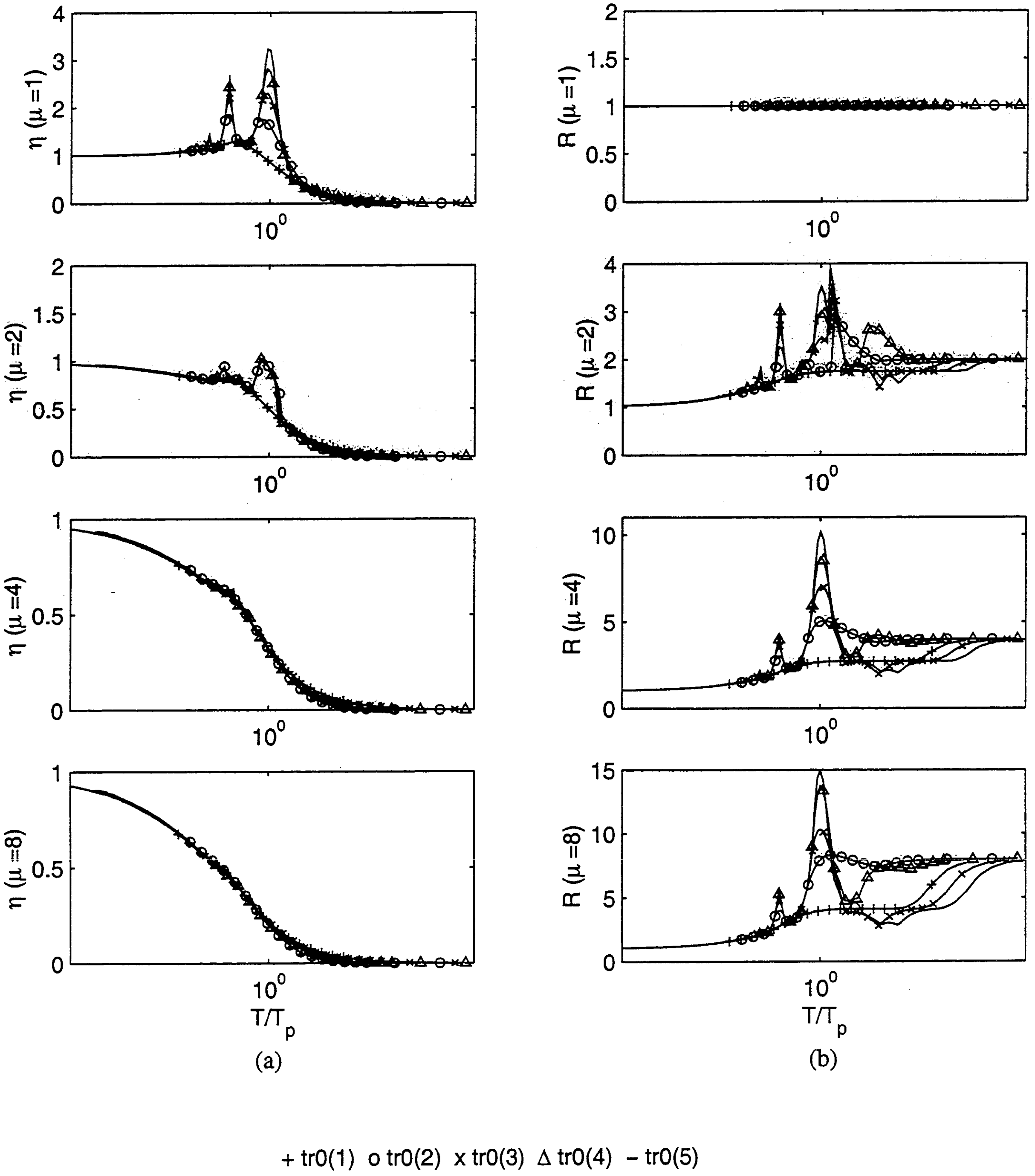

(a)

(b)

Figure 3.5: Overall response of systems with $\mu = 1$, 2, 4, and 8 subjected to quadratic pulses, (a) Strength parameter, η, vs. T/T_p; (b) R-factors vs. T/T_p

3.3.1.2 Short period systems

In Figs. 3.3 and 3.4 it can be seen that the pulse families sort into three groups with regard to the isoductile strengths of short period systems ($T/T_p < 0.5$):

1. *The gradual (qua, sin, trh) families and tr1(1) pulse*: isoductile strengths tend to unity as $T/T_p \rightarrow 0$, and small differences in strength cause large differences in ductility response (Fig. 3.3). As $T/T_p \rightarrow 0$, the yield strength approaches the product of the mass and the peak acceleration of the pulse, $m \cdot a_{g,max}$.

2. *The shock pulse families (rec and tr0)*: the strength parameter tends to unity for $\mu = 8$, and tends to an average of 1.848 for $\mu = 1$ as $T/T_p \rightarrow 0$ (Fig. 3.4). Closed-form solutions for undamped elastic systems subjected to shock loading show the strength parameter tends to 2 as $T/T_p \rightarrow 0$ [33, 7]. Figure 3.4 shows that the isoductile strengths are always higher for shock loading than for gradual loading as $T/T_p \rightarrow 0$.

3. *A hybrid pulse, tr1(2)*: this gradual loading pulse is discontinuous at $t_d/2$, resulting in a trend in between the two trends mentioned above.

3.3.1.3 Long period systems

The impulse-momentum principle is known to be applicable to long period systems ($T \gg T_p$). This principle holds that when the period of the system is large relative to the duration of the pulse, the system experiences the pulse as an impulse of magnitude, I_m, where I_m is equal to the integral of the pulse acceleration over its duration [6]. The overall isoductile strengths tend to zero as $t_d/T \rightarrow 0$ at a rate that depends on the ductility and on the integral of the pulse, independent of the pulse shape. Pulses with one incursion and amplitudes, $a_{g,max}$, set to 3/2, $\pi/4$, 1, 1, 1/2, and 1 for the qua(1), sin(1), trh(1), tr1(1), rec(1), and tr0(1) pulses, respectively, have area equal to $t_d/2$, where t_d is constant for all pulses. Accordingly, not only do the elastic responses have the same initial slopes (with respect to t_d/T) as $t_d/T \rightarrow 0$, but the strengths for each ductility value have equal slopes, with the slope decreasing as ductility increases. This is explained as follows. The work done in deforming an elasto-plastic system, E_s, is given by [31]:

$$E_s = \frac{V_y^2}{2m\omega^2}(2\mu - 1) \tag{3.2}$$

where ω is the circular frequency of the system ($\omega = 2\pi/T$). An elastic system responding to an impulse would have kinetic energy, E_k, given by $E_k = I_m^2/2m$. Equating E_s to E_k for an impulse having area, I_m, allows the required yield strength V_y, to be expressed as:

$$V_y = \frac{2\pi}{T}\frac{I_m}{\sqrt{2\mu - 1}} \tag{3.3}$$

Equation 3.3 applies for t_d/T up to about 0.25 for the 24 pulses considered. This limit is consistent with results reported in [6] for linear elastic systems, for which Equation 3.3 applies with $\mu = 1$. Since the systems in the present study are damped, the approximate strength (Eq. 3.3) is an upper bound. If pulses are balanced, the integral of the pulse acceleration is zero and the elastic and inelastic strengths have slopes equal to zero as $t_d/T \rightarrow 0$. If bilinear systems are considered, having post-yield stiffness equal to α times the initial stiffness, the work in defroming the system to a peak displacement $u_m = \mu\, u_y$, E_s, is given by:

$$E_s = \frac{V_y^2}{2m\omega^2}\left(2\mu - 1 + \alpha(\mu - 1)^2\right) \tag{3.4}$$

Equating E_s to E_k allows Equation 3.3 to be generalized to:

$$V_y = \frac{2\pi}{T}\frac{I_m}{\sqrt{2\mu - 1 + \alpha(\mu - 1)^2}} \tag{3.5}$$

3.3.2 Strength Reduction Factors

The strength reduction factor, R, also termed response modification factor, response ratio, and inelastic acceleration response ratio in the literature, is the ratio of the strength for $\mu = 1$ to the isoductile yield strength, V_y , as shown in Eq. 2.2 or, equivalently

$$R(\mu, T) = \frac{\eta(\mu = 1, T)}{\eta(\mu, T)} \tag{3.6}$$

Strength reduction factors are plotted in Figs. 3.6 and 3.7 for the gradual loading and shock loading pulses, respectively. R-factors obtained from the forced and overall isoductile strengths are plotted in each figure using different line types. Similar features can be observed in the spectra:

- The higher the ductility value is, the larger is the R-factor. The R-factor necessarily is equal to unity for $\mu = 1$, for all pulses. R-factors tend to asymptotic limits for short and long period systems.
- For each family of pulses, the larger the number of incursions, the larger the R-factor is in the region of $T \approx T_p$. R-factors are not sensitive to the number of incursions for $T/T_p < 0.5$, but are sensitive for longer periods. Thus, the $R(\mu, T)$ relation depends on the number of incursions when $T/T_p > 0.5$.
- R-factors for intermediate periods systems are very similar for pulses having the same number of incursions.
- Differences between R-factors for forced and overall responses are larger and extend over larger period ranges for unbalanced pulses (non-zero velocity at $t = t_d$). The largest differences are found in the intermediate period region, for $T/T_p > 0.5$.
- Peak spectral R-factors occur in the region $1 \leq T/T_p \leq 100$ for all the pulses except tr0(2). The ratio T/T_p at which R-factors are largest decreases as the number of incursions increases.

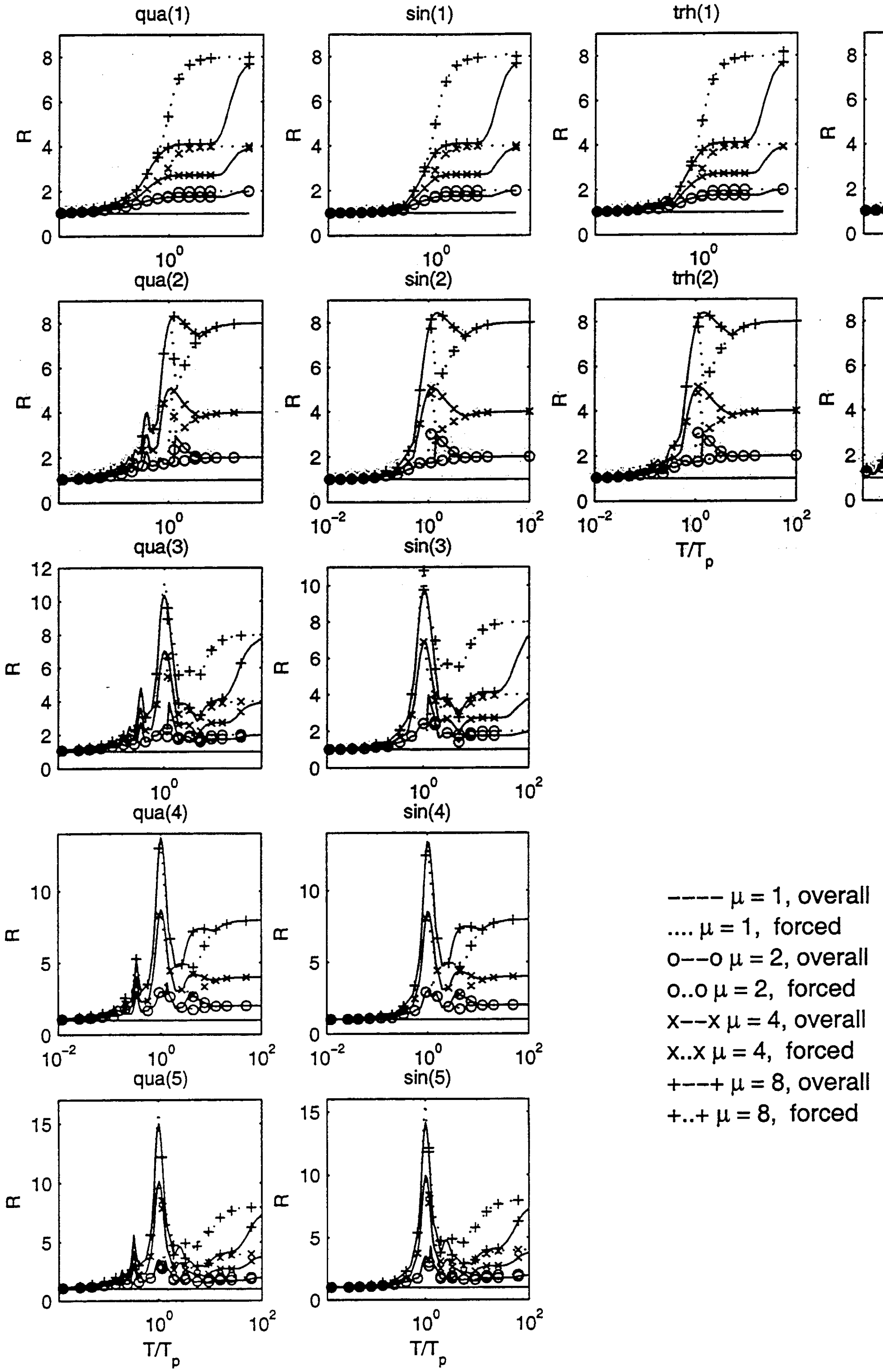

Figure 3.6: R-factor vs. T/T_p of systems with μ = 1, 2, 4, and 8. Forced and overall responses to gradual loading pulses

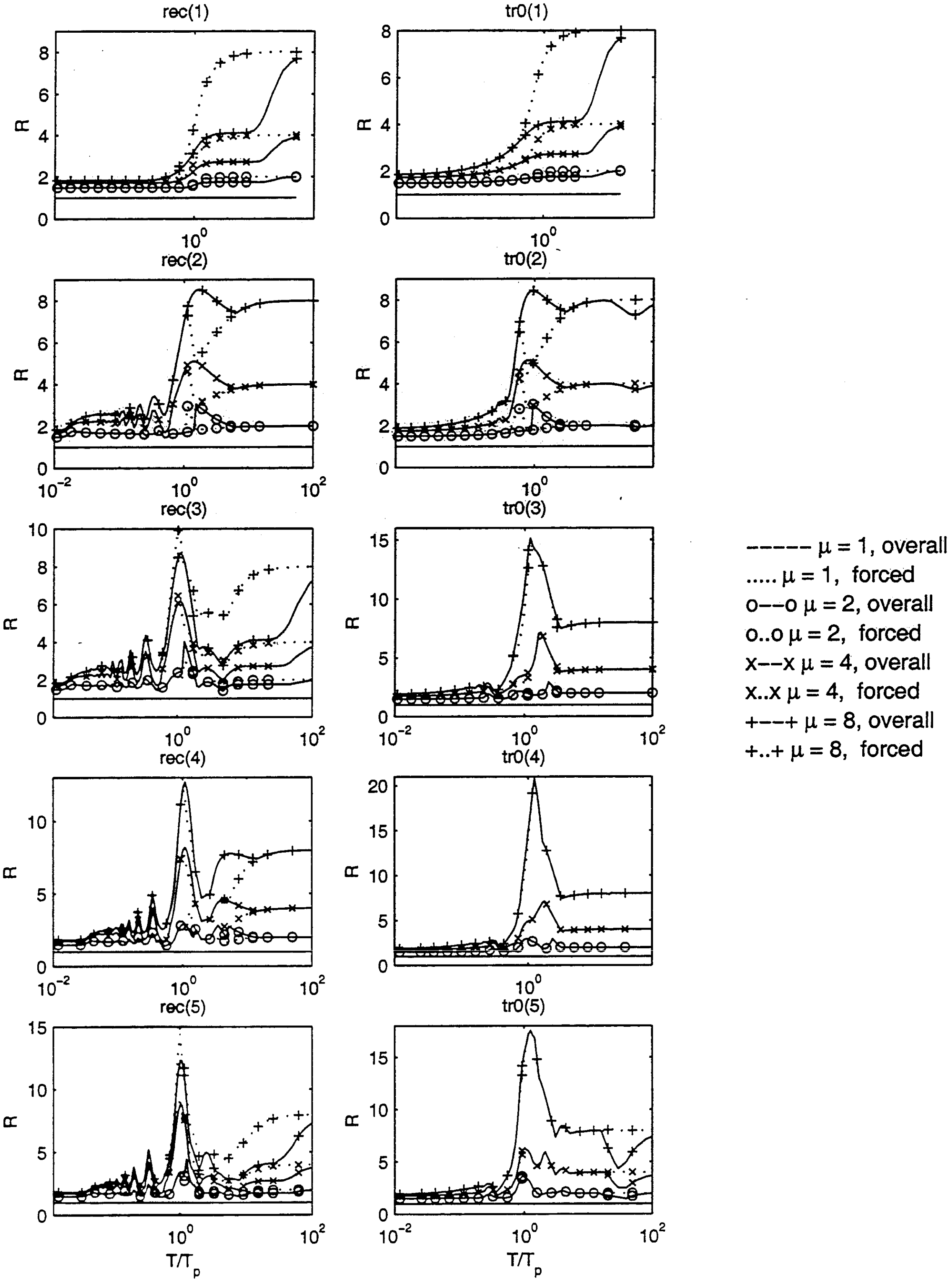

Figure 3.7: R-factor vs. T/T_p of systems with $\mu = 1$, 2, 4, and 8. Forced and overall responses to gradual loading pulses

- Peak spectral R-factors can exceed the ductility value for pulses with more than one incursion when $\mu \geq 2$.

- Peak spectral R-factors differed for forced and overall responses for $\mu \geq 2$ in 60 out of 72 cases (24 pulses and 3 ductilities).

3.4 Applicability of the Newmark and Hall Observations

Several physically-based idealizations have been used to gain insight into the R-factors obtained from ground motion records. These physical idealizations were developed in analytical studies of undamped systems subjected to a small number of pulses [20]. The pulses used in the original studies (the tr0 family and the trh(2) pulse) were included in the 24 pulses considered in the present study. The original observations for short, intermediate, and long period systems are described in Section 1.2.2. In this section the original Newmark and Hall observations are evaluated for the 24 pulses of this study for short, intermediate, and long period systems.

1. *Short period systems*: Figure 3.8a plots R vs. μ for short periods ($T/t_d = 0.01$) for forced vibration and overall responses to the 24 pulses. It can be observed that the R-factors for forced and overall response are the same for short period oscillators, because maximum response always occurs at $t < t_d$. The R-factors in Fig. 3.8a follow three trends. Oscillators subjected to shock pulses have R-factors that follow the equation of instantaneous acceleration change [20] (Eq. 1.5). For the gradual loading pulses (the qua, sin, and trh families and trl(1) pulse), the R-factor is nearly independent of ductility, since $R \approx 1$. As the ductility increases, the R-factors diverge slowly from unity, for small T/t_d. Finally, the pulse trl(2) follows a path that is intermediate between the two trends described above. This suggests that R-factors for short period systems have upper and lower bounds that appear to be given by Eqs. 1.5 and 1.6, respectively.

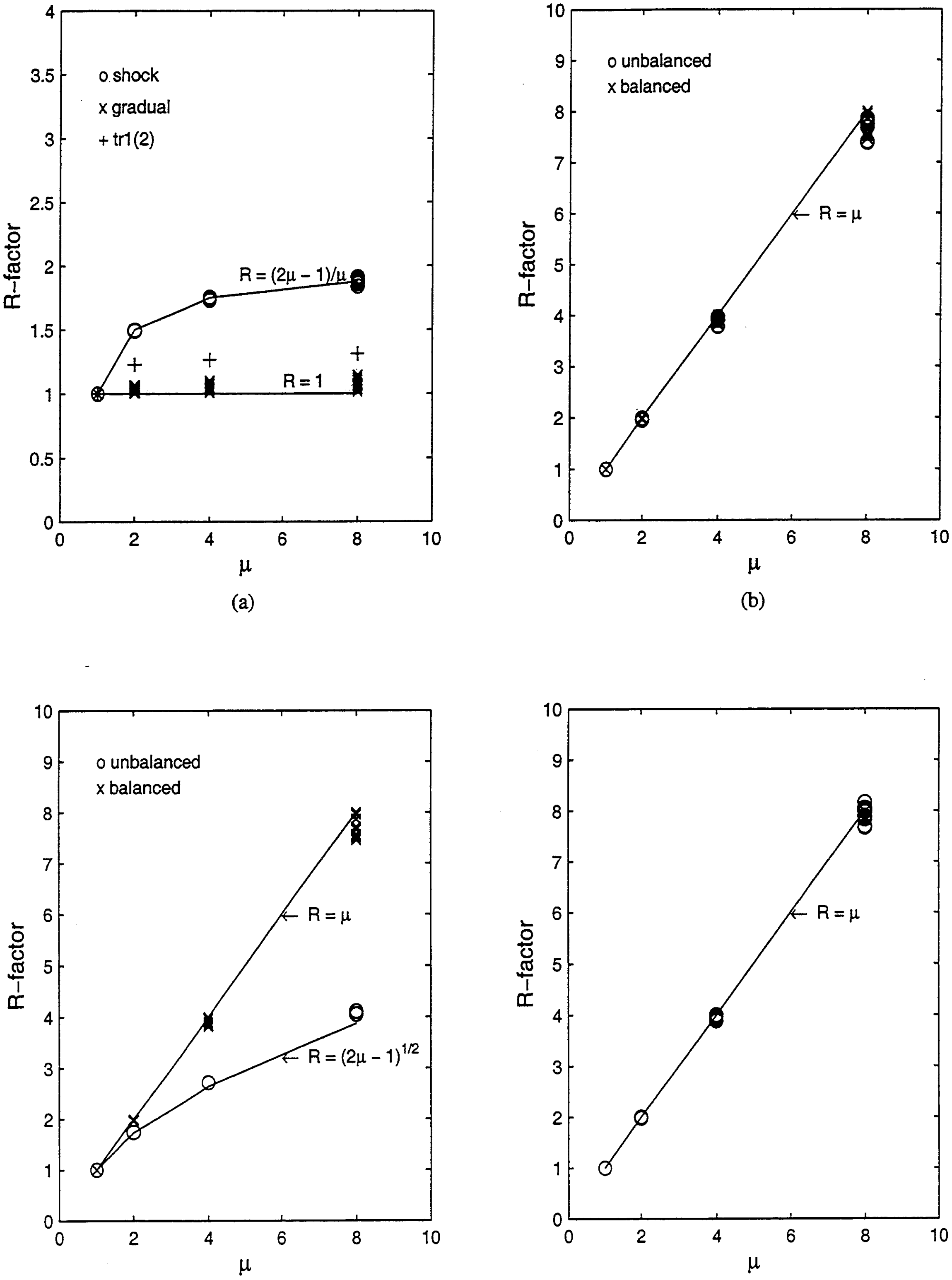

(a) (b)

(c) (d)

Figure 3.8: R-factor vs. ductility μ: (a) Forced and overall responses of systems having $T/t_d = 0.01$, (b) Forced response of systems having $T/t_d = 8$, (c) Overall response of systems having $T/t_d = 8$, and (d) Forced and overall responses of systems having $T/t_d = 100$

2. *Intermediate period systems*: The equal energy rule was said to be valid for intermediate period systems subjected to pulses having a single incursion and for systems whose elastic pseudo-velocity in response to pulses having two incursions and the tr0(3) pulse is from about 0.8-1 times the maximum ground velocity [20].

   In the intermediate period range no distinct trends are apparent except for a very narrow period range where differences in the response of balanced and unbalanced pulses determine the strengths of the systems. Figure 3.8b plots R vs. μ for the forced vibration response of systems for $T/t_d = 8$. It can be observed that the R-factor is independent of the pulse shape; the R-factors for all pulses follow the trend given by Eq. 1.8 (equal displacement rule). Figure 3.8c plots R vs. μ for the overall response of systems for $T/t_d = 8$. In this case, the data plot along two curves: balanced pulses follow the equal displacement rule (Eq. 1.8), while unbalanced pulses follow the equal energy rule (Eq. 1.7). These trends depend little on the pulse shape. Unbalanced pulses are received as an instantaneous velocity change when the overall response is considered. The R-factors deviate slightly from Eq. 1.7 because the systems studied here are damped.

   The range of applicability of Eq. 1.7 to the overall response to unbalanced pulses depends on the shape of the pulse, the number of incursions, and the ductility of the system. The larger the number of incursions and the larger the ductility, the narrower is the period range over which Eq. 1.7 applies. The range of applicability becomes more restricted as ductility increases. For example, the region of applicability of equal energy rule for the unbalanced pulse qua(1) is $T/t_d \,\epsilon\, [1.2 - 30]$ if $\mu = 2$, while $T/t_d \,\epsilon\, [1.6 - 20]$ if $\mu = 8$. For qua(5), $T/t_d \,\epsilon\, [4 - 20]$ for $\mu = 2$, and $T/t_d \,\epsilon\, [5 - 10]$ for $\mu = 8$. The R-factors for the balanced pulses do not exhibit any period region where the equal energy rule applies.

3. *Long period systems*: Figure 3.8d plots R vs. μ for long period systems ($T/t_d = 100^1$), for all pulses. The data follow a straight line corresponding to $R = \mu$. The maximum deformation is independent of the system behavior (elastic or elasto-plastic), type of loading (gradual or

shock), and type of response (forced vs. overall). Thus, the equal displacement rule (Eq. 1.8) is applicable to all 24 pulses for long period systems.

3.5 Summary

Based on the study of a large number of elasto-plastic SDOF oscillator responses to 24 simple pulses, the following conclusions result:

1. Isoductile strengths of short period systems are higher for shock loading than gradual loading pulses. Strengths are sensitive to the shape of the pulse for $T \leq T_p$.
2. The impulse-momentum principle is applicable to the elastic and inelastic response of long period systems, which experience the pulse as an impulse, independent of pulse shape.
3. The characteristic period, T_p, is an important time parameter that defines the regions of the spectra where maximum strengths or R-factors are present, with peak strengths located in $0 \leq T/T_p \leq 1$ and peak R-factors located in $1 \leq T/T_p \leq 100$.
4. Within any one family of pulses, R-factors depend on the number of incursions, since this number affects the elastic response substantially but has little effect on inelastic isoductile strengths.
5. Previous studies that focused on a subset of the pulses considered herein led to the preservation of the force, equal energy, and equal displacement rules that are widely accepted in earthquake engineering. The applicability and limitations of these rules for the set of 24 pulses are as follows:
    - The equal displacement rule applies to systems with high T/T_p ratios. The rule is valid for all pulses considered and for the forced and overall responses, consistent with prior findings.

---

[1] Except pulse tr0(2), which required $T/t_d = 300$ to converge to $R = \mu$.

- The equal energy rule applies only to the overall response of intermediate period systems subjected to only unbalanced pulses over a relatively narrow period range. The equal displacement rule is applicable to intermediate period systems subjected to balanced pulses (overall response) and to both balanced and unbalanced forced vibration responses. These observations are counter to conventional views, which hold that the equal energy rule is generally applicable to intermediate period systems.

- Short period systems subjected to shock pulses can be considered to be subject to an instantaneous acceleration change, consistent with prior findings.

- The strength required for short period systems subjected to gradual loading pulses is approximately $m \cdot a_{g,max}$ regardless of the ductility level, for the elasto-plastic cases considered. This is consistent with prior findings that force is preserved in short period systems, and relates to the observation that R-factors tend to unity as period tends to zero. Systems with positive post-yield stiffness are discussed in Chapter 5.

Chapter 4

Estimating Isoductile SDOF Response Spectra Using Pulse R-factors

4.1 Introduction

In this chapter a new approach is described for estimating inelastic response spectra for elasto-plastic SDOF systems subjected to strong ground motions. In this approach, inelastic spectra are estimated by applying strength reduction factors determined for a simple pulse to the elastic response spectrum of the ground motion. This approach relies upon similarities in the strength reduction factors computed for earthquake ground motions and for short duration pulses, indicating that strength reduction factors exhibit a degree of waveform independence. Based on the ground motions studied, these findings appear to be equally applicable to short and long duration ground motions and those having near-fault forward directivity effects.

Researchers have long been aware of similarities in the response of single-degree-of-freedom (SDOF) systems to ground motions and to pulse-type excitations (e.g. [20, 31, 30, 32]). Investigators recently have used pulses to represent near fault ground motions [38, 40, 37, 39, 35, 36]. Other investigators have studied large numbers of ground motions to determine mean or approximate strength reduction factors to obtain inelastic strengths associated with constant ductility demands (e.g. [27, 23, 24, 11, 26, 50]).

Observation of computed response indicates that only a few cycles of ground motion cause yielding in many of the systems of practical interest (Chapter 2 and [41]). These cycles describe a pulse of irregular form over a short interval of the ground motion and of sufficient intensity to cause yielding in a given structure [34, 20, 31, 42]. The equal displacement, equal energy, and equal acceleration rules were established first for pulses and were then applied to ground motions based on similarities between pulses and ground motions [20, 31, 30, 32, 44, 43, 51, 52]. While Chapter 3 identifies some exceptions to these rules, it should not be surprising that the R-factors determined for pulses resemble those determined for ground motions.

Sewell [45] found that the damaging characteristics of numerous ground motions can be separated into two distinct components: (1) an elastic contribution, given by the elastic pseudo-acceleration spectrum, and (2) a strength reduction factor, R, applied to the elastic spectrum to determine the strengths of nonlinear oscillators that result in constant ductility responses, referred to as "isoductile strengths." A systematic dependence of R-factors on earthquake magnitude and distance could not be identified, nor could Sewell identify a systematic dependence of R-factors on record duration.

Recognizing that a few cycles of the ground motion dominate the nonlinear response of many systems of interest, the approach developed in this chapter estimates inelastic spectra by applying the strength reduction factors determined for a simple pulse to the elastic response spectrum determined for the ground motion.

To illustrate this for a single case, Fig. 4.1 compares the response spectra of elasto-plastic systems having ductility demands of 2, 4, and 8 for the NS Newhall record of the 1994 Northridge earthquake (Table 2.1). The spectra plot the strength parameter, η, defined by Eq. 2.1. The strengths required for constant ductility responses to the record, η_r, are compared with the isoductile strengths η_p for a pulse called qua(2) (see Fig. 4.2). The strengths η_r are also compared with the strengths given by the elastic response spectrum for this record, η_e, divided by the strength reduction factors, R_p, for

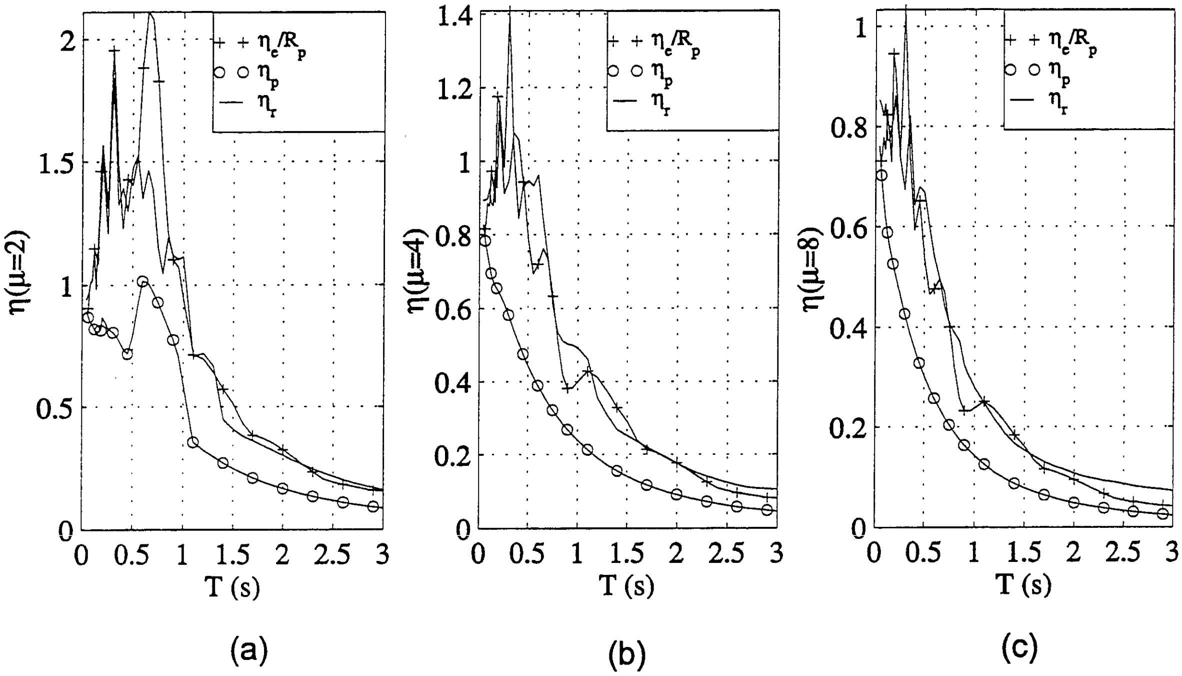

Figure 4.1: Comparison for NR94NWHL.360 record among the strength response spectra to the record, η_r, the overall response to the pulse qua(2), η_p, and the ratio of the elastic response spectrum to the record to the R-factor of the same pulse, $\eta_e/R_p(T_p = 0.75\,s)$. (a) Systems having $\mu = 2$, (b) Systems having $\mu = 4$, and (c) Systems having $\mu = 8$

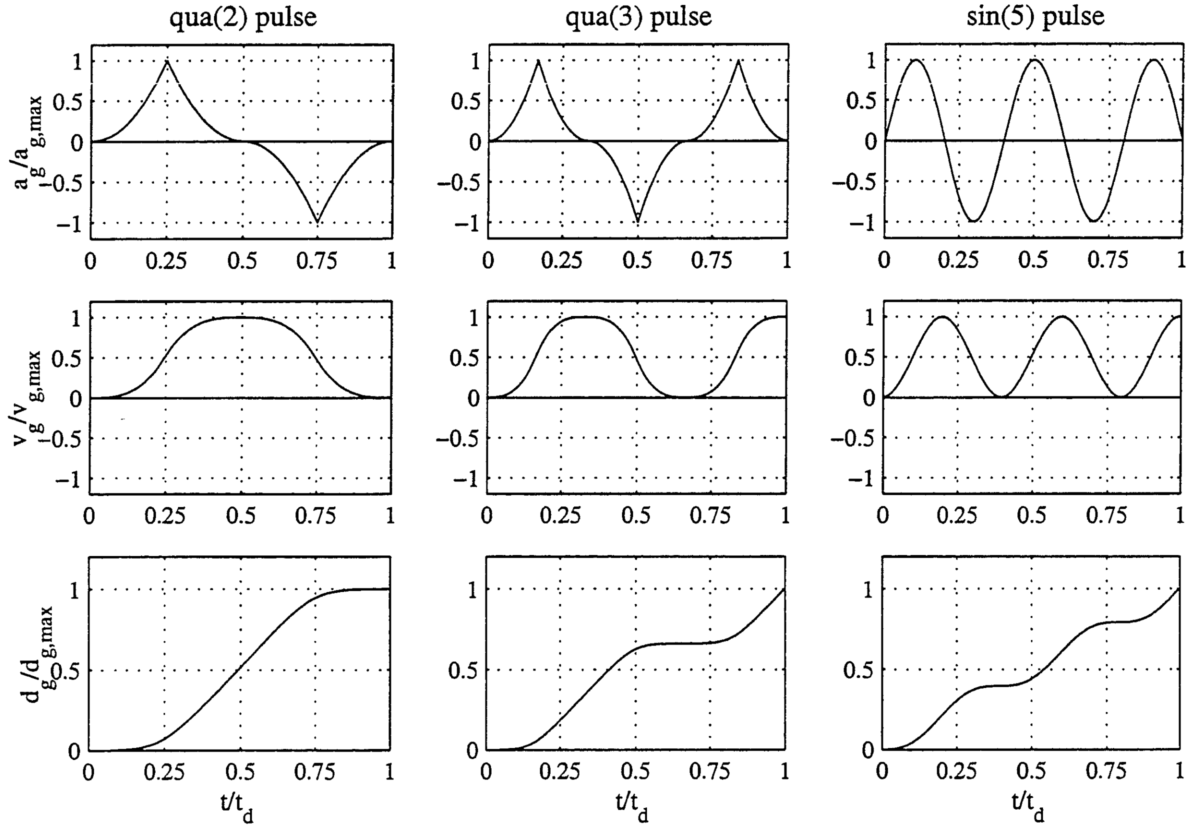

Figure 4.2: Normalized acceleration, velocity, and displacement time histories of the qua(2), qua(3), and sin(5) pulses

this pulse, with the duration of the pulse selected to be 0.75 s. Although η_p and η_r are dissimilar, Fig. 4.1 shows that the ratio η_e/R_p provides a very good estimate of η_r for each ductility value. This example shows that a simple pulse cannot represent the complex information contained within the ground motion that produces the elastic response spectrum, but the pulse contains sufficient information to characterize the strength reduction factor.

This chapter explores the possibility of using R-factors obtained from pulses to estimate the inelastic response spectra of 15 recorded strong ground motions. The set of 24 pulses considered in Chapter 3 were used together with the 15 recorded ground motions of Chapter 2, selected to represent short and long durations of shaking and the presence or absence of near-fault forward directivity conditions. Simplifications developed in this chapter lead to a single quadratic pulse recommended for all records except the soft soil 1985 Mexico City SCT record, for which a sinusoidal pulse is recommended.

4.2 Methodology

This section describes the SDOF systems, ground motions, and pulses considered in the study. Definitions of the strength parameters are provided along with the three error measures used to identify optimal pulse shapes for estimating the inelastic response spectra.

4.2.1 Systems

Elasto-plastic SDOF systems were considered, having 5% of critical damping and strengths required to achieve ductility responses μ = 1, 2, 4, and 8. The isoductile strengths for each ground motion were determined at 45 periods, T, between 0.04 and 3 s. The periods were spaced at 0.02, 0.05, and 0.1 s in the period intervals [0.04 - 0.2], [0.25 - 1], and [1 - 3] s, respectively.

As described in Chapter 3 and in Cuesta and Aschheim [43], strength response spectra were calculated for the pulses at 107 periods. The first 100 periods were distributed geometrically to provide greater resolution in the short period range, using Eq. 3.1 with $\kappa_1 = 0.01$ and $\kappa_N = \kappa_{100} = 15$. These are supplemented by 7 additional periods corresponding to $\kappa = 20, 25, 30, 40, 60, 80$, and 100. Accordingly, the duration of the pulse is constrained to $t_d \epsilon [0.01T, 100T]$, where T is the initial natural period of vibration of the system.

4.2.2 Ground Motions

The fifteen recorded ground motions in Chapter 2 and shown in Table 2.1 are selected for this study. The characteristic period T_g was chosen to coincide approximately with the first (lowest period) peak of the equivalent velocity spectrum and the period at which the transition occurs between the constant acceleration and constant velocity portions of a smoothed design spectrum fitted to the elastic spectrum [53, 54, 55]. This period approximately corresponds to the period T_s used to define smoothed elastic design spectra in the NEHRP Guidelines [2].

4.2.3 Pulse Waveforms

The 24 acceleration pulses used here are the same ones described in Chapter 3 and in Cuesta and Aschheim [43]. The pulses, shown in Table 4.1, are classified according to four criteria mentioned in Section 3.2.1. An index number is added to each cell to identify the pulses in future plots.

Section 3.2.3 showed that the response data were best organized with respect to a parameter termed the characteristic period of the pulse, T_p. For the families sin, qua, rec, trh, and trl, the duration of the pulse, t_d, having a complete cycle (2 incursions) defines the characteristic period ($T_p = t_d$). The characteristic period is the same for all pulses of the same family. For example, T_p equals the duration of the pulse qua(2). The pulse sin(5) has 2.5 cycles, and $T_p = 2t_d/5$ for this pulse.

Three of the 24 pulses studied are of particular significance in the present chapter. Two of these are the qua(2) and qua(3) pulses, characterized by quadratic rising and descending segments. The

Table 4.1: Index number of the acceleration pulses +

		WAVEFORM FAMILY					
		qua	sin	trh	tr1	rec	tr0
		GRADUAL LOADING				SHOCK LOADING	
NUMBER OF INCURSIONS	1	* 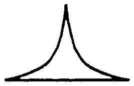 1	* 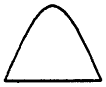 2	* 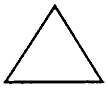 3	* 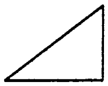 4	* 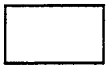 5	* 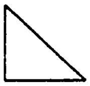 6
	2	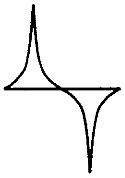 7	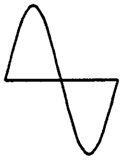 8	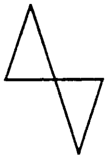 9	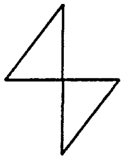 10	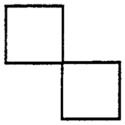 11	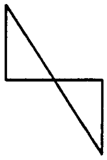 12
	3	* 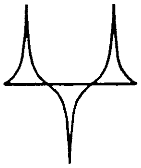 13	* 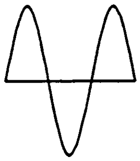 14	—	—	* 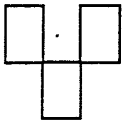 15	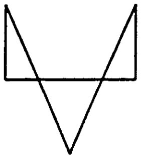 16
	4	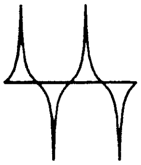 17	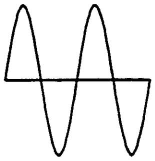 18	—	—	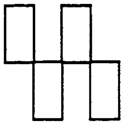 19	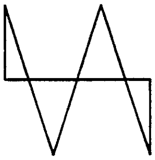 20
	5	* 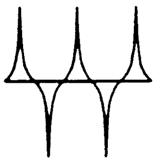 21	* 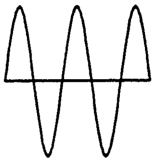 22	—	—	* 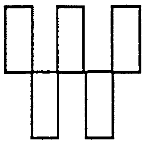 23	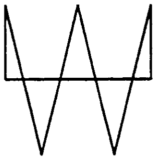 24

+ The number in the lower left-hand corner of each cell indicates the "pulse index number." An asterisk (*) indicates those pulses having nonzero final velocity.

initial rising segment, in normalized form is given by

$$\frac{a_g}{a_{g,max}} = \left(\frac{At}{t_d}\right)^2 \tag{4.1}$$

for $0 \leq \frac{t}{t_d} \leq \frac{1}{A}$, where $a_{g,max}$ is the peak acceleration of the pulse, and $A = 4$ or 6 for each pulse, respectively. The third pulse is the sin(5) pulse, with

$$\frac{a_g}{a_{g,max}} = sin\left(5\pi\frac{t}{t_d}\right) \tag{4.2}$$

for $0 \leq \frac{t}{t_d} \leq 1$. The acceleration, velocity, and displacement of these pulses are plotted versus a dimensionless time parameter, t/t_d, in Fig. 4.2. Further details are provided in Appendix A.

4.2.4 Isoductile Strength Spectra

The strengths required for each oscillator to achieve the specified ductilities were determined iteratively using the computer program PCNSPEC [48], a modified version of NONSPEC [47], as discussed in Section 2.2.2.1. The isoductile strengths of the oscillators subjected to the pulses were computed for two cases. As in Chapter 3, in the case of "forced" response, the duration of the response over which the ductility demands developed was limited to $0 < t/t_d \leq 1$. In the case of "overall" response, the maximum ductility demands may occur at any time, $0 < t/t_d \leq \infty$. Figures 4.3 and 4.4 present the strength response spectra and R-factors for the overall response to the qua(2) pulse, and the forced responses to the qua(3) and sin(5) pulses.

The isoductile strengths were normalized to obtain the dimensionless strength parameter, η_y, defined in Eq. 2.1. The estimated dimensionless isoductile strengths $\hat{\eta}_y$, are determined using the pulse R-factor as:

$$\hat{\eta}_y(\mu, T) = \frac{\eta_y(\mu = 1, T)}{R_p(\mu, T/T_p)} \tag{4.3}$$

where $\eta_y(\mu = 1, T)$ is the strength for elastic response to the ground motion, and R_p is the R-factor

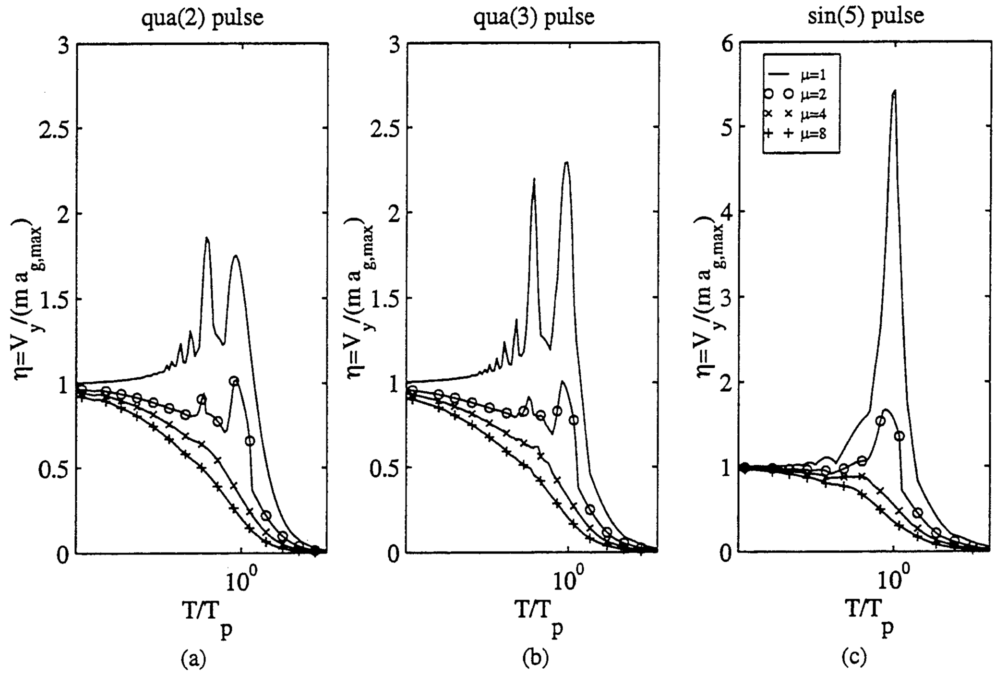

Figure 4.3: Isoductile strength response spectra for (a) overall response to qua(2), (b) forced response to qua(3), and (c) forced response to sin(5)

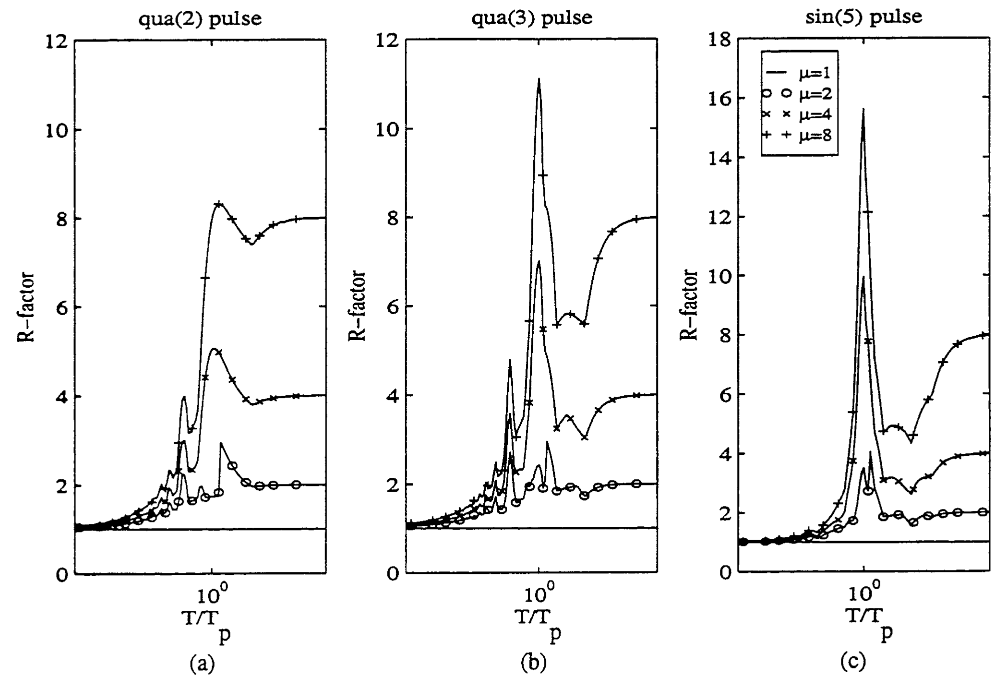

Figure 4.4: R-factor response spectra for (a) overall response to qua(2), (b) forced response to qua(3), and (c) forced response to sin(5)

computed for the pulse. For each period T_p, linear interpolation was used to determine the pulse R-factor at the periods (0.04 to 3 s) used to compute $\eta_y(\mu = 1, T)$.

4.2.5 Error Measures

To determine optimal pulses, comparisons between η_y (Eq. 2.1) and $\hat{\eta}_y$ (Eq. 4.3) were performed for each ground motion and for each pulse over a wide range of T_p. Three measures of the error in the estimated dimensionless strength parameters were developed, so that any conclusions made with respect to the pulses that minimize error are robust with regard to the error metric. These measures are particularly sensitive to the differences between η_y and $\hat{\eta}_y$ in the short period range, where strengths are largest. For a given ground motion, gm, ductility demand, d, pulse, i, and pulse duration, j, the three error functions for the estimated isoductile strength spectra are:

$$E^a_{gm,d}(i,j) = \frac{1}{n_p} \sum_{m=1}^{np} |\eta_{y,gm,d} - \hat{\eta}_{y,d}(i,j)| \tag{4.4}$$

$$E^b_{gm,d}(i,j) = \left(\frac{1}{n_p} \sum_{m=1}^{np} [\eta_{y,gm,d} - \hat{\eta}_{y,d}(i,j)]^2 \right)^{1/2} \tag{4.5}$$

$$E^c_{gm,d}(i,j) = \left(\frac{1}{n_p} \sum_{m=1}^{np} exp\left(|\eta_{y,gm,d} - \hat{\eta}_{y,d}(i,j)|\right) \right) - 1 \tag{4.6}$$

where:

- n_p = number of periods ($n_p = 45$, from 0.04 to 3 s)
- gm = ground motion index number (1 to 15)
- d = ductility index number (1 to 3, corresponding to μ = 2, 4, and 8, respectively)
- i = pulse index number (1 to 24 for forced response, and 25 to 48 for overall response)

- j = pulse characteristic period index number (1 to 41 in constant increments of 0.05 s in [0.2 - 2.2] s).

Note that other investigators have focused on accurately representing the R-factors. Had the measure of the error been expressed in terms of the R-factors, the error measure would be particularly sensitive to differences in the estimated and actual R-factors in the long period range, where the R-factors are largest. Equations 4.4 to 4.6 focus on minimizing errors in the strength estimate. This naturally emphasizes the need to provide adequate strength to structures responding nonlinearly, particularly for the short period structures where the required strengths are largest.

The minimum error for each ground motion, pulse, and ductility value is given by $E^s_{gm,d}(i,\hat{j})$, where $s = a$, b, c refers to the error measures given by Eqs. 4.4, 4.5, and 4.6, respectively; and $\hat{j}$ indicates the period T_p that minimizes this error. The error, $E^s_{gm,*}(i,\hat{j})$, is the minimum error for each record and pulse, where the asterisk ($*$) indicates an average over the ductility variable. Figure 4.5 shows E^a, E^b, and E^c versus T_p, for the case of the CH85LLEO.010 record ($gm = 6$), using the forced response of the qua(3) pulse ($i = 13$). It can be observed that the curves for $\mu =$ 8 have minimum values, $E^s_{6,3}(13,\hat{j})$, for $\hat{j} = 8$, which corresponds to $T_p = 0.55$ s.

Figures 4.6a and 4.6b plot $E^a_{4,*}(i,\hat{j})$ and $E^a_{11,*}(i,\hat{j})$ versus the pulse index number (Table 4.1), for the LP89CORR.090 ($gm = 4$) and the LN92LUCN.250 ($gm = 11$) records. Figure 4.6a shows that the error measure is smallest for pulses $i = 13$, 17 and 21, which are the qua(3), qua(4), and qua(5) pulses, respectively, for the first record, while pulses with one incursion ($i = 1$ to 6) produce the smallest error measure for the second record. The best pulse for each ground motion is given by $E^s_{gm,*}(\hat{i},\hat{j})$, with $\hat{i}$ identifying the pulse that minimizes the error measure over all ductility values, when the best values of T_p are selected, for the specified ground motion. Hence, using E^a, the optimal pulses are $\hat{i} = 21$ (forced response for the qua(5) pulse) for the LP89CORR.090 record and $\hat{i} = 30$ (overall response for the tr0(1) pulse) for the LN92LUCN.250 record when all ductilities are considered and T_p is the remained fixed for each ductility value.

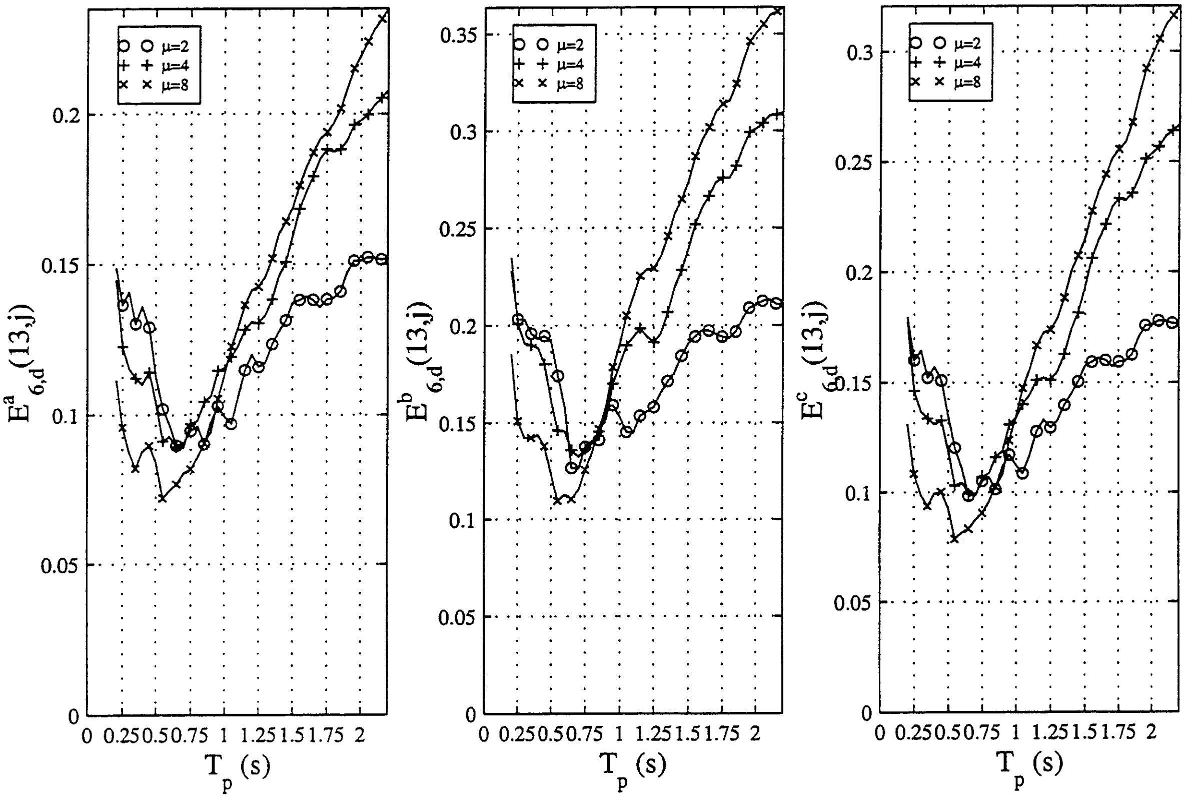

Figure 4.5: Errors $E^s_{6,d}(13,j)$ vs. the characteristic period of the pulse, T_p, in the estimate of the response to CH85LLEO.010 record with the R-factor of the forced response to the qua(3) pulse

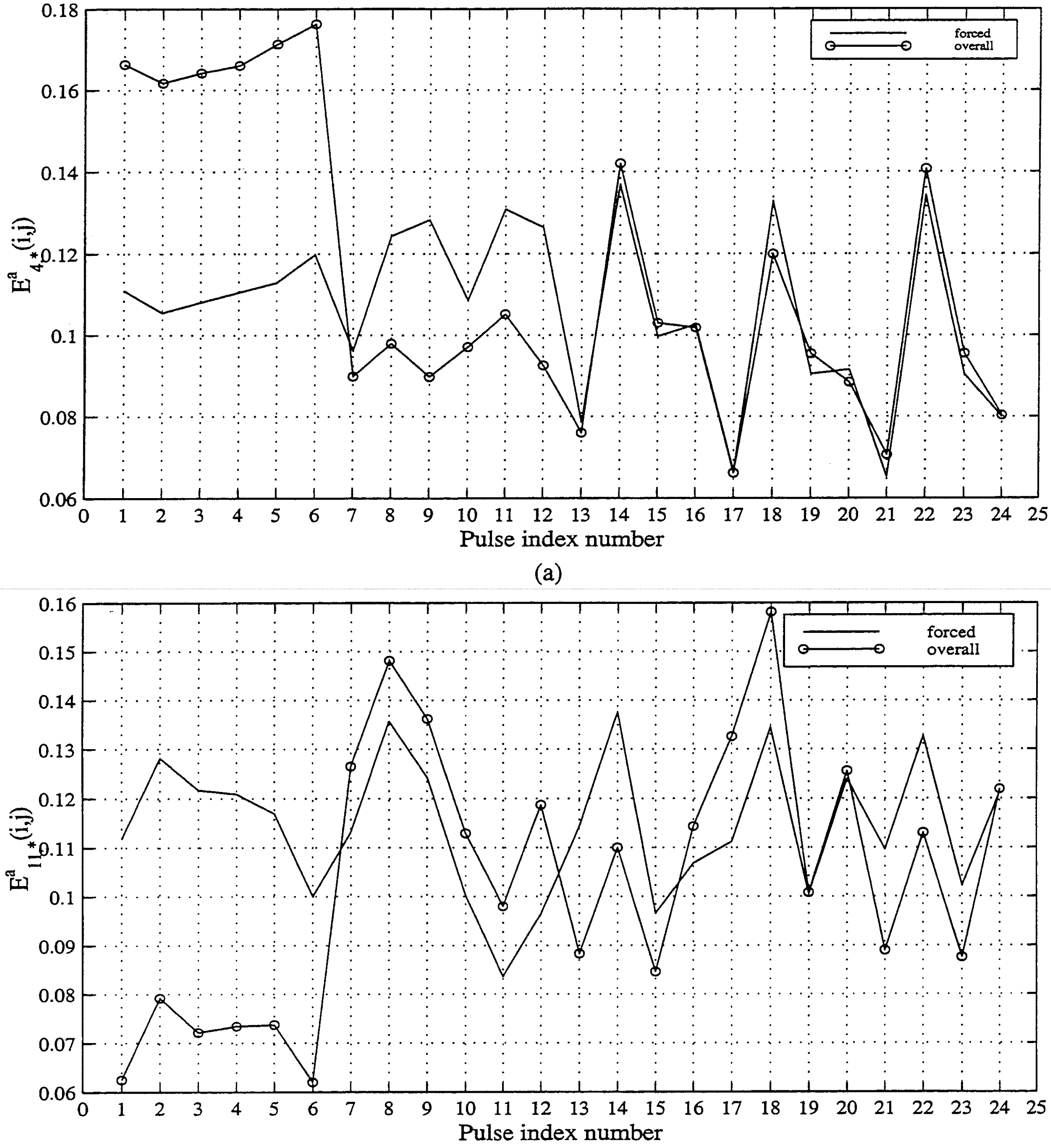

(a)

(b)

Figure 4.6: Minimum error, $E^a_{gm,*}(i,\hat{j})$, for: (a) the estimate of LP89CORR.090 (gm = 4), and (b) for the estimate of LN92LUCN.250 (gm = 11) records using 24 pulses in forced and overall response. Numbers 1, 7, 13, 17, and 21 correspond to the quadratic family of pulses

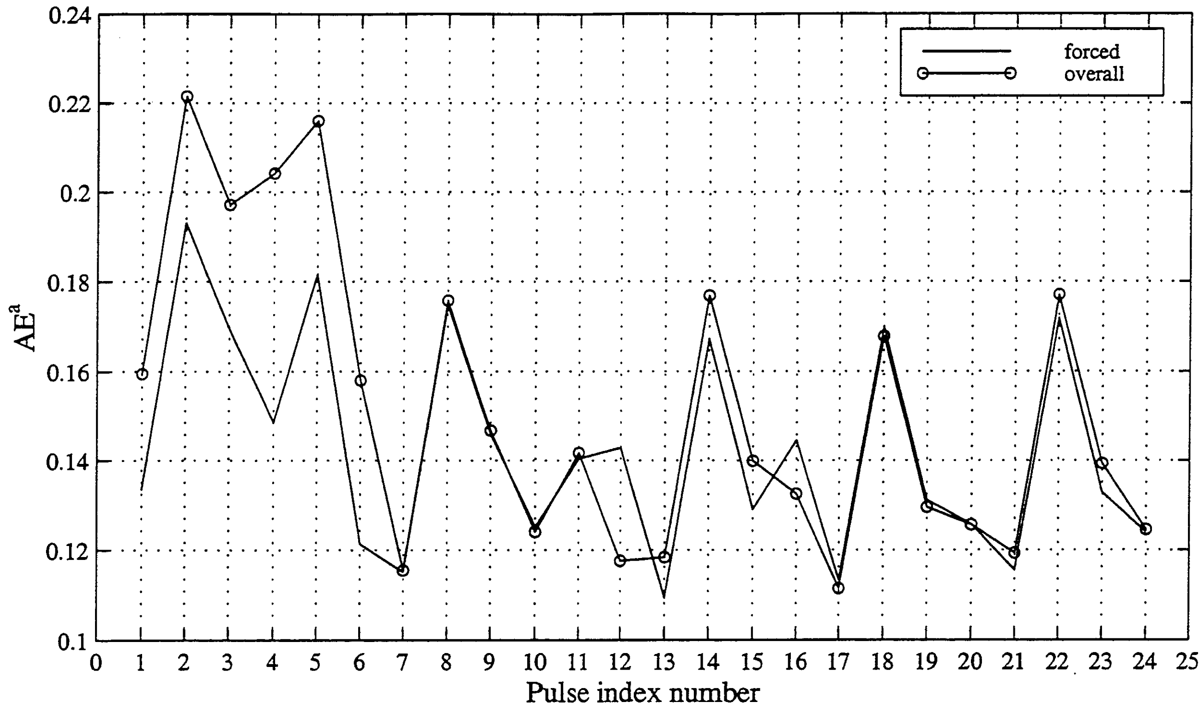

Figure 4.7: Average error, $AE^a = E^a_{*,*}(i,j)$, for the estimate of all the records using 24 pulses in forced and overall response with $T_p = T_g$. Numbers 1, 7, 13, 17, and 21 correspond to the quadratic family of pulses

The error $E^s_o = E^s_{gm,*}(\hat{i},\hat{j})$ is taken as a reference to gauge the error obtained when simplifications are introduced to identify a smaller set of pulses in place of the ones that minimize $E^s_{gm,*}(\hat{i},\hat{j})$. For a given ground motion, gm, pulse, i, and error measure, the normalized error given by the ratio $NE^s_{gm,*}(i,j) = E^s_{gm,*}(i,j)/E^s_o$ indicates how good the estimate is compared with the optimal pulse for the individual ground motion. Finally, the overall error is gauged over all the ground motions, $OE^s = NE^s_{*,*}(i,j)$; where the asterisk $(*)$ means an average of the $NE^s_{gm,*}(i,j)$ values over the ground motion variable. If the errors are not normalized by E^s_o, the average errors are given by $AE^s = E^s_{*,*}(i,j)$, where $E^s_{*,*}(i,j)$ is the average of $E^s_{gm,*}(i,j)$ over the ground motion variable. Figure 4.7 shows the average error, AE^a, for each pulse using $T_p = T_g$. With this constraint, the quadratic family of pulses gives the lowest AE^a values. Section 4.3 applies a consistent procedure to establish the pulses and characteristic periods that minimize the error measures.

4.3 Results

4.3.1 The Best Pulses

There is a pulse and associated period, T_p, that minimizes the error in the estimated inelastic strength spectra for each ground motion and a given ductility. The pulse T_p that minimizes E^s may differ for different ductilities and error functions. For example, E^a is minimized for μ = 2, 4, and 8 for the WN87MWLN.090 record using tr0(2), trl(2), and qua(4) pulses, respectively, at $T_p = 0.2$ s. The same pulse and T_p may happen to minimize the error measure for all ductilities, as with the BB92CIVC.360 record, for which the best pulse is sin(2) at $T_p = 0.2$ s. There are also ground motions where the best pulse and associated T_p differ for different ductilities. For example, the best pulses for the IV40ELCN.180 record are qua(4) at $T_p = 0.7$, qua(2) at $T_p = 0.4$, and trl(1) at $T_p = 0.3$ s for μ = 2, 4, and 8, respectively, using $E^s = E^a$.

If T_p is fixed for all ductilities, for a given record there is a single pulse and period $T_p = \hat{T}_o$, among all possible combinations of i and T_p, that minimizes the error $E^s_o = E^s_{gm,*}(\hat{\imath}, \hat{\jmath})$. Table 4.2 shows for each ground motion the optimal pulses, the error E^a_o, and the periods $T_p = \hat{T}_o$ where the minimum errors E^a_o, E^b_o, and E^c_o occur. It can be observed that each record has its own best pulses and particular $\hat{T}_o$ values. The set of optimal pulses for the 15 ground motions consists of 12 of the 24 pulses considered. It is interesting to notice that the optimal pulses can be classified into 2 groups. Where balanced pulses are optimal, it is for the overall response to the balanced pulses. Where unbalanced pulses are optimal, it is for the forced response to the unbalanced pulses. Only for the LN92LUCN.250 record did the best estimates occur for the overall response to an unbalanced pulse, in this case the tr0(1) and qua(1) pulses. Figure 4.6b plots the errors $E^a_o = E^a_{11,*}(i, \hat{\jmath})$ for this record, and it can be observed that the errors are smallest for the overall response to all the unbalanced pulses having one incursion (i = 1 to 6). Based on Chapter 3 and on Cuesta and Aschheim [43], this motion is a good example of the use of the equal energy rule to estimate R-factors of intermediate period systems. Figure 4.8 shows that the R-factors computed for this record and those determined

Table 4.2: Ground motion-pulse match classification +

Ground motion	**Best Pulse Match**	**Error** $\mathbf{E_o^a}$	**Period** $\hat{\mathbf{T}}_o$ **(s)**
WN87MWLN.090	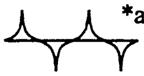 *abc	0.049	0.2
BB92CIVC.360	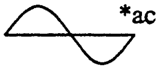 *ac 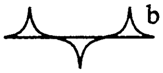 b	0.0565, 0.0612^{pb}	0.25^{ac}, 0.4^{b}
SP88GUKA.360	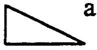 abc	0.056	0.25
LP89CORR.090	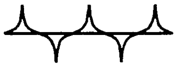 abc	0.065	0.7, 0.65^{b}
NR94CENT.360	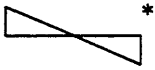 *ac 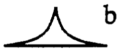 b	0.092, 0.095^{pb}	1^{ac}, 0.4^{b}
CH85LLEO.010	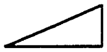 ac 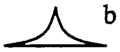 b	0.064, 0.066^{pb}	0.3^{ac}, 0.45^{b}
CH85VALP .070	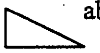 abc	0.094	0.45^{ac}, 0.5^{b}
IV40ELCN.180	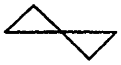 *ac 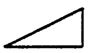 b	0.08, 0.083^{pb}	0.4^{ac}, 0.3^{b}
LN92JOSH.360	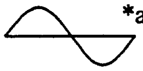 *abc	0.059	0.5
MX85SCT1.270	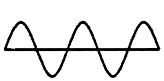 ac 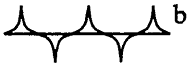 b	0.133, 0.139^{pb}	2.15
LN92LUCN.250	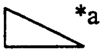 *a 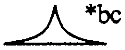 *bc	0.062, 0.0625^{pb}	0.45^{a}, 0.2^{bc}
LP89SARA.360	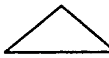 ac 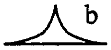 b	0.0722, 0.0724^{pb}	0.3^{ac}, 0.4^{b}
NR94NWHL.360	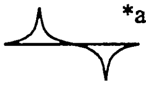 *abc	0.079	0.75^{ac}, 0.8^{b}
NR94SYLH.090	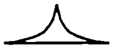 abc	0.07	0.7
KO95TTRI.360	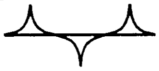 abc	0.13	1.35^{a}, 1.4^{bc}

$^{+}$ these are the best pulses for $\mu = 2, 4$, and 8 and the associated $T_p = \hat{T}_o$ for each ground motion using the three type of errors E_o^a, E_o^b, and E_o^c.

a, b, c define the error measures a, b, and c given by the errors E_o^a, E_o^b, and E_o^c, respectively.

* overall response.

^{pb} Error E_o^a using pulse given by error b.

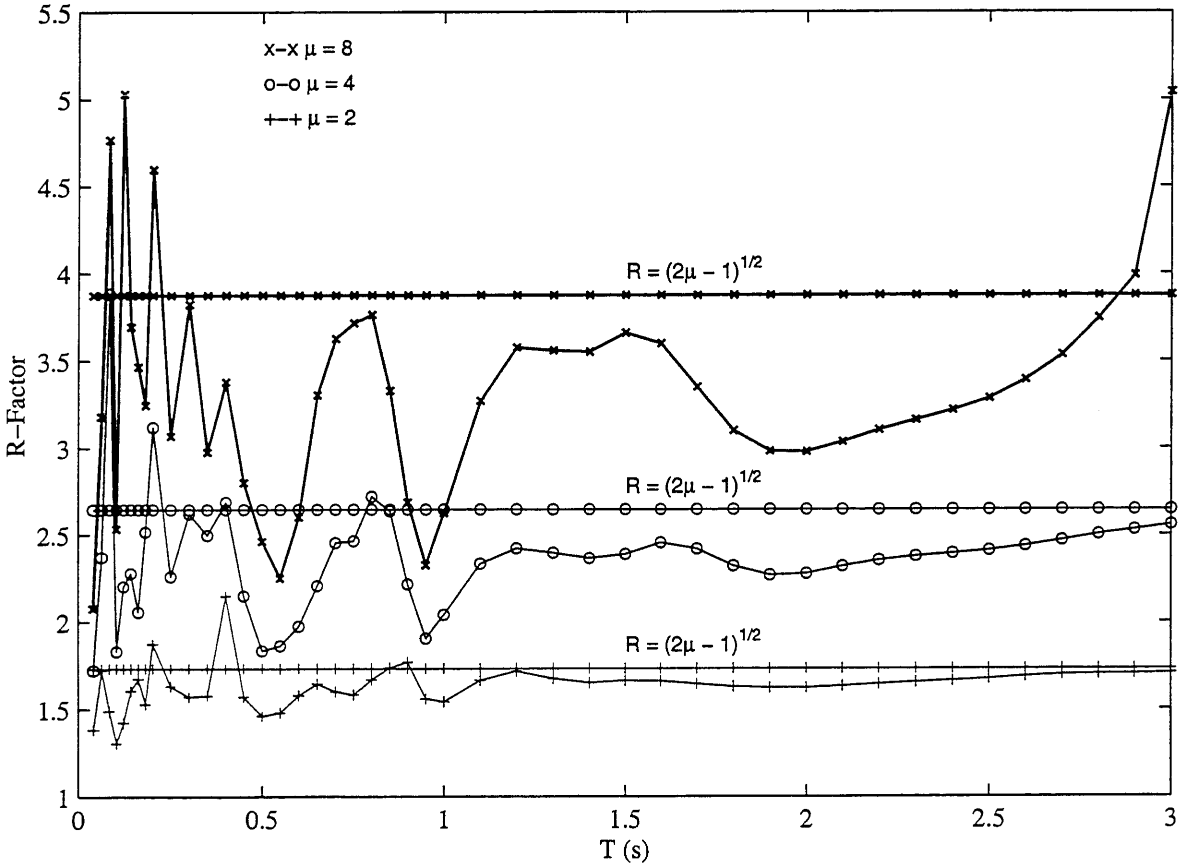

Figure 4.8: R-factor response spectra to the LN92LUCN.250 record and the equal energy rule R-factor, $R = \sqrt{2\mu - 1}$

using the equal energy rule for undamped elasto-plastic systems, given by $R = \sqrt{2\mu = 1}$, are very similar in the intermediate range of periods. For the rest of the ground motions, the optimal pulses (that minimize E^a) have R-factors that are not accurately represented by the equal energy rule for intermediate period systems. Thus, the equal energy rule would not be a good rule to follow for 14 of the 15 ground motions.

There is no finding that unbalanced pulses are better for some motions and balanced pulses are better for others. In fact, there are three ground motions (BB92CIVC.360, NR94CENT.360, and IV40ELCN.180) for which a balanced pulse minimizes one error measure and an unbalanced pulse minimizes another error measure. Table 4.2 shows that the errors $E_o^a = E_{11,*}^a(i, \hat{j})$ for the records that have different optimal pulses depending on the error measure to be minimized are very similar even for those records whose optimal pulses are a balanced and an unbalanced pulse. This indicates that the error computed over all periods is similar even though the R-factors of the pulses differ.

There are four records (SP88GUKA.360, NR94CENT.360, CH85VALP.070, and LN92LUCN.250) whose best estimates are obtained with shock pulses: the tr0(2) pulse for the Northridge Century City record and the tr0(1) pulse for the other three records. The R-factors for these records tend to unity for short period systems, resulting in little reduction in strength as μ increases. Nevertheless, the error over all periods was smallest using the shock pulses, for which short period systems respond to the excitation as an instantaneous change in ground acceleration, having $R = (2\mu - 1)/\mu$ [20]. For other records, the preceding formula is much less accurate, and gradual loading pulses, having $R = 1$, estimate the response of short period systems more accurately.

Within any one family of pulses, R-factors depend on the number of incursions, since this number affects the elastic response substantially (see Section 3.3.1). Table 4.2 shows the records (WN87MWLN.090, LP89CORR.090, and MX85SCT1.270) whose best pulses have a larger number of incursions; for these, the strengths for inelastic response are greatly reduced as ductility increases.

It also may be observed that the quadratic pulses minimize the E_o^b error more often than the other error measures. The best estimates for 11 of the 15 ground motions are quadratic pulses when using this error measure.

Figures 4.9, 4.10, and 4.11 plot isoductile strengths, η_y, and their estimates, $\hat{\eta}_y$, for the optimal pulses with respect to the error E^a_o for the SD, LD, and FD records, respectively.

Recognizing the basic finding, that pulse R-factors can be used to estimate inelastic spectra, it was desired to determine whether simplifications could be made in the selection of the pulses and the characteristic period T_p. Two simplifications are explored in the following sections.

4.3.2 Simplification No. 1 - Identifying a Subset of Best Pulses

Instead of identifying a different optimal pulse for each ground motion (Table 4.2), just one or two pulses may minimize the errors E^s sufficiently to obtain good estimates for the 15 ground motions. Two pulses were found that minimize the three error measures: the qua(3) pulse (forced response) and the qua(2) pulse (overall response). The qua(3) pulse minimizes each error measure for $\mu = 2$ and the qua(2) pulse minimizes each error measure for $\mu = 4$ and 8 (different values of T_p were associated with each ductility-pulse-ground motion combination). To further simplify, the possibility of using a single pulse for all ductilities was explored. Two cases are studied in detail and compared with the case where the qua(3) pulse is used for $\mu = 2$ and the qua(2) pulse is used for $\mu = 4$ and 8. First, the qua(2) pulse is used for all ductilities ($i = 31$) and second, the qua(3) pulse is used for all ductilities ($i = 13$). For each case, the periods $T_p = T^*_1$ that minimize $E^s_{gm,*}(i, \hat{j})$ were found for each ground motion (Table 4.3).

Table 4.4 shows that the average errors $AE^s_{*,d}(i, \hat{j})$, using these pulses with $T_p = T^*_1$, are lowest when the forced response of the qua(3) pulse is used for $\mu = 2$ and the overall response of qua(2) is used for $\mu = 4$ and 8. The errors decrease as ductility increases. The errors $NE^a_{gm,*}(i, \hat{j})$ are shown in Table 4.5 for the three cases with $T_p = T^*_1$. Two records, NR94NWHL.360 and KO95TTRI.360, have NE^a values less than unity when using qua(3) for $\mu = 2$ and qua(2) for $\mu = 4$ and 8 because the errors E^a_{13} and E^a_{15} are lower than E^a_o obtained with only one pulse for all ductilities. The smallest errors for the three cases are obtained for the SD motions; the LD motions have the

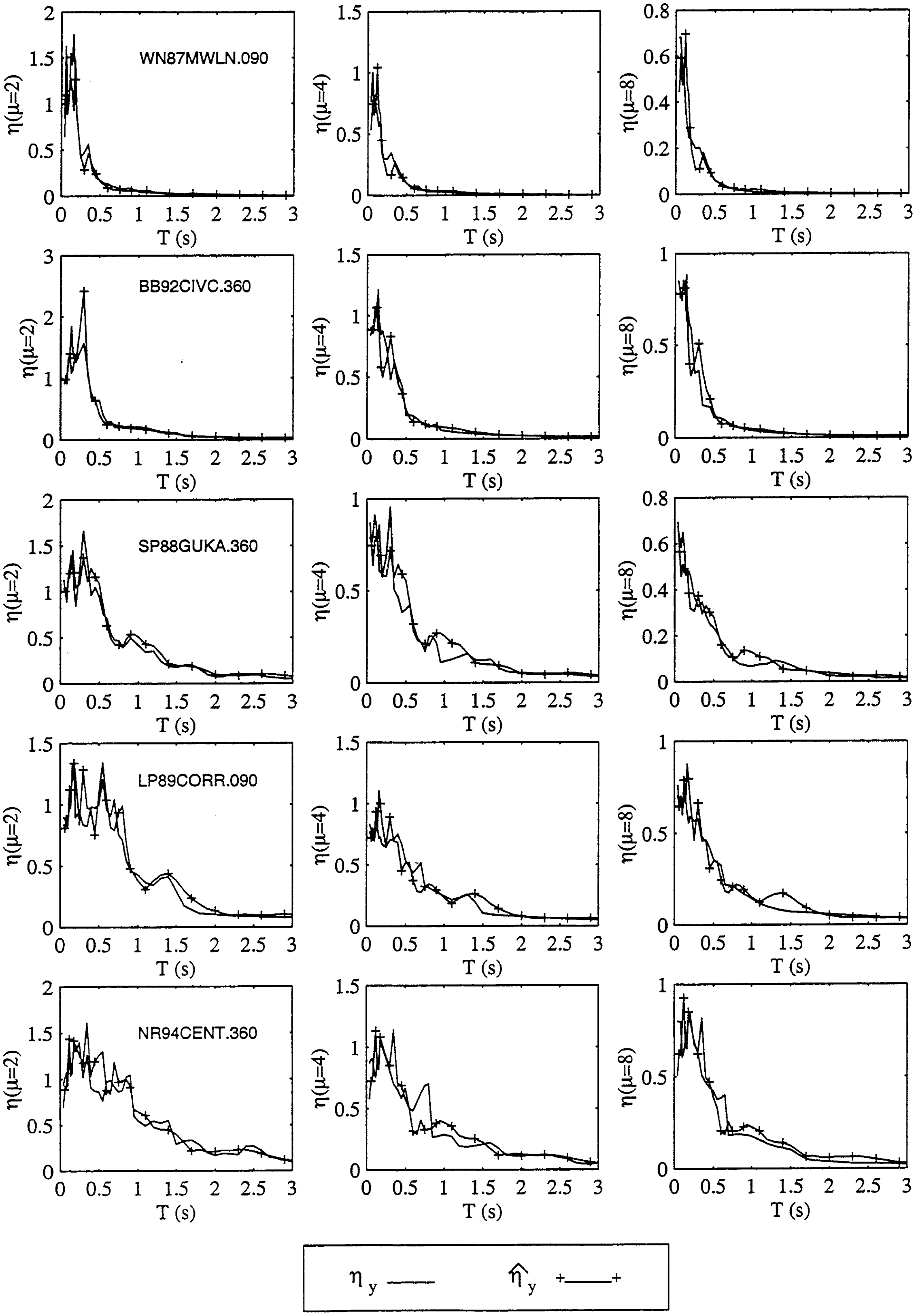

Figure 4.9: Isoductile strength response spectra to short duration records, η_y, and their estimates $\hat{\eta}_y$, with their best pulses at $T_p = \hat{T}_o$ given by E_o^a (see Table 4.2)

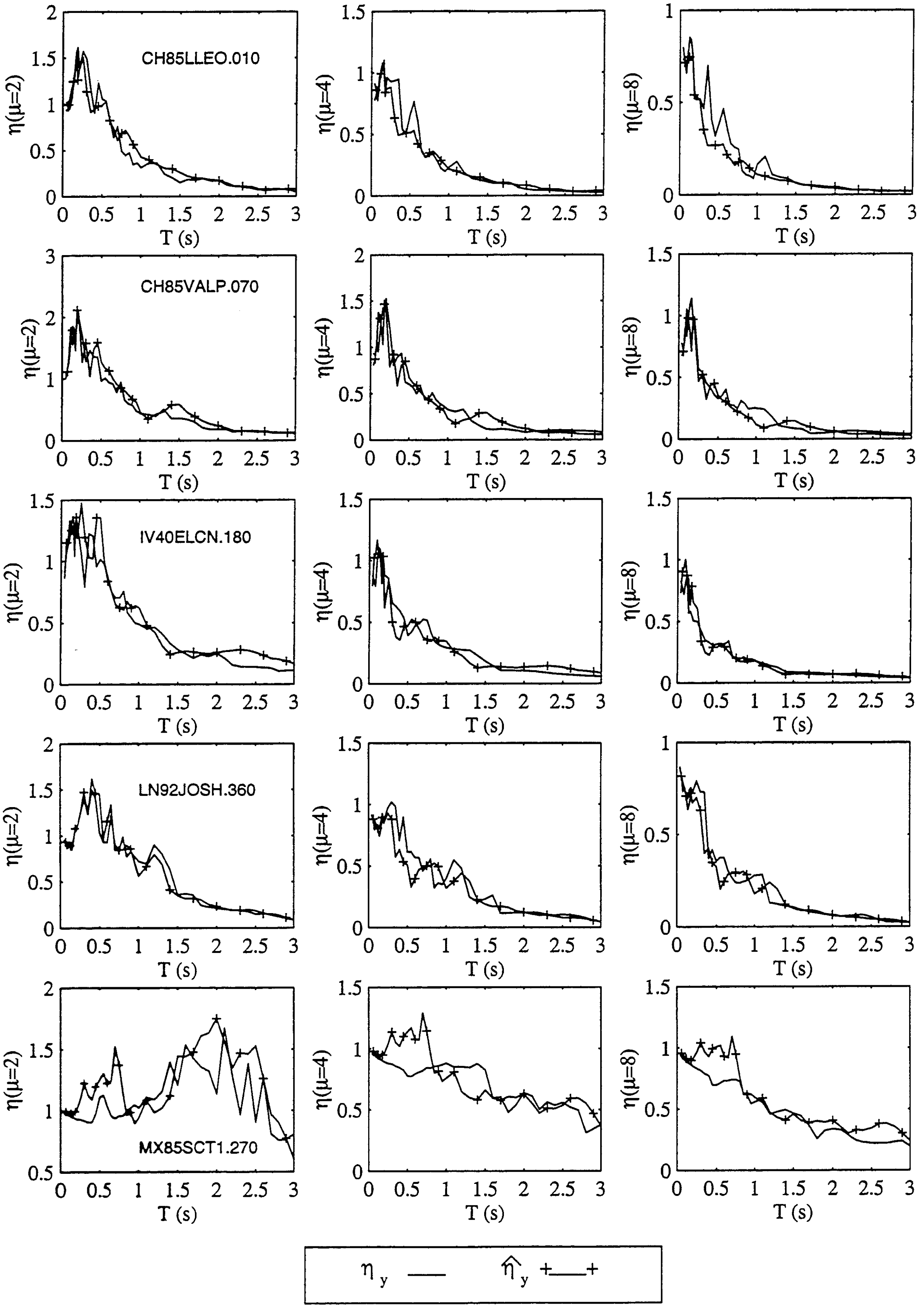

Figure 4.10: Isoductile strength response spectra to long duration records, η_y, and their estimates $\hat{\eta}_y$, with their best pulses at $T_p = \hat{T}_o$ given by E_o^a (see Table 4.2)

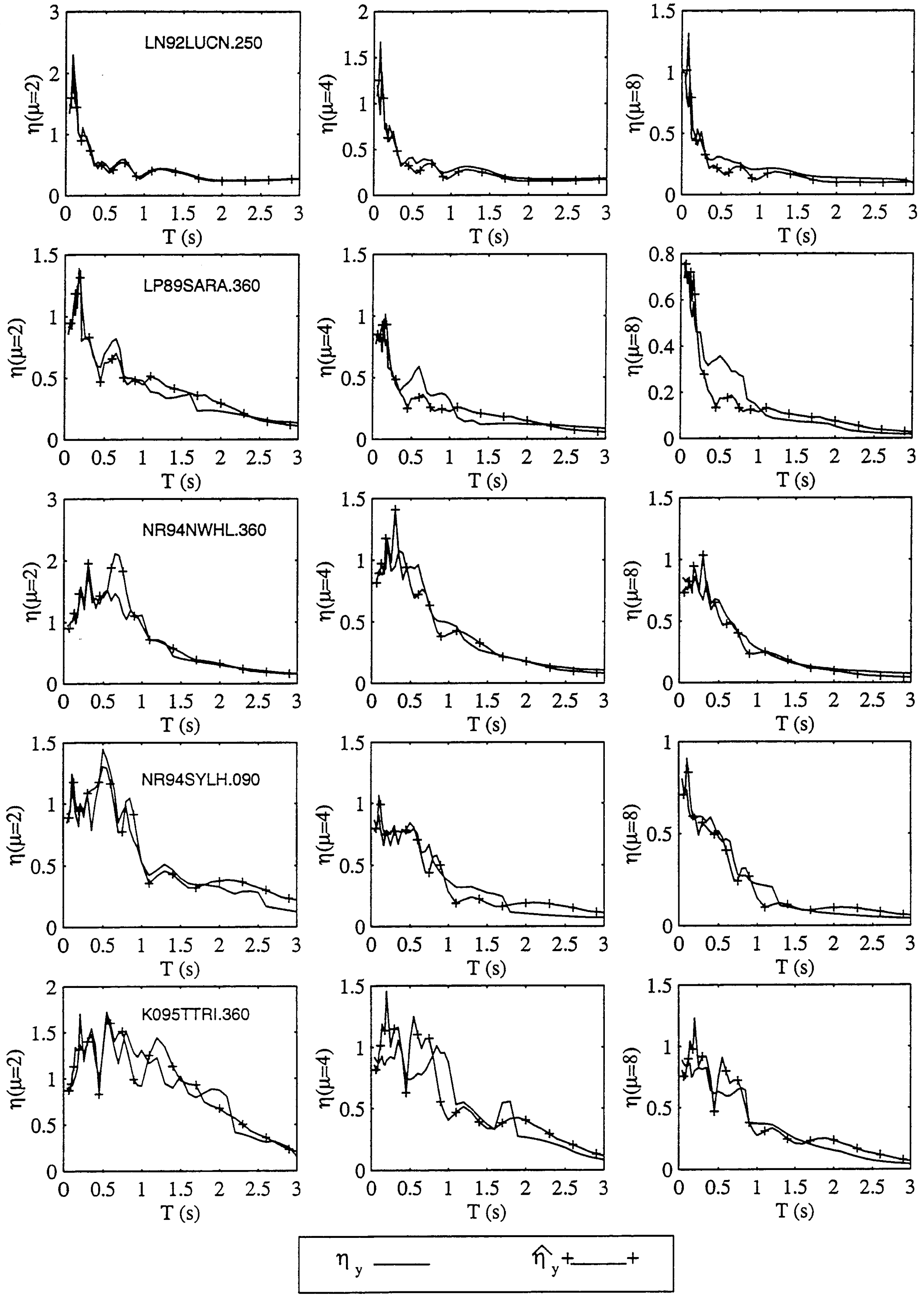

Figure 4.11: Isoductile strength response spectra to forward directive records, η_y, and their estimates $\hat{\eta}_y$, with their best pulses at $T_p = \hat{T}_o$ given by E_o^a (see Table 4.2)

Table 4.3: Characteristic pulse periods, T_p

Ground Motion	$T_p = T_1^*$ (s)			$T_p = T_g$ (s)
	qua(2),qua(3)	qua(2)	qua(3)	
WN87MWLN.090	0.20	0.20	0.20	0.20
BB92CIVC.360	0.40	0.45^a , 0.40^{bc}	0.40	0.40
SP88GUKA.360	0.25	0.30	0.30^a , 0.50^{bc}	0.55
LP89CORR.090	0.65^{ac}, 0.60^b	0.55	0.65	0.85
NR94CENT.360	0.70^{ac}, 0.65^b	0.70^{ac} , 0.65^b	0.70^{ac} , 0.65^b	1.00
CH85LLEO.010	0.65	0.55^{ac} , 0.65^b	0.65	0.30
CH85VALP.070	0.35	0.30^{ac} , 0.35^b	0.35	0.55
IV40ELCN.180	0.65	0.40	0.65^{ac} , 0.70^b	0.65
LN92JOSH.360	0.80	0.60	0.85	1.30
MX85SCT1.270	2.05^a, 2.00^{bc}	1.50^a , 1.35^{bc}	2.20	2.00
LN92LUCN.250	0.30^a, 0.25^{bc}	0.30^a , 0.25^{bc}	0.30^a , 0.25^{bc}	0.20
LP89SARA.360	0.85^a, 0.60^{bc}	0.60	1.10^a , 0.60^b , 1.00^c	0.40
NR94NWHL.360	0.75^{ac}, 0.80^b	0.75^{ac} , 0.80^b	0.80	0.80
NR94SYLH.090	1.10	1.10	1.10	0.90
KO95TTRI.360	1.30^{ab}, 1.35^c	0.75	1.35^a , 1.40^{bc}	1.40

a, b, and c identify the error measures E_o^a, E_o^b, and E_o^c, respectively

Table 4.4: Average errors $AE^s = E^s_{*,d}(i, \hat{j})$ using (a) qua(2) for $\mu = 4$ and 8, and qua(3) for $\mu = 2$, (b) qua(2) (i =31) for all ductilities, and (c) qua(3) (i =13) for all ductilities

μ	$T_p = T_1^*$			$T_p = T_1^*$			$T_p = T_g$		
	$qua(2,3)$	$qua(2)$	$qua(3)$	$qua(2,3)^1$	$qua(2)^1$	$qua(3)^1$	$qua(2,3)^2$	$qua(2)^2$	$qua(3)^2$
	AE^a	AE^a	AE^a	AE^a	AE^a	AE^a	AE^a	AE^a	AE^a
$\mu = 2$	0.113	0.116	0.115	0.105	0.108	0.106	0.118	0.132	0.118
$\mu = 4$	0.100	0.108	0.105	0.094	0.098	0.102	0.107	0.107	0.112
$\mu = 8$	0.076	0.081	0.079	0.071	0.072	0.075	0.082	0.082	0.083
$\forall\mu$	0.096	0.102	0.100	0.090	0.093	0.094	0.102	0.107	0.105
	AE^b	AE^b	AE^b	AE^b	AE^b	AE^b	AE^b	AE^b	AE^b
$\mu = 2$	0.172	0.179	0.172	0.159	0.173	0.158	0.172	0.204	0.172
$\mu = 4$	0.140	0.152	0.144	0.135	0.141	0.144	0.155	0.155	0.162
$\mu = 8$	0.107	0.114	0.112	0.103	0.105	0.110	0.123	0.123	0.124
$\forall\mu$	0.140	0.148	0.143	0.133	0.140	0.137	0.150	0.161	0.152
	AE^c	AE^c	AE^c	AE^c	AE^c	AE^c	AE^c	AE^c	AE^c
$\mu = 2$	0.136	0.137	0.139	0.122	0.128	0.122	0.136	0.159	0.136
$\mu = 4$	0.111	0.124	0.116	0.105	0.110	0.113	0.122	0.122	0.128
$\mu = 8$	0.082	0.090	0.087	0.076	0.078	0.083	0.091	0.091	0.092
$\forall\mu$	0.110	0.117	0.114	0.101	0.105	0.106	0.116	0.124	0.119

[1] The sin(5) pulse at $T_p = \hat{T}_o = 2.15$ s is used for the ground motion no. 10

[2] The sin(5) pulse at $T_p = 2$ s is used for the ground motion no. 10

Table 4.5: Normalized errors $NE^a_{gm,*}(\imath,\hat{\jmath})$ at $T_p = T_1^*$ and $T_p = T_g$, using (a) qua(2) for all ductilities, (b) qua(3) for all ductilities, (c) qua(2) for $\mu = 4$ and 8, and qua(3) for $\mu = 2$. Overall errors OE^a, for short duration (SD), long duration (LD), forward directive (FD), and all ground motions

Ground Motion	$T_p = T_1^*$			$T_p = T_1^*$			$T_p = T_g$		
	$qua(2,3)$	$qua(2)$	$qua(3)$	$qua(2,3)^1$	$qua(2)^1$	$qua(3)^1$	$qua(2,3)^2$	$qua(2)^2$	$qua(3)^2$
Record	NE^a	NE^a	NE^a	NE^a	NE^a	NE^a	NE^a	NE^a	NE^a
1	1.157	1.369	1.043	1.157	1.369	1.043	1.157	1.369	1.043
2	1.044	1.211	1.074	1.044	1.211	1.074	1.044	1.205	1.074
3	1.238	1.191	1.454	1.238	1.191	1.454	1.498	1.525	1.529
4	1.238	1.385	1.209	1.238	1.385	1.209	1.602	1.862	1.471
5	1.048	1.016	1.177	1.048	1.016	1.177	1.329	1.361	1.285
6	1.211	1.144	1.331	1.211	1.144	1.331	1.705	1.553	1.791
7	1.152	1.096	1.191	1.152	1.096	1.191	1.347	1.436	1.420
8	1.009	1.075	1.068	1.009	1.075	1.068	1.009	1.185	1.068
9	1.544	1.780	1.583	1.544	1.780	1.583	2.051	2.080	2.066
10	1.692	1.981	1.538	0.977	1.000	1.000	1.063	1.063	1.063
11	1.990	2.040	1.845	1.990	2.040	1.845	2.145	2.214	2.042
12	1.217	1.054	1.290	1.217	1.054	1.290	1.383	1.353	1.451
13	0.930	1.000	1.129	0.930	1.000	1.129	0.958	1.019	1.129
14	1.266	1.214	1.431	1.266	1.214	1.431	1.357	1.331	1.550
15	0.974	1.054	1.000	0.974	1.054	1.000	0.988	1.104	1.006
Category	OE^a	OE^a	OE^a	OE^a	OE^a	OE^a	OE^a	OE^a	OE^a
SD	1.145	1.234	1.191	1.145	1.234	1.191	1.326	1.464	1.280
LD	1.322	1.415	1.342	1.179	1.219	1.235	1.435	1.463	1.482
FD	1.275	1.273	1.339	1.275	1.273	1.339	1.366	1.386	1.436
$\forall g.m.$	1.247	1.307	1.307	1.200	1.242	1.255	1.376	1.438	1.399

[1] The sin(5) pulse at $T_p = \hat{T}_o = 2.15$ s is used for the ground motion no. 10

[2] The sin(5) pulse at $T_p = 2$ s is used for the ground motion no. 10

largest errors. The overall error, OE^a, increased between 24.7 and 30.7% with respect to having used the best pulse from Table 4.2 for each ground motion. It can be observed that the error for MX85SCT1.270 record increased considerably. Poor estimates are obtained for this particular ground motion, recorded on soft soils, using these quadratic pulses; estimates are much improved with the sinusoidal sin(5) pulse. Accordingly, a second set of optimal pulses is considered in Table 4.4. If the sin(5) pulse with $T_p = \hat{T}_o = 2.15$ s is used in conjunction with qua(2) and qua(3) for the remaining 14 records, the errors $AE^s_{*,d}(i, \hat{j})$ are reduced as shown in Table 4.4, resulting in overall errors, OE^a, between 20.0 and 25.5% higher than if the best pulse had been used for each ground motion (Table 4.2). Although it was not formally part of this study, a sinusoidal pulse with 6 incursions did not improve the estimate given by sin(5) for MX85SCT1.270. The qua(2), qua(3), and sin(5) pulses are characterized by $R = 1$ for short period systems and $R = \mu$ for long period systems (Fig. 4.4).

4.3.3 Simplification No. 2 – Identifying Characteristic Periods for the Best Pulses

The characteristic pulse periods $T_p = T_1^*$ that minimize the errors obtained with the qua(2) and qua(3) pulses in Table 4.3, and the periods $T_p = \hat{T}_o$ that minimize the errors obtained with the best pulses in Table 4.2, often are similar to the characteristic periods of the ground motions, T_g, reported in Table 4.3. These T_g values were determined prior to this study and are reported in FEMA-307 [46]. Using these values of T_g to estimate the isoductile strength spectra ($T_p = T_g$) results in the average errors $AE^s_{*,d}(i, \hat{j})$ shown in Table 4.4 using the pulses qua(2) and qua(3) for all ductilities and using qua(3) for $\mu = 2$, and qua(2) for $\mu = 4$ and 8, for the three errors $s =$ a, b, and c. Considering all pulses individually (with $T_p = T_g$), the qua(3) pulse is the best for μ = 2, while qua(2) is best for $\mu = 4$ and 8. If both pulses are joined, using qua(3) for $\mu = 2$ and qua(2) for $\mu = 4$ and 8 for all records except the MX85SCT1.270 record for which the sin(5) pulse is used, the errors $AE^s_{*,*}$ are reduced with respect to using only the quadratic pulses for all the ground motions. The normalized errors for each ground motion, $NE^a_{gm,*}(i,\hat{j})$, and overall errors OE^a are given in Table 4.5, using $T_p = T_g$. The overall error OE^a is 1.438 and 1.399 using qua(2) and qua(3), respectively, an increase of 13.1 and 10.8% over OE^a using $T_p = T_1^*$. The overall errors for SD, LD, and FD categories ranged from 1.144 to 1.415 when $T_p = T_1^*$, and now range from 1.280 to 1.482 when $T_p = T_g$.

Although the qua(3) pulse gave a smaller error, the increase in error if the simpler qua(2) pulse is used instead is small. The qua(2) pulse may be recommended for all ductilities and all ground motions except the soft soil MX85SCT1.270 record. The use of the qua(2) pulse (overall response) with $T_p = T_g$ is illustrated in Figs. 4.14, 4.13, and 4.12 for 14 of the 15 records with the overall response of sin(5) used for the MX85SCT1.270 record. These figures plot the spectra of the strength responses, η_y, and their estimates, $\hat{\eta}_y$ for the SD, LD, and FD records. Chapert 5 will identify another characteristic period, T_2^*, which improves the error measures over those calculated with $T_p = T_g$.

4.3.4 Near-Fault Ground Motions

Near-fault ground motions have been recorded in the 1971 San Fernando, 1979 Imperial Valley, 1994 Northridge, and 1995 Kobe earthquakes. These records are characterized by large velocity pulses. Two types of near-fault motion have been described. The original concept of a near-fault "fling" [56] refers to the ground displacement that takes place as the fault slip causes a near-fault location to displace permanently. More recently Iwan, Hall, and Somerville [57, 58, 40, 38] among others have identified a second phenomenon in which shear waves emitted from the moving fault rupture zone superpose at locations ahead of the fault rupture to produce large amplitude velocity pulses having relatively long durations. For a strike-slip fault, superposition of the waves emitted from the propagating rupture zone results in large velocity pulses that are perpendicular to the fault, increasing the strengths required for elastic response in the long period range of the spectrum.

Iwan [57, 58] reported that the Landers and Northridge earthquakes generated near-fault ground motions characterized by a small number or even just one velocity pulse of short duration, large amplitude, and very high input energy. He concluded that:

1. The shape of the response spectrum for near-fault earthquakes was very similar to the response spectrum for more distant earthquake ground motions.
2. For short period systems, isoductile yield strengths are nearly equal to the strengths required for elastic response ($R = 1$), given by $V_y = V_e = m \cdot a_{g,max}$.
3. For long period systems the relative displacement of the SDOF system tends to the peak ground displacement, resulting in $R = \mu$.

Several researchers [38, 37, 35, 36, 40, 39] have suggested the use of idealized near-fault pulses to replace the large amplitude velocity pulse(s) associated with forward directivity, for estimating the response of MDOF systems. The idealized pulses are characterized by linear acceleration histories similar to the rectangular family of pulses of this study (rec) and having one or two incursions in the velocity histories.

The results of the present study on SDOF systems have some bearing on this topic. First, the shock pulses used by these researchers produce in short period systems larger isoductile strength demands than the gradual pulses, for which the strength reduction factors are larger than unity ($R = (2\mu - 1)/\mu$, in Section 3.4). Even if the rec family were to give the correct elastic spectrum the inelastic spectra would be incorrect for the short period range. Table 4.2 shows that responses to the FD records are best estimated with the quadratic family of pulses which have $R = 1$ for short period systems rather than with shock pulses. This result is also supported by Baez and Miranda [59] who state that for extremely short period systems $R = 1$ for all ground motions regardless of near-fault effects. Second, the linear acceleration histories used by these researchers are not required to obtain velocity pulses. The gradual pulse qua(2) proposed herein for estimating the R-factors of the FD, SD, and LD motions, also has a velocity pulse in the time history, as shown in Fig. A.1. Many other pulses considered in this study also have velocity pulses (see Appendix A).

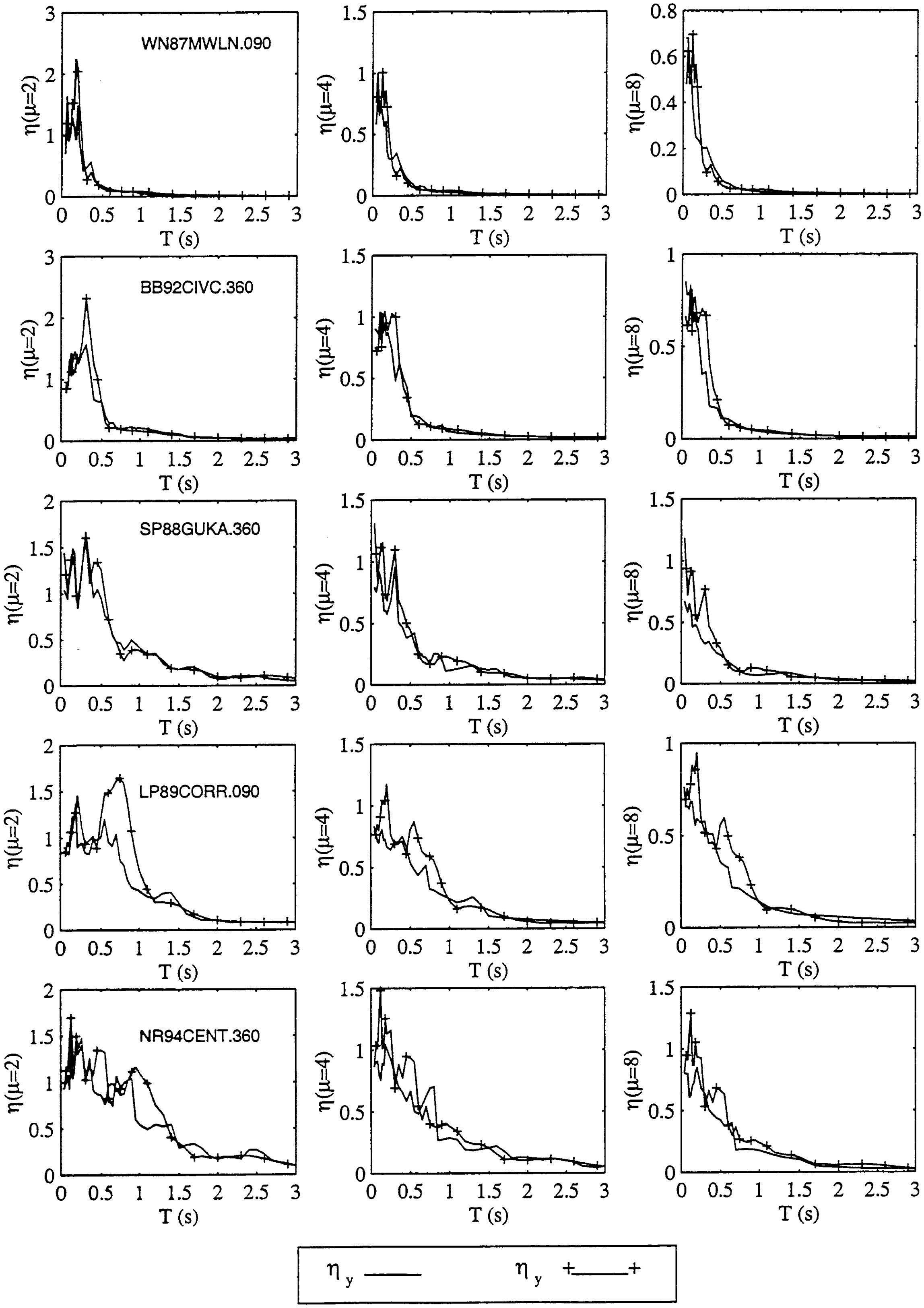

Figure 4.12: Isoductile strength response spectra to short duration records, η_y, and their estimates $\hat{\eta}_y$, with the qua(2) pulse at $T_p = T_g$ (see Table 4.3)

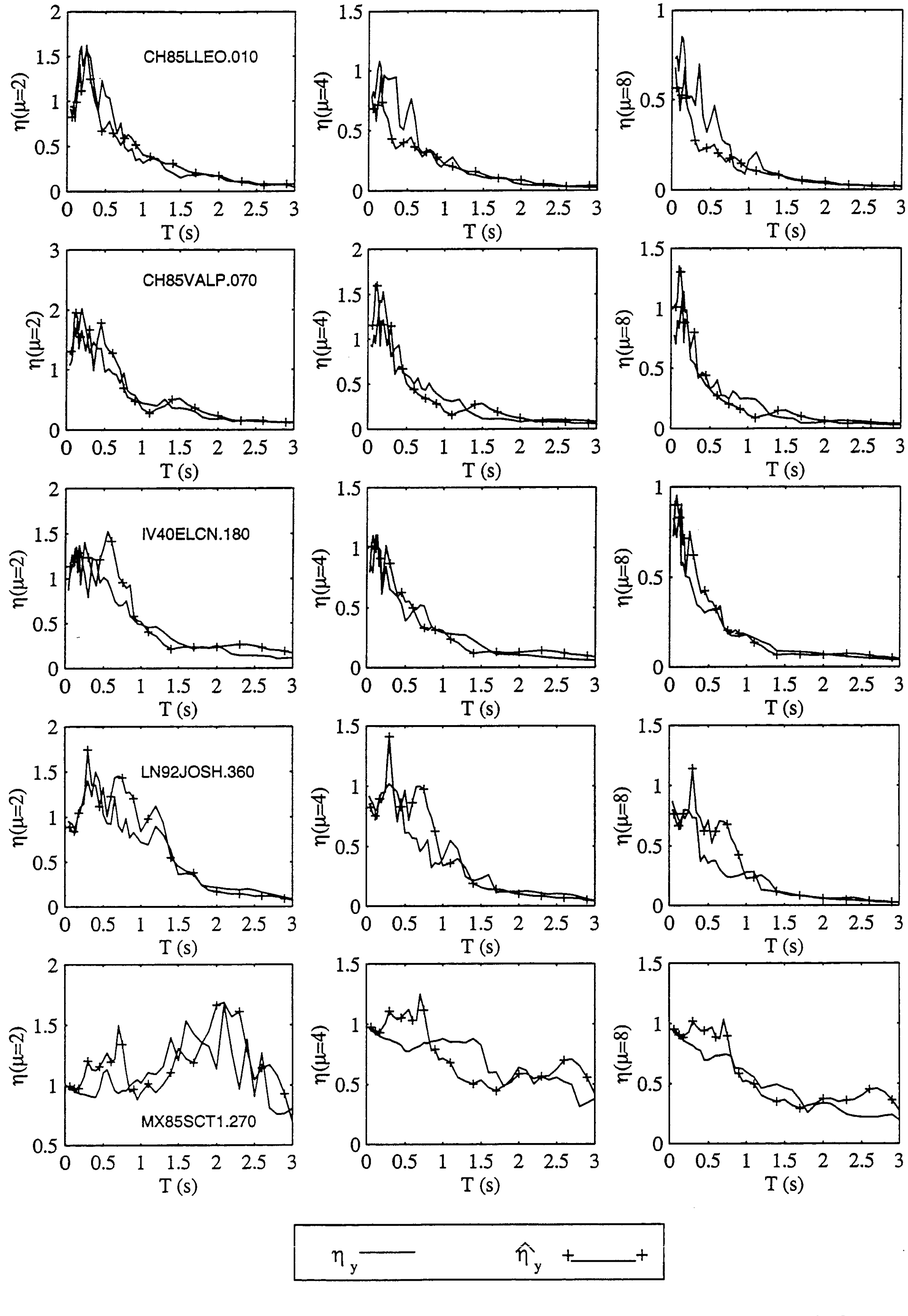

Figure 4.13: Isoductile strength response spectra to long duration records, η_y, and their estimates $\hat{\eta}_y$, with the qua(2) pulse for all records except MX85SCT1.270, for which the sin(5) pulse was used, at $T_p = T_g$ (see Table 4.3)

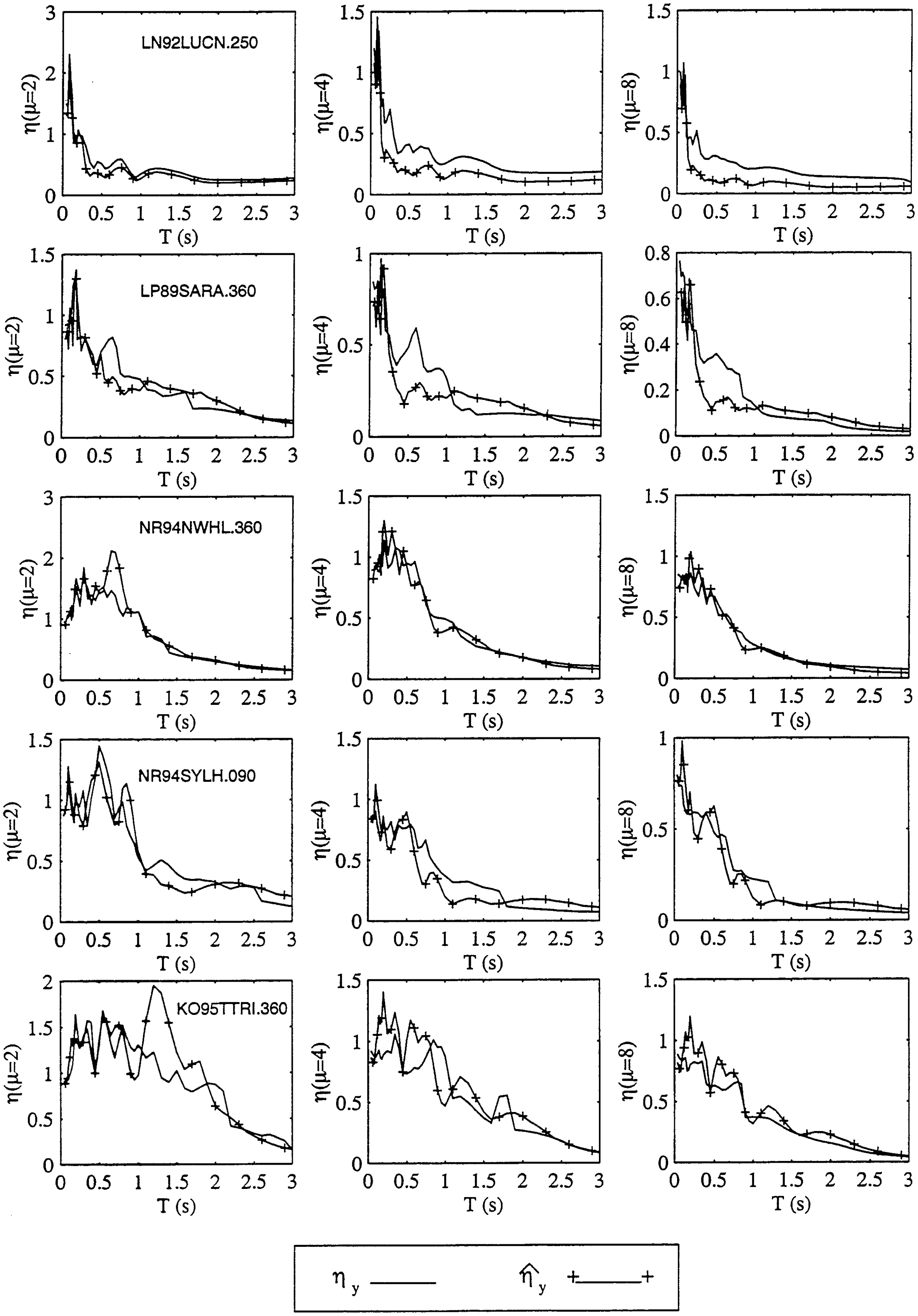

Figure 4.14: Isoductile strength response spectra to forward directive records, η_y, and their estimates $\hat{\eta}_y$, with the qua(2) pulse at $T_p = T_g$ (see Table 4.3)

The R-factors obtained from such pulses are applicable to ground motions recorded far from the fault. The quadratic pulse gives R-factors that work well for SD, LD, and FD motions, but these R-factors must be applied to the correct elastic spectrum. The elastic spectrum involves contributions from a broad range of frequencies present in the ground motion, which produce varying degrees of resonance in the elastic SDOF systems. A simple pulse is unlikely to contain the appropriate range of frequencies and is unlikely to excite resonance similar to the richer and more complex longer-duration ground motions. Thus, it is unlikely that a simple pulse can generate appropiate spectra. Furthermore, even if a single pulse could generate correct spectra, the phasing of higher mode responses resulting from a pulse will surely be different, in general from the phasing of higher mode responses to a ground motion, and thus it is doubtful that such a pulse would result in an accurate representation of potential demands on MDOF systems.

4.4 Summary

This chapter shows that R-factors exhibit a sufficient degree of waveform independence, and that R-factors determined for simple pulses may be used in conjunction with elastic response spectra for purposes of estimating the inelastic response spectra of elasto-plastic systems subjected to earthquake ground motions. Based on Sewell [45], this conclusion should be valid across a large range of earthquake magnitudes and distances.

The quadratic pulses qua(2) (overall response for systems with $\mu = 4$ and 8) and qua(3) (forced response for systems with $\mu = 2$) are adequate for 14 of the 15 records studied, while the sinusoidal pulse sin(5) is necessary to estimate the inelastic spectra for the soft soil SCT record of the 1985 Michoacan earthquake (MX85SCT1.270). For simplicity and with little increase in error, the R-factor for the overall response to the qua(2) pulse may be used for ductilities of 2, 4, and 8 for all records except the 1985 Michoacan record. The goodness of the pulse R-factors seems to be independent of the classification of the records into the SD, LD, and FD categories. This result is particularly useful because:

1. a single pulse shape can be used for generating the R-factors suitable for different load-deformation and hysteretic characteristics rather than requiring separate $R-\mu-T$ relations to be developed for each case of interest, and

2. gross features of waveform independence demonstrated in this chapter suggest that $R-\mu-T$ relations may be used for estimating the inelastic response spectra of unknown future ground motions, an issue of particular interest where recorded ground motions are not available because historic seismicity preceded the relatively recent deployment of strong motion instrumentation.

The characteristic period of the ground motion, T_g, may be estimated as the transition period between the constant acceleration and constant velocity portions of a smoothed elastic design spectrum. The characteristic periods of the ground motions, T_g, are nearly equal to the characteristic periods of the pulses, T_p, that minimized the errors of the estimated isoductile strengths using the qua(2), qua(3), and sin(5) pulses.

Chapter 5

Comparisons of Inelastic Response Spectra Determined Using Conventional and Pulse R-Factors

5.1 Introduction

Chapter 4 showed that inelastic response spectra may be estimated by dividing elastic response spectra by R-factors derived from the response to a simple pulse. The pulse R-factor depends on the pulse shape, ductility (μ), load-deformation model, and the period of the system (T) relative to the characteristic period of the pulse (T_p). In this chapter, inelastic spectra estimated using pulse R-factors are compared with those obtained using other contemporary $R - \mu - T$ relationships for elasto-plastic, bilinear, and stiffness-degrading SDOF systems. Strong motion records used in this chapter are the same ones described in Section 2.2.1. The accuracy of the estimates is not found to depend strongly on duration or presence of forward directivity features, but is influenced by the characteristic period and the presence of soft soil deposits that lead to nearly harmonic waveforms. In this chapter, pulse R-factors are found to be slightly better than the $R - \mu - T$

relations determined by other investigators for the 15 ground motions studied. Because the pulse R-factors are defined implicitly by the specification of the pulse shape, they may be useful for a variety of load-deformation models having varied hysteretic relationships.

Several researchers (e.g. [21, 29, 22, 23, 25, 24, 26]) have estimated isoductile response spectra for single-degree-of-freedom (SDOF) systems subjected to ground motions by applying a strength reduction factor (R) to elastic response spectra. The recommended R-factors describe the trends observed for the ground motions and load-deformation behaviors that were investigated. In some cases, response was computed for a large number of ground motions, and mean R-factor curves were then approximated by analytical functions of ductility and period. In some cases the recommended $R - \mu - T$ relations apply uniformly without regard to characteristics of the ground motion.

Chapter 4 and Cuesta and Aschheim [44, 43, 51, 60, 52] showed that the strength reduction factors can be obtained from a simple pulse. As described in Chapter 2, peak ductility demands are not reached throughout the duration of the record, but rather in one or several irregular cycles traced by the record and having a fraction of the record duration [41, 34]. Since these pulses can not be known *a priori*, Chapter 4 and Cuesta and Aschheim [44, 43, 51] focused on a variety of simple pulse shapes. This chapter shows that the R-factors determined by simple pulses are similar to those determined by other inverstigators in empirical studies of large numbers of ground motions. In Chapter 4, a pulse waveform having quadratic acceleration components was adequate for estimating the inelastic response spectra for elasto-plastic SDOF systems having 5% of critical damping (see Fig. 5.1a) for 14 of the 15 ground motions studied. A sinusoidal pulse was necessary for estimating the inelastic spectra of the Mexico City SCT ground motion, which was recorded on soft lakebed deposits that gave rise to nearly harmonic motion.

This chapter compares the isoductile response spectra generated using pulse R-factors with those determined using the $R - \mu - T$ relations recommended by other investigators for elasto-plastic, bilinear, and stiffness degrading oscillators. The comparisons indicate the pulse R-factors result in slightly more accurate estimates of strength than can be determined using other contemporary

$R-\mu-T$ relations for the 15 ground motions used in this study. These ground motions include motions identified as having short or long duration and those having near fault forward directivity effects.

5.2 Framework of Study

This section describes the SDOF systems that were studied, the set of 15 ground motions, the two pulses used to define the R-factors, and the empirical $R-\mu-T$ relations recommended by other investigators that are compared with the pulse R-factors.

Ground Motions

The 15 records used in Chapter 2, described in Section 2.2.1, and Table 2.1, are also used to estimate and compare the strength response spectra of the systems studied in this chapter.

SDOF Systems and Load-Deformation Relations

As in previous chapters, strengths required for each oscillator to achieve specified ductilities of 2, 4, and 8 were determined iteratively using the computer program PCNSPEC [48], a modified version of NONSPEC [47].

Six load-deformation models were used to develop the $R-\mu-T$ relations (described in Section 1.2.2) that are compared with the pulse R-factors in this chapter. Because each $R-\mu-T$ relation might be best-suited to the particular load-deformation model on which it is based, all six load-deformation models used in the development of the six $R-\mu-T$ relations of Section 1.2.2 are used in this study. The SDOF models comprise elasto-plastic systems having damping, β, equal to 2, 5, or 10% of critical damping; bilinear systems having $\beta = 5\%$ and a post-yield stiffness, α, equal to 2 or 10% of the initial stiffness; and, stiffness degrading systems having $\beta = 5\%$ and $\alpha = 2\%$. The stiffness-degrading model is the same as the one described by Mahin and Lin [47], applicable to systems that do not exhibit substantial degradation or pinching.

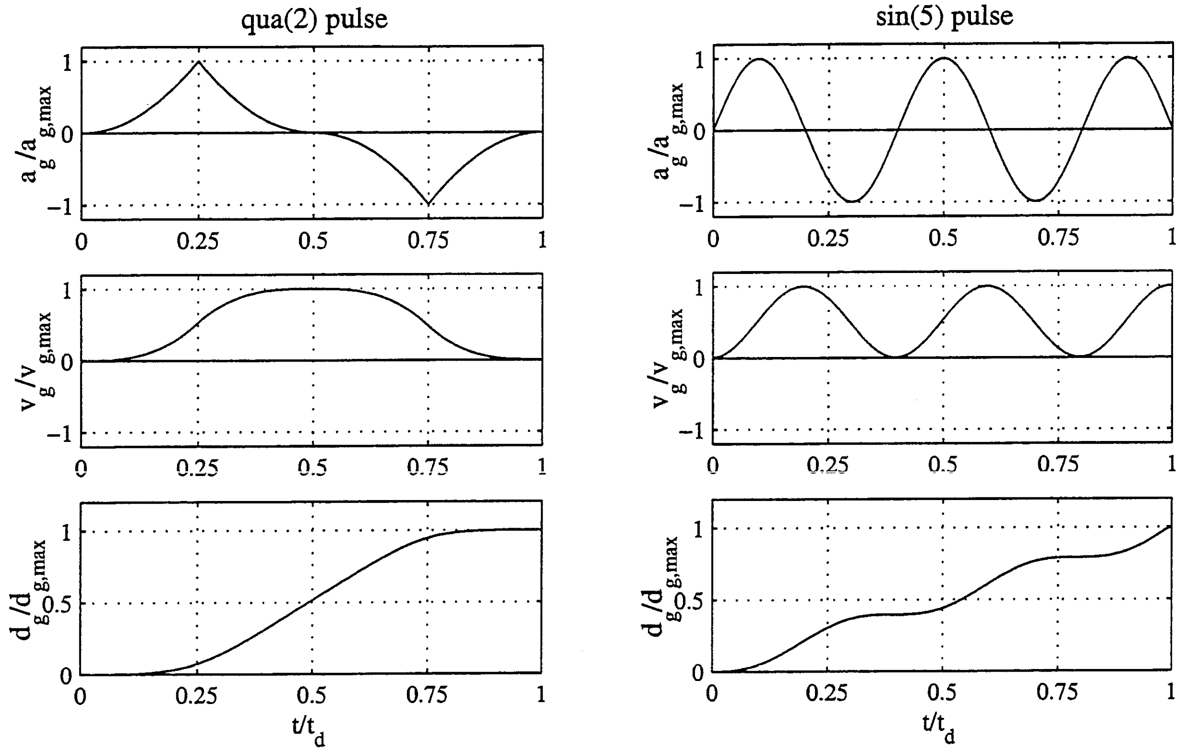

Figure 5.1: Normalized acceleration, velocity, and displacement time histories of the qua(2) and sin(5) pulses

As in Chapter 4, for each record, R-factors were computed for forty-five initial periods of vibration, T, varying from 0.04 to 3 s, with the periods spaced at 0.02 s in the range 0.04-0.2 s, 0.05 s in the range 0.2-1 s, and 0.1 s in the range 1-3 s.

Pulse R-Factor Model

Two pulse waveforms were used to generate the pulse R-factors. The pulse R-factors then were applied to the elastic spectra of the ground motions to generate the estimated inelastic response spectra. The two pulses were identified in Chapter 4 as capable of representing the R-factors of the 15 ground motions with T_p set equal to T_g. The pulse R-factors were computed for 112 periods, ranging from $0.005t_d$ to $100t_d$, where t_d is the duration of the pulse having peak acceleration $a_{g,max}$. The two pulses are:

1. *Quadratic pulse.* The quadratic pulse, qua(2), was used for all but one of the ground motion records. For this pulse (Fig. 5.1a), strengths are computed to limit the ductility demand that

may develop at any time during the response of the oscillator ($0 < t/t_d \leq \infty$). A parameter termed the characteristic period of the pulse, T_p, was defined to equal the duration of this pulse ($T_p = t_d$). The acceleration time history, a_g, in normalized form is

$$\frac{a_g}{a_{g,max}} = \begin{cases} 16\left(\frac{t}{t_d}\right)^2 & 0 \leq \frac{t}{t_d} < \frac{1}{4} \\ 16\left(\frac{t}{t_d} - \frac{1}{2}\right) & \frac{1}{4} \leq \frac{t}{t_d} < \frac{1}{2} \\ -16\left(\frac{t}{t_d} - \frac{1}{2}\right)^2 & \frac{1}{2} \leq \frac{t}{t_d} < \frac{3}{4} \\ -16\left(\frac{t}{t_d} - 1\right)^2 & \frac{3}{4} \leq \frac{t}{t_d} < 1 \end{cases} \tag{5.1}$$

2. *Sinusoidal pulse.* The qua(2) pulse was not capable of generating accurate R-factors in the case of the nearly harmonic SCT record of the 1985 Michoacan earthquake. For this record a sinusoidal pulse called sin(5) was used, consisting of 5 half cycles of a sine wave, as illustrated in Fig. 5.1b. For this pulse, isoductile strengths are determined to limit the peak ductility response that occurs during the pulse excitation ($0 < t/t_d \leq 1$). The characteristic period of this pulse was defined to equal 2/5 of the duration of the pulse. The acceleration, a_g, in normalized form is is given by Eq. 4.2.

The inelastic spectra estimated using the pulses R-factors are compared with estimates made using six models developed over the last three decades: Newmark and Hall [21], Riddell, Hidalgo, and Cruz [22], Nassar and Krawinkler [23], Miranda [24], Vidic, Fajfar, and Fischinger [25], and Ordaz and Pérez-Rocha [26]. These models are described in Section 1.2.2.

5.3 Analytical Results

The isoductile strengths, computed to obtain a specified ductility for each ground motion, were normalized to obtain the dimensionless strength parameter, η_y, defined in Eq. 2.1. The estimated dimensionless isoductile strengths, $\hat{\eta}_y$, are given by the ratio

$$\hat{\eta}_y(\mu, T) = \frac{\eta_y(\mu = 1, T)}{R(\mu, T)} \tag{5.2}$$

where:

- $\eta_y(\mu = 1, T)$ is the strength for elastic response to the ground motion
- $R(\mu, T)$ is the strength reduction factor given in Eqs. 1.9 to 1.14 or given by the pulse R-factor.

The pulse R-factor is calculated as

$$R(\mu, T/T_p) = \frac{\eta_y(\mu = 1, T/T_{p)}}{\eta_y(\mu, T/T_p)} \tag{5.3}$$

The pulse R-factors at the periods of interest (0.04 to 3 s) were calculated by linear interpolation of a predetermined data set that is indexed by the dimensionless parameter T/T_p. This was done after first specifying the value of T_p to be used.

Figures 5.2 and 5.3 show the R-factor spectra versus T/T_p for systems subjected to the qua(2) pulse and the sin(5) pulse, respectively. It can be observed (Fig. 5.4) that for short period systems the R-factor follows the curve $R = 1+\alpha(\mu-1)$, independent of the damping of the system, reflecting the strength available to resist the relatively slowly applied seismic loading. Long period systems subjected to these pulses have $R = \mu$, for the types of hysteresis behavior studied. The maximum strength reduction factor occurs around $T/T_p = 1$ for both pulses. The pulse R-factors are described as functions of μ and T/t_d or T/T_p, while the ground motion R-factors are described as functions of μ and T. The R-factor spectra generated using the pulses are smoother than those generated using the more irregular ground motions records.

Figure 5.5 shows the R-factor spectra determined using the six conventional $R-\mu-T$ relations (represented by Eqs. 1.9 to 1.14) for the case of the 1940 El Centro earthquake (IV40ELCN.180 record, $T_g = 0.65$ s, $\alpha = 0\%$, $\beta = 5\%$). The R-factor spectra are similar to each other and resemble

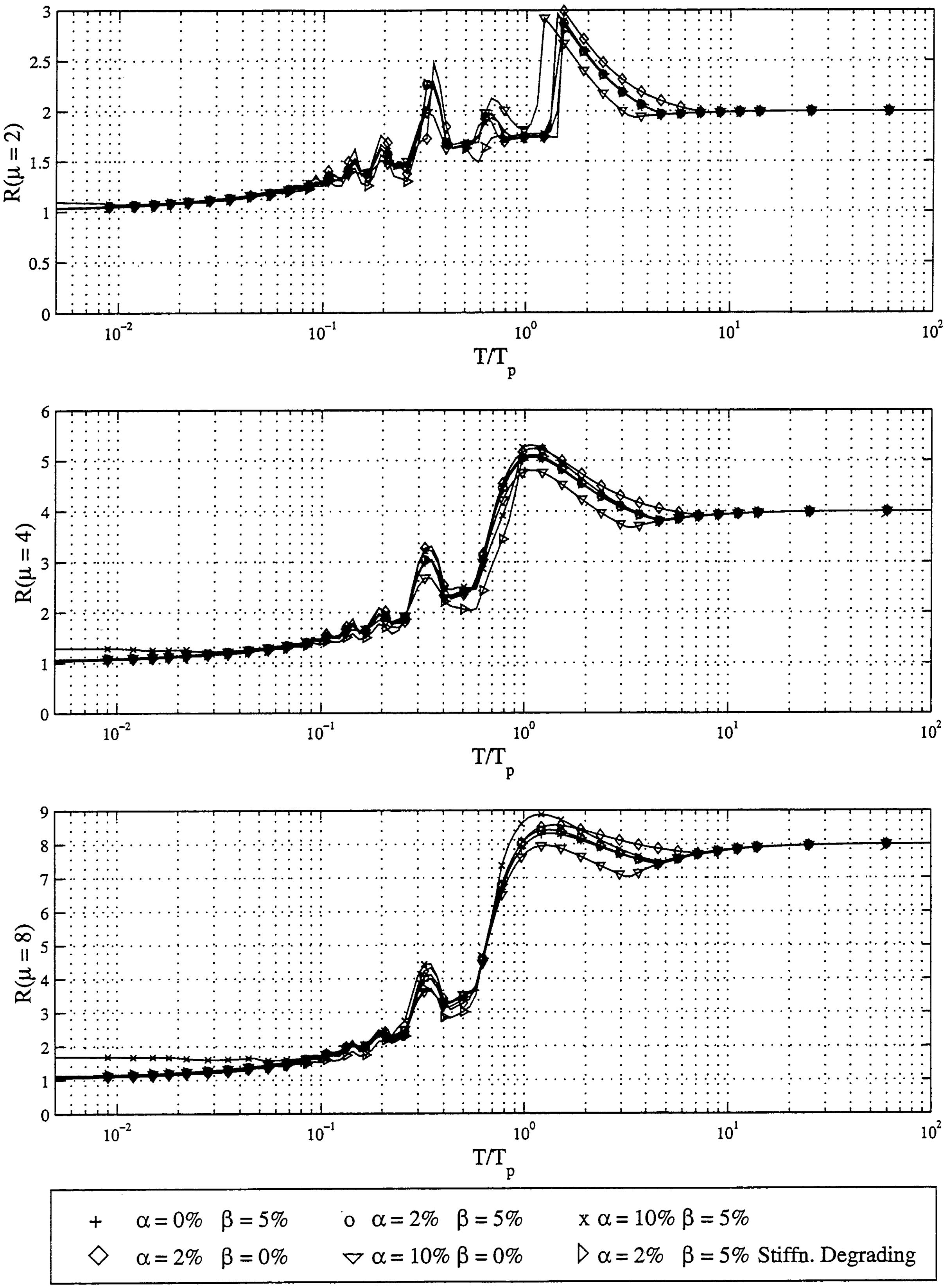

Figure 5.2: R-factor response spectra to the qua(2) pulse

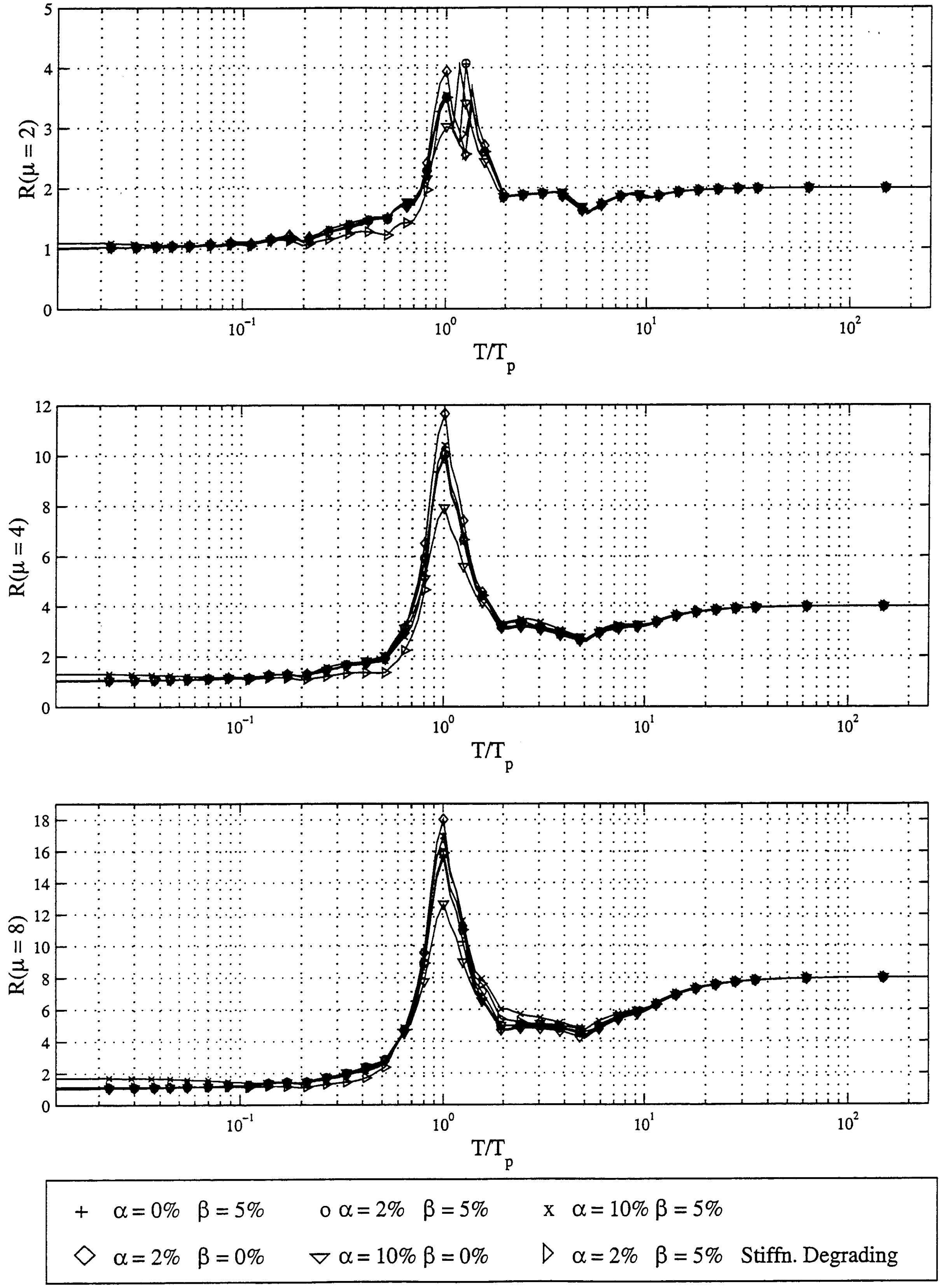

Figure 5.3: R-factor response spectra to the sin(5) pulse

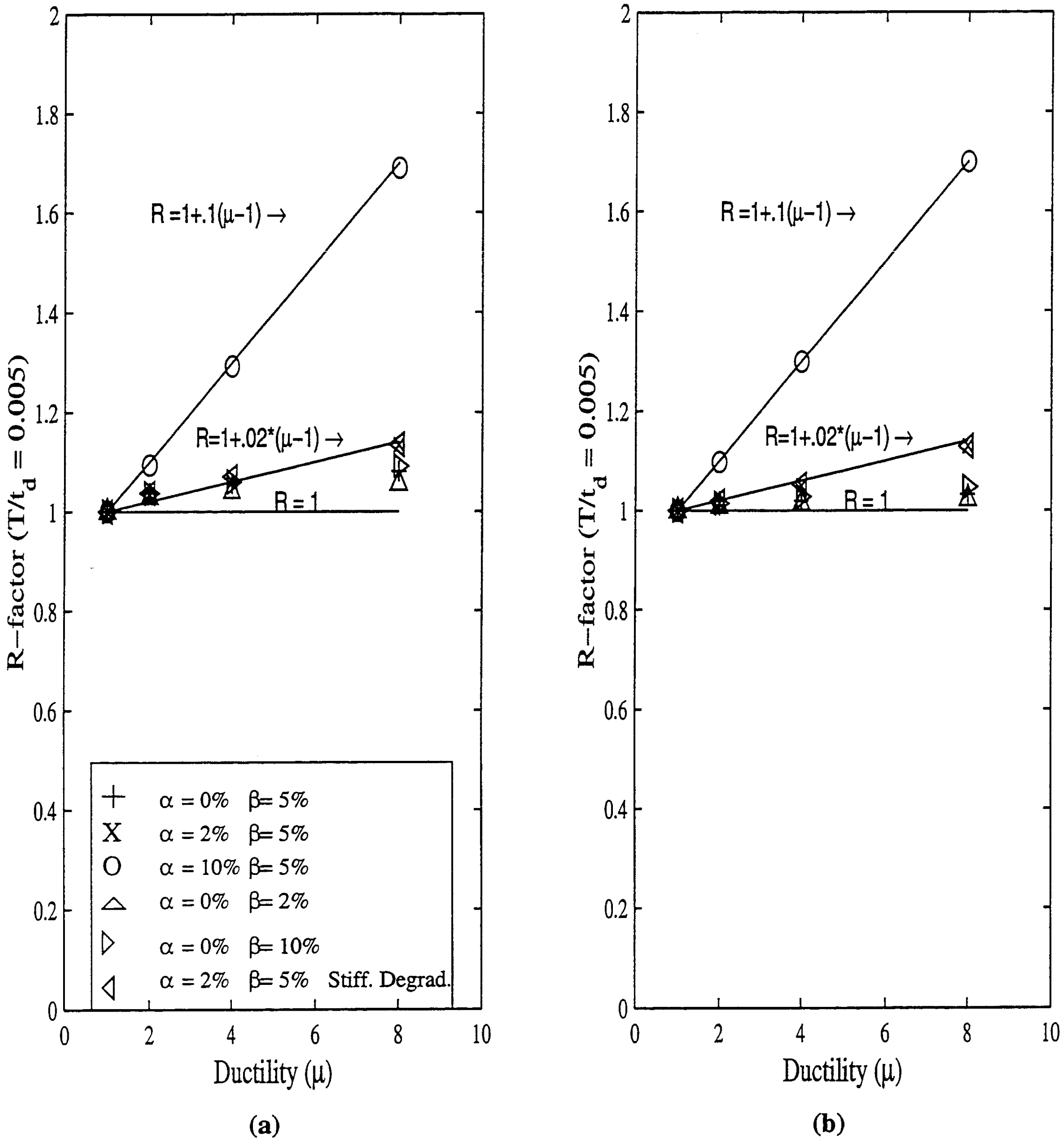

Figure 5.4: R-factor vs. ductility μ for short period systems $T/t_d = 0.005$; (a) to the qua(2) pulse, (b) to the sin(5) pulse

the pulse R-factor spectra (Fig. 5.2), particularly in the short and long period regions. Differences among the R-factor models are more prominent at intermediate periods.

5.3.1 Error Measures

Comparisons between η_y and $\hat{\eta}_y$ were performed for each ground motion and ductility level. Three measures of the error in the strength parameters were developed in Section 4.2.5. For a given ground motion, gm, and ductility, d, the errors given in Eqs. 4.4, 4.5, and 4.6 for estimating the isoductile strength spectra are simplified to:

$$E^{a}_{gm,d} = \frac{1}{n_p} \sum_{m=1}^{np} |\eta_{y,gm,d} - \hat{\eta}_{y,d}| \tag{5.4}$$

$$E^{b}_{gm,d} = \left(\frac{1}{n_p} \sum_{m=1}^{np} [\eta_{y,gm,d} - \hat{\eta}_{y,d}]^2 \right)^{1/2} \tag{5.5}$$

$$E^{c}_{gm,d} = \left(\frac{1}{n_p} \sum_{m=1}^{np} exp\left(|\eta_{y,gm,d} - \hat{\eta}_{y,d}|\right) \right) - 1 \tag{5.6}$$

where:

- n_p = number of periods (n_p = 45 from 0.04 to 3 s)
- gm = ground motion index number (1 to 15)
- d = ductility index number (1 to 3 corresponding to μ = 2, 4, and 8, respectively)

The average error for each ground motion, gm, is given by $E^{s}_{gm,*}$, where the asterisk ($*$) means an average over the ductility variable, and s = a, b, c refers to the error functions given by Eqs. 5.4, 5.5, and 5.6, respectively. The average error over all the records is given by $AE^s = E^{s}_{*,*}$, where the asterisks ($*$) indicate an average over the ground motion and ductility variables.

To estimate strength spectra using the pulse R-factors, it is necessary to first determine the value of the characteristic period of the pulse, T_p, to be used. Three approaches were used to identify

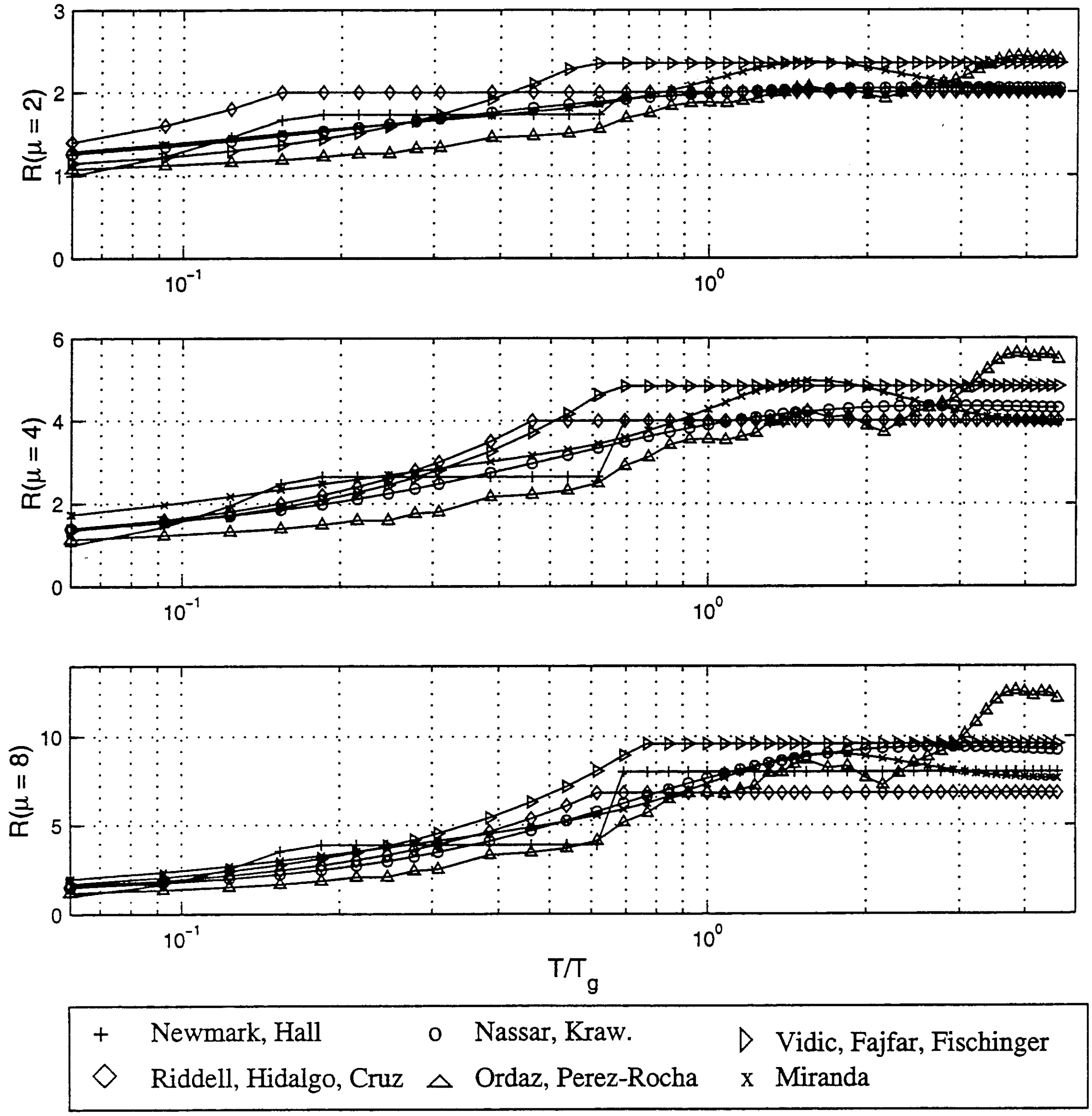

Figure 5.5: Estimated R-factor response spectra for the 1940 N-S component of El Centro earthquake (IV40ELCN.180 record, $T_g = 0.65$ s)

the characteristic periods. In the first approach, the periods $T_p = T_1^*$ were determined to minimize the error function $E^a_{gm,*}$ for elasto-plastic systems having $\beta = 5\%$ (Table 5.2). In the second, T_p was equated to the characteristic period of the ground motion, $T_p = T_g$, determined prior to this study and reported in Table 2.1 and in FEMA-307 [46]. The second approach recognizes that applications to unknown future ground motions will not have the opportunity to fit values of T_1^*, although the specification of a smoothed elastic design response spectrum locates T_g approximately at the intersection of the constant acceleration and constant velocity portions of the spectrum. In the third approach, T_p was equated to the period T_2^*, defined as

$$T_2^* = 2\pi \frac{(S_v)_{max}}{(S_a)_{max}} \tag{5.7}$$

where

- S_v = elastic pseudo-velocity spectrum for elasto-plastic systems having $\beta = 5\%$
- S_a = elastic pseudo-acceleration spectrum for elasto-plastic systems having $\beta = 5\%$

Because $S_a(T) = \eta(T) \cdot a_{g,max}$ and $S_v(T) = \frac{T}{2\pi} S_a(T)$, Eq. 5.7 can be expressed equivalently as:

$$T_2^* = \frac{|T \cdot \eta(T)|_{max}}{|\eta(T)|_{max}} \tag{5.8}$$

Figure 5.6 illustrates the graphical determination of the period T_2^* according to Eq. 5.8 for the CH85VALP.070 record. The curves $T \cdot \eta(T)$ and $\eta(T)$ are plotted as well as the maximum values of both curves. The period $T^a = 1.5$ s defines the period of maximum $T \cdot \eta(T)$, and $\eta^a = 1.173$ is the elastic strength at this period. Since the maximum of $\eta(T)$ is 3.482, Eq. 5.8 provides $T_2^* = \frac{1.173 * 1.5s}{3.482} = 0.505$ s. Figure 5.6 also indicates a graphical method for establishing T_2^*: Various curves proportional to $1/T$ are drawn to intersect the plot of $\eta(T)$. The largest valued $1/T$ curve to intersect $\eta(T)$ does so precisely at the location that ηT is a maximum. This intersection defines the period T and strength parameter $\eta(T)$ at which ηT is easily identified from the plot. The

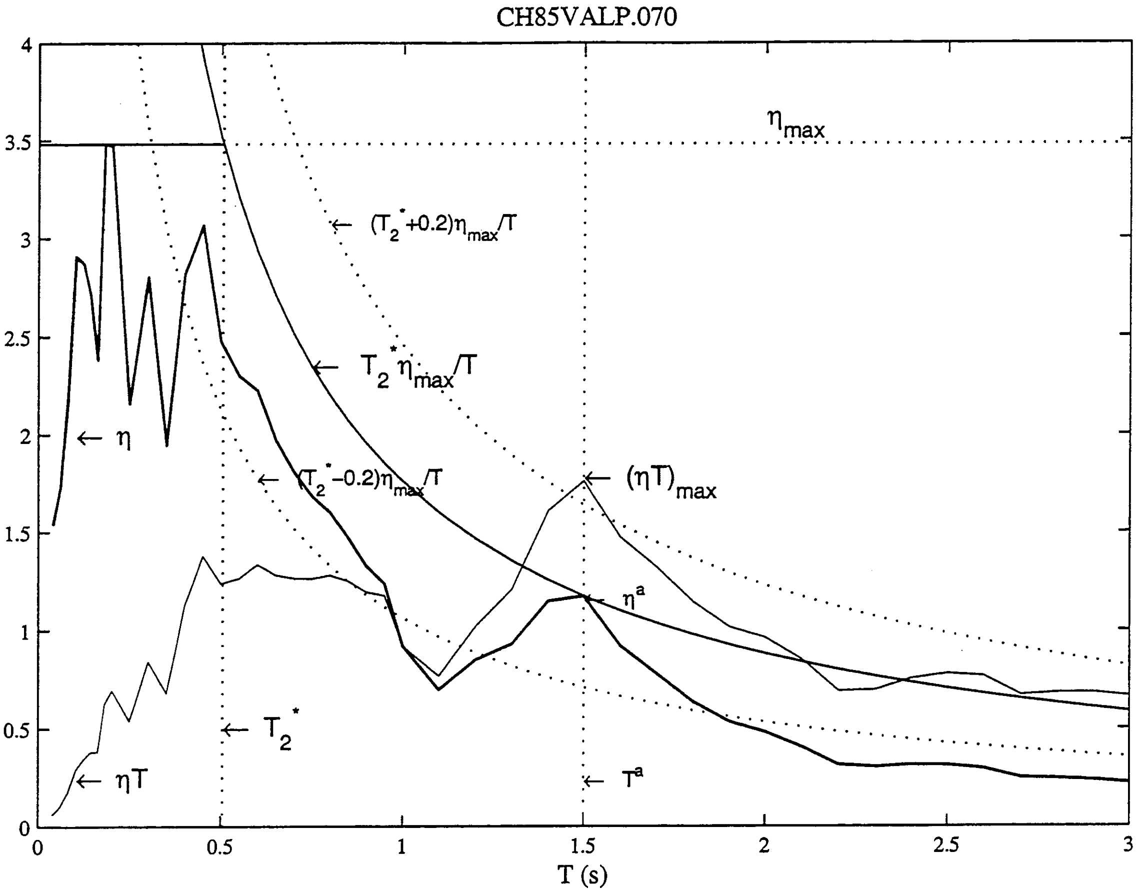

Figure 5.6: Graphical determination of the period T_2^* for the CH85VALP.070 record

values of $|T \cdot \eta(T)|_{max}$ and $|\eta(T)|_{max}$ so determined can be used in Eq. 5.8 to determine T_2^*, or the intersection of the corresponding constant strength and largest valued $1/T$ curves can be determined graphically, with this intersection identifying T_2^*. This graphical intersection is seen to correspond exactly to the intersection of the constant acceleration and constant velocity portions of a smoothed design spectrum.

This technique works perfectly well for harmonic pulses as shown in Figure 5.7 for the sin(5) pulse. In this case peak $T \cdot \eta(T)$ and $\eta(T)$ are reached at the same period ratio $T/T_p = 1$; therefore, $T_2^* = T_p$, resulting in a definition for T_2^* that also is consistent with the period of the harmonic excitation.

Returning to the 15 ground motions, Table 5.1 shows the periods T_g, T_1^*, and T_2^* for each ground motion along with the values T_a determined using the equations proposed by Newmark and Hall

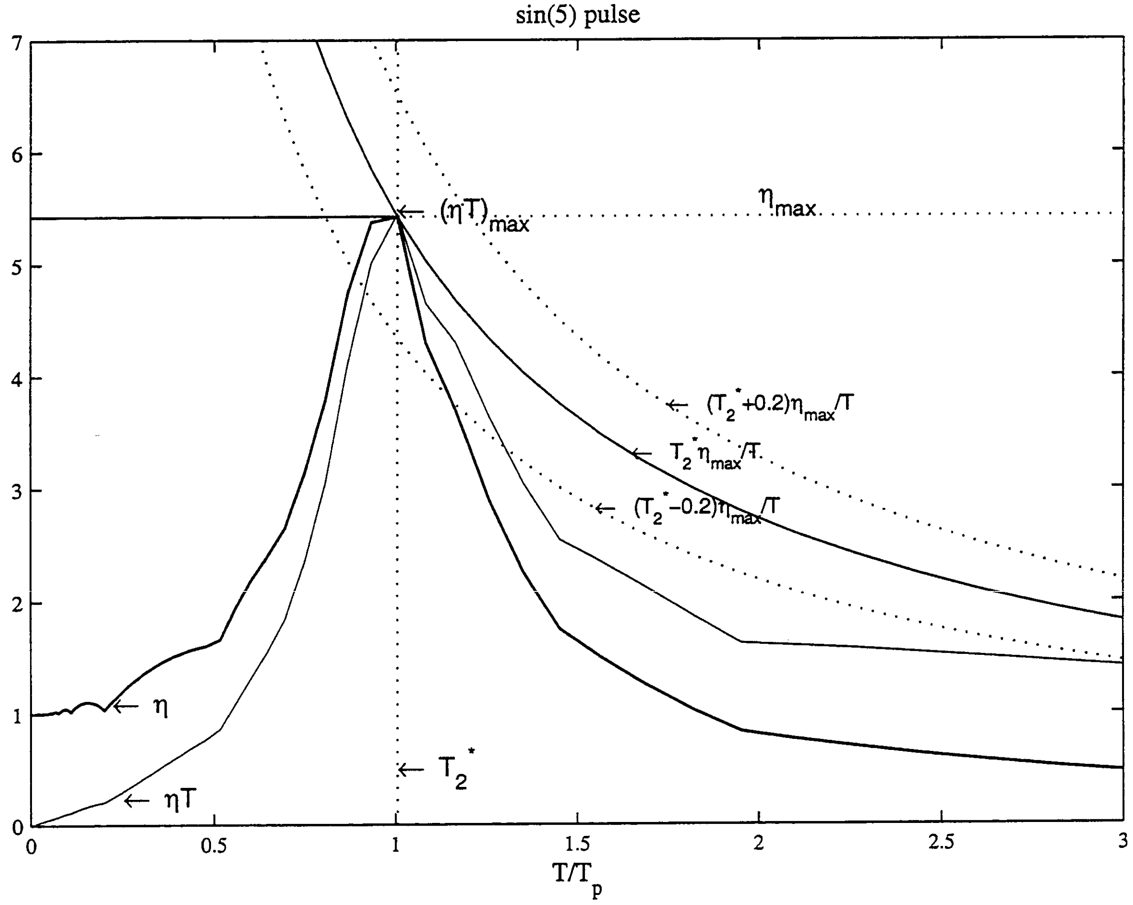

Figure 5.7: Graphical determination of the period T_2^* for the sin(5) pulse

Table 5.1: Periods (in s)

Ground motion	T_g	T_2^*	T_1^*	T_a (Ne.-Hall)	T_a (Vidic)
WN87MWLN.090	0.20	0.17	0.20	0.11	0.11
BB92CIVC.360	0.40	0.30	0.45	0.29	0.29
SP88GUKA.360	0.55	0.40	0.30	0.38	0.42
LP89CORR.090	0.85	0.77	0.55	0.46	0.46
NR94CENT.360	1.00	0.73	0.70	0.52	0.52
CH85LLEO.010	0.30	0.41	0.55	0.26	0.38
CH85VALP.070	0.55	0.51	0.30	0.38	0.55
IV40ELCN.180	0.65	0.56	0.40	0.43	0.43
LN92JOSH.360	1.30	0.86	0.60	0.46	0.46
MX85SCT1.270	2.00	2.00	2.15	1.63	2.53
LN92LUCN.250	0.20	0.41	0.30	0.89	0.89
LP89SARA.360	0.40	0.59	0.60	0.38	0.38
NR94NWHL.360	0.80	0.69	0.75	0.74	0.74
NR94SYLH.090	0.90	0.75	1.10	0.59	0.59
KO95TTRI.360	1.40	1.25	0.75	0.89	1.00

and Vidic et al. for use with their R-factor relations (Eqs. 1.9 and 1.13, respectively). The values of T_a determined for the Newmark-Hall and Vidic equations are similar, while there is greater spread among the values of T_g, T_1^*, and T_2^*, with T_2^* often intermediate between T_1^* and T_g.

The error $E_o^s = E_{gm,*}^s$ determined using the qua(2) pulse or the sin(5) pulse with $T_p = T_1^*$ is taken as a reference to gauge the error obtained when the pulses are used with $T_p = T_g$ and $T_p = T_2^*$, and when the six R-factor models are applied. The normalized error, given by the ratio $NE_{gm,*}^s = E_{gm,*}^s / E_o^s$ indicates how good the estimate is compared to the reference value. If $NE_{gm,*}^a < 1$, the estimate is better than the one obtained with the pulses using $T_p = T_1^*$, and is worse if $NE_{gm,*}^a > 1$. Finally, the overall error is the average of $NE_{gm,*}^s$ over all the ground motions, $OE^s = NE_{*,*}^s$.

5.3.2 Findings

Table 5.2 shows the normalized errors $NE_{gm,*}^a$ and the overall errors $OE_{*,*}^a$ for the 5% damped elasto-plastic systems. The errors were computed for the six contemporary $R - \mu - T$ relations and for the pulse R-factors obtained using $T_p = T_g$, T_1^*, and T_2^*, where T_2^* is described in Section

5.3.1. All the R-factor relations except the pulse R-factor and the Ordaz and Pérez-Rocha relation give poor estimates of isoductile strengths for the MX85SCT1.270 record, where the largest $NE^{a}_{gm,*}$ values occur (1.726 to 3.331). No clear difference in the error estimates emerges with respect to the classification of SD, LD, and FD records. The best SD estimates are made using the pulses having $T_p = T_1^*$ (1.000) and the Vidic et al. $R-\mu-T$ relation (0.978); the best LD and FD estimates are made using the pulses having $T_p = T_1^*$. The rest of the models do not present a consistent trend. Considering all 15 ground motions, the smallest OE^a occurs using the pulses with $T_p = T_1^*$, (1.000) followed by the pulses with $T_p = T_2^*$ (1.111), Vidic et al. (1.157), the pulses with $T_p = T_g$ (1.162), and Ordaz and Pérez-Rocha (1.164) relations. The other models have OE^a ranging from 1.209 to 1.389.

Each of the six contemporary $R-\mu-T$ relations was developed for specific load-deformation models, defined by particular values of α, β, and the choice of hysteretic relation. Average errors, $AE^s = E^s_{*,*}$, determined using these $R-\mu-T$ relations are reported in Table 5.4 for a variety of load-deformation responses, along with the errors resulting when the pulse R-factors are determined for each particular load-deformation response. For each case, the pulse R-factors are determined for $T_p = T_g$, T_1^*, and T_2^*. The periods T_1^*, obtained for the systems having $\alpha = 0\%$ and $\beta = 5\%$, were used for systems having other hysteretic or damping characteristics. The largest errors in the strength estimates occurred for systems having $\alpha = 0\%$ and $\beta = 2\%$, the smallest errors were obtained for systems having $\alpha = 0\%$ and $\beta = 10\%$, and the errors are similar and intermediate between the best and worst cases for the remaining systems ($\alpha = 0$, 2, and 10% with $\beta = 5\%$, and the stiffness degrading systems). This result applies for each error measure and for each of the R-factor models (including the pulses), indicating that damping has a greater influence in reducing scatter in isoductile strengths than does the hysteretic behavior of the system (systems with negative values of α were not part of this study but also may be prone to large scatter in isoductile strengths). Nevertheless, the errors given by the pulse estimates with $T_p = T_g$, T_1^*, and T_2^* are similar to or smaller than the errors obtained using the other models for the six types of systems studied, for each of the three error measures. Only the Vidic et al. relation gives similar accuracy. Both the

Table 5.2: Errors $NE^a_{gm,*}$ and OE^a using the pulses and 6 R-factor models. The pulse R-factors are calculated with T_p equal to T_1^*, T_2^*, and T_g. The errors are computed for elasto-plastic SDOF systems having 5% damping

G. M.	Pulses			Newm., Hall	Riddell, et al.	Nassar, Kraw.	Miran.*	Vidic et al.*	Ordaz, P-R
	$T_p = T_1^*$	$T_p = T_2^*$	$T_p = T_g$						
Records	E_o^a	$NE^a_{gm,*}$	$NE^a_{gm,*}$	$NE^a_{gm,*}$	$NE^a_{gm,*}$	$NE^a_{gm,*}$	$NE^a_{gm,*}$	$NE^a_{gm,*}$	$NE^a_{gm,*}$
1	0.067	0.904	1.000	0.851	1.388	1.776	1.373	0.881	0.657
2	0.069	1.184	1.000	1.116	0.986	1.159	1.261	0.957	0.841
3	0.067	1.209	1.269	1.254	1.119	1.299	1.418	1.030	1.537
4	0.090	1.244	1.344	1.144	1.300	1.133	1.122	1.000	1.233
5	0.094	1.040	1.330	1.170	1.234	0.968	1.064	1.021	1.128
6	0.073	1.200	1.356	1.301	1.178	0.890	0.877	1.315	1.178
7	0.103	1.291	1.311	1.049	1.068	1.058	1.097	1.126	1.175
8	0.086	1.121	1.105	1.186	1.209	1.023	1.058	0.895	1.395
9	0.105	1.041	1.171	1.133	1.333	1.067	1.152	1.181	0.629
10	0.133	1.063	1.060	2.165	3.331	3.008	1.887	1.726	1.105
11	0.127	1.039	1.039	1.559	1.016	1.008	0.961	1.433	1.819
12	0.076	0.991	1.276	1.079	1.132	0.947	1.053	1.211	1.237
13	0.079	1.182	1.025	1.633	1.671	1.354	1.304	1.228	1.557
14	0.085	1.120	1.094	1.106	1.447	1.129	1.459	1.341	1.035
15	0.137	1.027	1.044	1.000	1.431	1.175	1.051	0.993	0.942
Category	OE^a	OE^a	OE^a	OE^a	OE^a	OE^a	OE^a	OE^a	OE^a
SD	1.000	1.116	1.189	1.107	1.205	1.267	1.248	0.978	1.079
LD	1.000	1.143	1.201	1.367	1.624	1.409	1.214	1.250	1.096
FD	1.000	1.072	1.096	1.275	1.339	1.123	1.165	1.241	1.318
$\forall g.m.$	1.000	1.111	1.162	1.250	1.389	1.266	1.209	1.157	1.164

* Model not developed for elasto-plastic SDOF systems

Table 5.4: Average errors AE^s for the six types of hysteresis SDOF systems using 6 R-factor models and the pulses with $T_p = T_1^*$, T_2^*, and T_g

	Bilinear model					Stiff. Deg.	
$R-\mu-T$ Relation	$\alpha = 0\%$ $\beta = 5\%$	$\alpha = 0\%$ $\beta = 2\%$	$\alpha = 0\%$ $\beta = 10\%$	$\alpha = 2\%$ $\beta = 5\%$	$\alpha = 10\%$ $\beta = 5\%$	$\alpha = 2\%$ $\beta = 5\%$	Row Average
	AE^a	AE^a	AE^a	AE^a	AE^a	AE^a	
Newmark et al[x]	0.119	0.173	0.093	0.119	0.125	0.125	0.126
Riddell et al[x]	0.135	0.173	0.112	0.132	0.126	0.139	0.136
Nassar et al	0.121	0.173	0.097	0.120	0.112	0.128	0.125
Miranda[+]	0.112	0.160	0.092	0.112	0.110	0.122	0.118
Vidic et al[+]	0.109	0.147	0.091	0.104	0.101	0.111	0.111
Ordaz et al[x]	0.108	0.158	0.082	0.113	0.132	0.113	0.118
Pulses, $T_p = T_g$	0.107	0.164	0.077	0.105	0.107	0.115	0.113
Pulses, $T_p = T_2^*$	0.102	0.153	0.075	0.101	0.100	0.108	0.106
Pulses, $T_p = T_1^*$	0.093	0.142	0.073	0.090	0.092	0.101	0.099
	AE^b	AE^b	AE^b	AE^b	AE^b	AE^b	
Newmark et al[x]	0.188	0.283	0.146	0.189	0.197	0.194	0.200
Riddell et al[x]	0.187	0.255	0.154	0.184	0.177	0.187	0.191
Nassar et al	0.177	0.272	0.135	0.174	0.162	0.181	0.184
Miranda[+]	0.167	0.252	0.130	0.167	0.167	0.177	0.177
Vidic et al[+]	0.164	0.235	0.132	0.158	0.155	0.167	0.169
Ordaz et al[x]	0.171	0.262	0.125	0.182	0.210	0.178	0.189
Pulses, $T_p = T_g$	0.161	0.257	0.111	0.159	0.164	0.174	0.171
Pulses, $T_p = T_2^*$	0.156	0.250	0.109	0.155	0.156	0.164	0.165
Pulses, $T_p = T_1^*$	0.143	0.230	0.107	0.139	0.141	0.156	0.153
	AE^c	AE^c	AE^c	AE^c	AE^c	AE^c	
Newmark et al[x]	0.155	0.300	0.110	0.158	0.168	0.165	0.176
Riddell et al[x]	0.162	0.246	0.128	0.159	0.152	0.169	0.169
Nassar et al	0.147	0.253	0.110	0.145	0.133	0.156	0.157
Miranda[+]	0.131	0.217	0.102	0.131	0.131	0.144	0.143
Vidic et al[+]	0.129	0.207	0.101	0.123	0.122	0.133	0.136
Ordaz et al[x]	0.133	0.237	0.093	0.141	0.169	0.142	0.153
Pulses, $T_p = T_g$	0.124	0.217	0.084	0.122	0.125	0.135	0.135
Pulses, $T_p = T_2^*$	0.119	0.204	0.082	0.117	0.117	0.126	0.127
Pulses, $T_p = T_1^*$	0.106	0.182	0.079	0.103	0.105	0.117	0.115

[x] Model developed for elasto-plastic SDOF systems

[+] Model developed for bilinear SDOF systems

Vidic et al. relation and the pulse R-factor model depend on the frequency characteristics of the ground motion (via the terms T_g, T_1^*, T_2^*, and T_a), indicating the need to explicitly consider ground motion frequency content in the specification of the strength-reduction factor.

The pulse R-factors only require specification of the pulse shape and a characteristic period of the ground motion, whether described by T_g or T_2^*. The Vidic et al. relation requires specification of T_a, which is based on estimates of the pseudo-velocity and pseudo-acceleration derived from peak ground velocity and peak ground acceleration. In many ways T_g, T_2^*, and T_a describe similar characteristics (note they vary together with the ground motions in Table 5.1) but are evaluated by different procedures. Both T_2^* and T_a depend on details of the ground motions that may not be known well prior to the event, while the values of T_g that are reported in FEMA-307 [46] were determined by eye to match approximately the intersection of the constant acceleration and constant velocity regions of a smoothed spectrum fit to the 5% damped elastic spectrum, with consideration given to the equivalent velocity spectrum. The manner of defining T_g and T_2^* make them correspond approximately to the period T_s used in the NEHRP *Provisions* [2], where smoothed design spectra are used. Both T_2^* and T_a may be determined easily when ground motion records are available. Given the goodness of the bilinear relation used by Vidic et al., the precise curve described by the pulse R-factor may not be of critical importance, and a bilinear approximation such as employed by Vidic et al. may be appropiate given the uncertainties inherent in establishing future ground motions and their response spectra. Compared with a bilinear approximation, the pulse R-factors, however, are also applicable to soft soil sites, and because of their implicit definition, may be useful for systems with load-deformation responses that differ from those studied in previous investigations. Other contemporary approaches were less accurate and in some cases require posterior knowledge of the ground motion characteristics (e.g. Newmark and Hall [21], Vidic et al [25], and Ordaz and Pérez-Rocha [26]).

5.4 Summary

Inelastic spectra were estimated with reasonable accuracy using the quadratic pulse qua(2) for 14 of the 15 records studied. A sinusoidal pulse was needed for the soft soil SCT record of the 1985 Michoacan earthquake. The estimates of the strength response spectra using these pulses tended to have less error relative to the estimates made using six contemporary $R-\mu-T$ relations. The pulse R-factors require the identification of a characteristic pulse period, T_p, or pulse duration, t_d. The isoductile strengths were estimated with greatest accuracy when the characteristic period of the pulse, T_p, was set equal to the period T_1^*. Estimates obtained by setting T_p equal to the characteristic period of the ground motion, T_g, or the period T_2^* also proved to be acceptable, as did the estimates made using the Vidic et al. relation. That the smallest errors in the estimates of inelastic response spectra were obtained using the pulse R-factors and those recommended by Vidic et al. suggest that $R-\mu-T$ relations should be formulated in terms of T/T_g, T/T_2^*, or T/T_a rather than T alone, to explicitly address ground motion frequency characteristics.

Even though it was found necessary to use a harmonic pulse to generate suitable R-factors for the Mexico City SCT record, R-factors clearly exhibit a degree of waveform independence that allows R-factors determined for simple pulses to be used to estimate the inelastic response spectra of a highly varied set of ground motions. Furthermore, the estimates tended to be slightly better than those obtained using contemporary $R-\mu-T$ relations. Since the R-factors are implicit once the pulse shape and duration have been identified, they can be generated for different load-deformation and hysteretic relations, while the parameters that define contemporary $R-\mu-T$ relations require numerical evaluation by considering the response of a specific load-deformation model for a large number of ground motions.

Chapter 6

Estimating the Response of Multistory Buildings Using Pulse R-Factors

6.1 Introduction

This chapter applies pulse R-factors to estimate the peak response of multi-degree-of-freedom (MDOF) systems. Previous chapters have shown that the response of inelastic SDOF systems to ground motions can be estimated using pulse R-factors instead of the more precise R-factors computed for each specific ground motion. This chapter addresses whether this simplification applies to buildings with more than one degree-of-freedom.

The parameters by which the dynamic response of multistory buildings is assessed in this chapter are the peak roof displacement and interstory drift index (IDI). These quantities are computed by nonlinear dynamic analysis using the program DRAIN-2DX [61]. Estimates of peak roof displacement and IDIs are determined using the "equivalent" SDOF modeling technique [62, 63] to transform a MDOF system into an equivalent SDOF system. The nonlinear response of the equivalent SDOF system is estimated using $R-\mu-T$ relations determined from the pulse R-factor model, the Vidic et al. [25] recommendations, and the actual response to each ground motion record. Four moment-resistant frame buildings originally designed by Black [64] are analyzed.

Three methods to estimate the interstory drift index are presented. One of the methods requires only the first mode of vibration, and the other two utilize both the first and second modes of vibration, as discussed by Black [64].

6.2 Equivalent SDOF Modeling of Multistory Buildings

Equivalent SDOF models of multistory buildings have become widely used during recent years. Experimental and analytical studies have shown equivalent SDOF models to result in good estimates of the displacement responses of buildings [33, 64, 54, 53]. Moreover, ATC-40 [62] and FEMA-273/274 [63] have presented equivalent SDOF approaches for the evaluation of multistory buildings.

The assumptions involved in replacing a MDOF system with an equivalent SDOF system are that the lateral displacement response is mainly in a single mode, and that the mode shape may be assumed to remain constant throughout the response. The transformation of the MDOF system to an equivalent SDOF system is derived in Chapter 3 of FEMA-274 and also in Black's thesis [64].

Following the terminology used by several researchers [64, 7, 6], the MDOF system having mass lumped at each story level is approximated by a SDOF system with a specified yield displacement and yield strength. The equivalent SDOF yield displacement, u_y^{sdof}, is given by

$$u_y^{sdof} = \frac{M_{eq}}{L_{eq}} u_y^{mdof} \tag{6.1}$$

where:

- u_y^{mdof} = yield displacement of the MDOF system obtained with a nonlinear static (pushover) analysis

- $\frac{L_{eq}}{M_{eq}}$ = participation factor, given by

$$\frac{L_{eq}}{M_{eq}} = \frac{\{\phi\}^T M \{1\}}{\{\phi\}^T M \{\phi\}} \tag{6.2}$$

  where:

  - M_{eq} = mass of the equivalent SDOF system, with $M_{eq} = \{\phi\}^T M \{\phi\}$, where $\{\phi\}$ is the mode shape vector and M is the diagonal mass matrix of the MDOF system
  - L_{eq} = modal earthquake excitation factor, with $L_{eq} = \{\phi\}^T M \{1\}$. The column $\{1\}$ represents a unit static translation at the base of the structure producing directly a unit displacement of all degrees of freedom [7].

  The value L_{eq}/M_{eq} depends on the manner in which $\{\phi\}$ is normalized. This thesis adopts the common convention in which $\{\phi\}$ is normalized to have unit amplitude at the roof. This quantity depends on the characteristics of the structure only. If the input motion has uniform frequency content (white noise), L_{eq}/M_{eq} represents the extent to which the motion excites response in the assumed mode [7].

The equivalent SDOF yield strength parameter, η_y^{sdof} is given by

$$\eta_y^{sdof} = \frac{V_y^{mdof}}{\alpha_e \cdot W_t} \cdot \frac{g}{a_{g,max}} \tag{6.3}$$

where:

- V_y^{mdof}= yield strength of the MDOF system
- $a_{g,max}$ = peak ground acceleration, given in Table 2.1
- g = gravity acceleration
- W_t = total weight of the building, $W_t = M_t \cdot g$, where $M_t = \{1\}^T M \{1\}$ is the total mass of the system

- α_e = effective modal mass coefficient, given by

$$\alpha_e = \frac{L_{eq}^2}{M_{eq} \cdot M_t} = \frac{\{\phi\}^T M\{1\}\,\{\phi\}^T M\{1\}}{\{\phi\}^T M\{\phi\}\,\{1\}^T M\{1\}} \tag{6.4}$$

the term L_{eq}^2/M_{eq} is called the effective modal mass and has dimensions of mass.

6.3 Methodology Using the Pulse R-Factors

This section describes the steps to be used to estimate peak roof displacements and interstory drift indices of the building frames. These steps are applied to the 4-story and 12-story frames in Section 6.4. The first four steps to develop the estimates of peak roof displacements and interstory drift indices consist of calculating the equivalent SDOF system corresponding to the MDOF system. These four steps are:

1. Determine the first and second periods of vibration, T_1 and T_2, the first and second mode shapes of the MDOF system, $\{\phi_1\}$ and $\{\phi_2\}$, normalized to unity at the top of the building, based on elastic vibration properties (mass and stiffness).
2. Determine the yield displacement and yield strength of the MDOF system with a pushover analysis, u_y^{mdof} and V_y^{mdof}, respectively. The building is subjected to either a monotonically increasing set of lateral forces or a monotonically increasing set of lateral displacements until a given target displacement is reached. Consistent with many researchers, lateral forces proportional to the product of the modal amplitude and floor mass are applied at each floor level in this thesis. Because mass was uniform over the height of the building, this happens to coincide with applying lateral forces proportional to the mode shape. Thus, the lateral forces have a shape similar to the deformed shape of the building when subjected to the ground motion, that is, the first and second modes of vibration, which determine the yield strength and yield displacement associated with each mode. A plot of roof displacement versus base shear force is defined as the "capacity curve."

3. Determine the participation factor L_{eq}/M_{eq} (Eq. 6.2) and the effective modal mass coefficient α_e (Eq. 6.4) for each mode of vibration.

4. Determine the yield displacement and yield strength of the equivalent SDOF system using Eqs. 6.1 and 6.3, u_y^{sdof} and η_y^{sdof}, respectively, for the two modes of vibration. Often this requires fitting a bilinear curve to the computed capacity curve, with the yield strength and yield displacement determined by the break point in the bilinear curve

Accurate estimates of peak roof displacement often may be obtained using only the first mode of vibration. Interstory drift index estimates often require data corresponding to two or more modes; only the first two modes are considered here.

6.3.1 Estimating Peak Displacement Using the Pulse R-Factors

The buildings to be analyzed were designed assuming viscous damping equal to 5% of critical damping in the first mode of vibration [64]. The pushover analyses of the buildings under study show that the load-deformation capacity curves can be represented approximately as bilinear systems with post-yield stiffness equal to approximately 10% of the initial stiffness. To achieve "equivalence" in representing the response of a multistory structure responding in a single mode by a SDOF system, the pulse R-factor response spectra used in estimating the responses of the multistory buildings should have similar damping (5%) and post-yield stiffness (10%). Only the yield displacement and yield strength of the building in the first mode of vibration are required to estimate the peak roof displacement. After following steps 1 to 4 of Section 6.3, the next steps to estimate the peak displacement of the MDOF system are the following, where each ground motion has the characteristic period, T_g, given in Table 2.1:

1. Calculate the equivalent SDOF elastic strength parameter, $\eta_e^{sdof} = \eta(\mu = 1, T = T_1)$.

2. If $\eta_e^{sdof} > \eta_y^{sdof}$ (Eq. 6.3), then, the strength reduction factor is the ratio

$$R^{sdof} = \frac{\eta_e^{sdof}}{\eta_y^{sdof}} \tag{6.5}$$

otherwise, the response is elastic and the strength reduction factor is given by $R^{sdof} = 1$.

3. Determine the ductility demand of the SDOF system, using a SDOF system having period T_1 and a strength reduction factor R^{sdof} for a specified pulse shape having a characteristic period T_p equal to the characteristic period of the ground motion,

$$\mu = \mu(R = R^{sdof}, T = T_1, T_p = T_g) \tag{6.6}$$

4. Estimate the peak roof displacement of the MDOF system as

$$u_u^{mdof} = \frac{L_{eq}}{M_{eq}} \cdot \mu \cdot max(u_{el}^{sdof}) \tag{6.7}$$

where $max(u_{el}^{sdof})$ is the maximum elastic displacement of the equivalent SDOF system. If the response of the systems is elastic, ($R^{sdof} = 1$), then $max(u_{el}^{sdof}) = u_e^{sdof}$, where

$$u_e^{sdof} = \frac{T_1^2}{4\pi^2} \cdot a_{g,max} \cdot \eta_e^{sdof} \tag{6.8}$$

If the response is nonlinear, $R^{sdof} > 1$, then $max(u_{el}^{sdof}) = u_y^{sdof}$. Using Eq. 6.1, Eq. 6.7 results in $u_u^{mdof} = \mu \cdot u_y^{mdof}$.

6.3.2 Estimating Interstory Drift Index Using the Pulse R-Factors

The interstory drift index (IDI) is a measure used to quantify local damage in a building. It is defined as the displacement of any floor relative to the floor immediately below, normalized by the story height. Although the peak IDI of each story can be reached at different times during the response of the building, the equivalent SDOF methodology assumes that the deformed shape remains constant during the response and the peak IDI of each story is reached with the same deformed shape given.

According to several investigators that have studied the IDI over the last years [65, 55, 54], the peak IDI can be related to the roof drift index (defined as the peak roof displacement normalized by the building height) by a quantity known as the coefficient of distortion (COD). The coefficient of distortion is, therefore, based on the deformed shape of the building when the maximum roof displacement occurs. Estimates of IDI will be made using three different but related techniques, following Black [64]. The estimates of IDI require independent estimates of the peak roof displacement given by Eq. 6.7 for each of the first two modes of vibration. The following three techniques and equations are employed for estimating the maximum IDI of all separate floor IDI maxima:

1. The IDI depends only on one deformed shape, corresponding to the fundamental mode of vibration as follows

$$IDI_i^a = u_{u1}^{mdof} \cdot IDI_i(\phi_1) \tag{6.9}$$

2. Two IDI estimates that depend on two deformed shapes, associated with the first and second mode of vibration

$$IDI_i^b = \sqrt{\sum_{j=1}^{2} (u_{uj}^{mdof} \cdot IDI_i(\phi_j))^2} \tag{6.10}$$

$$IDI_i^c = \sum_{j=1}^{2} \mid u_{uj}^{mdof} \cdot IDI^i(\phi_j) \mid \tag{6.11}$$

where:

- IDI_i^s = estimated interstory drift index for the i^{th} story, where $s = a, b, c$ corresponds to the techniques (a), (b), and (c). Each estimated IDI is named IDI^a, IDI^b, and IDI^c to refer to Eqs. 6.9, 6.10, and 6.11, respectively.

- u_{uj}^{mdof}= peak roof displacement given by Eq. 6.7 for the j^{th} mode of vibration.

- $IDI_i(\phi_j)$ = modal interstory drift index for the i^{th} story, defined as the interstory drift index calculated for the assumed deformed mode shape $\{\phi_j\}$.

6.4 Peak Roof Displacement and IDI Estimates for 4- and 12-Story Frames

6.4.1 Characteristic of the Frames

Four moment-resistant steel frame buildings having three bays were used for the MDOF systems; two 4-story frames representing low-rise buildings and two 12-story frames representing medium-height buildings. Each building of each pair was designed by Black [64] to achieve a roof drift of 1.5% under a design earthquake ground motion, corresponding to the drift limit recommended in Vision 2000 [66] for the life safety performance objective. Relatively weak earthquake ground motions were used for the design of buildings labeled "Flexible" while relatively strong ground motions were used for the design of the buildings labeled "Rigid". No gravity load was applied since the frames were only designed and analyzed only for lateral force. The resulting buildings were named Flexible-4, Rigid-4, Flexible-12, and Rigid-12, and were designed to resist the LN92LUCN.270, NR94NWHL.360, MX85SCT1.270, and KO95TTRI.360 records (Table 2.1), respectively.

Mass- and stiffness- proportional damping factors were set to produce 5% damping in the 1^{st} and 4^{th} modes for the 4-story frames, and in the 1^{st} and 6^{th} modes for the 12-story frames. The damping associated with the 2^{nd} mode of vibration was 2.8% for the 4- and 12-story frames.

All the buildings have uniform mass distribution, with columns fixed at the base, and a lower story height of 5 meters and the remaining stories each 4 meters high. The total weight of each 4-story building was 2,204 kN, and each 12-story building weighed 6,612 kN. Each bay is 8 meters wide from center to center of the columns. The steel is Grade A36. More details of the buildings can be found in Black's thesis [64].

Table 6.1: Characteristics of the buildings for the 1^{st} mode of vibration

	Flexible-4	Rigid-4	Flexible-12	Rigid-12
$\frac{L_{eq}}{M_{eq}}$	1.266	1.308	1.372	1.406
α_e	0.875	0.846	0.786	0.766
V_y^{mdof} (kN)	585	1500	1145	3100
u_y^{mdof} (m)	0.129	0.133	0.353	0.335
T_1 (s)	1.16	0.71	2.17	1.25

Table 6.2: Characteristics of the buildings for the 2^{nd} mode of vibration

	Flexible-4	Rigid-4	Flexible-12	Rigid-12
$\frac{L_{eq}}{M_{eq}}$	0.363	0.401	0.568	0.615
α_e	0.096	0.121	0.118	0.125
V_y^{mdof} (kN)	575	1250	954	2150
u_y^{mdof} (m)	0.035	0.030	0.110	0.091
T_2 (s)	0.38	0.25	0.80	0.48

Table 6.1 shows the values of the participation factor, L_{eq}/M_{eq}, the effective modal mass coefficient, α_e, the MDOF yield strength and yield displacements obtained with a push-over analysis in the first mode of vibration, and the fundamental period of vibration of each building. Table 6.2 shows the same information but for the second mode of vibration. Tables 6.3 and 6.4 show the first and second mode shapes, normalized to unity at the top of the building, and the modal IDI for each mode shape for the 4-story frames and 12-story frames, respectively. Figure 6.1 shows the first and second modes of vibration of the 4- and 12-story buildings.

Table 6.3: Mode shapes and modal interstory drift indices of the 4-story buildings for the first and second mode of vibration

Story No.	Story Height	Flexible-4				Rigid-4			
	(m)	$\{\phi_1\}$	$IDI(\phi_1)$	$\{\phi_2\}$	$IDI(\phi_2)$	$\{\phi_1\}$	$IDI(\phi_1)$	$\{\phi_2\}$	$IDI(\phi_2)$
4	4	1.0000	3.66%	1.0000	27.74%	1.0000	5.03%	1.0000	31.14%
3	4	0.8536	6.45%	-0.1097	23.34%	0.7989	7.08%	-0.2457	21.33%
2	4	0.5957	7.06%	-1.0432	-3.35%	0.5157	6.04%	-1.0989	-5.88%
1	5	0.3134	6.27%	-0.9093	-18.19%	0.2743	5.49%	-0.8638	-17.28%

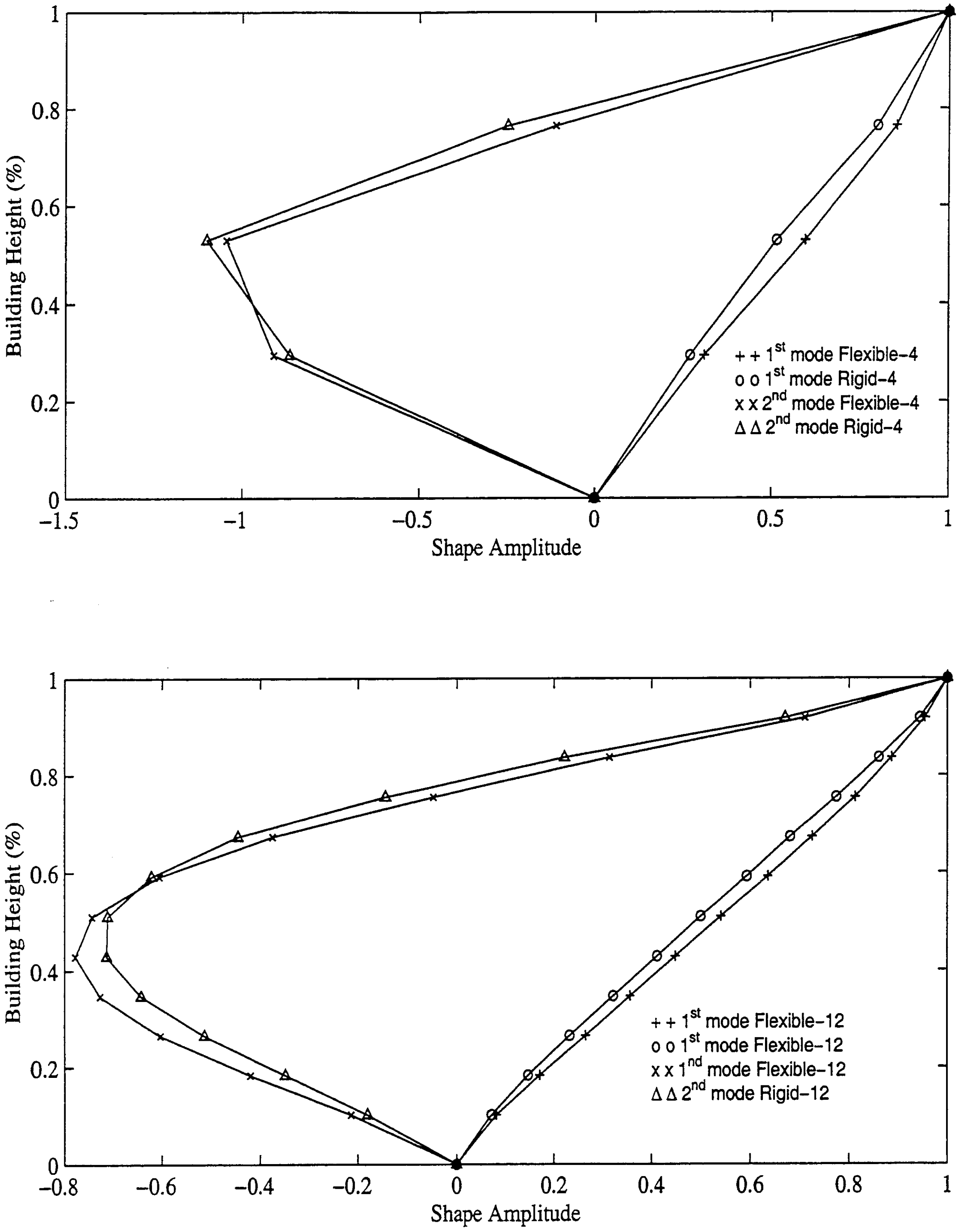

Figure 6.1: First and second mode shapes for the 4- and 12-story buildings

Table 6.4: Mode shapes and modal interstory drift indices of the 12-story buildings for the first and second mode of vibration

Story No.	Story Height	Flexible-12				Rigid-12			
	(m)	$\{\phi_1\}$	$IDI(\phi_1)$	$\{\phi_2\}$	$IDI(\phi_2)$	$\{\phi_1\}$	$IDI(\phi_1)$	$\{\phi_2\}$	$IDI(\phi_2)$
12	4	1.0000	1.13%	1.0000	7.23%	1.0000	1.40%	1.0000	8.24%
11	4	0.9546	1.70%	0.7109	9.96%	0.9442	2.09%	0.6703	11.23%
10	4	0.8868	1.87%	0.3124	9.04%	0.8605	2.15%	0.2211	9.15%
9	4	0.8120	2.17%	-0.0490	8.15%	0.7747	2.35%	-0.1448	7.53%
8	4	0.7254	2.24%	-0.3751	5.77%	0.6806	2.18%	-0.4460	4.39%
7	4	0.6356	2.37%	-0.6057	3.45%	0.5932	2.31%	-0.6215	2.25%
6	4	0.5409	2.29%	-0.7437	0.86%	0.5008	2.23%	-0.7113	0.04%
5	4	0.4492	2.34%	-0.7780	-1.28%	0.4117	2.28%	-0.7129	-1.78%
4	4	0.3556	2.29%	-0.7267	-3.08%	0.3205	2.22%	-0.6419	-3.20%
3	4	0.2640	2.34%	-0.6034	-4.58%	0.2317	2.13%	-0.5138	-4.13%
2	4	0.1704	2.19%	-0.4203	-5.17%	0.1465	1.84%	-0.3487	-4.21%
1	5	0.0828	1.66%	-0.2136	-4.27%	0.0728	1.46%	-0.1804	-3.61%

6.4.2 Peak Displacement Estimates

This section presents estimates of the peak roof displacement of the four frames, each subjected to 15 ground motions. Results are presented in Section 6.4.2.2 and discussed in Section 6.4.2.3. An example, below, illustrates the calculation.

6.4.2.1 Example of Peak Displacement Estimation

The following example illustrates the estimation of the peak roof displacement of a MDOF system using the pulse R-factors. Consider the Flexible-4 and Rigid-4 buildings subjected to the 1940 N-S component of the El Centro earthquake (IV40ELCN.180), characterized by a peak acceleration, $a_{g,max} = 3.417\ m/s^2$ and characteristic period, $T_g = 0.65$ s. Steps 1 to 3 of Section 6.3 result in the values shown in Table 6.1. Step 4 consists of calculating the yield displacement and yield strength of the equivalent SDOF systems (Eqs. 6.1 and 6.3, respectively). Using the data of Table 6.1 for Flexible-4,

$$u_y^{sdof} = \frac{0.129m}{1.266} = 0.102m$$

$$\eta_y^{sdof} = \frac{585\,kN}{0.876 \cdot 2204\,kN} \cdot \frac{9.807 m/s^2}{3.417 m/s^2} = 0.871$$

Applying the same procedure to Rigid-4 results in $u_y^{sdof} = 0.1017$ m and $\eta_y^{sdof} = 2.307$.

The four steps of Section 6.3.1 come next:

1. The elastic strength parameter for the fundamental period of vibration is obtained from the strength spectrum of the bilinear SDOF systems having 5% damping and 10% post yield stiffness, for the IV40ELCN.180 record. For the Flexible-4 frame, $\eta_e^{sdof} = \eta(\mu = 1, T = T_1 = 1.16s) = 1.01$, and for the Rigid-4 frame, having $T_1 = 0.71s$, $\eta_e^{sdof} = 1.757$.
2. The Flexible-4 building behaves nonlinearly, since $\eta_e^{sdof} > \eta_y^{sdof}$, therefore, the reduction factor is given by $R^{sdof} = \frac{1.01}{0.871} = 1.158$. The Rigid-4 building behaves linearly in the first mode, therefore, $R^{sdof} = 1$.
3. Once the fundamental period of vibration and the R-factor are known, the next step is to calculate the ductility of the system associated with the first mode. The ductility is obtained from the overall response of bilinear SDOF systems having 5% damping and 10% post yield stiffness subjected to the qua(2) pulse (Fig. 4.2) having a strength reduction factor equal to R^{sdof}. The characteristic period of the pulse is equated to the period of the ground motion, $T_p = T_g = 0.65$ s. Figure 6.2 shows the R-factor spectrum for this pulse. The dotted lines indicate the periods of vibration of the buildings. For the Flexible-4 frame, $\mu = \mu(R = R^{sdof} = 1.158, T = T_1 = 1.16s) = 1.093$, and for the Rigid-4 frame, $\mu = 1$ since it behaves linearly.
4. The peak roof displacement of the MDOF system is now calculated using Eq. 6.7. For the Flexible-4 frame,

$$u_u^{mdof} = 1.266\,(1.093)\,(0.102m) = 0.141m \tag{6.12}$$

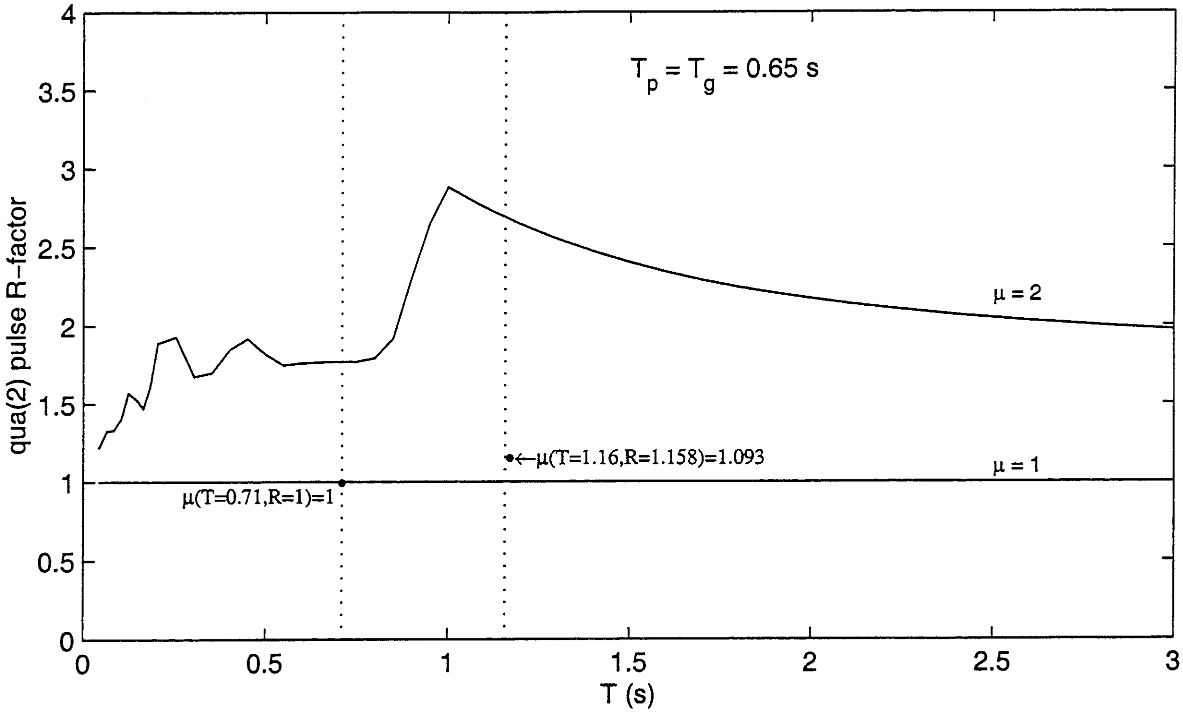

Figure 6.2: Ductility values associated with the first mode for the 4-story buildings subjected to the IV40ELCN.180 record ($T_g = 0.65$ s, $\alpha = 10\%$, $\beta = 5\%$)

The Rigid-4 frame is elastic and the peak roof displacement is given by the elastic displacement of the SDOF system (Eq. 6.8), $u_e^{sdof} = \frac{0.71^2}{4\pi^2}(3.417)(1.757) = 0.76$ m. Therefore, the estimated peak roof displacement of the Rigid-4 building is $u_u^{mdof} = 1.308\,(1)\,(0.766m) = 0.100$ m.

6.4.2.2 Numerical Results

Three methods to estimate peak displacement are evaluated with respect to the peak roof displacement computed by nonlinear dynamic analysis with the DRAIN-2DX program. The results are plotted and mean and standard deviation statistics are reported. The following tables and figures show the peak roof displacement estimates that result from each of the methods and from nonlinear dynamic analysis with DRAIN-2DX. The latter result is taken as the correct value, and was obtained by applying the recorded ground motions in their natural state, that is, without any scaling of amplitude or time. The methods consider the elastic spectrum of the ground motions and the R-factors derived from:

a) the ground motion R-factor, which is the most accurate implementation of an equivalent SDOF system, but requires knowledge of ground motion history,

b) Vidic's $R-\mu-T$ relation which often is very accurate, based on Chapter 5, but requires knowledge of $a_{g,max}$ and $v_{g,max}$, and,

c) the pulse R-factor, which only requires knowledge of the pulse shape and the characteristic period T_p.

It is expected that (c) will be least accurate, but less information is required, and hence (c) may be more suitable for design situations in which only the elastic spectrum is known. The estimates given by the methods (a) and (b) are obtained following processes similar to the example mentioned in Section 6.4.2.

The R-factor that results from the overall response of SDOF systems having 5% damping and 10% post-yield stiffness subjected to the qua(2) pulse was used for all ground motions, except the 1985 Michoacan earthquake (MX85SCT1.270 record) for which the forced response of the sin(5) pulse was used (see Chapter 4). Figure 5.1 plots the acceleration, velocity, and displacement time histories of these two pulses. Two cases were considered when using the pulse R-factors. In one case the period of the pulse is considered to be equal to the characteristic ground period, $T_p = T_g$. In the other case, $T_p = T_1^*$, where T_1^* is the period that minimizes the error given in Eq. 4.4 (see Table 4.3).

Tables 6.5 to 6.9 present the peak roof displacements computed and estimated for each of the four buildings subjected to the 15 ground motions (Table 2.1). The first column shows the identifier name of each ground motion. The second column shows the ductility of the building for each record, given by the ratio $u_{u,DRAIN-2DX}^{mdof} \big/ u_y^{mdof}$ associated with the first mode. The following columns show the result from the nonlinear analyses performed with DRAIN-2DX, $u_{u,DRAIN-2DX}^{mdof}$, the estimates calculated with Eq. 6.7 using the R-factor of the equivalent SDOF subjected to the record, $u_{u,record}^{mdof}$, the estimates given by Vidic's R-factor, $u_{u,vidic}^{mdof}$, the estimates using the pulses R-factor having $T_p = T_1^*$, $u_{u,pul(T_1^*)}^{mdof}$, and the estimates calculated for $T_p = T_g$, $u_{u,pul(T_g)}^{mdof}$. Tables 6.10 to 6.13 present

Table 6.5: Peak roof displacements for Flexible-4 (cm)

Ground motion	μ^*	$u^{mdof}_{u,DRAIN-2DX}$	$u^{mdof}_{u,record}$	$u^{mdof}_{u,vidic}$	$u^{mdof}_{u,pul(T_1^*)}$	$u^{mdof}_{u,pul(T_g)}$
WN87MWLN.090	Linear	0.96	0.91	0.91	0.91	0.91
BB92CIVC. 360	Linear	8.63	7.18	7.18	7.18	7.18
SP88GUKA.360	Linear	7.78	7.33	7.33	7.33	7.33
LP89CORR.090	1.40	18.11	15.94	16.22	15.90	16.57
NR94CENT.360	1.01	13.02	13.47	13.66	13.47	14.22
CH85LLEO.010	1.38	17.75	17.88	19.77	19.11	21.78
CH85VALP.070	Linear	5.16	5.91	5.91	5.91	5.91
IV40ELCN.180	1.01	12.99	14.32	14.41	14.58	14.11
LN92JOSH.360	1.20	15.55	17.04	19.18	18.23	24.13
MX85SCT1.270	Linear	10.91	11.62	11.62	11.62	11.62
LN92LUCN.250	1.88	24.09	25.79	19.84	21.88	22.53
LP89SARA.360	1.38	17.80	18.04	19.10	18.15	19.81
NR94NWHL.360	2.27	29.35	32.32	41.75	39.10	39.50
NR94SYLH.090	1.53	19.78	22.02	17.85	21.60	20.05
KO95TTRI.360	4.02	51.82	60.98	67.59	70.38	81.93

*in the first mode, independent of the others

the ratios of the estimated peak roof displacements to the nonlinear DRAIN-2DX values for each of the 15 records.

Table 6.7: Peak roof displacements for Rigid-4 (cm)

Ground motion	μ^*	$u^{mdof}_{u,DRAIN-2DX}$	$u^{mdof}_{u,record}$	$u^{mdof}_{u,vidic}$	$u^{mdof}_{u,pul(T_1^*)}$	$u^{mdof}_{u,pul(T_g)}$
WN87MWLN.090	Linear	0.57	0.53	0.53	0.53	0.53
BB92CIVC. 360	Linear	5.34	4.97	4.97	4.97	4.97
SP88GUKA.360	Linear	2.87	2.89	2.89	2.89	2.89
LP89CORR.090	1.48	19.70	18.03	19.77	22.71	24.78
NR94CENT.360	Linear	7.49	7.20	7.20	7.20	7.20
CH85LLEO.010	1.10	14.62	14.16	14.30	14.75	14.28
CH85VALP.070	Linear	5.50	5.13	5.13	5.13	5.13
IV40ELCN.180	Linear	10.38	10.02	10.02	10.02	10.02
LN92JOSH.360	Linear	11.26	10.94	10.94	10.94	10.94
MX85SCT1.270	Linear	5.73	5.70	5.70	5.70	5.70
LN92LUCN.250	Linear	11.37	10.92	10.92	10.92	10.92
LP89SARA.360	Linear	9.96	9.83	9.83	9.83	9.83
NR94NWHL.360	1.68	22.29	25.92	29.21	33.36	34.39
NR94SYLH.090	1.01	13.41	14.11	13.73	13.95	14.03
KO95TTRI.360	1.62	21.51	24.62	24.12	27.81	33.86

*in the first mode, independent of the others

Table 6.8: Peak roof displacements for Flexible-12 (cm)

Ground motion	μ^*	$u^{mdof}_{u,DRAIN-2DX}$	$u^{mdof}_{u,record}$	$u^{mdof}_{u,vidic}$	$u^{mdof}_{u,pul(T_1^*)}$	$u^{mdof}_{u,pul(T_g)}$
WN87MWLN.090	Linear	0.98	0.97	0.97	0.97	0.97
BB92CIVC. 360	Linear	11.51	7.70	7.70	7.70	7.70
SP88GUKA.360	Linear	7.14	5.95	5.95	5.95	5.95
LP89CORR.090	Linear	23.62	14.65	14.65	14.65	14.65
NR94CENT.360	Linear	17.86	17.07	17.07	17.07	17.07
CH85LLEO.010	Linear	34.22	27.15	27.15	27.15	27.15
CH85VALP.070	Linear	10.94	9.56	9.56	9.56	9.56
IV40ELCN.180	Linear	33.64	29.96	29.96	29.96	29.96
LN92JOSH.360	Linear	22.77	17.47	17.47	17.47	17.47
MX85SCT1.270	1.96	69.03	75.01	109.07	73.48	78.85
LN92LUCN.250	1.44	50.69	52.76	43.99	47.25	47.15
LP89SARA.360	1.08	38.14	38.94	39.03	39.98	40.48
NR94NWHL.360	1.47	51.80	52.41	51.25	53.08	52.40
NR94SYLH.090	1.72	60.82	57.48	63.05	59.21	62.87
KO95TTRI.360	2.38	84.09	92.63	122.38	142.16	115.51

*in the first mode, independent of the others

Table 6.9: Peak roof displacements for Rigid-12 (cm)

Ground motion	μ^*	$u^{mdof}_{u,DRAIN-2DX}$	$u^{mdof}_{u,record}$	$u^{mdof}_{u,vidic}$	$u^{mdof}_{u,pul(T_1^*)}$	$u^{mdof}_{u,pul(T_g)}$
WN87MWLN.090	Linear	0.98	0.93	0.93	0.93	0.93
BB92CIVC. 360	Linear	10.04	7.92	7.92	7.92	7.92
SP88GUKA.360	Linear	8.52	8.20	8.20	8.20	8.20
LP89CORR.090	Linear	23.39	23.00	23.00	23.00	23.00
NR94CENT.360	Linear	16.35	15.12	15.12	15.12	15.12
CH85LLEO.010	Linear	25.47	25.22	25.22	25.22	25.22
CH85VALP.070	Linear	9.07	8.75	8.75	8.75	8.75
IV40ELCN.180	Linear	17.50	15.25	15.25	15.25	15.25
LN92JOSH.360	Linear	28.37	26.49	26.49	26.49	26.49
MX85SCT1.270	Linear	14.3	15.61	15.61	15.61	15.61
LN92LUCN.250	Linear	29.27	28.89	28.89	28.89	28.89
LP89SARA.360	Linear	26.45	25.24	25.24	25.24	25.24
NR94NWHL.360	1.65	55.45	49.45	52.64	48.04	47.76
NR94SYLH.090	Linear	28.47	28.30	28.30	28.30	28.30
KO95TTRI.360	1.94	65.01	73.19	93.47	85.13	103.79

*in the first mode, independent of the others

Table 6.10: Estimate peak roof displacement/Drain peak roof displacement ratio for Flexible-4

Ground motion	$Ratio_{record}$	$Ratio_{vidic}$	$Ratio_{pul(T_1^*)}$	$Ratio_{pul(T_g)}$
WN87MWLN.090	0.950	0.950	0.950	0.950
BB92CIVC. 360	0.832	0.832	0.832	0.832
SP88GUKA.360	0.941	0.941	0.941	0.941
LP89CORR.090	0.881	0.896	0.878	0.915
NR94CENT.360	1.035	1.049	1.035	1.092
CH85LLEO.010	1.008	1.114	1.077	1.227
CH85VALP.070	1.146	1.146	1.146	1.146
IV40ELCN.180	1.102	1.109	1.122	1.086
LN92JOSH.360	1.096	1.234	1.172	1.552
MX85SCT1.270	1.066	1.066	1.066	1.066
LN92LUCN.250	1.071	0.824	0.908	0.935
LP89SARA.360	1.014	1.073	1.020	1.113
NR94NWHL.360	1.101	1.422	1.332	1.346
NR94SYLH.090	1.113	0.902	1.092	1.013
KO95TTRI.360	1.177	1.304	1.358	1.581

Table 6.11: Estimate peak roof displacement/Drain peak roof displacement ratio for Rigid-4

Ground motion	$Ratio_{record}$	$Ratio_{vidic}$	$Ratio_{pul(T_1^*)}$	$Ratio_{pul(T_g)}$
WN87MWLN.090	0.929	0.929	0.929	0.929
BB92CIVC. 360	0.930	0.930	0.930	0.930
SP88GUKA.360	1.005	1.005	1.005	1.005
LP89CORR.090	0.915	1.003	1.153	1.258
NR94CENT.360	0.961	0.961	0.961	0.961
CH85LLEO.010	0.969	0.978	1.009	0.977
CH85VALP.070	0.933	0.933	0.933	0.933
IV40ELCN.180	0.965	0.965	0.965	0.965
LN92JOSH.360	0.971	0.971	0.971	0.971
MX85SCT1.270	0.994	0.994	0.994	0.994
LN92LUCN.250	0.960	0.960	0.960	0.960
LP89SARA.360	0.987	0.987	0.987	0.987
NR94NWHL.360	1.162	1.310	1.496	1.542
NR94SYLH.090	1.052	1.024	1.040	1.047
KO95TTRI.360	1.145	1.121	1.293	1.574

Table 6.12: Estimate peak roof displacement/Drain peak roof displacement ratio for Flexible-12

Ground motion	$Ratio_{record}$	$Ratio_{vidic}$	$Ratio_{pul(T_1^*)}$	$Ratio_{pul(T_g)}$
WN87MWLN.090	0.998	0.998	0.998	0.998
BB92CIVC. 360	0.668	0.668	0.668	0.668
SP88GUKA.360	0.834	0.834	0.834	0.834
LP89CORR.090	0.620	0.620	0.620	0.620
NR94CENT.360	0.995	0.995	0.995	0.995
CH85LLEO.010	0.794	0.794	0.794	0.794
CH85VALP.070	0.874	0.874	0.874	0.874
IV40ELCN.180	0.891	0.891	0.891	0.891
LN92JOSH.360	0.767	0.767	0.767	0.767
MX85SCT1.270	1.087	1.580	1.064	1.142
LN92LUCN.250	1.041	0.868	0.932	0.930
LP89SARA.360	1.021	1.023	1.048	1.061
NR94NWHL.360	1.012	0.989	1.025	1.012
NR94SYLH.090	0.945	1.037	0.974	1.034
KO95TTRI.360	1.102	1.455	1.691	1.374

Table 6.13: Estimate peak roof displacement/Drain peak roof displacement ratio for Rigid-12

Ground motion	$Ratio_{record}$	$Ratio_{vidic}$	$Ratio_{pul(T_1^*)}$	$Ratio_{pul(T_g)}$
WN87MWLN.090	0.951	0.951	0.951	0.951
BB92CIVC. 360	0.789	0.789	0.789	0.789
SP88GUKA.360	0.962	0.962	0.962	0.962
LP89CORR.090	0.983	0.983	0.983	0.983
NR94CENT.360	0.925	0.925	0.925	0.925
CH85LLEO.010	0.990	0.990	0.990	0.990
CH85VALP.070	0.946	0.946	0.946	0.946
IV40ELCN.180	0.872	0.872	0.872	0.872
LN92JOSH.360	0.934	0.934	0.934	0.934
MX85SCT1.270	1.089	1.089	1.089	1.089
LN92LUCN.250	0.987	0.987	0.987	0.987
LP89SARA.360	0.954	0.954	0.954	0.954
NR94NWHL.360	0.892	0.949	0.866	0.861
NR94SYLH.090	0.994	0.994	0.994	0.994
KO95TTRI.360	1.126	1.438	1.309	1.597

Figures 6.3 to 6.6 provide a graphic comparison among the different methods used to estimate the peak roof displacements and the results obtained by nonlinear dynamic analysis. The upper part of these figures plots the estimated peak roof displacement versus the DRAIN-2DX peak roof displacement. The diagonal line represents perfect estimation; points below the line indicate underestimation, while points above indicate overestimation of the peak roof displacement. The vertical dashed line indicates the separation between elastic displacements $u^{mdof}_{u,DRAIN-2DX} < u^{mdof}_{y}$ and nonlinear displacements $u^{mdof}_{u,DRAIN-2DX} > u^{mdof}_{y}$ based on first mode behavior. This plot shows the accuracy of each estimate model with respect to the nonlinear displacement. Differences between the "record" estimate and the DRAIN-2DX value represent the effects of higher modes. Differences between the estimates (pulses and Vidic) and the "record" values represent errors in estimating nonlinear response based on R-factors applied to an elastic response spectrum. The lower part of each figure shows ratios of the estimated peak roof displacement and the DRAIN-2DX peak roof displacement for each ground motion. In this case, the horizontal line represents perfect estimation; points below indicate underestimation of peak displacement; points above indicate overestimation. This plot shows the accuracy of each estimate with respect to each ground motion. Data to produce these graphics are presented in Tables 6.5 to 6.13.

6.4.2.3 Analysis of Results

If the buildings have not reached their roof yield displacement, the estimated peak roof displacement of each building is the same independently of the model used to estimate it. The reason is because linear elastic response is identified in the first mode with the elastic spectrum of the SDOF systems subjected to the considered ground motion. Therefore, the peak roof displacements, u^{mdof}_{u}, given in Tables 6.5 to 6.9 are the same using the equivalent SDOF systems subjected to the record, Vidic's model, and the pulse model.

However, if the response of the buildings is nonlinear, differences in u^{mdof}_{u} appear among the estimates. In general, the peak roof displacement estimates are less accurate when the R-factor obtained

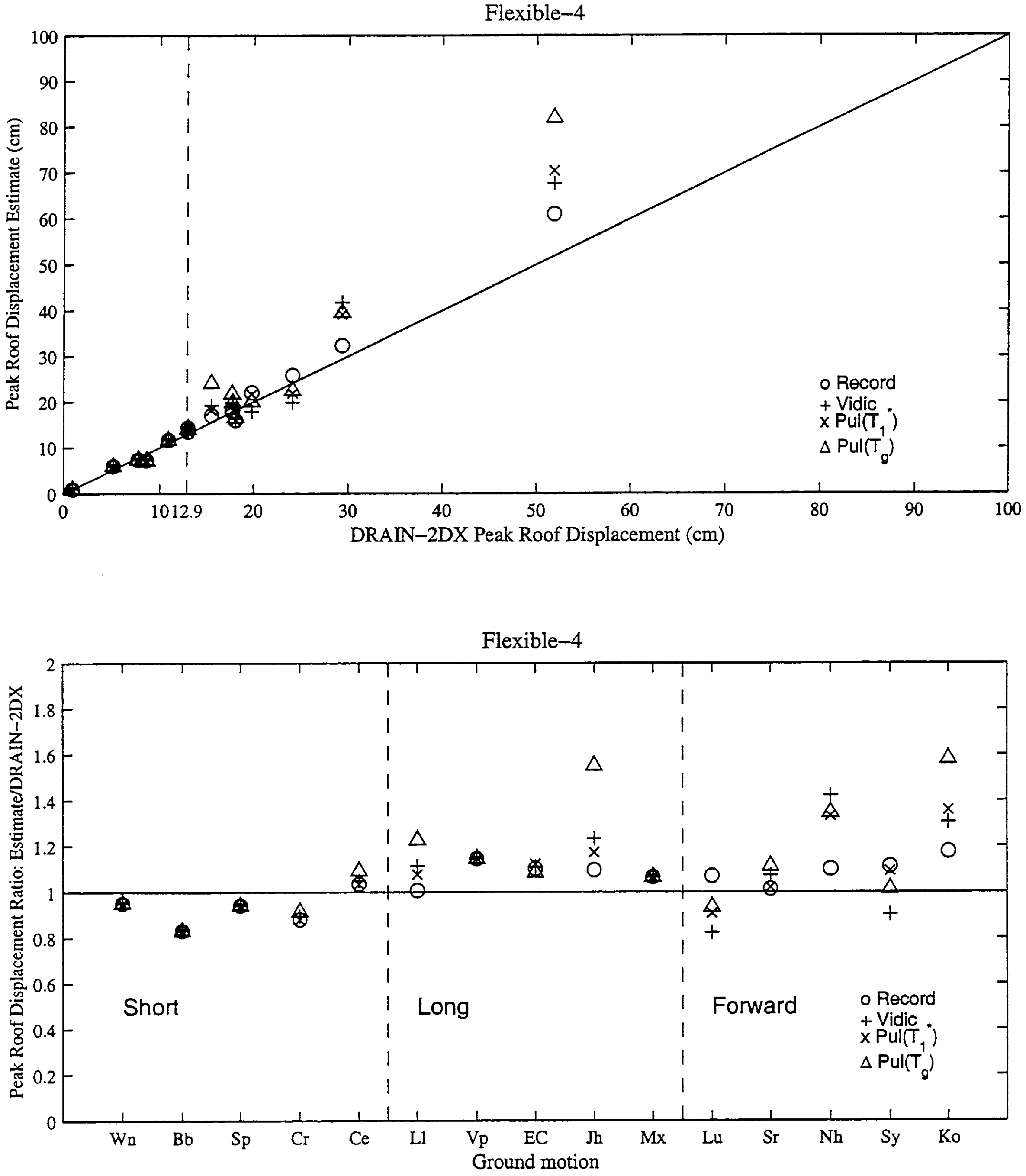

Figure 6.3: Peak roof displacement comparisons for the Flexible-4 building

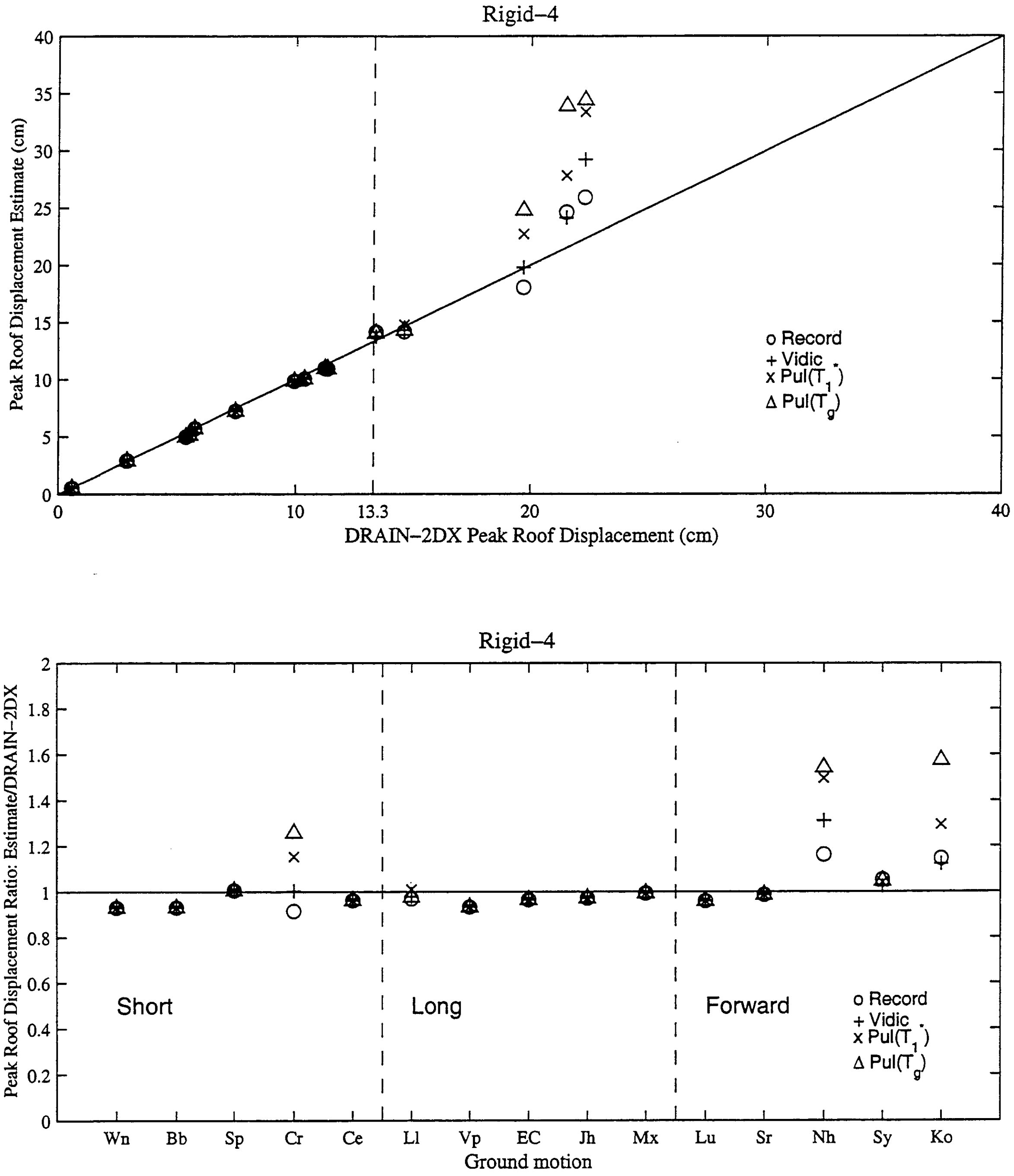

Figure 6.4: Peak roof displacement comparisons for the Flexible-4 building

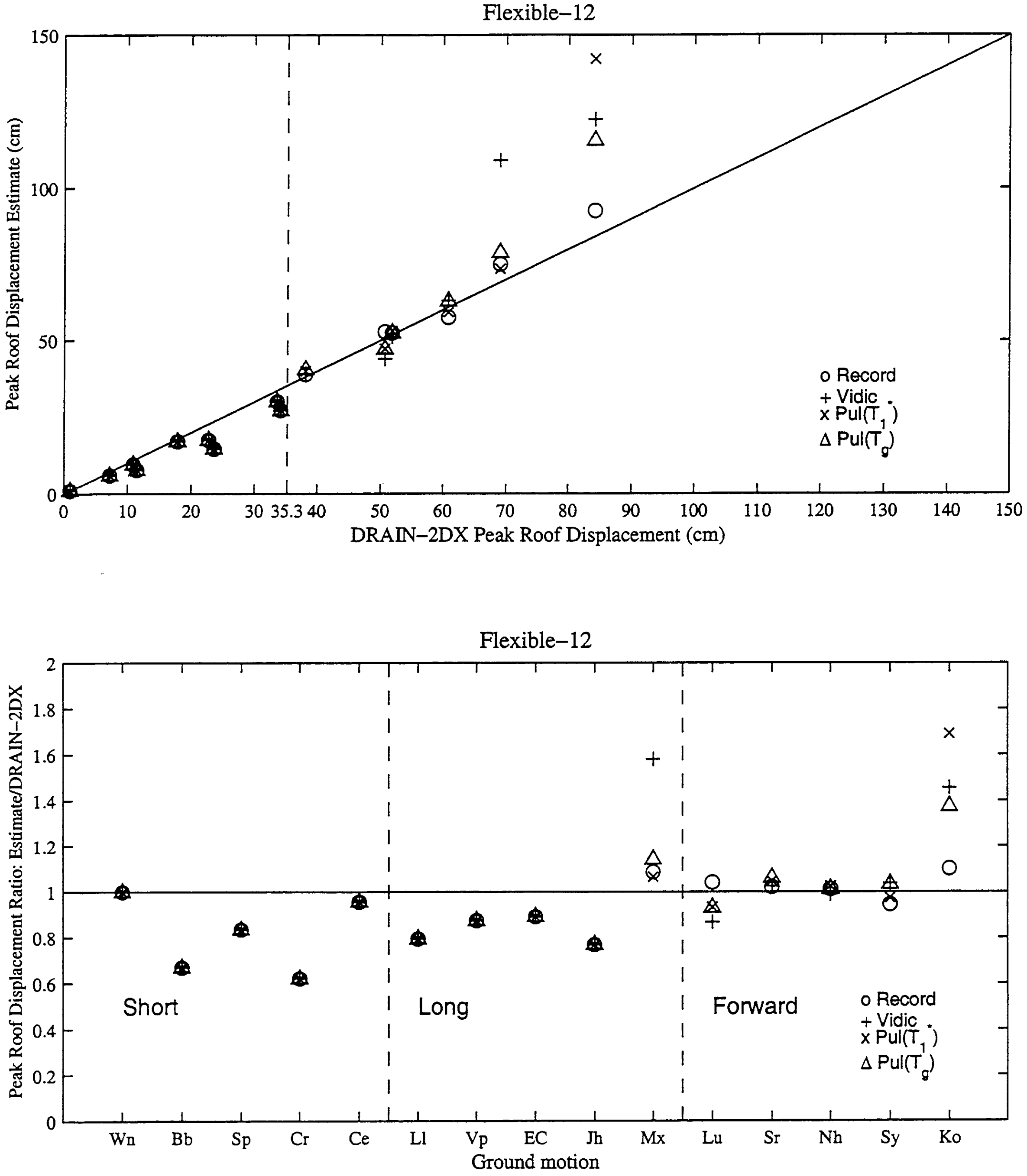

Figure 6.5: Peak roof displacement comparisons for the Flexible-12 building

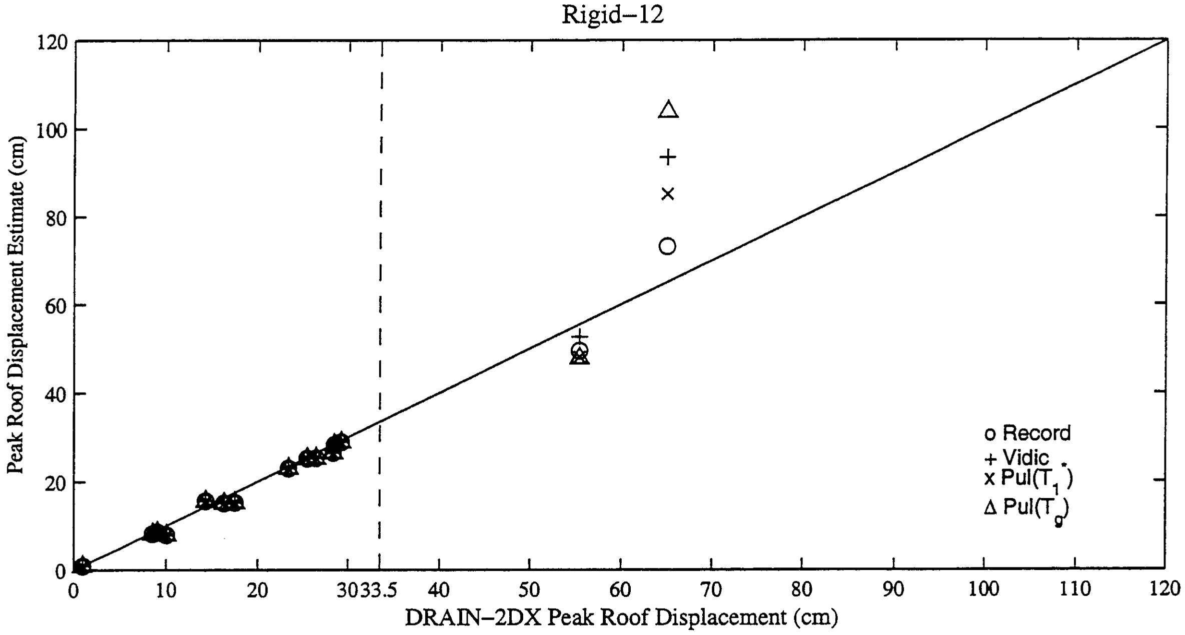

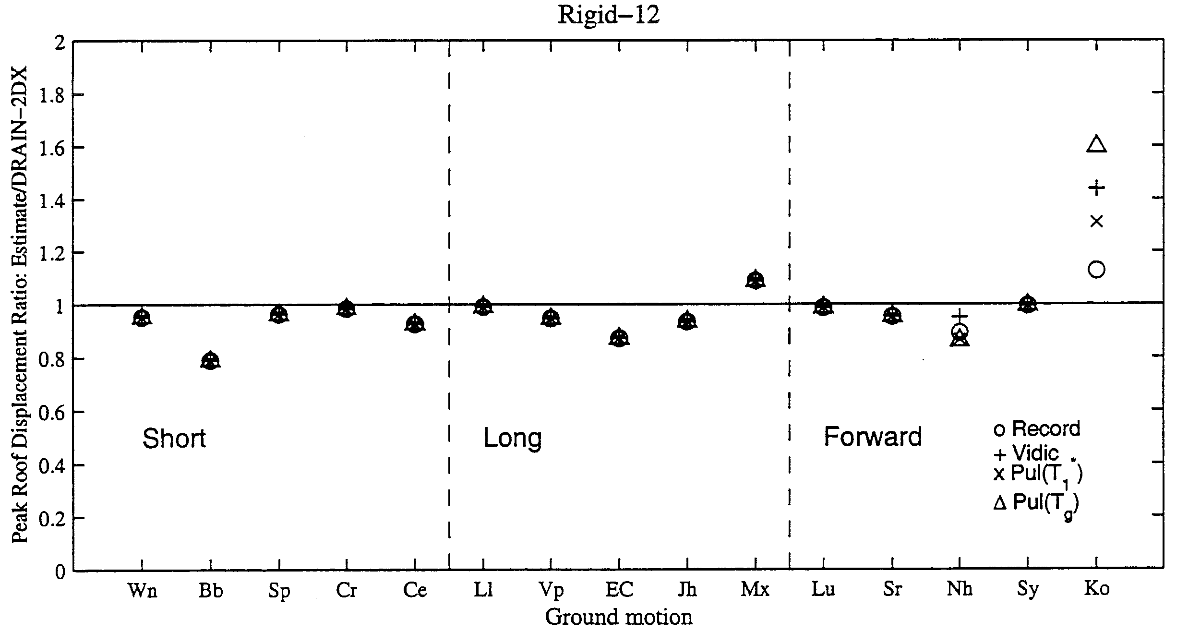

Figure 6.6: Peak roof displacement comparisons for the Rigid-12 building

Table 6.14: Results for all cases

	Record		Vidic		Pulse, $T_p = T_1^*$		Pulse, $T_p = T_g$	
Frame	Mean	Std. Dev.	Mean	Std. Dev.	Mean	Std. Dev.	Mean	Std. Dev.
Flexible-4	1.035	0.098	1.057	0.173	1.062	0.152	1.120	0.223
Rigid-4	0.992	0.074	1.005	0.097	1.042	0.158	1.069	0.214
Flexible-12	0.907	0.147	0.957	0.260	0.942	0.246	0.930	0.190
Rigid-12	0.960	0.081	0.984	0.141	0.970	0.116	0.989	0.182
All	0.974	0.112	1.001	0.177	1.004	0.177	1.027	0.211

from the ground motions is replaced by the R-factor given by Vidic or the pulses. The difference between Vidic and the pulse estimates and the nonlinear response given by DRAIN-2DX is especially large in all buildings subjected to the 1995 Hyogo-Ken Nambu earthquake (KO95TTRI.360 record), where the largest peak roof displacements are found. The buildings subjected to this record present the largest peak roof displacements, ranging from $u_{u,DRAIN-2DX}^{mdof} = 21.5$ cm for Rigid-4 to 84.1 cm for Flexible-12, and the pulses, using $T_p = T_g$, overestimate $u_{u,DRAIN-2DX}^{mdof}$ by 30, 12, 31, and 38 cm for the Flexible-4, Rigid-4, Flexible-12, and Rigid-12, respectively.

There are 23 nonlinear cases out of the 15 records x 4 buildings = 60 cases under study. Among these cases, the estimated peak displacements using the pulses having $T_p = T_g$ are larger than using the same pulses but having $T_p = T_1^*$ in 16 cases, which corresponds to 70% of the nonlinear cases.

Table 6.14 shows the mean and standard deviations of the ratio of the estimated peak roof displacement and the nonlinear DRAIN-2DX peak roof displacement, for each building, using the record, Vidic, and the pulses having $T_p = T_1^*$ and $T_p = T_g$, (the pulses consist of the sin(5) pulse for the 1985 Michoacan earthquake and the qua(2) pulse for the rest of the records). The mean ratios indicate that the peak roof displacement for the four-story buildings is overestimated in general, while the 12-story building peak roof displacements are underestimated, for the set of linear and nonlinear responses in Table 6.14. Often, the best results occur when the R-factor used to estimate the response comes from Vidic or from the pulse having $T_p = T_1^*$. For both cases the dispersion is larger than for the estimates given by the record R-factor. The standard deviation is smallest for the record (0.112), followed by Vidic and the pulses having $T_p = T_1^*$ (0.177). Using the pulses with $T_p = T_g$ leads to slightly greater dispersion. The accuracy of the record estimate, as reflected

Table 6.15: Results for nonlinear cases

Frame	Record		Vidic		Pulse, $T_p = T_1^*$		Pulse, $T_p = T_g$	
	Mean	Std. Dev.	Mean	Std. Dev.	Mean	Std. Dev.	Mean	Std. Dev.
Flexible-4	1.060	0.081	1.093	0.190	1.099	0.158	1.186	0.238
Rigid-4	1.049	0.108	1.087	0.136	1.198	0.200	1.280	0.275
Flexible-12	1.034	0.056	1.159	0.287	1.122	0.283	1.092	0.154
Rigid-12	1.009	0.166	1.194	0.345	1.088	0.313	1.229	0.520
All	1.046	0.084	1.118	0.209	1.126	0.204	1.186	0.243

in the mean and standard deviation, indicate the first mode analogy captures nearly all of the displacement response, that is, higher modes are seen to have little effect on the mean peak roof displacement estimate. More significant are differences in the estimated $R - \mu - T$ relationship relative to the actual $R - \mu - T$ relation computed for the ground motion.

Table 6.15 shows the mean and standard deviation values of the ratio of the displacement estimate and the nonlinear DRAIN-2DX displacement of only the cases where the buildings behave nonlinearly. The average is also presented. The mean ratios indicate that the record and estimate methods tend to overestimate peak displacement response, albeit by less than 20% on average for most of the building frames. The record estimates tend to be higher for the 4-story buildings than the 12-story buildings, repeating a trend observed in Table 6.14. However, this pattern does not extend to the Vidic and pulse estimates for the nonlinear cases. In general, the means and standard deviations are larger than those presented in Table 6.14 where the linear and nonlinear cases where mixed. The lowest mean (1.046) and standard deviation (0.084) correspond to the estimates given by the record R-factor. Vidic and the pulse ($T_p = T_1^*$) have similar overall means (1.118 and 1.126) and standard deviations (0.209 and 0.204). The pulse with $T_p = T_g$ has a larger mean (1.186) and standard deviation (0.243). The standard deviations are higher for the nonlinear estimates (Table 6.15) than for the set of all cases (Table 6.14), except for the record estimates. This reflects the error introduced by using the estimates of R-factors.

6.4.3 IDI Estimates

As described in Section 6.3.2, interstory drift indices are estimated using three techniques. One mode of vibration is used in Eq. 6.9 and two modes are used in Eqs. 6.10 and 6.11. Modal amplitudes are estimated assuming independence, even when nonlinear response is known to develop. Thus, the peak roof displacement is estimated for each mode independently of the response in the other modes. These equations are used to estimate and compare the IDI obtained using the estimated ductility responses of the systems subjected to the record, to the pulses having $T_p = T_1^*$ and $T_p = T_g$, and using Vidic's $R-\mu-T$ relation. The modal interstory drift indices for each building are presented in Table 6.3 for the 4-story buildings and in Table 6.4 for the 12-story buildings.

The peak roof displacement generated with the second mode of vibration was obtained for equivalent SDOF systems having 10% post-yield stiffness and 2.8% of critical damping, which corresponds to the damping assigned to the second mode of vibration of the MDOF system in the nonlinear analysis generated by DRAIN-2DX, for the four buildings.

An example of how the IDI of a story of a MDOF system is estimated using the pulse R-factors is now presented. The Flexible-4 building was subjected to the 1940 N-S component of the El Centro record (IV40ELCN.180), characterized by a peak acceleration, $a_{g,max} = 3.417$ m/s^2 and characteristic period, $T_g = 0.65$ s. Following Section 6.4.2, the peak roof displacement associated with the second mode is calculated by the same procedure used for the first mode. Table 6.2 contains the data needed for the second mode of vibration: $\frac{L_{eq}}{M_{eq}} = 0.363$, $\alpha_e = 0.096$, $V_y^{mdof} = 575$ kN, $u_y^{mdof} = 0.035$ m, and $T_2 = 0.38$ s. The yield displacement and yield strength of the equivalent SDOF system is obtained with Eqs. 6.1 and 6.3, respectively. In this case, $u_y^{sdof} = \frac{0.035}{0.363} = 0.096$ m, and $\eta_y^{sdof} = \frac{575}{0.096 \cdot 2204} \cdot \frac{9.807}{3.417} = 7.77$.

Following the four steps in Section 6.3.1:

1. The elastic response of a bilinear SDOF system having 2.8% damping and 10% post-yield stiffness subjected to the IV40ELCN.180 record is used to determine the elastic strength

parameter. The result for the Flexible-4 building is $\eta_e^{sdof} = \eta(\mu = 1, T = T_2 = 0.38s) = 2.07$.

2. The Flexible-4 building behaves linearly, since $\eta_e^{sdof} < \eta_y^{sdof}$, therefore, the reduction factor is given by $R^{sdof} = 1$.

3. Since the response is elastic, the ductility is $\mu = 1$.

4. The peak roof displacement of the MDOF system is now calculated using Eq. 6.8 as $u_e^{sdof} = \frac{0.38^2 s^2}{4\pi^2}\,(3.417m/s^2)\,(2.07) = 0.026$ m. Therefore, the estimated peak roof displacement associated with the second mode of vibration of the building is

$$u_u^{mdof} = 0.363\,(1)\,(0.026m) = 0.01m \tag{6.13}$$

The peak roof displacement associated with the first mode is 0.141 m, from Eq. 6.12.

Having estimated the maximum modal responses (assuming the modes to respond independently), interstory drift indices can now be estimated. For example, for the top story of Flexible-4, Eqs. 6.9 to 6.11 result in $IDI_4(\phi_1) = 3.66\%$ and $IDI_4(\phi_2) = 27.74\%$, as shown in Table 6.3. Therefore, using Eq. 6.9,

$$IDI_4^a = 0.141 \cdot 3.66\% = 0.52\% \tag{6.14}$$

Eq. 6.10 leads to

$$IDI_4^b = \sqrt{(0.141 \cdot 3.66\%)^2 + (0.01 \cdot 27.74\%)^2} = 0.58\% \tag{6.15}$$

and Eq. 6.11,

$$IDI_4^c = \mid 0.141 \cdot 3.66\% \mid + \mid 0.01 \cdot 27.74\% \mid = 0.79\% \tag{6.16}$$

Similar calculations were done for each story of each building and for each of the 15 ground motion records.

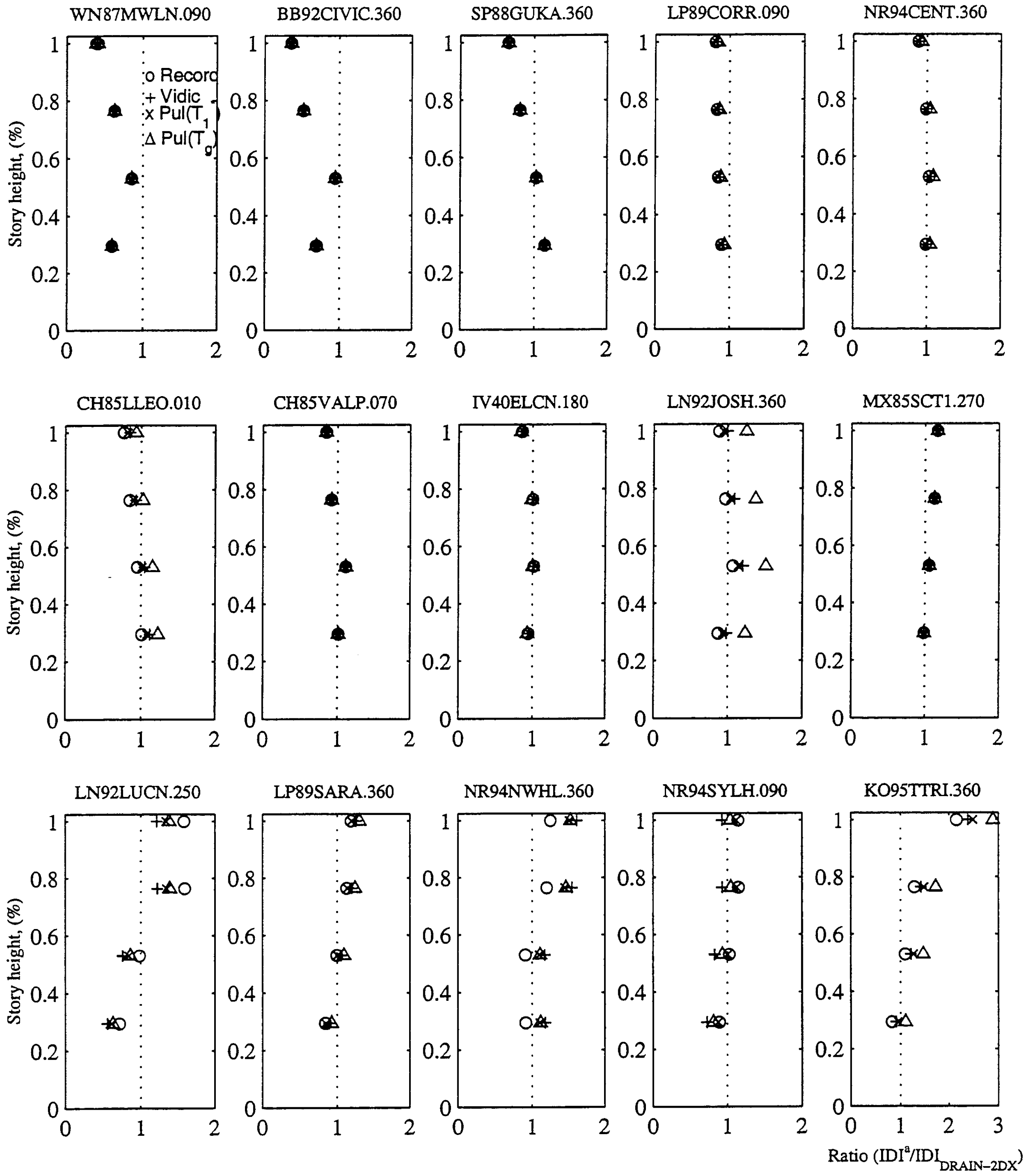

Figure 6.7: Ratio $IDI^a/IDI_{DRAIN-2DX}$ for Flexible-4 building subjected to each ground motion

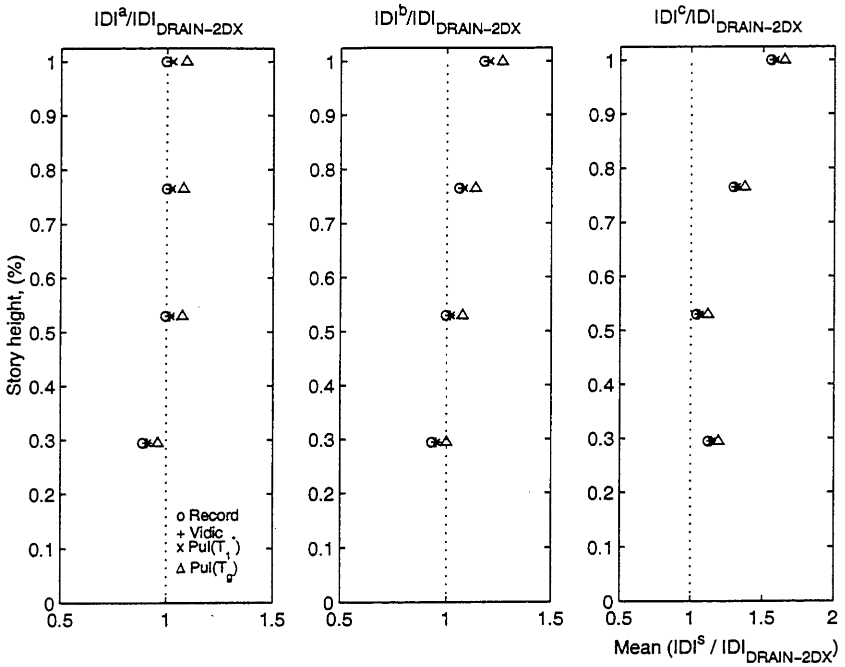

Figure 6.8: Mean ratio $IDI^s/IDI_{DRAIN-2DX}$, $s = a, b, c$, per story for Flexible-4 building over all records

6.4.3.1 Numerical Results

Figure 6.7 shows for Flexible-4, the ratio for each story of the IDI estimated using Eq. 6.9 to the IDI obtained with the nonlinear analysis of the MDOF buildings using the DRAIN-2DX program ($IDI_{DRAIN-2DX}$). The estimates are labeled, Record, Vidic, Pul(T_1^*), and Pul(T_g) for the estimates using the record $R - \mu - T$ relation, Vidic's $R - \mu - T$ relation, and the pulse $R - \mu - T$ relation having $T_p = T_1^*$ and $T_p = T_g$, respectively. The IDI^s is based on combinations of individual modal peaks, while $IDI_{DRAIN-2DX}$ is the maximum IDI at each story over all time. The peak IDI obtained in the nonlinear dynamic analysis for each story, in general, occurred at different instants in time.

Appendix B presents figures containing the ratio $IDI^s/IDI_{DRAIN-2DX}$, $s = a, b, c$ for each story using Eq. 6.9 (Figs. B.1 to B.4), Eq. 6.10 (Figs. B.5 to B.8), and Eq. 6.11 (Figs. B.9 to B.12) for the Flexible-4, Rigid-4, Flexible-12, and Rigid-12 buildings.

Figures 6.8 to 6.11 show, for each building, the mean ratio $IDI^s/IDI_{DRAIN-2DX}$, $s = a, b, c$ for each story over all ground motions using Eqs. 6.9, 6.10, and 6.11, respectively. The vertical dashed line represents perfect correlation. Values to the right means the IDI for a given story

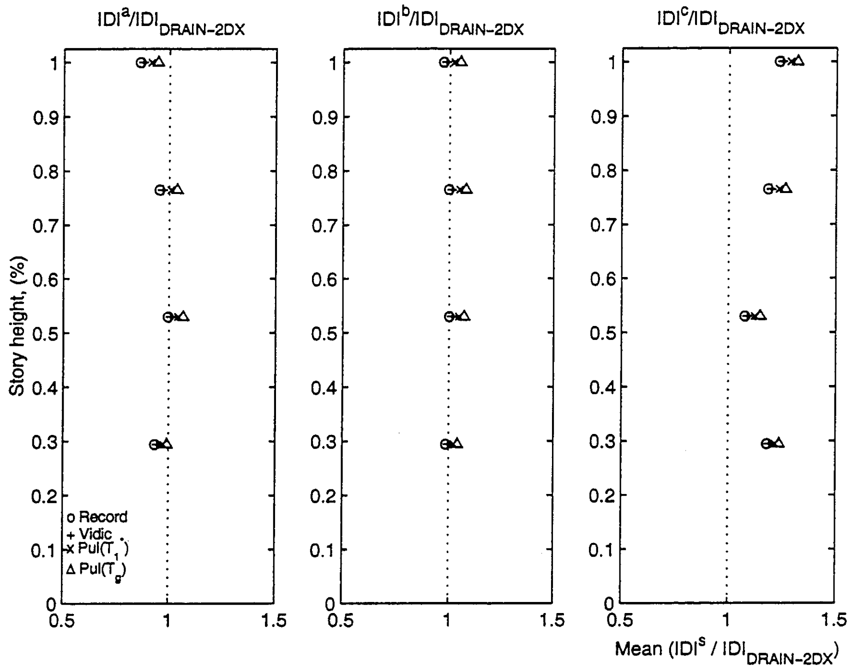

Figure 6.9: Mean ratio $IDI^s/IDI_{DRAIN-2DX}$, $s = a, b, c$, per story for Rigid-4 building over all records

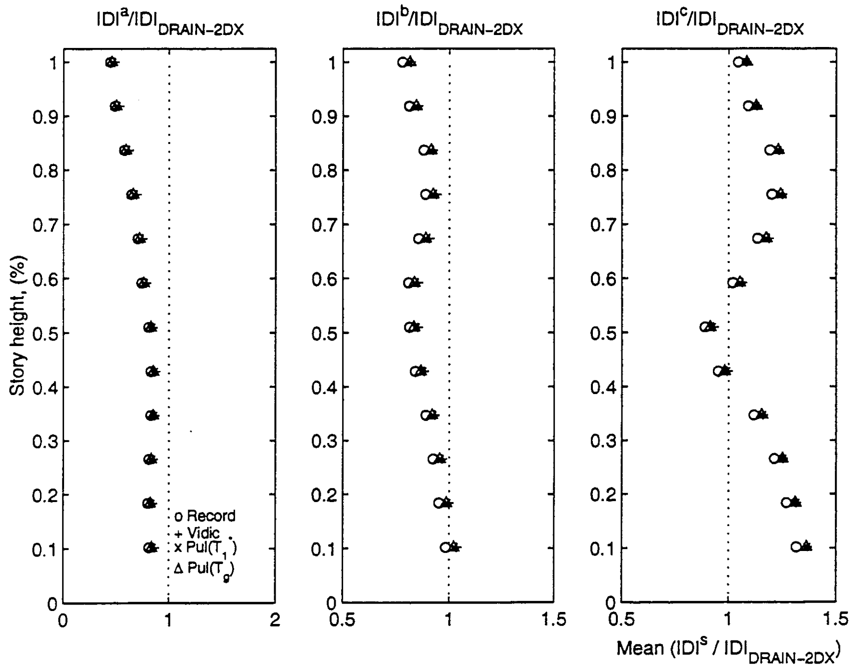

Figure 6.10: Mean ratio $IDI^s/IDI_{DRAIN-2DX}$, $s = a, b, c$, per story for Flexible-12 building over all records

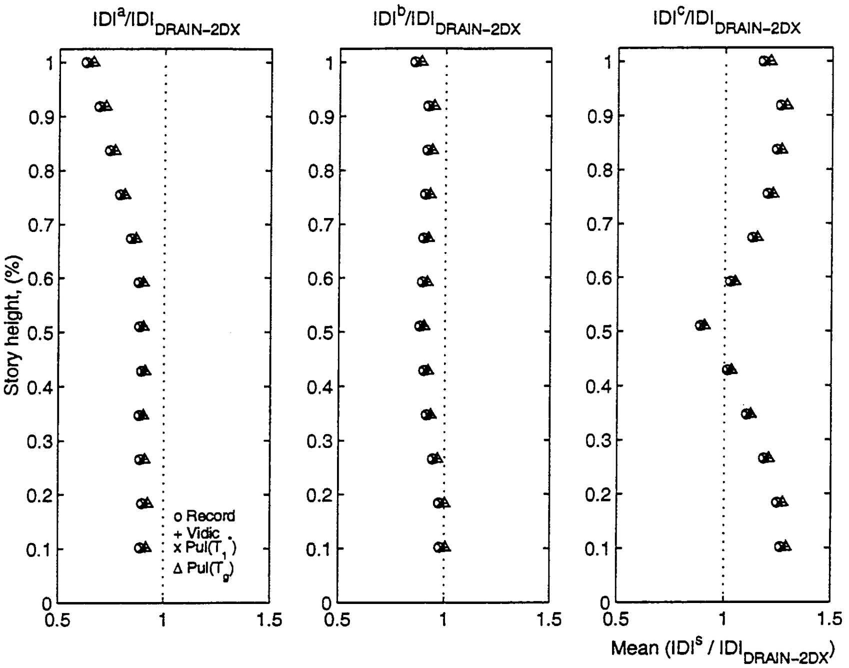

Figure 6.11: Mean ratio $IDI^s/IDI_{DRAIN-2DX}$, $s = a, b, c$, per story for Rigid-12 building over all records

is overestimated, and values to the left means the IDI is underestimated. Ratios less than unity obtained using the "Record" indicate that higher modes play a more significant role in the peak IDI than is represented in the technique applied.

Figure 6.12 shows the mean and standard deviation statistics of the IDI ratios $IDI^s/IDI_{DRAIN-2DX}$, $s = a, b, c$, computed for each building over all the ground motions, with the IDI ratios computed for each floor. If the IDI estimates were perfect, the average of the IDI ratios would be precisely equal to unity, represented by the horizontal dashed line of Figure 6.12. However, systematic over and underestimation could also lead to mean ratios equal to unity (values of unity are a necessary but not sufficient condition to indicate perfect estimation).The horizontal dashed line at zero on the standard deviation plot represents similar condition. Vertical dashed lines divide the results for each estimate model, given by the record, Vidic, pulse at T_1^*, and pulse at T_g. The data for these plots are in Table 6.16.

Figure 6.13 shows the mean and standard deviation of the IDI ratios, $IDI^s/IDI_{DRAIN-2DX}$, $s = a, b, c$, calculated over all the buildings, stories, and ground motions. If the IDI estimates

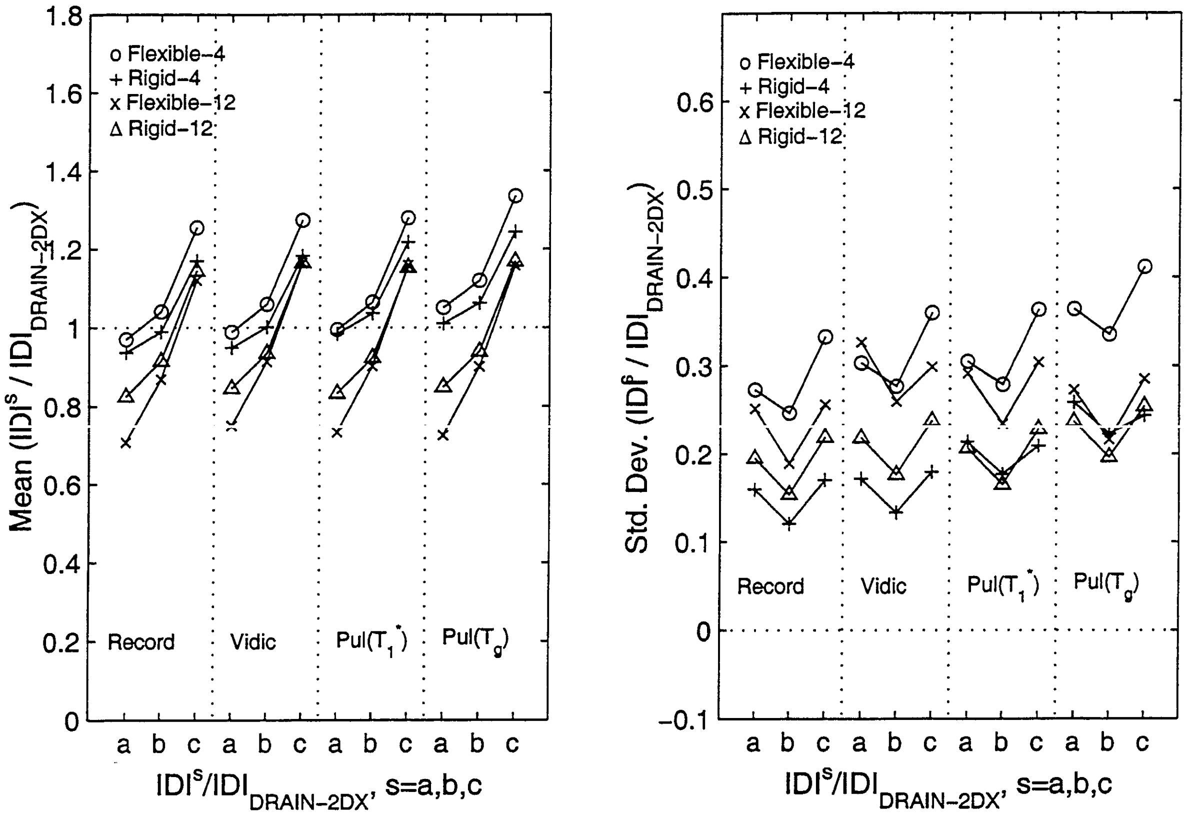

Figure 6.12: Mean and standard deviation of the IDI ratios, for each building and IDI model over all stories and ground motions

Table 6.16: Mean and standard deviation of the IDI ratios, $IDI^s/IDI_{DRAIN-2DX}$, $s = a,b,c$ for each building averaged for all stories and ground motions

Frame	Record			Vidic			Pulse T_1^*			Pulse T_g		
	IDI^a	IDI^b	IDI^c	IDI^a	IDI^b	IDI^c	IDI^a	IDI^b	IDI^c	IDI^a	IDI^b	IDI^c
	Mean											
Flexible-4	0.97	1.04	1.25	0.99	1.06	1.27	1.00	1.06	1.28	1.05	1.12	1.33
Rigid-4	0.94	0.99	1.17	0.95	1.00	1.18	0.98	1.04	1.22	1.01	1.06	1.24
Flexible-12	0.71	0.87	1.12	0.75	0.91	1.16	0.73	0.90	1.16	0.73	0.90	1.16
Rigid-12	0.82	0.92	1.14	0.85	0.94	1.16	0.83	0.92	1.15	0.85	0.94	1.17
	Standard Deviation											
Flexible-4	0.27	0.25	0.33	0.30	0.28	0.36	0.30	0.28	0.36	0.36	0.34	0.41
Rigid-4	0.16	0.12	0.17	0.17	0.13	0.18	0.21	0.18	0.21	0.26	0.22	0.24
Flexible-12	0.25	0.19	0.26	0.33	0.26	0.30	0.29	0.23	0.30	0.27	0.22	0.28
Rigid-12	0.19	0.15	0.22	0.22	0.18	0.24	0.21	0.16	0.23	0.24	0.20	0.25

Table 6.17: Mean and standard deviation of the IDI ratios, $IDI^s/IDI_{DRAIN-2DX}$, $s = a, b, c$, over all buildings, stories, and ground motions

Record			Vidic			Pulse T_1^*			Pulse T_g		
IDI^a	IDI^b	IDI^c	IDI^a	IDI^b	IDI^c	IDI^a	IDI^b	IDI^c	IDI^a	IDI^b	IDI^c
Mean											
0.81	0.92	1.15	0.84	0.95	1.18	0.84	0.95	1.18	0.85	0.96	1.19
Standard Deviation											
0.24	0.19	0.25	0.28	0.23	0.27	0.27	0.22	0.28	0.30	0.24	0.29

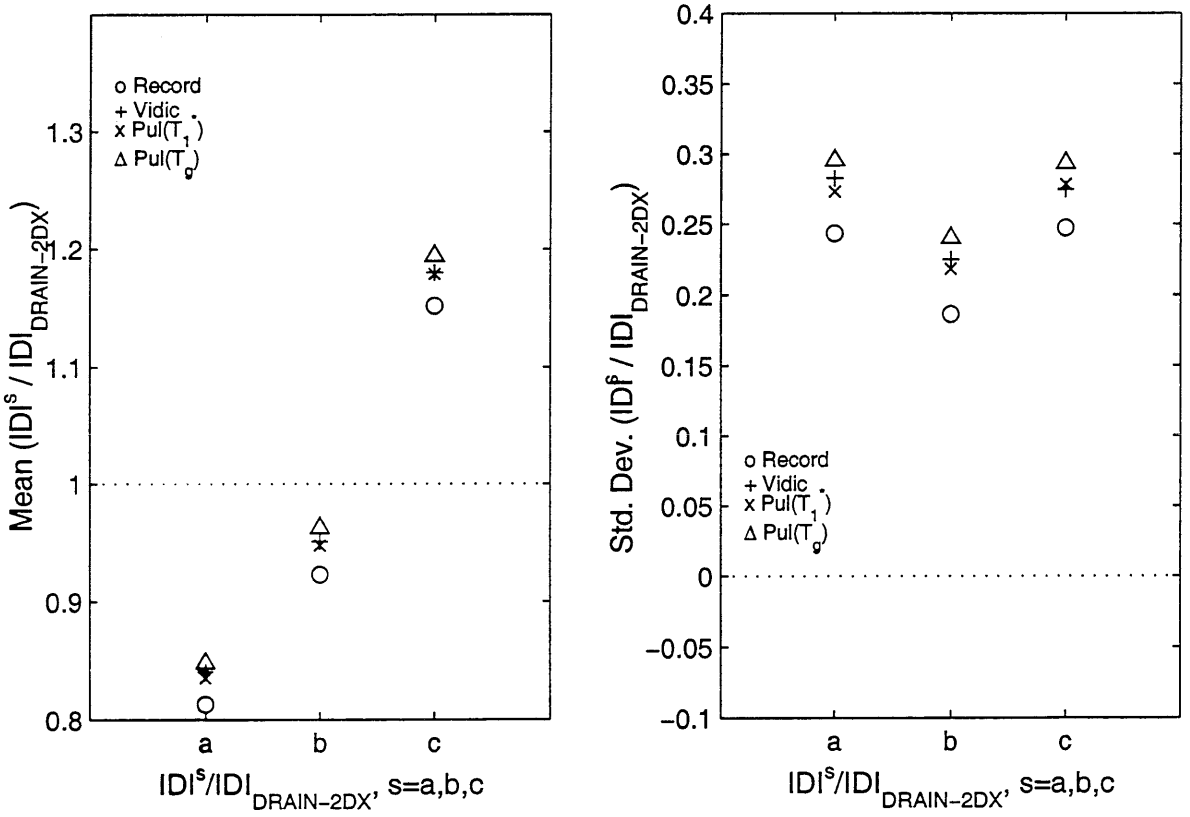

Figure 6.13: Mean and standard deviation of the IDI ratios for each IDI model, over all buildings, stories, and ground motions

were perfect, the average of the IDI ratios would be precisely equal to unity, represented by the horizontal dashed line of Figure 6.13. The horizontal dashed line at zero on the standard deviation plot represents similar condition. Table 6.17 shows the values of the means and standard deviations depicted in Fig. 6.13.

6.4.3.2 Analysis of Results

Figures 6.8 to 6.11 show that the top and lower story IDIs of the 4- and 12-story buildings are underestimated when using only one mode of vibration (Eq. 6.9, IDI^a), are overestimated when summing the absolute values given by two modes (Eq. 6.11, IDI^b), and are intermediate between these values when using the SRSS combination (Eq. 6.10, IDI^c). For intermediate stories (2^{nd} story for 4-story buildings and 6^{th} story for 12-story buildings), the IDI are of similar accuracy regardless of the equation used.

Figure 6.12 represents the mean over all the peak IDI of each story for each building given by the four estimates. For each estimate, IDI^s, the same pattern of underestimating using only one mode, overestimating using the absolute sum, and estimating intermediate between these two using the SRSS equation is found. Peak IDIs for the 4-story buildings are accurately estimated using only one mode of vibration; they are highly overestimated when using two modes, especially using the absolute sum technique. Peak IDIs for the 12-story buildings are highly underestimated when using only one mode (IDI^a), slightly underestimated when using the SRSS combination (IDI^b), and overestimated when using the absolute sum (IDI^c). The dispersion is somewhat smaller for all buildings and R-factor models using IDI^b. The smallest dispersion is obtained using the record R-factor.

Mean IDI values are similar for the buildings whether estimated by Record, Vidic, or the pulses $R-\mu-T$ relations. IDI estimates tend to be low for the taller (12-story) buildings than the 4-story buildings, regardless of the strength of the buildings ("rigid" vs. "flexible"). Within this overall trend, estimates made by IDI^c tend to be high, those made by IDI^a tend to be low, and

IDI^b tends to result in the most accurate estimates of IDI. Standard deviation statistics for the estimates are nearly equal to those obtained for the record, indicating that most of the deviation in IDI estimates (relative to computed peaks) results from higher modes and/or lack of independence in modal combinations. Approximating nonlinear response using Vidic or pulse at T_1^* $R - \mu - T$ relations does little to the standard deviation statistics. There is a lot of dispersion in IDI estimates by a, b, and c, and adding dispersion in R is of little consequence.

Figure 6.13 shows the mean and standard deviation of the the estimated peak IDI ratios $IDI^s/IDI_{DRAIN-2DX}$, over all buildings, stories, and ground motions. While Eq. 6.9 (IDI^a) underestimates interstory drifts for the three R-factor models, Eq. 6.11 (IDI^c) overestimates the drifts. The SRSS combination (IDI^b, Eq. 6.10) gives the best results of the three models. The dispersion is smallest for the estimate using the record R-factor, followed by the estimate using the pulse R-factor having $T_p = T_1^*$. Estimates using $T_p = T_2^*$ were not computed but are expected to be in the vicinity of the T_1^* and T_g estimates.

In Fig. 6.13 the effect of estimating R-factors can be seen as the increase in standard deviation results relative to the record values (circle symbols). The pulse R-factors (T_1^*) are seen to be as good as the Vidic R-factors, with the largest errors coming from the inability to estimate modal contributions well. Potential sources of inaccuracy in the estimates include (1) the phasing of modal peaks, (2) the assumptions that the modal responses are independent and may be superposed, and (3) the contributions of the 3^{rd} and higher modes. The errors associated with modal combinations are dominant and are likely to persist since it is unlikely that the timing of modal peaks will ever be described accurately in site-specific hazard evaluations.

6.5 Inelastic Response of the Flexible-4 Building

Previous sections in this chapter have described the estimates of the peak roof displacements and peak interstory drift indices of two 4-story and two 12-story moment-resistant frame buildings subjected to 15 ground motion records based on equivalent SDOF models using various combinations of the first and second modal responses.

As noted in Section 6.4, in many cases, the buildings responded elastically. For these cases, the estimated elastic response of the building is independent of the R-factor model because $R(\mu = 1, T) = 1$. Only 23 out of 60 cases produced nonlinear response and these were precisely the cases where the scatter between the estimates of peak roof displacements and IDIs, and the nonlinear DRAIN-2DX values were the largest. The equivalent SDOF system technique assumes that the first mode is dominant. Knowing that higher modes affect the response as the number of stories and fundamental period of the building increase, it is clear that the estimates for the 12-story buildings should be less accurate than those obtained for the 4-story buildings. For the sake of completeness, the nonlinear response of the Flexible-4 building described in Section 6.4.1 is now studied in more detail, knowing beforehand that the estimates will worsen, not only for the approximate R-factor relations given by Vidic and the pulses instead of the record R-factor, but also for the record R-factor since modal peaks are assumed to be independent and then combined.

Rather than subjecting different buildings to a set of recorded motions, producing varied ductility responses, as was done in Section 6.4, this section studies the response of only one building (Flexible-4) to the 15 ground motions scaled to produce ductility responses of approximately 2, 4, and 8 in the first mode. The building frame is invariant throughout this process, and the period of the building remains constant.

6.5.1 Scaling the acceleration records.

The equivalent SDOF yield strength parameter corresponding to a given building is given in Eq. 6.3 as a function of the peak ground acceleration. The yield strength parameter can also be determined as the ratio of the elastic strength parameter to the R-factor (Eq. 6.5). Combining both definitions, the peak ground acceleration can be expressed as

$$a_{g,max} = \frac{V_y^{mdof}}{\alpha_e W_t} \cdot \frac{R^{sdof}(\mu, T)}{\eta_e^{sdof}(T)} \cdot g \tag{6.17}$$

The parameters of the Flexible-4 building associated with the first mode, found in Table 6.1, are $V_y^{mdof} = 585$ kN, $\alpha_e = 1.266$, and $T_1 = 1.16$ s. The total weight of the building, W_t, is 2,204 kN, and the acceleration of gravity, g, is 9.81 m/s^2. Considering the isoductile strength spectra of SDOF systems having 10% post-yield stiffness, 5% damping, and ductility demands of $\mu = 1$, 2, 4, and 8, for the 15 ground motion records, the elastic strength is given by $\eta_e^{sdof}(\mu = 1, T_1)$. The necessary R-factor to obtain a desired ductility is obtained by setting the period of the system equal to the first mode of vibration of Flexible-4, ($T = T_1$). The acceleration scale factors, χ, to be applied to the ground motion (Table 6.18), are given by the ratio

$$\chi = \frac{a_{g,max}}{a'_{g,max}} \tag{6.18}$$

where

- $a'_{g,max}$ is the required peak ground accelerations to achieve the R-factor for the ductility demands of 2, 4, and 8 (Eq. 6.17).
- $a_{g,max}$ is the recorded peak ground acceleration, given in Table 2.1

Notice that the record scale factor is determined to obtain the R-factor associated with obtaining target ductilities of 2, 4, or 8 based on the response of the equivalent SDOF system to the ground motion. The nonlinear response of Flexible-4 building subjected to the scaled records computed using the DRAIN-2DX program can result in larger or smaller roof displacements, depending on higher mode contributions. The data presented in the next figures and tables are described in terms of the nominal ductility values of $\mu \sim 2$, $\mu \sim 4$, and $\mu \sim 8$, reflecting the expected ductility responses if response was entirely in the first mode.

6.5.2 Peak displacement estimates

Peak roof displacement estimates were made following the steps in Section 6.3.1. The following figures show the peak roof displacement resulting from a) the ground motion $R - \mu - T$ relation,

Table 6.18: Acceleration scale factor, χ

Ground motion	$\mu = 2$	$\mu = 4$	$\mu = 8$
WN87MWLN.090	46.43	90.16	228.64
BB92CIVC.360	3.45	11.04	19.10
SP88GUKA.360	4.66	11.00	19.84
LP89CORR.090	1.83	2.677	6.954
NR94CENT.360	2.57	6.30	11.51
CH85LLEO.010	1.65	4.22	8.04
CH85VALP.070	4.59	9.07	19.18
IV40ELCN.180	2.10	3.93	7.73
LN92JOSH.360	1.84	3.91	8.80
MX85SCT1.270	1.64	2.08	2.89
LN92LUCN.250	1.00	1.50	2.37
LP89SARA.360	1.59	3.78	6.47
NR94NWHL.360	0.72	1.83	2.91
NR94SYLH.090	1.14	1.65	3.59
KO95TTRI.360	0.40	0.83	1.63

b) the Vidic et al.'s $R - \mu - T$ relation, and c) the pulse $R - \mu - T$ relation having $T_p = T_1^*$ and $T_p = T_g$. Figures 6.14 to 6.16 depict a graphic comparison among the different methods used to estimate the peak roof displacements with the results obtained by nonlinear dynamic analysis. The upper part of these figures plots the estimated peak roof displacement versus the DRAIN-2DX peak roof displacement. The diagonal line represents perfect estimation; points below the line indicate underestimation, while points above indicate overestimation of the peak roof displacement. The results obtained indicate that most of the estimated peak roof displacements using the Vidic R-factor and the pulse R-factors highly overestimate the nonlinear peak roof displacement. Meanwhile, the results using the record R-factor are rather constant for all ground motions, with a tendency to slightly overestimate the peak roof displacement.

The more or less horizontal line described by the record (circle symbol) results from specifying χ to achieve a peak roof displacement estimate based on the first mode equal to μ times the first mode yield displacement. The variation in peak roof displacement computed in DRAIN-2DX indicates the influence of higher modes. The higher modes are seen to bias the peak roof displacement towards values less than the first mode response. That the circles do not describe a perfectly horizontal line reflect minor round off errors and minor differences in the precision of the response calculations made by the various software programs.

The lower part of each figure shows ratios of the estimated peak roof displacement and the DRAIN-2DX peak roof displacement for each ground motion. In this case, the horizontal line represents perfect estimation; points below indicate underestimation of peak displacement, and above, overestimation. These plots shows the record R-factor tends to estimate the peak roof displacement best since there is no error in the R-factor, while some scatter results for the Vidic and the pulse R-factors. The scatter increases with ductility, and no difference is aparent among SD, LD, and FD motions, nor with T_g as T_g varies across the SD, LD, and FD motions.

Figure 6.17 plots the mean and standard deviation statistics of the peak roof displacement ratios over all ductility values and stories, for each ground motion. The mean values indicate that the peak roof displacement is overestimated except for the MX85SCT1.270, LN92LUCN.250, and NR94SYLH.360 records using the Vidic and the pulse R-factor models. In general, the smallest means and standard deviations correspond to the record R-factor model, the largest values corresponding to the pulse R-factor models, and intermediate values are obtained for the Vidic R-factor model. This is sensible because the record R-factors are exact, causing differences in peak displacements to be due to higher mode contributions.

Table 6.19 presents the mean and standard deviation of the estimated peak roof displacements to the nonlinear peak roof displacement ratios computed over all 15 ground motions and 4 stories for the target ductilities 2, 4, and 8, and the average over all ductilities. The average mean using the record R-factor is very good (1.092) compared with Vidic's (1.181) and the pulses (1.334 and 1.359). The average dispersion obtained with the record R-factor (0.097) is significantly lower than for the R-factor models, which have standard deviations ranging from 0.396 to 0.513. All methods are seen to systematically overestimate the peak roof displacement. Because peak roof displacements are overestimated even when the record R-factor is used, it appears that higher modes may systematically reduce the peak roof displacement relative to the estimate made using the first mode.

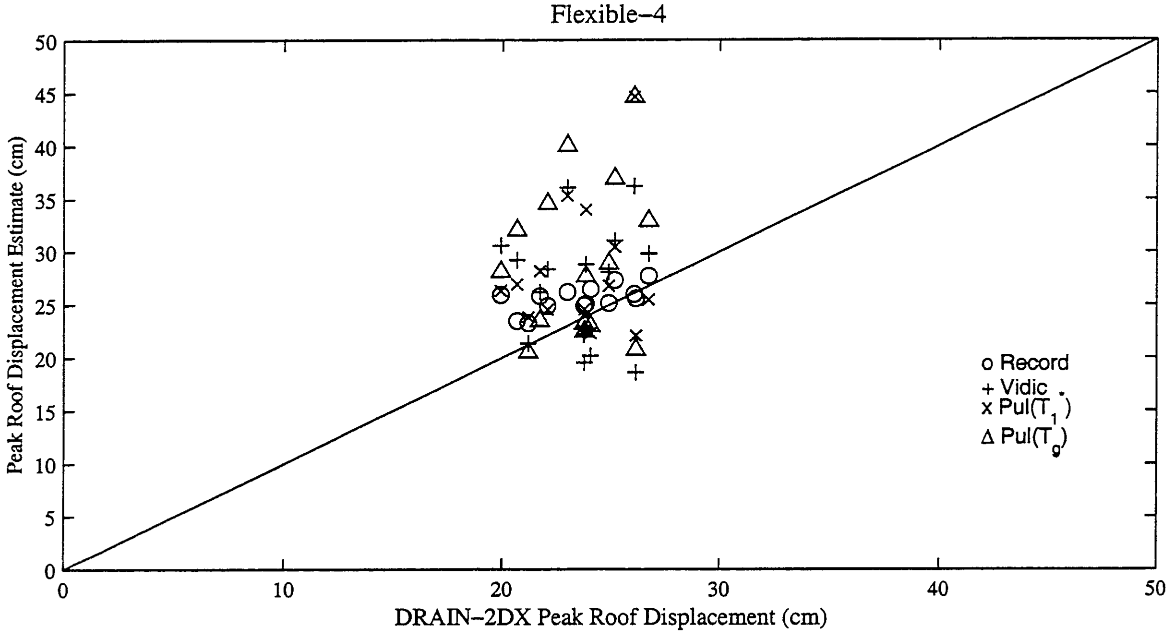

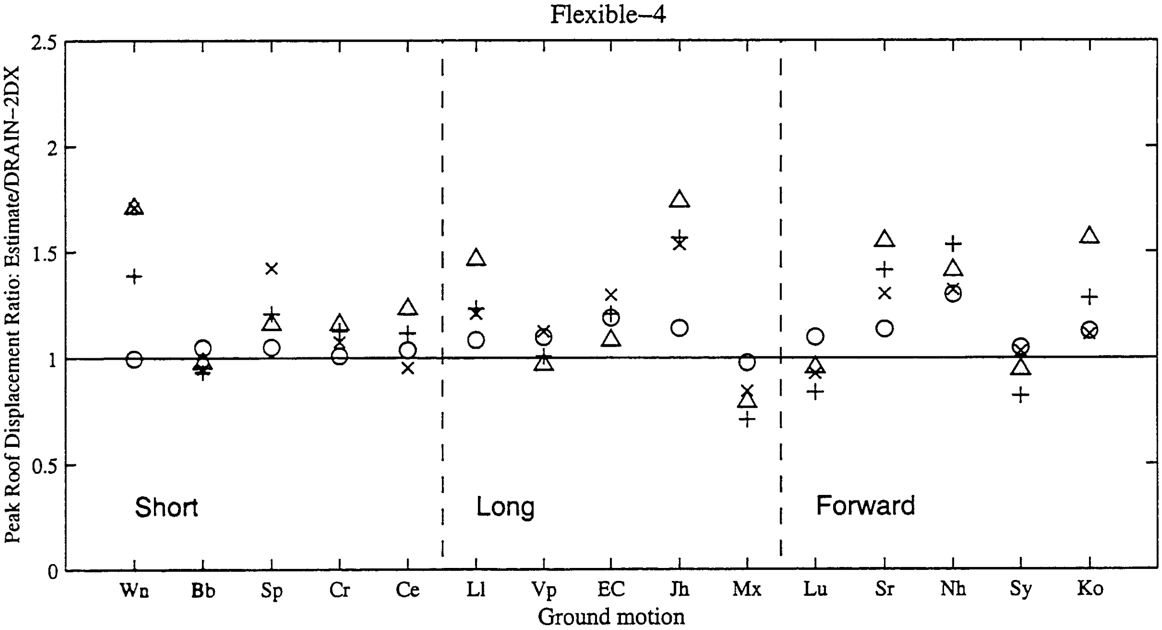

Figure 6.14: Peak roof displacement comparisons for the Flexible-4 building, $\mu \sim 2$

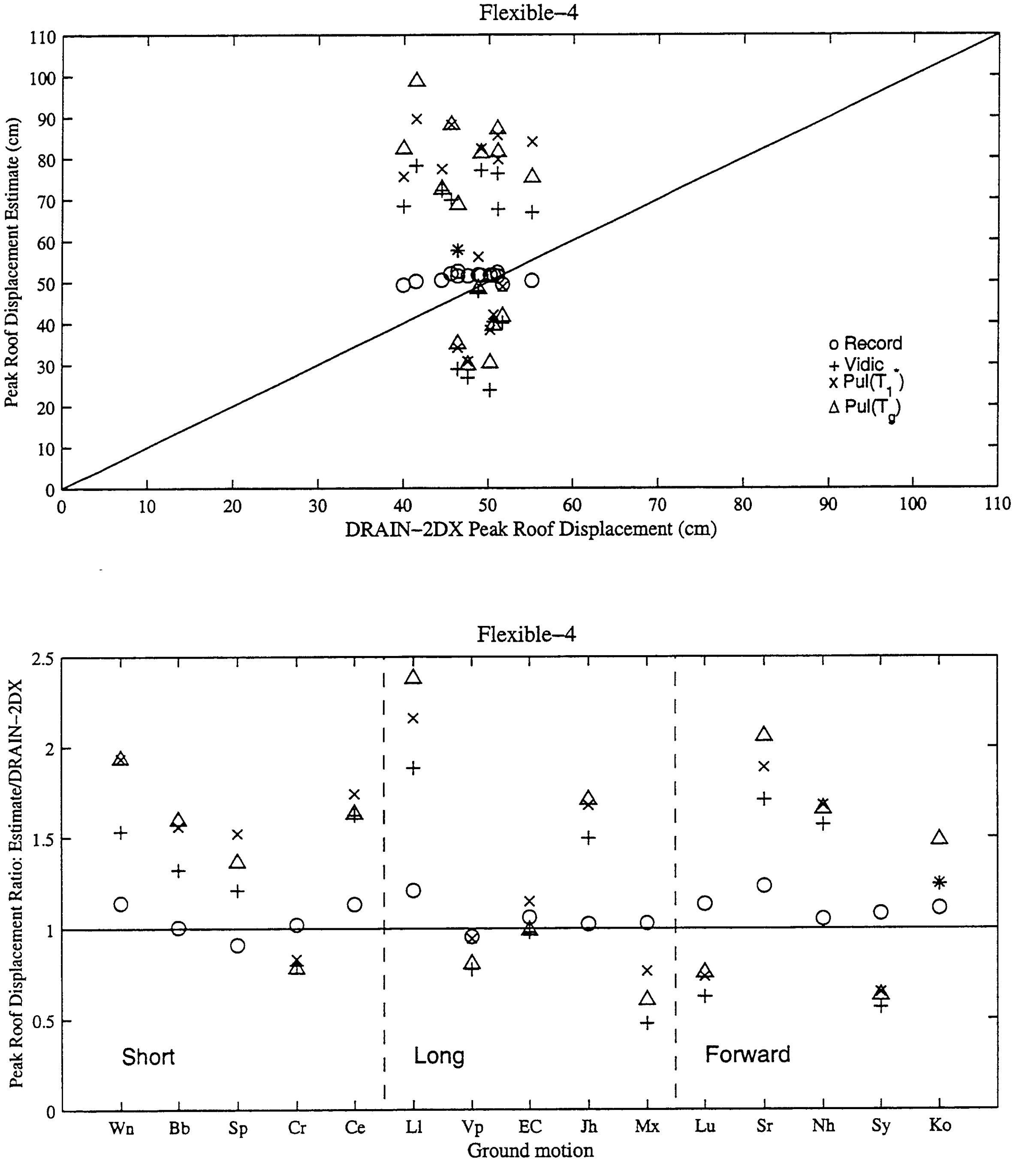

Figure 6.15: Peak roof displacement comparisons for the Flexible-4 building, $\mu \sim 4$

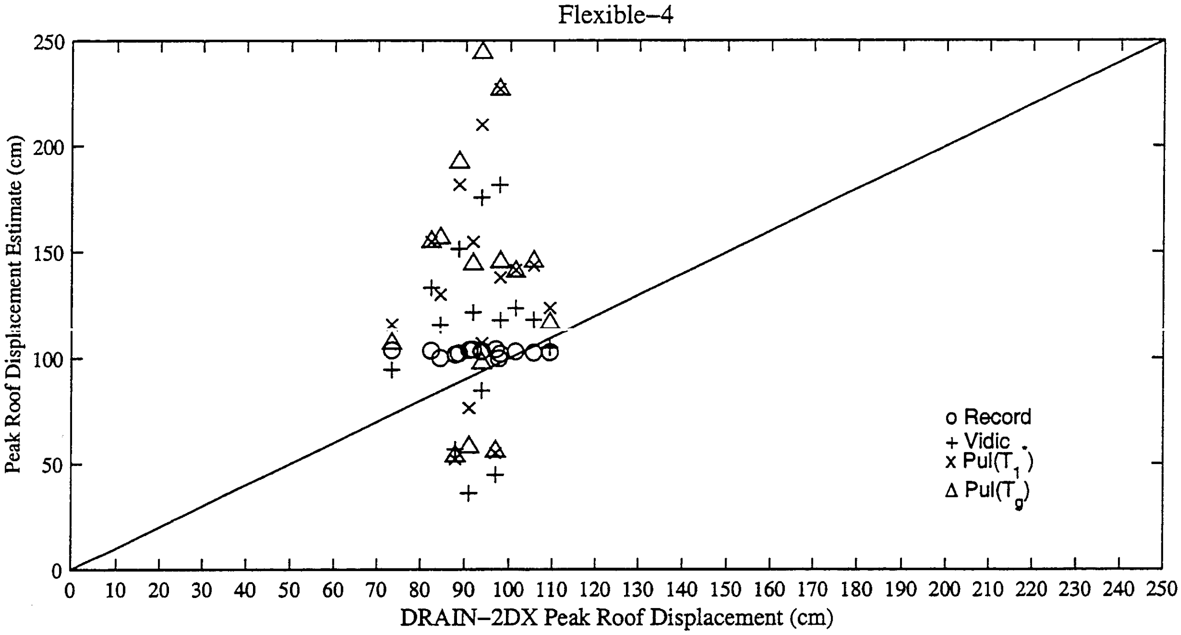

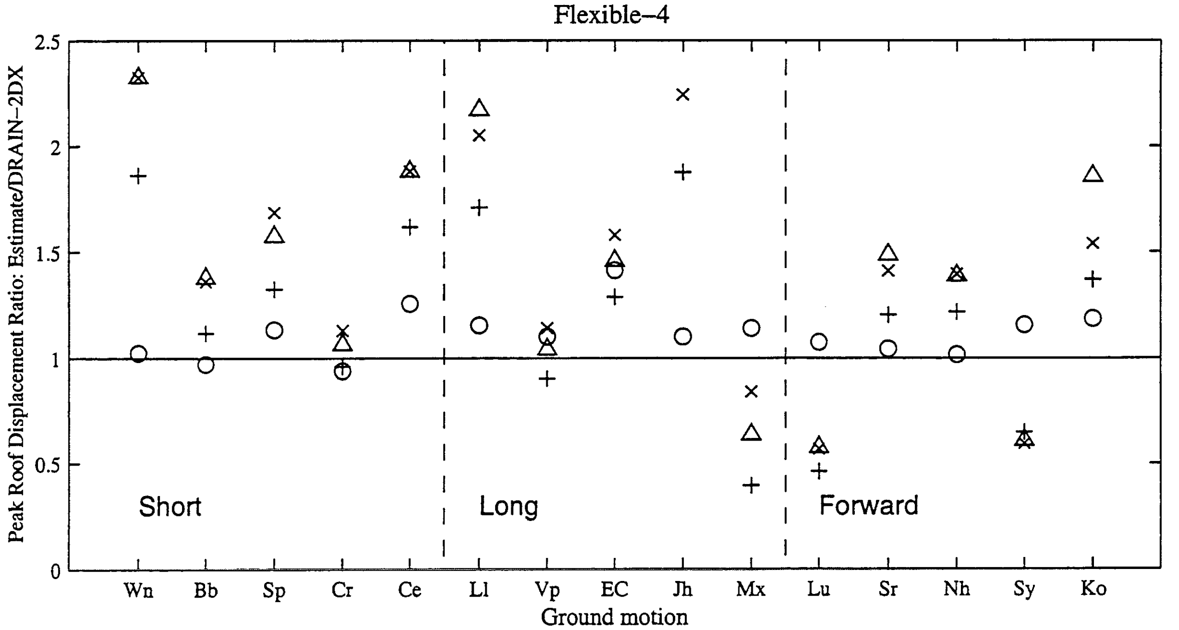

Figure 6.16: Peak roof displacement comparisons for the Flexible-4 building, $\mu \sim 8$

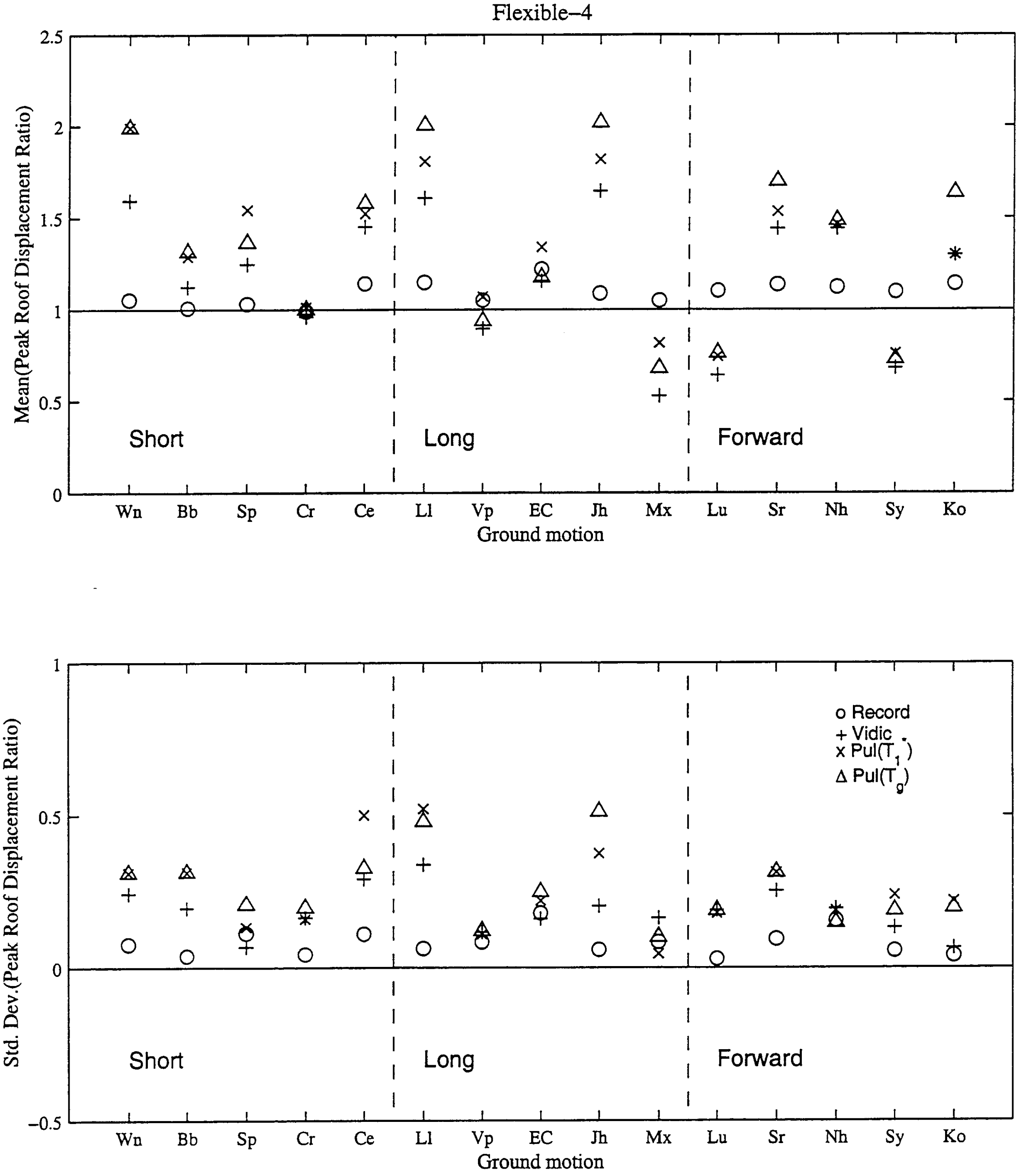

Figure 6.17: Mean and standard deviations for the peak roof displacement ratio over all ductility value

Table 6.19: Estimate peak roof displacement/Drain peak roof displacement ratio for Flexible-4, over all ground motion records and stories

Target Ductility	$Ratio_{record}$		$Ratio_{vidic}$		$Ratio_{pul(T_1^*)}$		$Ratio_{pul(T_g)}$	
	Mean	St. Dev.	Mean	St. Dev.	Mean	St. Dev.	Mean	St. Dev.
$\mu \sim 2$	1.089	0.083	1.158	0.260	1.187	0.245	1.247	0.305
$\mu \sim 4$	1.073	0.089	1.186	0.456	1.365	0.495	1.358	0.565
$\mu \sim 8$	1.115	0.118	1.197	0.465	1.450	0.542	1.471	0.624
$\forall \mu$	1.092	0.097	1.181	0.396	1.334	0.450	1.359	0.513

6.5.3 IDI estimates

Interstory drift indices are estimated using the three techniques described in Section 6.3.2. The first mode of vibration is used in Eq. 6.9 and the first two modes are combined in Eqs. 6.10 and 6.11.

Peak roof displacements associated with the first and second mode of vibration are computed according to Section 6.3.1 using the record, Vidic, and the pulse (having $T_p = T_g$ and $T_p = T_1^*$) R-factor models to estimate the peak roof displacements. The peak roof displacement in the first and second mode of vibration was estimated for equivalent SDOF systems having 10% post-yield stiffness, the first mode having 5% of the critical damping, and the second mode having 2.8% of the critical damping, which corresponds to the damping assigned to the first and second modes of vibration of the MDOF system in the nonlinear analysis computed with DRAIN-2DX.

Figures 6.18 to 6.20 shows the ratios $IDI^s/IDI_{DRAIN-2DX}$ averaged for all ductility values for each story of the Flexible-4 building subjected to the 15 ground motions scaled to get ductilities μ = 2, 4, and 8. The ratios are calculated for each story of the building using three estimates and then averaged. The estimates are: a) the record R-factor, b)the Vidic R-factor, and c) the pulse R-factor having $T_p = T_1^*$ and $T_p = T_g$. These are labeled Record, Vidic, Pul(T_1^*), and Pul(T_g), respectively in the figures.

Appendix B shows the figures of the ratios $IDI^a/IDI_{DRAIN-2DX}$ (Figs. B.13 to B.15 for $\mu \sim 2$), $IDI^b/IDI_{DRAIN-2DX}$ (Figs. B.16 to B.18, for $\mu \sim 4$), and $IDI^c/IDI_{DRAIN-2DX}$ (Figs. B.19 to B.21, for $\mu \sim 8$) for each story of the Flexible-4 building subjected to the 15 ground motions scaled to get ductilities $\mu = 2, 4, 8$. The general tendency in each figure (for any ductility and their average)

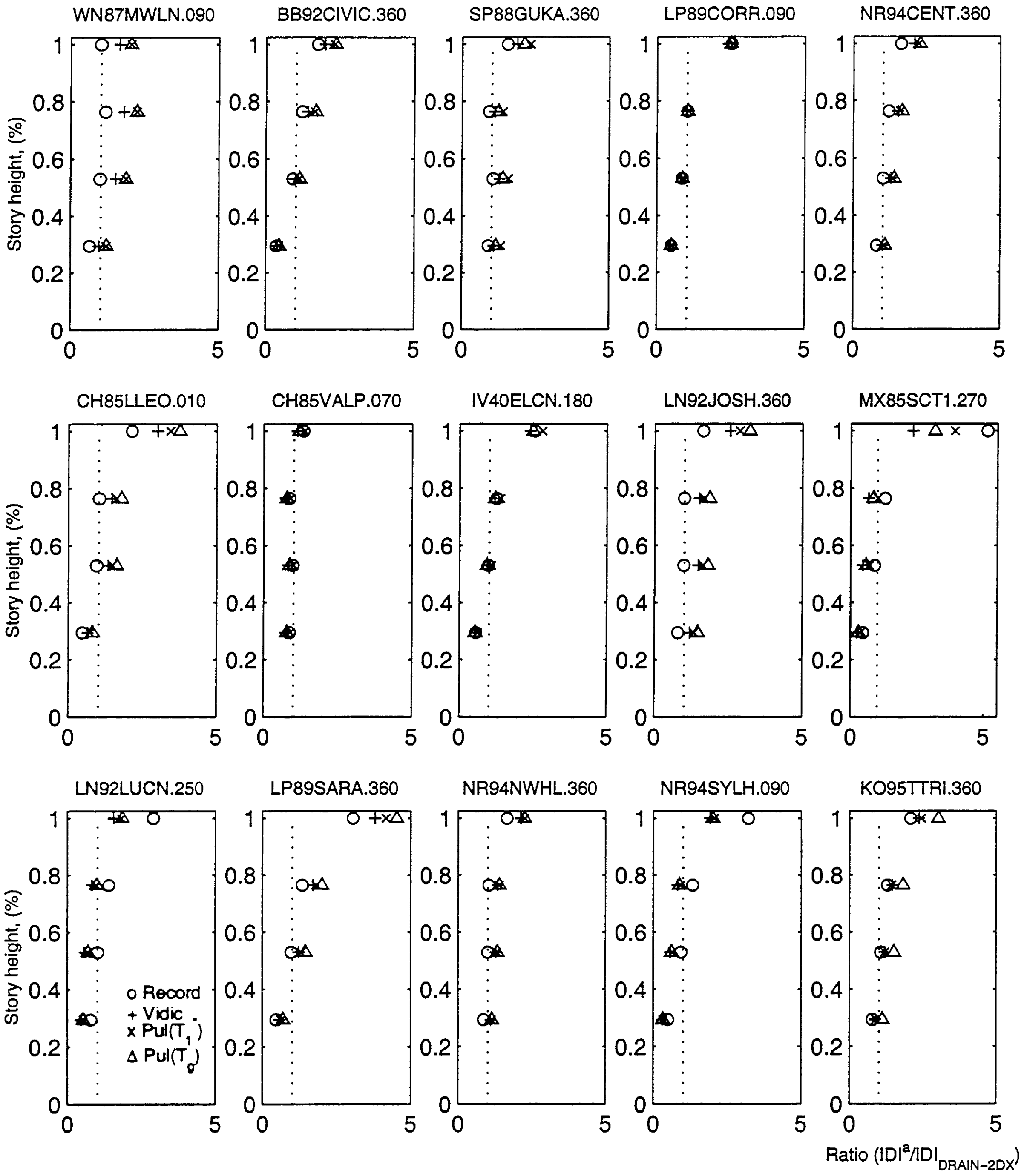

Figure 6.18: Ratio $IDI^a/IDI_{DRAIN-2DX}$ for Flexible-4 building subjected to each ground motion scaled, over all ductility value using Eq. 6.9

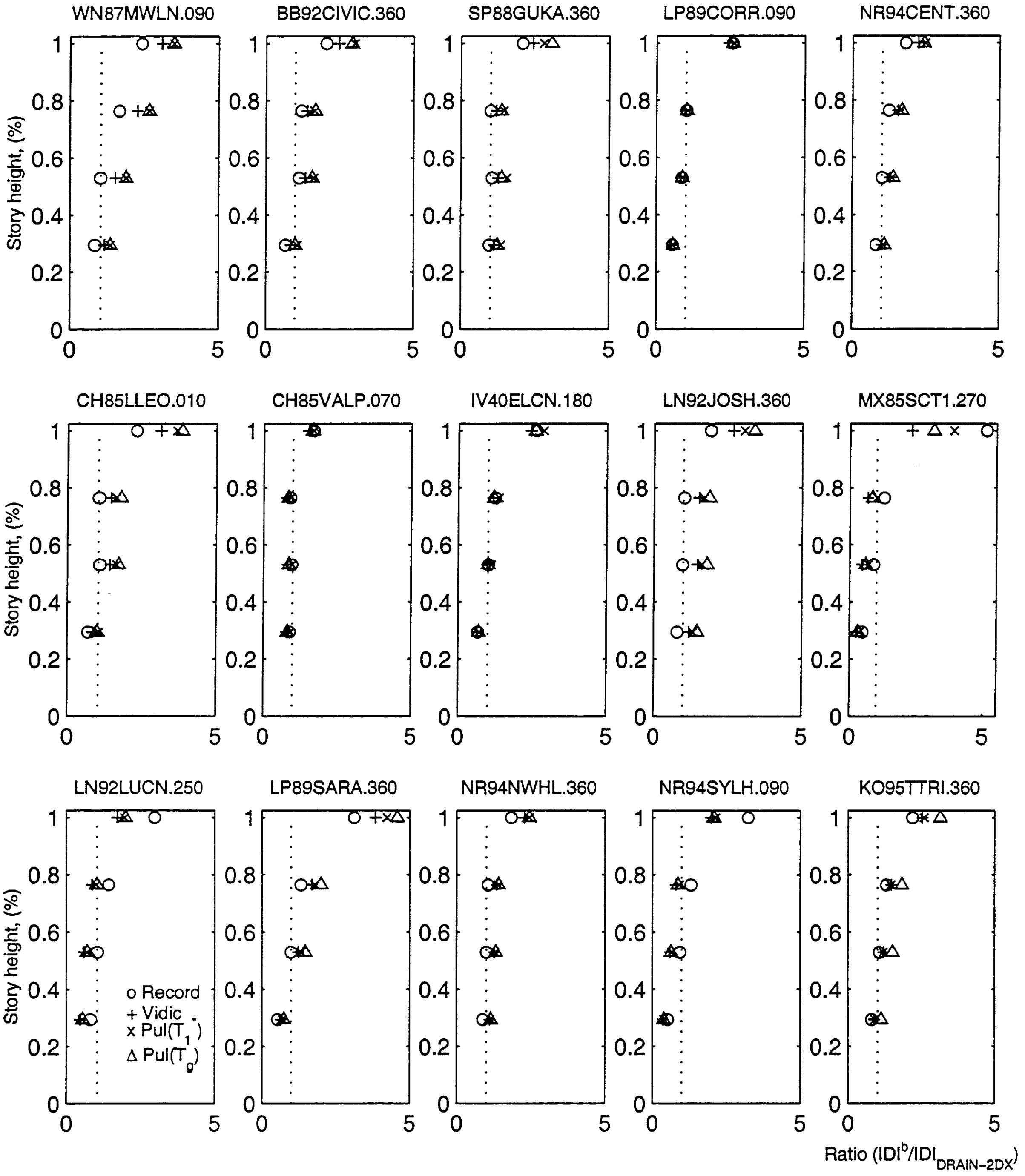

Figure 6.19: Ratio $IDI^b/IDI_{DRAIN-2DX}$ for Flexible-4 building subjected to each scaled ground motion, over all ductility values using Eq. 6.10

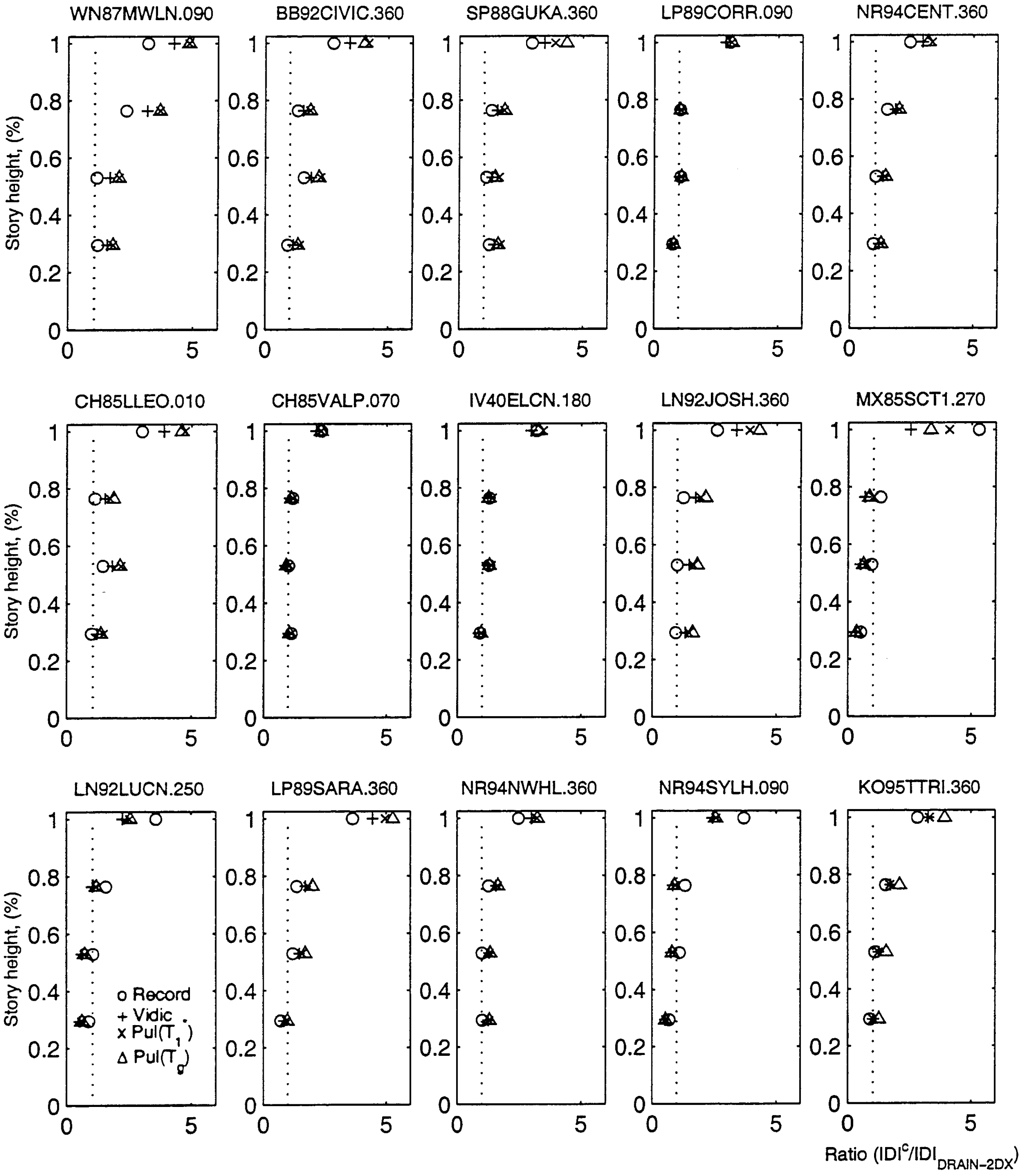

Figure 6.20: Ratio $IDI^c/IDI_{DRAIN-2DX}$ for Flexible-4 building subjected to each scaled ground motion, over all ductility values using Eq. 6.11

Table 6.20: Mean and standard deviation of the ratios $IDI^a/IDI_{DRAIN-2DX}$ over all ground motions and ductility values

	Record		Vidic		Pulse, $T_p = T_1^*$		Pulse, $T_p = T_g$	
Story	Mean	Std. Dev.	Mean	Std. Dev.	Mean	Std. Dev.	Mean	Std. Dev.
4	2.26	1.33	2.19	1.01	2.55	1.33	2.57	1.36
3	1.15	0.23	1.22	0.45	1.39	0.52	1.42	0.59
2	0.96	0.10	1.04	0.35	1.17	0.40	1.19	0.44
1	0.64	0.20	0.70	0.32	0.79	0.36	0.80	0.37
All	1.25	0.91	1.29	0.81	1.47	1.00	1.49	1.03

Table 6.21: Mean and standard deviation of the ratios $IDI^b/IDI_{DRAIN-2DX}$ over all ground motions and ductility values

	Record		Vidic		Pulse, $T_p = T_1^*$		Pulse, $T_p = T_g$	
Story	Mean	Std. Dev.	Mean	Std. Dev.	Mean	Std. Dev.	Mean	Std. Dev.
4	2.52	1.29	2.47	1.12	2.85	1.48	2.88	1.51
3	1.20	0.26	1.27	0.51	1.43	0.60	1.47	0.65
2	1.00	0.11	1.08	0.36	1.23	0.42	1.24	0.45
1	0.72	0.18	0.79	0.31	0.89	0.35	0.89	0.36
All	1.36	0.96	1.40	0.92	1.60	1.12	1.62	1.15

is that the IDI ratio of the top story is highly overestimated compared to the IDI ratios of the other stories. Estimates in the lowest story are low, even for IDI^c in some cases. Since the absolute sum of the two modal IDIs may be considered a reasonable upper bound, underestimation of the lowest story IDI using IDI^c requires some explanation. A possible explanation is that rapid reversals of the ground may concentrate large interstory drifts in the lowest stories. This result is present more or less equally in the elastic and inelastic IDI responses, in the SD, LD, and FD motions, and for different T_g.

Tables 6.20, 6.21, and 6.22 present the values of the means and standard deviations of the ratios

Table 6.22: Mean and standard deviation of the ratios $IDI^c/IDI_{DRAIN-2DX}$ for all ground motions and ductility values

	Record		Vidic		Pulse, $T_p = T_1^*$		Pulse, $T_p = T_g$	
Story	Mean	Std. Dev.	Mean	Std. Dev.	Mean	Std. Dev.	Mean	Std. Dev.
4	3.14	1.37	3.14	1.43	3.63	1.88	3.66	1.91
3	1.38	0.37	1.48	0.69	1.66	0.82	1.70	0.87
2	1.13	0.20	1.23	0.43	1.40	0.53	1.41	0.53
1	0.91	0.23	0.99	0.38	1.11	0.44	1.12	0.43
All	1.64	1.14	1.71	1.19	1.95	1.46	1.97	1.48

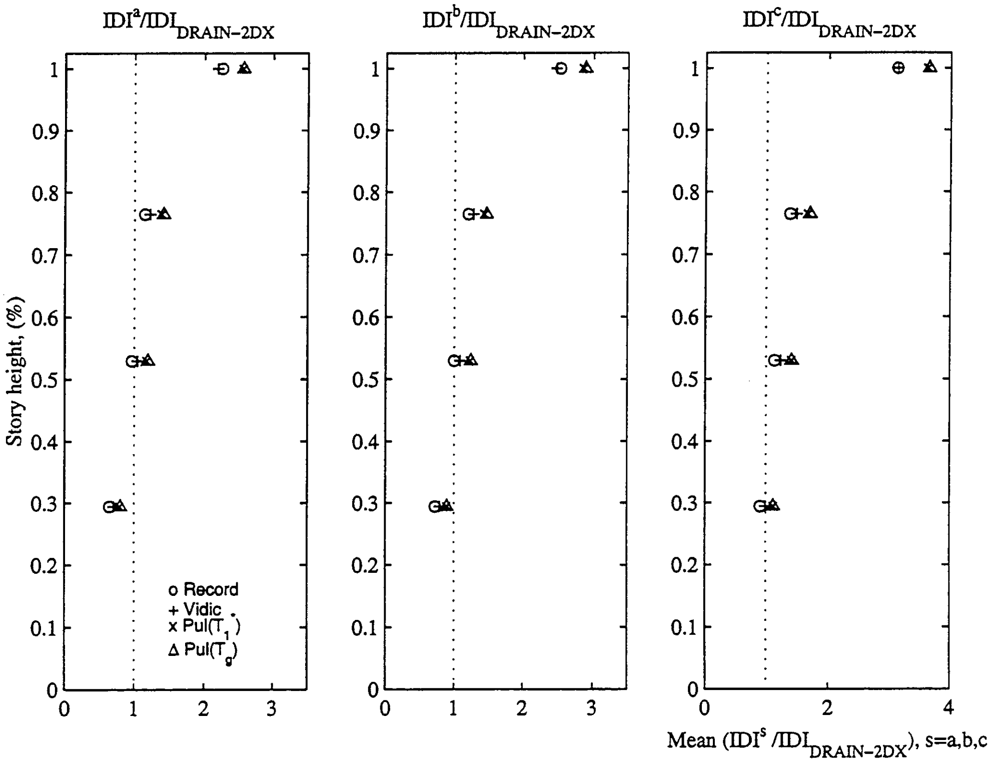

Figure 6.21: Mean ratios $IDI^s/IDI_{DRAIN-2DX}$, $s = a, b, c$ for Flexible-4 building, for each story, over all scaled ground motions and ductility values

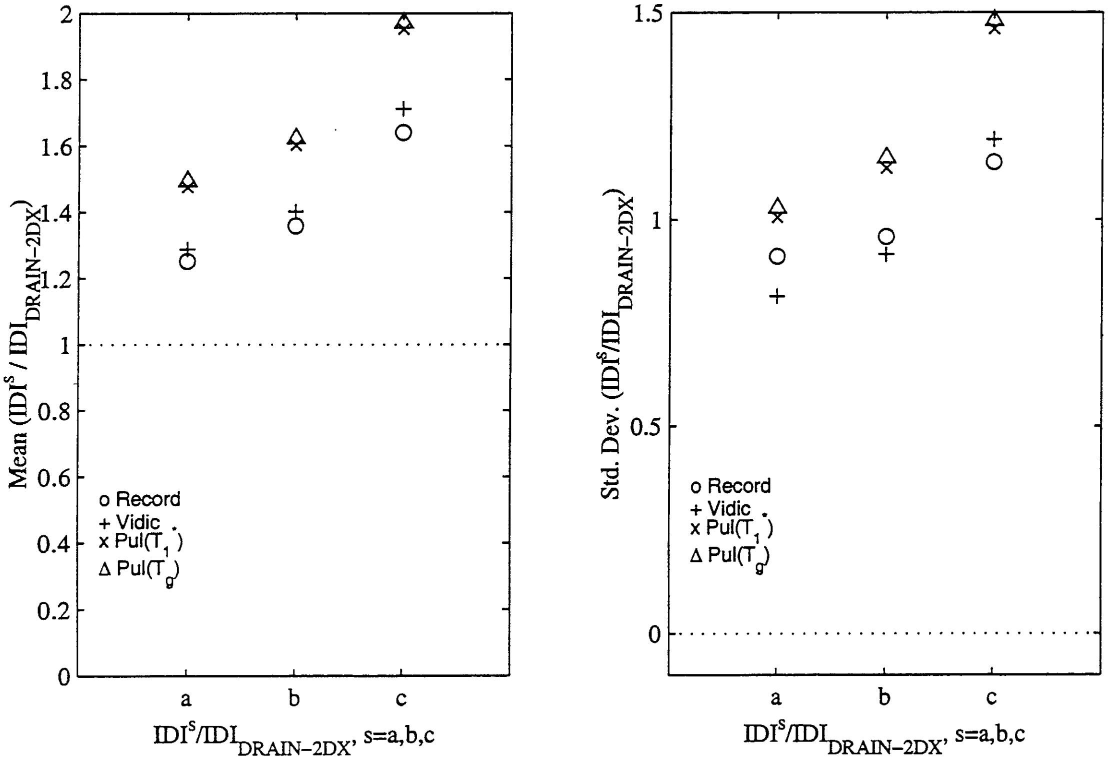

Figure 6.22: Mean and standard deviation of the IDI ratios, $IDI^s/IDI_{DRAIN-2DX}$, $s = a, b, c$ for Flexible-4 building, over all scaled ground motions, stories, and ductility values

$IDI^s/IDI_{DRAIN-2DX}$, $s = a, b, c$ for each story over all ground motions and ductility values using Eqs. 6.9 ($s = a$), 6.10 ($s = b$), and 6.11 ($s = c$), respectively, for the four estimates: the record, Vidic, and the pulses having $T_p = T_g$ and $T_p = T_1^*$. Figure 6.21 is the graphic representation of the mean values for each story and for each IDI equation. The vertical dashed line represents perfect correlation. Values to the right indicate the IDI for a given story is overestimated, and values to the left indicate underestimation. The three IDI ratios give similar results for all estimates and for each story: the first story IDI is underestimated, the second and third stories are slightly overestimated, and the top story is highly overestimated. The first story IDI is better estimated with IDI^b and IDI^c, and the second, third, and top stories are better estimated by IDI^a.

Figure 6.22 plots the mean and standard deviations of the sum of each ratio $IDI^s/IDI_{DRAIN-2DX}$, $s = a, b, c$ obtained for each ground motion, ductility value, and story using Eqs. 6.9 ($s = a$), 6.10 ($s = b$), and 6.11 ($s = c$), respectively, for the four R-factor estimates: the record, the Vidic, and the pulses having $T_p = T_g$ and $T_p = T_1^*$ (values displayed also in Tables 6.20 to 6.22). This figure shows that the means and deviations, although very large for all IDI ratios, are best estimated with the IDI^a ratio. The estimated IDI are better using the record and the Vidic R-factor relations compared with the estimates given by the pulses, but, in any case, none is very accurate.

6.6 Summary

An approach of using pulse R-factors instead of the record R-factors has been presented to estimate the peak roof displacement and interstory drift indices (IDI) of two 4-story and two 12-story buildings.

Peak displacement estimates were obtained with four R-factor models and compared with the response computed by nonlinear dynamic analysis using the DRAIN-2DX program. Three estimates of IDI were calculated using various combinations of the first and second modes of vibration. Results of the estimates were also compared using simple statistics.

With regard to estimates of peak roof displacement, when the two 4-story and the two 12-story buildings behave linearly, the peak roof displacement is generally estimated well (Table 6.14) using the equivalent SDOF system technique. A tendency to slightly overestimate the peak roof displacement was observed when using a first mode equivalent SDOF system when response was linear. When the buildings respond nonlinearly, the estimates given by the record R-factor are still good (Table 6.15), although the overestimation of the peak roof displacement response is reduced and more scatter is observed as ductility increases. The estimates obtained using the R-factor models (Vidic and the pulses) get worse, often highly overestimating the roof displacement response as ductility increases, with dispersion increasing considerably with respect to the dispersion associated with the record R-factor. Thus, accurate estimates of the peak roof displacement of the 4- and 12-story buildings can be obtained using a first mode equivalent SDOF system if the $R-\mu-T$ relation for the ground motion record is known.

With regard to estimates of peak interstory drift, when linear and nonlinear responses are mixed, the peak IDIs of the four-story buildings are best estimated using only one mode of vibration, indicating that the response is mainly controlled by the first mode of vibration, for the four R-factor models. The peak IDIs of the 12-story buildings are best estimated with the SRSS technique considering the first and second modes of vibrations (IDI^b).

The study of the nonlinear response of the Flexible-4 building showed that:

- The peak IDIs for the first, second, and third story are well estimated using only the first mode of vibration.
- The peak IDI of the top story is highly overestimated (Fig. 6.21), independent of the R-factor model used. This effect is larger whe response is nonlinear, as compared with the mixed linear and nonlinear responses. The overestimation of the peak IDI of the top story increases as the ductility demand of the system increases.
- The peak IDI of the first story is systematically underestimated using the three estimates (the record, Vidic et al and the pulse R-factors). This may be due to rapid reversals of the ground

that may concentrate large interstory drifts in the lowest stories.

These observations suggest that estimates of IDI are prone to significant errors for buildings behaving nonlinearly, due to assumptions that: a) response is predominantly in a single mode, and b) the mode shape remains constant throughout the response. These errors are larger when the record R-factor is approximated with other relations such as Vidic or the pulse R-factor relations. Higher mode effects appear to significantly effect the interstory drifts in the 4- and 12-story buildings. The goodness of the estimate of peak roof displacement using a single mode of vibration shows that nonlinear MDOF response can be estimated using an equivalent SDOF system with all nonlinearity represented in the R-factor determined for the SDOF oscillator responding to a simple pulse.

Chapter 7

Conclusions and Future Research

7.1 Conclusions

This thesis investigates the possibility of estimating the nonlinear response of SDOF and MDOF systems to strong ground motion records of short and long duration as well as records with near-fault forward directivity features, using information provided by the response of SDOF systems subjected to simple pulses having different shapes and durations.

Observations of the computed response of elasto-plastic SDOF systems subjected to 15 ground motions (Chapter 2) indicate that typically only one or several cycles of ground motion cause yielding in many of the systems studied. These cycles, characterized by their short duration and complex and irregular shape, produce maximum response displacements in the systems at occurrence times that are not known *a priori*. This observation suggests that the inelastic response to simple pulses may be capable of representing response to more complex earthquake ground motions using the strength associated with the pulses. In general, a simple pulse cannot contain the relatively rich range of frequencies that often are present in earthquake ground motions. The R-factor, however, relates to the ductility that develops in just one or several cycles of ground motion, and thus it is observed that the R-factors for ground motions often are similar to those determined for pulses.

For pulse R-factors to work, an accurate estimate of elastic spectra is needed, since elastic spectral amplitudes are strongly affected by resonance.

Sewell [45] found that the damaging characteristics of numerous ground motions can be separated into two distinct components: (1) an elastic contribution, given by the elastic pseudo-acceleration response, and (2) a strength reduction factor, R, (given by the ratio of the strength required for elastic response to the strength required for a given ductility demand) applied to the elastic spectrum to determine the strengths of nonlinear oscillators that result in constant ductility responses.

In order to determine if simple pulses might lead to proper estimates of the required strengths of the systems, isoductile strengths and strength reduction (R) factors were determined for elasto-plastic SDOF systems, defined by the initial period of the system (T) and ductility response (μ) to 24 idealized pulse waveforms (Chapter 3). A characteristic period of each pulse, T_p, was identified, which separates the regions of the spectra where peak strengths (to the left of $T = T_p$) and peak R-factors (to the right of $T = T_p$) are located. The study of a large number of elasto-plastic SDOF oscillator responses to the 24 simple pulses allowed the following conclusions and trends to be identified:

1. Isoductile strengths of short period systems are higher for shock loading than for gradual loading pulses. Strengths are sensitive to the shape of the pulse for $T \leq T_p$.
2. The impulse-momentum principle is applicable to the elastic and inelastic response of long period systems, which experience the pulse as an impulse, independent of pulse shape.
3. Within any one family of pulses, R-factors depend on the number of incursions, since this number affects the elastic response substantially but has little effect on inelastic isoductile strengths.
4. Previous studies that focused on a subset of the pulses considered herein led to the preservation of force, equal energy, and equal displacement rules that are widely accepted in earthquake engineering. The applicability and limitations of these rules for the set of 24 pulses are as

follows:

- The equal displacement rule applies to systems with high T/T_p ratios. The rule is valid for all pulses considered and for forced response (peak response at $t < t_d$, where t_d = pulse duration) and overall response (peak response at any time), consistent with prior findings.
- The equal energy rule applies only to the overall response of intermediate period systems subjected only to unbalanced pulses over a relatively narrow period range. The equal displacement rule is applicable to intermediate period systems subjected to balanced pulses (overall response) and to both balanced and unbalanced forced vibration responses. These observations are counter to conventional views, which hold that the equal energy rule is generally applicable to intermediate period systems.
- Short period systems subjected to shock pulses can be considered to be subject to an instantaneous acceleration change, consistent with prior findings.
- The strength required for short period elasto-plastic systems subjected to gradual loading pulses is approximately $m \cdot a_{g,max}$ regardless of the ductility level, for the cases considered. This is consistent with prior findings that force is preserved in short period systems, and relates to the observation that R-factors tend to unity as period tends to zero. Systems with post yield stiffness equal to α times the initial stiffness subjected to gradual pulses must have yield strengths equal to $m \cdot a_{g,max}/(1+\alpha(\mu-1))$ to limit the ductility response to μ, as discussed in Chapter 5.

In Chapter 4, inelastic spectra of SDOF systems subjected to strong ground motions are estimated by applying strength reduction factors determined for a simple pulse to the elastic response spectrum of the ground motion. This approach relies upon similarities in the strength reduction factors computed for earthquake ground motions and for short duration pulses.

Three measures of the error in the estimated dimensionless strength parameters were developed. The three measures of error were used so that any conclusions made with respect to the pulses that minimize error are robust with regard to the error metric. These measures are particularly sensitive to the differences in the strengths associated with the ground motion and the estimated strengths in the short period range, where the strengths are largest. Using these error measures it was found that:

1. The quadratic pulses qua(2) (overall response for systems with $\mu = 4$ and 8) and qua(3) (forced response for systems with $\mu = 2$) are adequate for 14 of the 15 records studied, while the sinusoidal pulse sin(5) is necessary to estimate the inelastic spectra for the soft soil SCT record of the 1985 Michoacan earthquake (MX85SCT1.270).
2. For simplicity and with little increase in error, the R-factor for the overall response to the qua(2) pulse may be used for ductilities of 2, 4, and 8 for all records except the 1985 Michoacan record.

The goodness of the pulse R-factors appears to be independent of the classification of the records into the SD, LD, and FD categories. This result is particularly useful because:

1. A single pulse shape may be useful for generating the R-factors suitable for different load-deformation and hysteretic characteristics, rather than requiring separate $R-\mu-T$ relations to be developed along traditional lines for each case of interest, and,
2. Features of waveform independence demonstrated in Chapter 4 suggest that pulse R-factors and $R-\mu-T$ relations may be used for estimating the inelastic response spectra of unknown future ground motions, an issue of particular interest where recorded ground motions are not available because historic seismicity preceded the relatively recent deployment of strong motion instrumentation.

In Chapter 5, isoductile strengths of bilinear and stiffness-degrading SDOF systems having ductility demands $\mu = 2$, 4, and 8, subjected to the 15 ground motions, were compared with the estimated isoductile strengths, given by the ratio between the strength required for elastic response of the system subjected to the ground motion and the strength reduction (R) factor of the same system subjected to a simple pulse. While the R-factors determined for earthquakes are dependent on the period of the system T, the R-factors determined for pulses depend on the dimensionless time parameter T/T_p, where T_p is the characteristic period of the pulse. The success in approximately reproducing the R-factors of the ground motions depends in large degree on the relation between T_p and the "frequency content" of the ground motion. A characteristic period of the ground motion, T_g, is defined as the intersection period of the constant acceleration and constant velocity portions of a smoothed elastic response spectrum for damping equal to 5% of critical damping. Results indicate that very good estimates of inelastic response spectra can be obtained when the pulse R-factor is applied to the elastic spectrum computed for the ground motion if the characteristic period of the pulse T_p was set equal to the characteristic period of the ground motion, T_g (Table 2.1). The period T_2^* (Eq. 5.7), at the intersection of the constant acceleration and constant velocity portions of the spectrum, also resulted in very good estimates of the inelastic spectra. While the period T_g was determined by eye, the period T_2^* gave a consistant and useful definition for all ground motions, and is also valid for harmonic pulses ($T_p = T_2^*$). These periods, T_g and T_2^*, are nearly equal to the characteristic periods of the pulses, T_1^*, that minimized the errors of the estimated isoductilie strengths using the qua(2), qua(3), and sin(5) pulses.

Good estimates of the inelastic response spectra were also obtained using the Vidic et al. relation. This relation is a function of the ratio T/T_a, where T_a is also related to an estimate of this intersection period (Section 1.2.2). Together these two results strongly suggest that $R - \mu - T$ relations instead should be formulated in terms of T/T_g, rather than T alone, to explicitly address ground motion frequency characteristics. Conveniently, T_g is readily discerned from typical code spectra [67, 2, 68], for example, as the period T_s used to define smoothed elastic design spectra in the *NEHRP Provisions* [2].

Among all the pulses considered in this study, a pulse called qua(2) (see Fig. 5.1), with duration equal to T_p and pulse shape having quadratic components in the acceleration history, represented well the R-factors of bilinear and stiffness-degrading systems subjected to 14 of the 15 earthquake ground motions. A sinusoidal pulse was needed for the soft soil SCT record of the 1985 Michoacan earthquake. Even though it was found necessary to use a harmonic pulse to generate suitable R-factors for the Mexico City SCT record, the overall finding supports the idea that R-factors exhibit a sufficient degree of waveform independence that R-factors determined from simple pulses can be used to estimate the inelastic response spectra of a highly varied set of earthquake ground motions, when used in conjunction with the elastic response spectra computed for these ground motions. Based on Sewell [45] this finding should be equally applicable to records obtained from sites at varied distances and for earthquakes of varied magnitudes. Furthermore, the estimates of isoductile strength response spectra using these pulses tended to have less error relative to the estimates made using six contemporary $R-\mu-T$ relations (Chapter 5 applies the Newmark and Hall [21], Riddell, Hidalgo, and Cruz [22], Nassar and Krawinkler [23], Miranda [24], Vidic, Fajfar, and Fischinger [25], and Ordaz and Pérez-Rocha [26] relations). The Vidic et al. relation was found to be similar in accuracy to the qua(2) pulse. Other contemporary approaches were less accurate and in some cases also require posterior knowledge of ground motion characteristics. Given the goodness of the bilinear relation used by Vidic et al., the precise curve described by the pulse R-factor does not appear to be of critical importance, and a bilinear approximation such as employed by Vidic et al. appears suitable, given the uncertainties inherent in future ground motions. The pulse R-factors, however, are also applicable to soft soil sites, and because of their implicit definition (once the pulse shape and duration have been identified), they can be generated for different load-deformation and hysteretic relations, while the parameters that define contemporary $R-\mu-T$ relations can be established only by extensive numerical computations for a large number of ground motions for the set of parameter values that characterize the specific load-deformation (hysteretic) model of interest. This implicit specification may allow the effects of different hysteretic responses to be evaluated by considering the response of such oscillators to a simple pulse such as the qua(2) pulse. The implications of these findings are significant for the determination of future $R-\mu-T$ relations. These findings indicate that ground motion frequency characteristics should be explicitly reflected in the R-factor formulations, and that the pulses are conceptually sufficient to represent the phenomenon of yielding when the peak response to earthquake ground motions develops.

While similarities in the nonlinear response of SDOF systems to earthquake ground motions and to simple pulse waveforms have been known for several decades [41, 34], only very recently have researchers recommended that pulses be used in place of near-fault records to represent forward directivity effects [38, 35, 36, 39] in earthquake-resistant design. The use of pulses as substitutes for near-fault records must contend with several difficulties, including:

1. Simple pulses cannot reproduce the elastic spectra generated by earthquake ground motions.
2. The use of shock loading pulses leads to inappropiate values of the R-factor for short period systems. The shock pulses produce larger isoductile strength demands in short period systems than occur with gradual pulses and the earthquake records considered herein, and have reduction factors $R = (2\mu - 1)/\mu$ that exceed unity (see Section 3.4).
3. The phasing of higher modes with a pulse is unlikely to be consistent with the phasing associated with richer, more complex, and longer duration motions such as earthquake ground motions.

Table 4.2 shows that responses to FD records are best estimated with the quadratic family of pulses (which have $R = 1$ for short period systems) rather than with shock pulses. This result is also supported by Baez and Miranda [59], who state that for extremely short period systems $R = 1$ for all ground motions regardless of near-fault effects. Shock loading pulses are not necessary to generate pulses in the velocity histories. The recommended gradual pulse qua(2) has a velocity pulse in the time history, as shown in Fig. A.1, as do many other pulses (see Appendix A). The qua(2) pulse R-factor was found to be equally valid for the SD, LD, and FD records; there was no indication in this study that suggested different R-factors were necessary for the FD records.

Although this study is mainly focused on the response of SDOF systems, the nonlinear response of a limited number of MDOF systems was estimated using pulse R-factors. The technique employed consisted of reducing a MDOF system to an equivalent SDOF system and approximating the R-factor associated with SDOF response to the ground motion with the pulse R-factor. Results indicated that good estimates of the peak roof displacements and IDI can be obtained using the pulse R-factor, but these estimates worsen as the ductility demand of the systems increases. Often the single mode estimates of peak roof displacement exceeded the peak roof displacements computed by nonlinear analysis of the MDOF structure.

Equivalent SDOF representations of MDOF response were accurate when the R-factor is determined precisely for the equivalent SDOF system and the ground motion. The use of the pulse R-factor reduces accuracy somewhat. Even so, the two simplifications indicate that peak roof displacements occurring in the nonlinear response of a MDOF structure to an earthquake ground motion can be represented approximately by the nonlinear response of an equivalent SDOF system, where the nonlinearity is contained in the $R - \mu - T$ relation associated with response to a simple pulse. While some inaccuracy in peak roof displacements and IDIs is associated with uncertainty in the R-factor, other sources of dispersion in these estimates appear to be more significant. These include (1) variability in the phasing of modal peaks, (2) the assumption that modal contributions are independent and may be superposed, and (3) the contributions of the 3^{rd} and higher modes.

7.2 Future Research

Despite the magnitude of the effort represented in the present work, further research may be fruitful in the following areas:

1. A deeper study of the pulses that best characterize the R-factor for a larger number of ground motions should be performed. The present study only considered bilinear and stiffness-degrading systems. SDOF systems having stiffness and strength degradation, negative post-yield stiffness, and pinching should also be investigated.

2. The comparison of the isoductile strengths of SDOF systems with the estimated strengths resulted in very good results even though two simplifications were undertaken. The first simplification was to consider a single pulse for all ductility values, although the optimal pulse differs for each ductility demand. The second simplification was to consider the characteristic period T_p to be fixed for all ductilities, knowing that the period T_p that improves the estimated strengths for any given pulse and ground motion also depends on the ductility demand of the system. These two simplifications should be confirmed using a broader set of ground motion records and pulses.

3. Optimal pulses and the possibility of bilinear simplifications similar to those done by Vidic et al. should be further explored, along with the use of parameters such as T_2^* to characterize the ground motion frequency content and the characteristic period of the pulse.

Appendix A

Description of the 24 Simple Pulse Waveforms

Tables A.1 to A.6 present the acceleration equations of the 24 pulses used in the thesis. Each table describes one pulse family, identifying the names of the pulses and the equations of the time history of pulse acceleration normalized by peak ground acceleration:

$$\frac{a_g}{a_{g,max}}$$

where:

- a_g = pulse acceleration, as a function of the dimensionless time parameter $\frac{t}{t_d}$
- $a_{g,max}$= peak pulse acceleration
- t = time
- t_d = duration of the pulse

The acceleration, velocity, and displacement of the pulse families are plotted versus t/t_d, in Figs. A.1 to A.5.

Table A.1: Quadratric family

Pulse name	Acceleration equation
$qua(1)$	$\frac{a_g}{a_{g,max}} = \begin{cases} 4\left(\frac{t}{t_d}\right)^2 & 0 \le \frac{t}{t_d} < \frac{1}{2} \\ 4\left(1-\frac{t}{t_d}\right)^2 & \frac{1}{2} \le \frac{t}{t_d} \le 1 \end{cases}$
$qua(2)$	$\frac{a_g}{a_{g,max}} = \begin{cases} 16\left(\frac{t}{t_d}\right)^2 & 0 \le \frac{t}{t_d} < \frac{1}{4} \\ 16\left(\frac{1}{2}-\frac{t}{t_d}\right)^2 & \frac{1}{4} \le \frac{t}{t_d} < \frac{1}{2} \\ -16\left(\frac{1}{2}-\frac{t}{t_d}\right)^2 & \frac{1}{2} \le \frac{t}{t_d} < \frac{3}{4} \\ -16\left(1-\frac{t}{t_d}\right)^2 & \frac{3}{4} \le \frac{t}{t_d} \le 1 \end{cases}$
$qua(3)$	$\frac{a_g}{a_{g,max}} = \begin{cases} 6^2\left(\frac{t}{t_d}\right)^2 & 0 \le \frac{t}{t_d} < \frac{1}{6} \\ 6^2\left(\frac{1}{3}-\frac{t}{t_d}\right)^2 & \frac{1}{6} \le \frac{t}{t_d} < \frac{1}{3} \\ -6^2\left(\frac{1}{3}-\frac{t}{t_d}\right)^2 & \frac{1}{3} \le \frac{t}{t_d} < \frac{1}{2} \\ -6^2\left(\frac{2}{3}-\frac{t}{t_d}\right)^2 & \frac{1}{2} \le \frac{t}{t_d} < \frac{2}{3} \\ 6^2\left(\frac{2}{3}-\frac{t}{t_d}\right)^2 & \frac{2}{3} \le \frac{t}{t_d} < \frac{5}{6} \\ 6^2\left(1-\frac{t}{t_d}\right)^2 & \frac{5}{6} \le \frac{t}{t_d} \le 1 \end{cases}$
$qua(4)$	$\frac{a_g}{a_{g,max}} = \begin{cases} 8^2\left(\frac{t}{t_d}\right)^2 & 0 \le \frac{t}{t_d} < \frac{1}{8} \\ 8^2\left(\frac{1}{4}-\frac{t}{t_d}\right)^2 & \frac{1}{8} \le \frac{t}{t_d} < \frac{2}{8} \\ -8^2\left(\frac{1}{4}-\frac{t}{t_d}\right)^2 & \frac{2}{8} \le \frac{t}{t_d} < \frac{3}{8} \\ -8^2\left(\frac{1}{2}-\frac{t}{t_d}\right)^2 & \frac{3}{8} \le \frac{t}{t_d} < \frac{4}{8} \\ 8^2\left(\frac{1}{2}-\frac{t}{t_d}\right)^2 & \frac{4}{8} \le \frac{t}{t_d} < \frac{5}{8} \\ 8^2\left(\frac{3}{4}-\frac{t}{t_d}\right)^2 & \frac{5}{8} \le \frac{t}{t_d} < \frac{6}{8} \\ -8^2\left(\frac{3}{4}-\frac{t}{t_d}\right)^2 & \frac{6}{8} \le \frac{t}{t_d} < \frac{7}{8} \\ -8^2\left(1-\frac{t}{t_d}\right)^2 & \frac{7}{8} \le \frac{t}{t_d} \le 1 \end{cases}$
$qua(5)$	$\frac{a_g}{a_{g,max}} = \begin{cases} 10^2\left(\frac{t}{t_d}\right)^2 & 0 \le \frac{t}{t_d} < \frac{1}{10} \\ 10^2\left(\frac{1}{5}-\frac{t}{t_d}\right)^2 & \frac{1}{10} \le \frac{t}{t_d} < \frac{2}{10} \\ -10^2\left(\frac{1}{5}-\frac{t}{t_d}\right)^2 & \frac{2}{10} \le \frac{t}{t_d} < \frac{3}{10} \\ -10^2\left(\frac{2}{5}-\frac{t}{t_d}\right)^2 & \frac{3}{10} \le \frac{t}{t_d} < \frac{4}{10} \\ 10^2\left(\frac{2}{5}-\frac{t}{t_d}\right)^2 & \frac{4}{10} \le \frac{t}{t_d} < \frac{5}{10} \\ 10^2\left(\frac{3}{5}-\frac{t}{t_d}\right)^2 & \frac{5}{10} \le \frac{t}{t_d} < \frac{6}{10} \\ -10^2\left(\frac{3}{5}-\frac{t}{t_d}\right)^2 & \frac{6}{10} \le \frac{t}{t_d} < \frac{7}{10} \\ -10^2\left(\frac{4}{5}-\frac{t}{t_d}\right)^2 & \frac{7}{10} \le \frac{t}{t_d} < \frac{8}{10} \\ 10^2\left(\frac{4}{5}-\frac{t}{t_d}\right)^2 & \frac{8}{10} \le \frac{t}{t_d} < \frac{9}{10} \\ 10^2\left(1-\frac{t}{t_d}\right)^2 & \frac{9}{10} \le \frac{t}{t_d} \le 1 \end{cases}$

Table A.2: Sinusoidal family

Pulse name	Acceleration Equation
$sin(A)\ A = 1, ..., 5$	$\frac{a_g}{a_{g,max}} = sin\left(A\pi\frac{t}{t_d}\right) \quad 0 \leq \frac{t}{t_d} \leq 1$

Table A.3: Triangular trh family

Pulse name	Acceleration equation
$trh(1)$	$\frac{a_g}{a_{g,max}} = \begin{cases} 2\frac{t}{t_d} & 0 \leq \frac{t}{t_d} < \frac{1}{2} \\ 2\left(1 - \frac{t}{t_d}\right) & \frac{1}{2} \leq \frac{t}{t_d} \leq 1 \end{cases}$
$trh(2)$	$\frac{a_g}{a_{g,max}} = \begin{cases} 4\frac{t}{t_d} & 0 \leq \frac{t}{t_d} < \frac{1}{4} \\ 4\left(\frac{1}{2} - \frac{t}{t_d}\right) & \frac{1}{4} \leq \frac{t}{t_d} \leq \frac{3}{4} \\ -4\left(1 - \frac{t}{t_d}\right) & \frac{3}{4} \leq \frac{t}{t_d} \leq 1 \end{cases}$

Table A.4: Triangular trl family

Pulse name	Acceleration equation
$tr1(1)$	$\frac{a_g}{a_{g,max}} = \frac{t}{t_d} \quad 0 \leq \frac{t}{t_d} \leq 1$
$tr1(2)$	$\frac{a_g}{a_{g,max}} = \begin{cases} 2\frac{t}{t_d} & 0 \leq \frac{t}{t_d} < \frac{1}{2} \\ -2\left(1 - \frac{t}{t_d}\right) & \frac{1}{2} \leq \frac{t}{t_d} \leq 1 \end{cases}$

Table A.5: Rectangular family

Pulse name	Acceleration Equation
$rec(1)$	$\frac{a_g}{a_{g,max}} = 1 \quad 0 \leq \frac{t}{t_d} \leq 1$
$rec(2)$	$\frac{a_g}{a_{g,max}} = \begin{cases} 1 & 0 \leq \frac{t}{t_d} < \frac{1}{2} \\ -1 & \frac{1}{2} \leq \frac{t}{t_d} \leq 1 \end{cases}$
$rec(3)$	$\frac{a_g}{a_{g,max}} = \begin{cases} 1 & 0 \leq \frac{t}{t_d} < \frac{1}{3} \\ -1 & \frac{1}{3} \leq \frac{t}{t_d} < \frac{2}{3} \\ 1 & \frac{2}{3} \leq \frac{t}{t_d} \leq 1 \end{cases}$
$rec(4)$	$\frac{a_g}{a_{g,max}} = \begin{cases} 1 & 0 \leq \frac{t}{t_d} < \frac{1}{4} \\ -1 & \frac{1}{4} \leq \frac{t}{t_d} < \frac{1}{2} \\ 1 & \frac{1}{2} \leq \frac{t}{t_d} < \frac{3}{4} \\ -1 & \frac{3}{4} \leq \frac{t}{t_d} \leq 1 \end{cases}$
$rec(5)$	$\frac{a_g}{a_{g,max}} = \begin{cases} 1 & 0 \leq \frac{t}{t_d} < \frac{1}{5} \\ -1 & \frac{1}{5} \leq \frac{t}{t_d} < \frac{2}{5} \\ 1 & \frac{2}{5} \leq \frac{t}{t_d} < \frac{3}{5} \\ -1 & \frac{3}{5} \leq \frac{t}{t_d} < \frac{4}{5} \\ 1 & \frac{4}{5} \leq \frac{t}{t_d} \leq 1 \end{cases}$

Table A.6: Triangular tr0 family

Pulse name	Acceleration equation
$tr0(1)$	$\frac{a_g}{a_{g,max}} = 1 - \frac{t}{t_d} \quad 0 \le \frac{t}{t_d} \le 1$
$tr0(2)$	$\frac{a_g}{a_{g,max}} = 2\left(\frac{1}{2} - \frac{t}{t_d}\right) \quad 0 \le \frac{t}{t_d} \le 1$
$tr0(3)$	$\frac{a_g}{a_{g,max}} = \begin{cases} 4\left(\frac{1}{4} - \frac{t}{t_d}\right) & 0 \le \frac{t}{t_d} < \frac{1}{2} \\ -4\left(\frac{3}{4} - \frac{t}{t_d}\right) & \frac{1}{2} \le \frac{t}{t_d} \le 1 \end{cases}$
$tr0(4)$	$\frac{a_g}{a_{g,max}} = \begin{cases} 6\left(\frac{1}{6} - \frac{t}{t_d}\right) & 0 \le \frac{t}{t_d} < \frac{1}{3} \\ -6\left(\frac{1}{2} - \frac{t}{t_d}\right) & \frac{1}{3} \le \frac{t}{t_d} < \frac{2}{3} \\ 6\left(\frac{5}{6} - \frac{t}{t_d}\right) & \frac{2}{3} \le \frac{t}{t_d} \le 1 \end{cases}$
$tr0(5)$	$\frac{a_g}{a_{g,max}} = \begin{cases} 8\left(\frac{1}{8} - \frac{t}{t_d}\right) & 0 \le \frac{t}{t_d} < \frac{1}{4} \\ -8\left(\frac{3}{8} - \frac{t}{t_d}\right) & \frac{1}{4} \le \frac{t}{t_d} < \frac{1}{2} \\ 8\left(\frac{5}{8} - \frac{t}{t_d}\right) & \frac{1}{2} \le \frac{t}{t_d} < \frac{3}{4} \\ -8\left(\frac{7}{8} - \frac{t}{t_d}\right) & \frac{3}{4} \le \frac{t}{t_d} \le 1 \end{cases}$

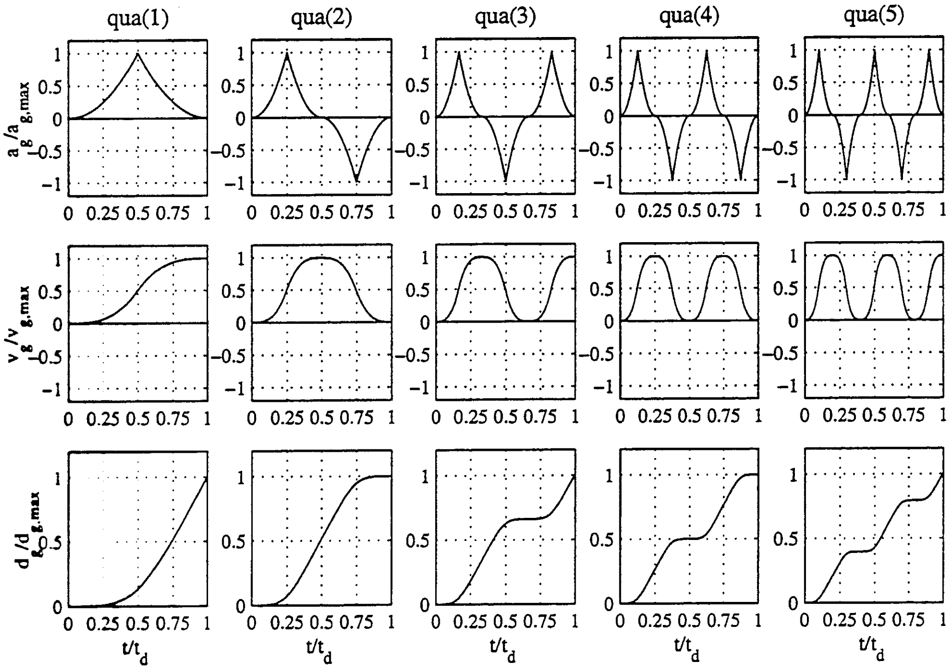

Figure A.1: Normalized acceleration, velocity, and displacement time histories of the quadratic family of pulses

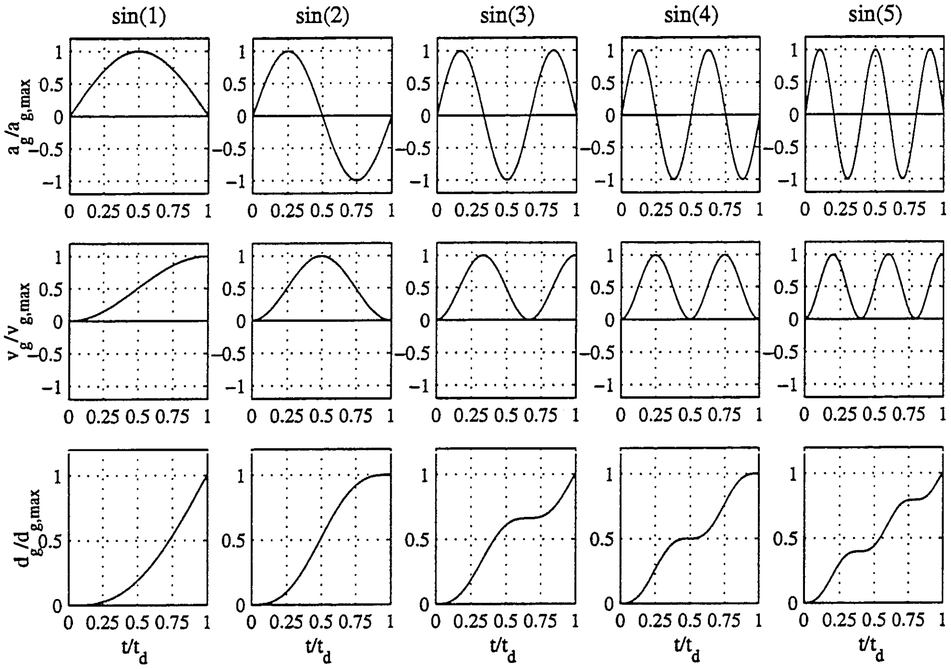

Figure A.2: Normalized acceleration, velocity, and displacement time histories of the sinusoidal family of pulses

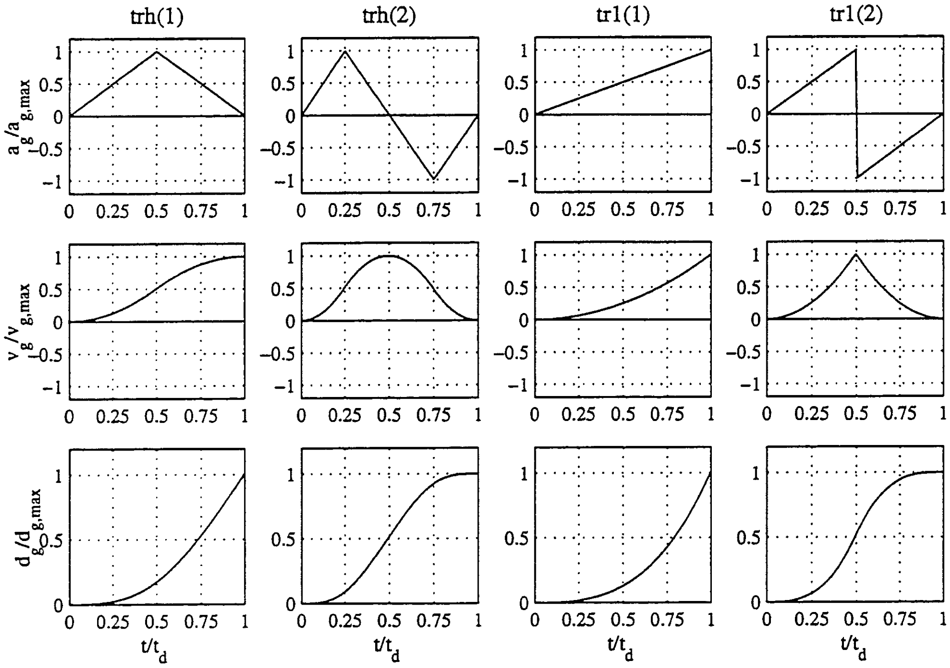

Figure A.3: Normalized acceleration, velocity, and displacement time histories of the triangular families of pulses trh and trl, having rise times, t_r, equal to 1/2 and 1 times the duration of the first incursion

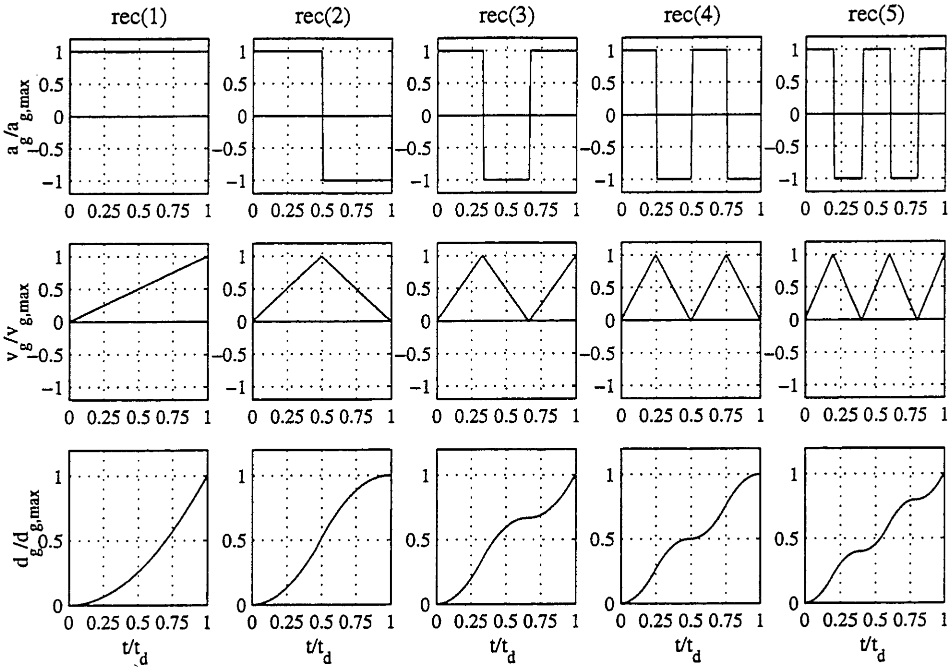

Figure A.4: Normalized acceleration, velocity, and displacement time histories of the rectangular family of pulses

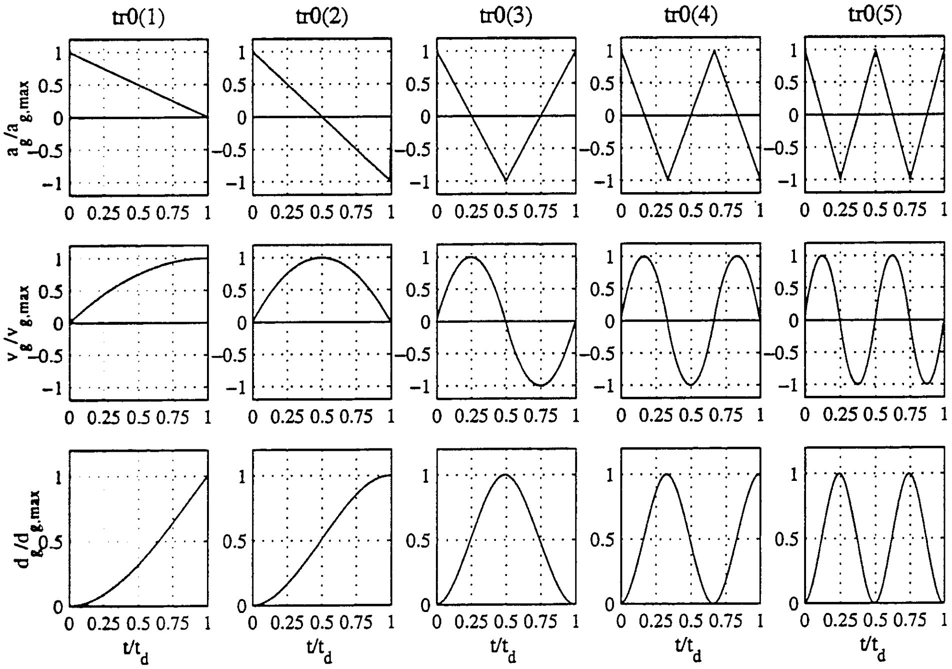

Figure A.5: Normalized acceleration, velocity, and displacement time histories of the triangular family of pulses having rise time, t_r, equal to 0 times the duration of the first incursion

Appendix B

IDI Figures

This appendix includes:

1. The figures of the ratios $\frac{IDI^a}{IDI_{DRAIN-2DX}}$ (Figs. B.1 to B.4), $\frac{IDI^b}{IDI_{DRAIN-2DX}}$ (Figs. B.5 to B.8), and $\frac{IDI^c}{IDI_{DRAIN-2DX}}$ (Figs. B.9 to B.12) for the Flexible-4, Rigid-4, Flexible-12, and Rigid-12 buildings subjected to each ground motion. The ratios are calculated for each story of the building using four estimates: a) the record R-factor, b) Vidic R-factor, c) the pulse R-factor having $T_p = T_1^*$, and d) the pulse R-factor having $T_p = T_g$.

2. The figures of the ratios $\frac{IDI^a}{IDI_{DRAIN-2DX}}$ (Figs. B.13 to B.15), $\frac{IDI^b}{IDI_{DRAIN-2DX}}$ (Figs. B.16 to B.18), and $\frac{IDI^c}{IDI_{DRAIN-2DX}}$ (Figs. B.19 to B.21) for the Flexible-4 building subjected to the 15 ground motions scaled to get ductilities $\mu = 2, 4, 8$ as explained in Section 6.5. The ratios are calculated for each story of the building using four estimates: a) the record R-factor, b) Vidic R-factor, c) the pulse R-factor having $T_p = T_1^*$, and d) the pulse R-factor having $T_p = T_g$, labeled *Record*, *Vidic*, $Pul(T_1^*)$, and $Pul(T_g)$, respectively.

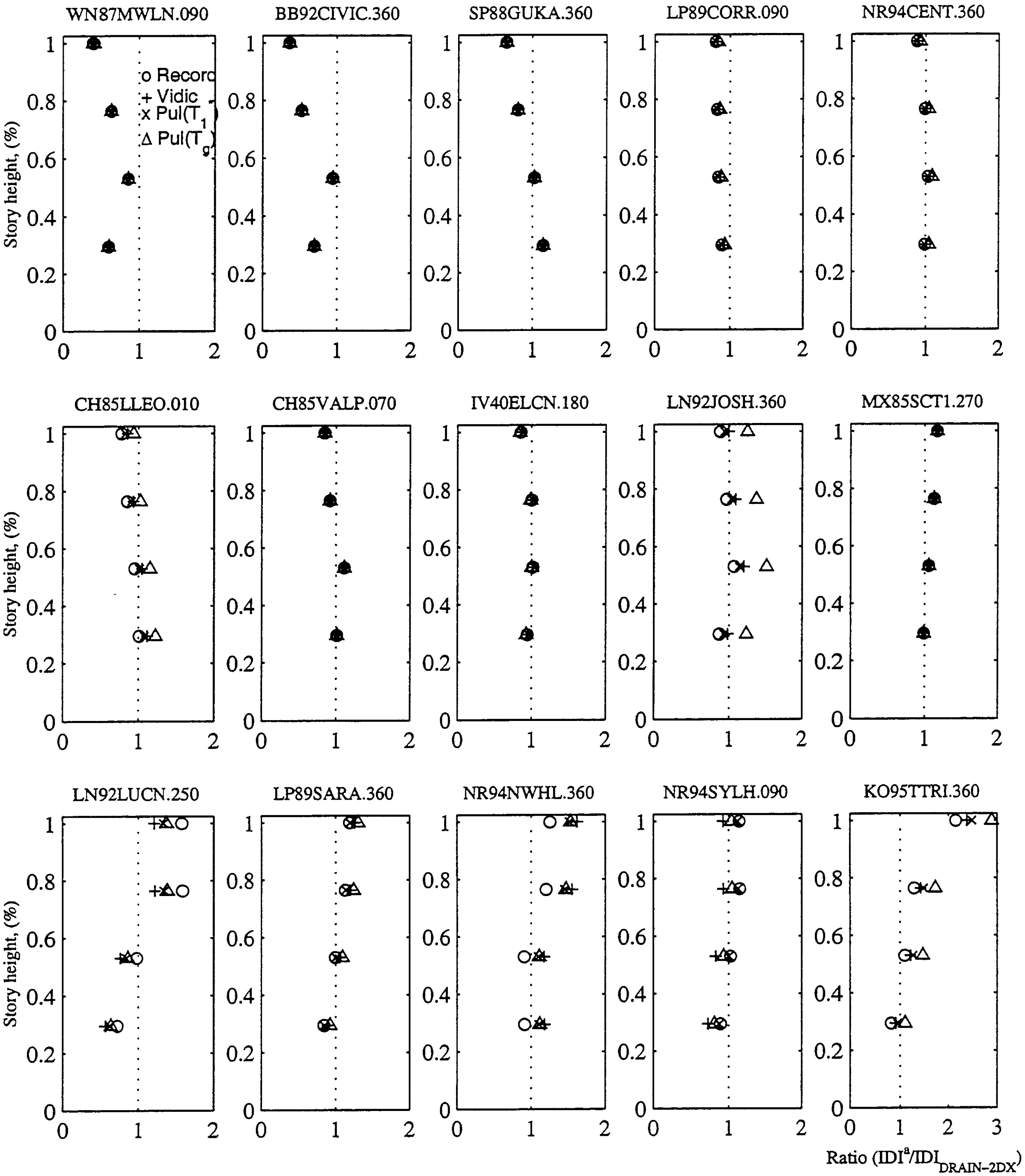

Figure B.1: Ratio $IDI^a/IDI_{DRAIN-2DX}$ for Flexible-4 building subjected to each ground motion using Eq. 6.9

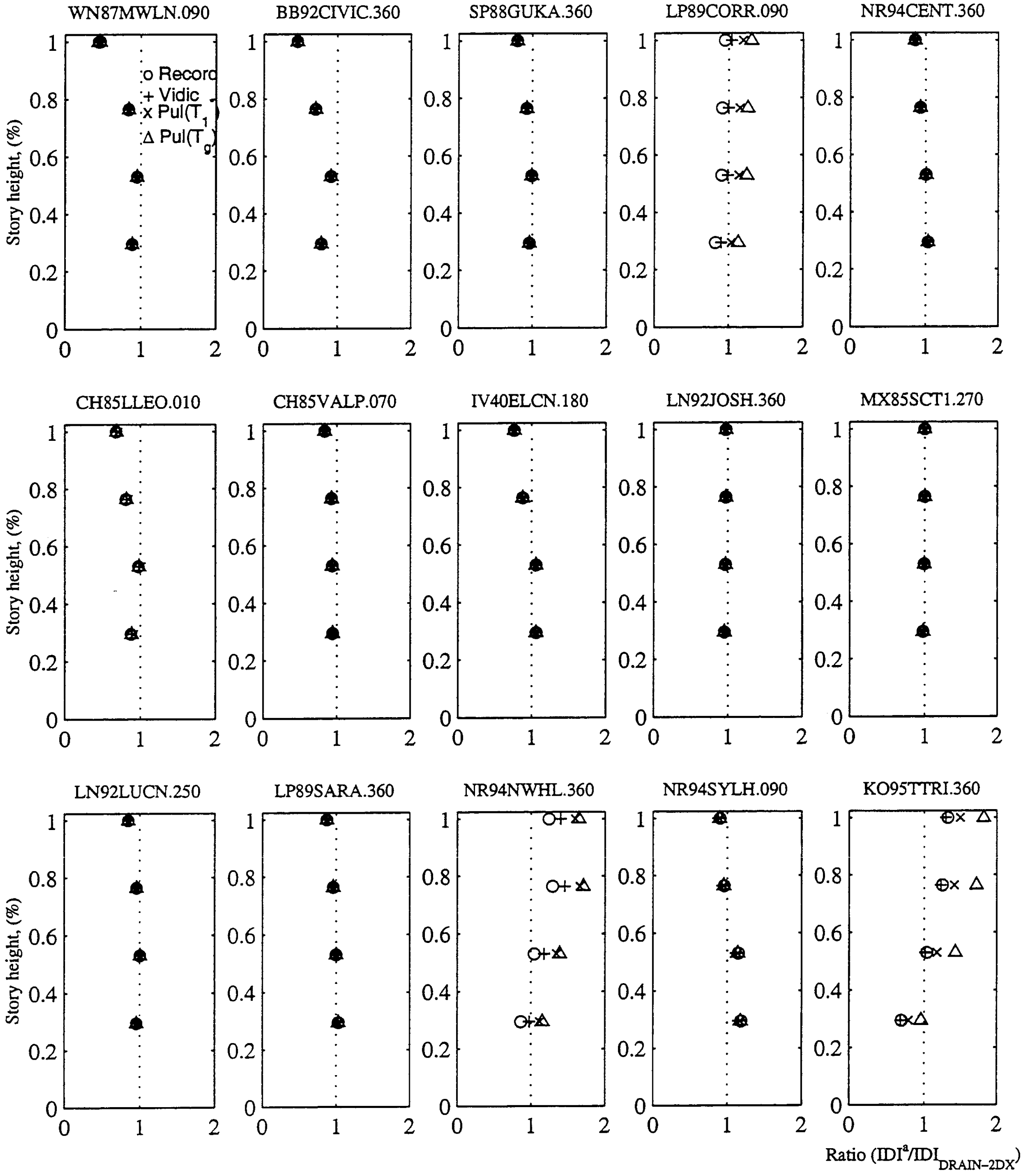

Figure B.2: Ratio $IDI^a/IDI_{DRAIN-2DX}$ for Rigid-4 building subjected to each ground motion using Eq. 6.9

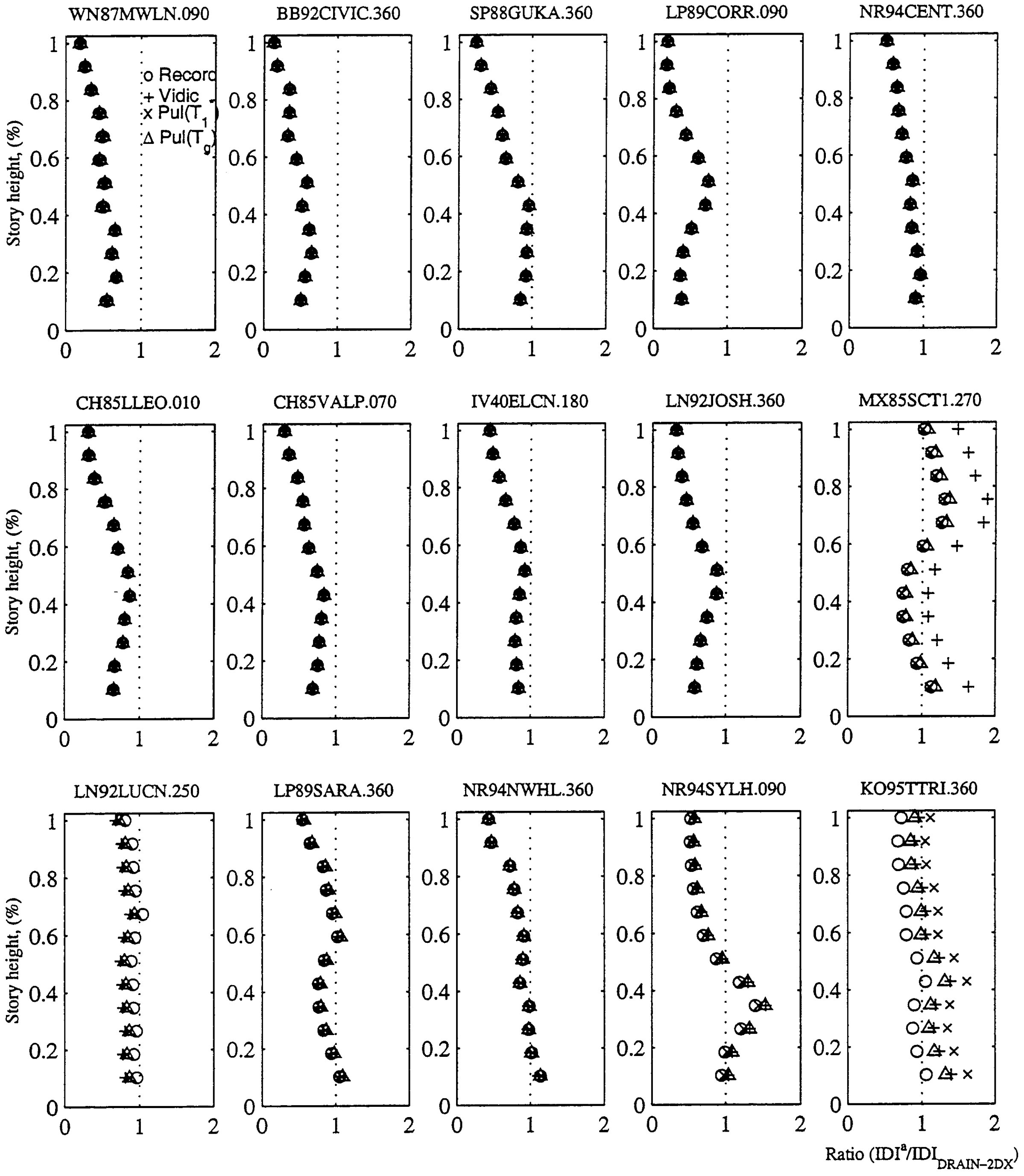

Figure B.3: Ratio $IDI^a/IDI_{DRAIN-2DX}$ for Flexible-12 building subjected to each ground motion using Eq. 6.9

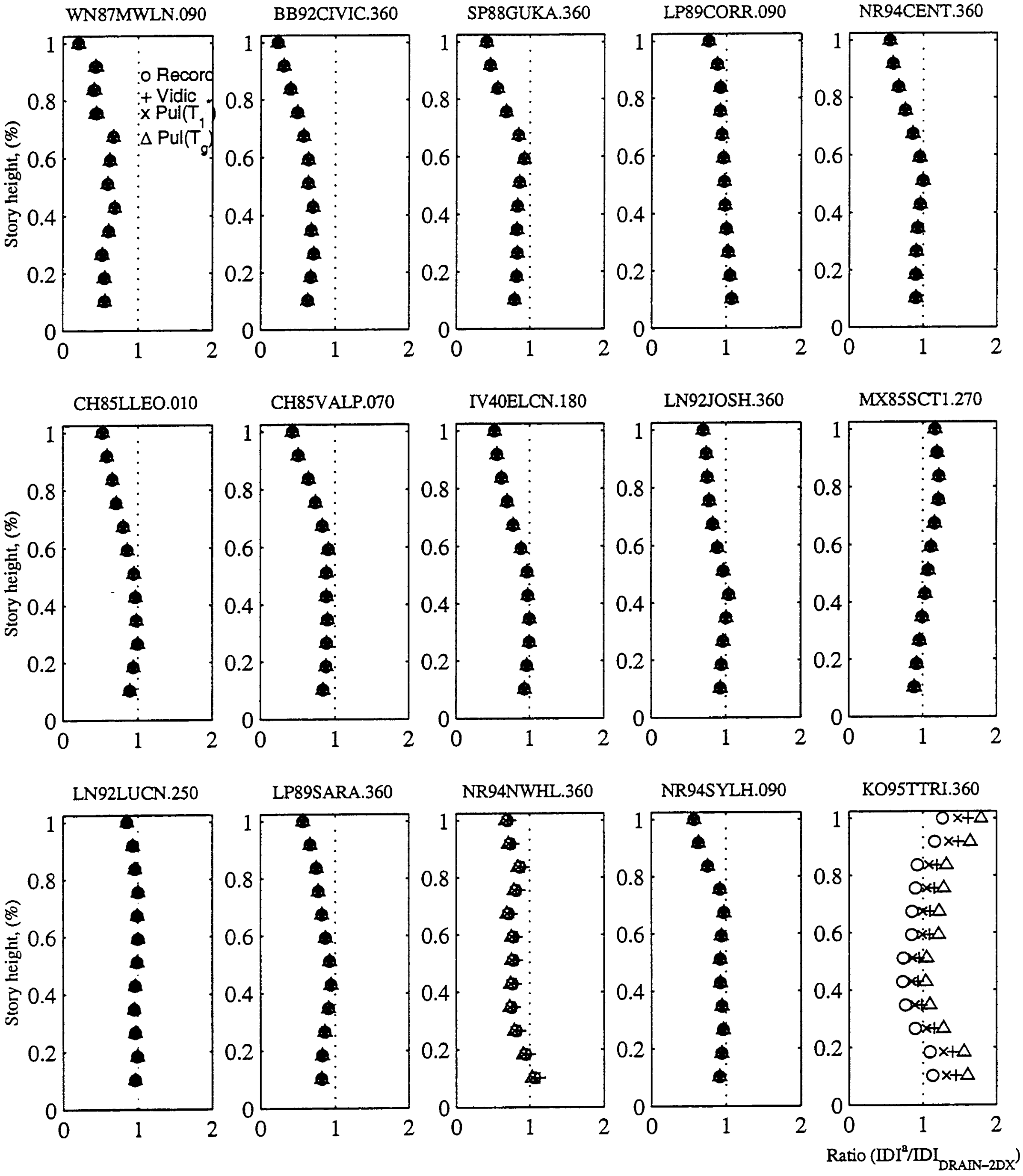

Figure B.4: Ratio $IDI^a/IDI_{DRAIN-2DX}$ for Rigid-12 building subjected to each ground motion using Eq. 6.9

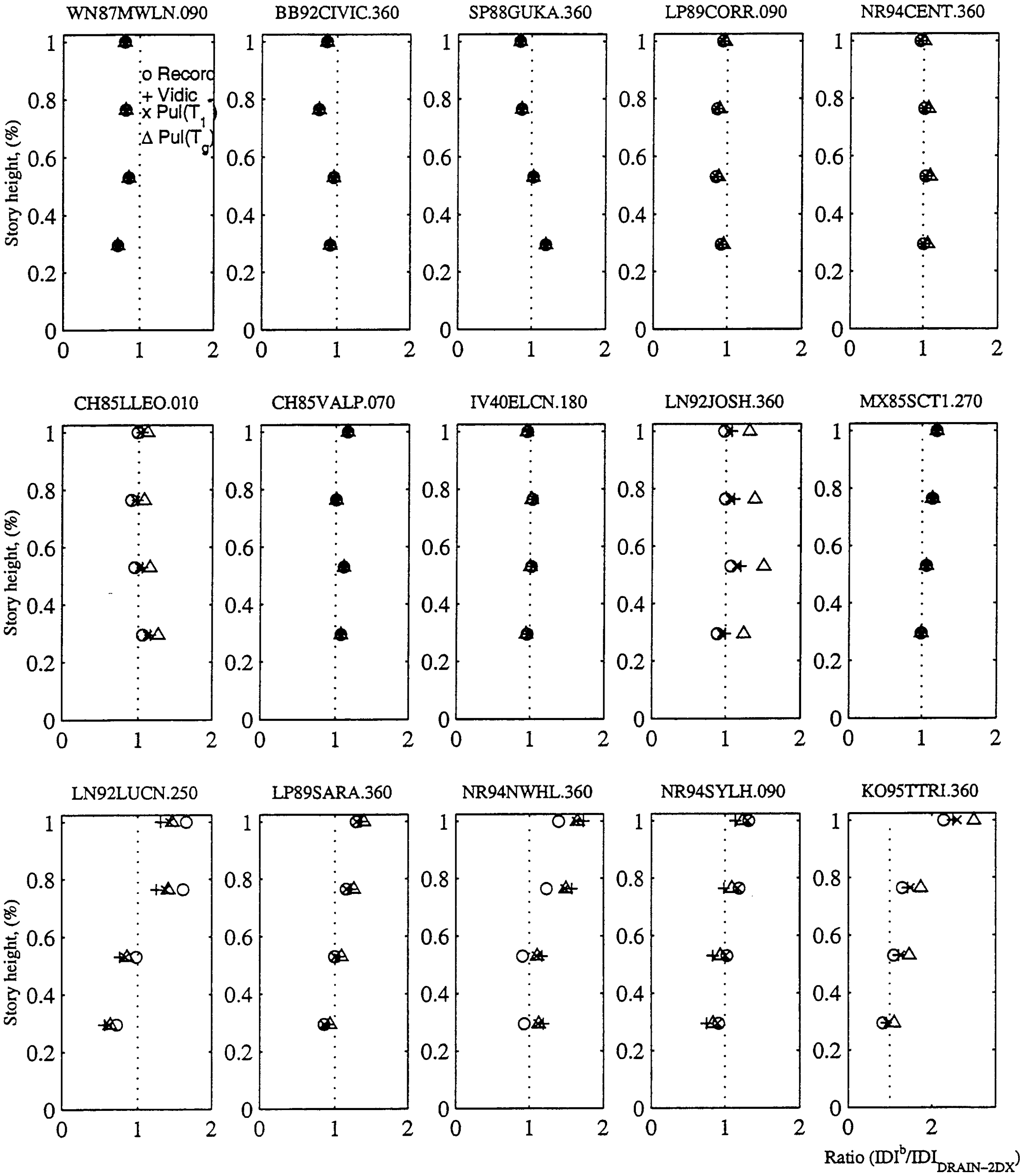

Figure B.5: Ratio $IDI^b/IDI_{DRAIN-2DX}$ for Flexible-4 building subjected to each ground motion using Eq. 6.10

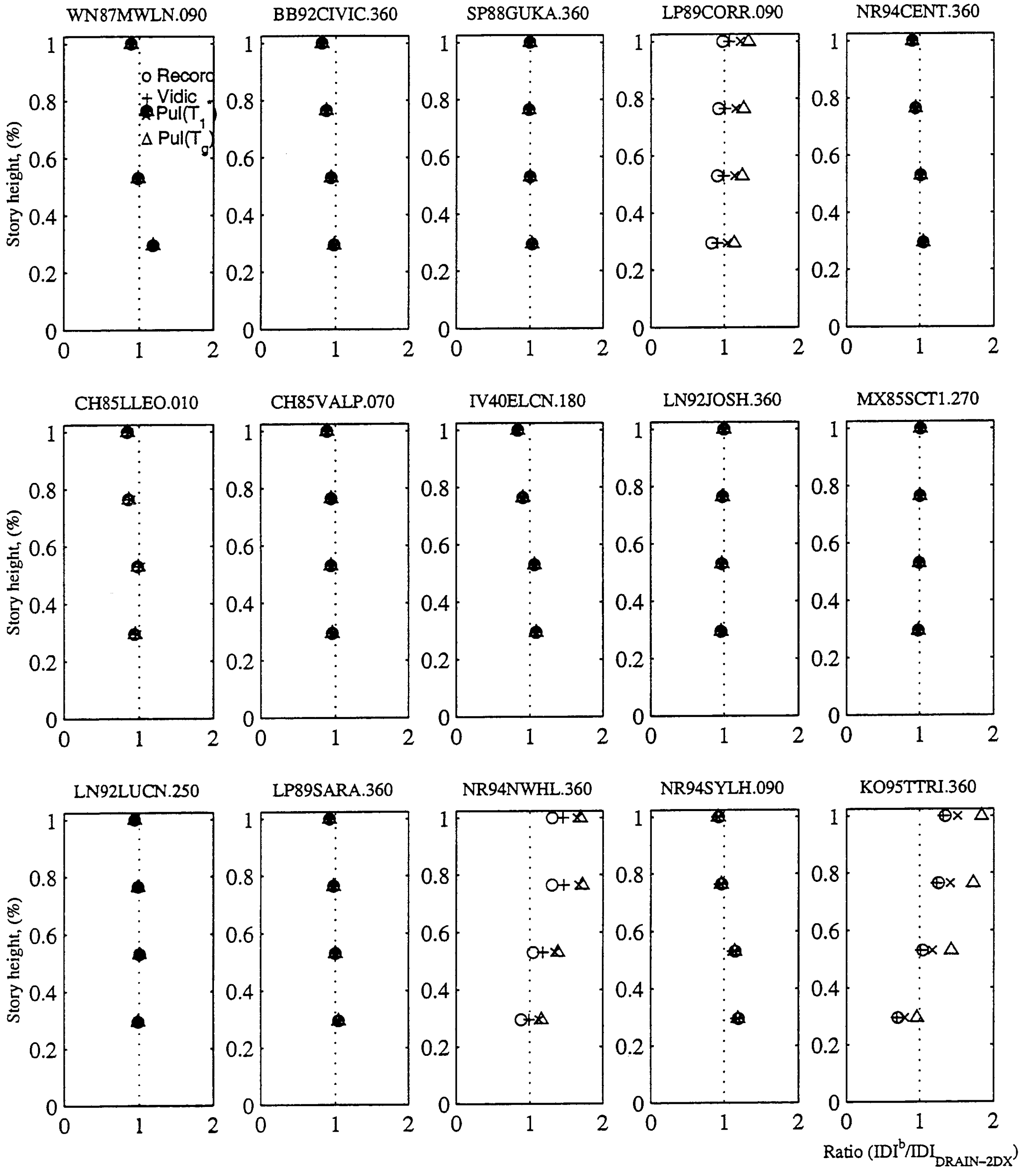

Figure B.6: Ratio $IDI^b/IDI_{DRAIN-2DX}$ for Rigid-4 building subjected to each ground motion using Eq. 6.10

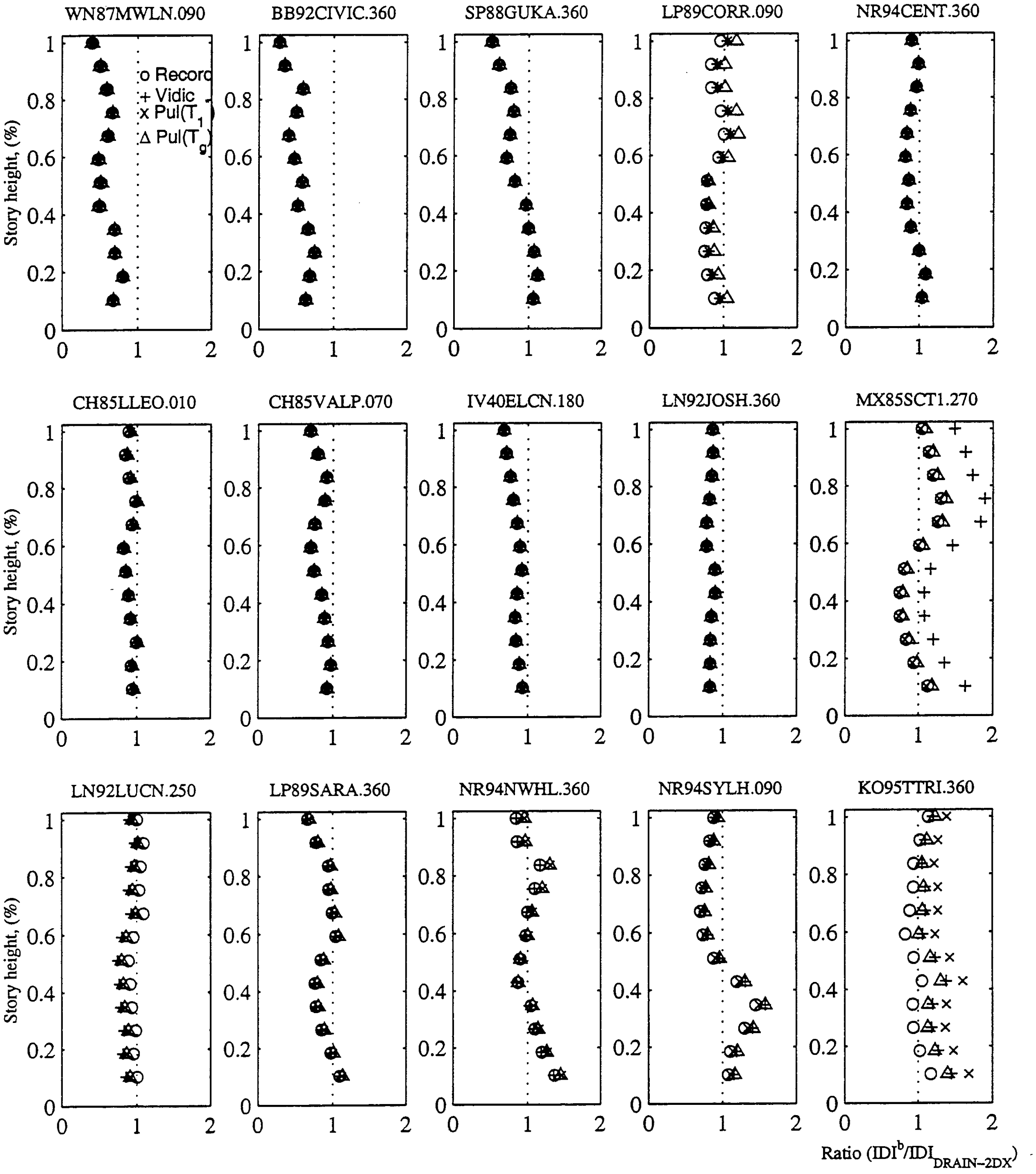

Figure B.7: Ratio $IDI^b/IDI_{DRAIN-2DX}$ for Flexible-12 building subjected to each ground motion using Eq. 6.10

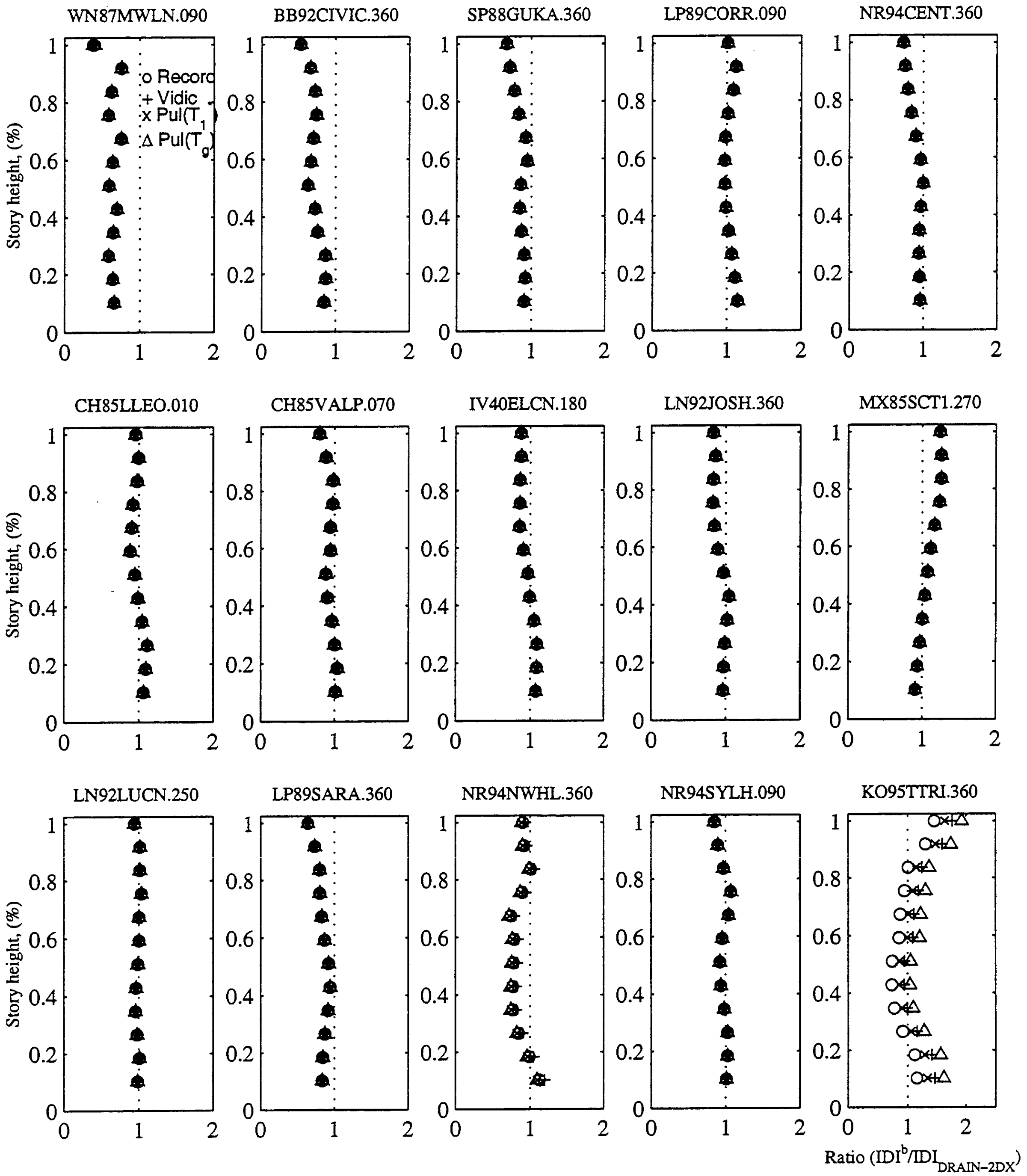

Figure B.8: Ratio $IDI^b/IDI_{DRAIN-2DX}$ for Rigid-12 building subjected to each ground motion using Eq. 6.10

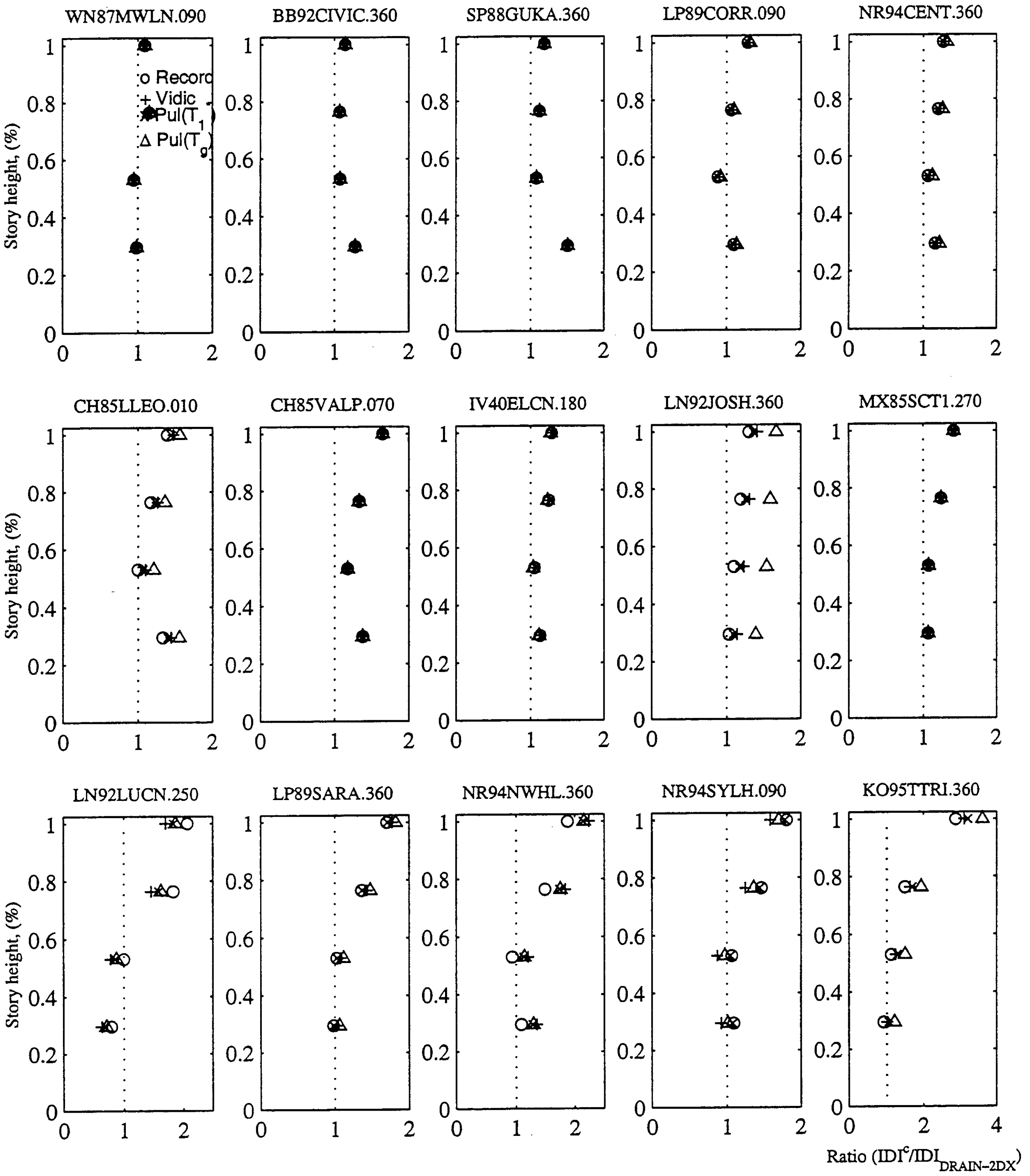

Figure B.9: Ratio $IDI^c/IDI_{DRAIN-2DX}$ for Flexible-4 building subjected to each ground motion using Eq. 6.11

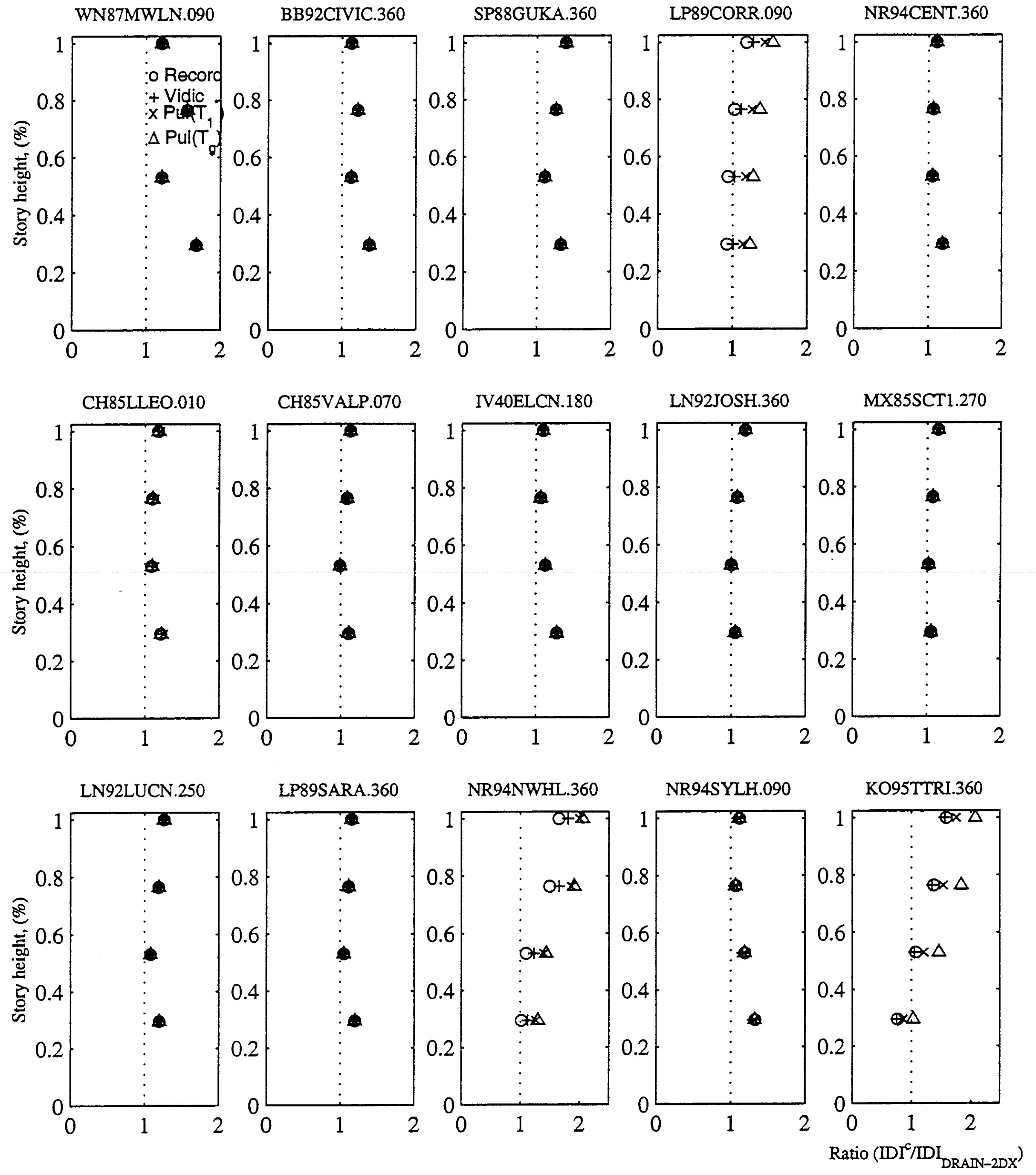

Figure B.10: Ratio $IDI^c/IDI_{DRAIN-2DX}$ for Rigid-4 building subjected to each ground motion using Eq. 6.11

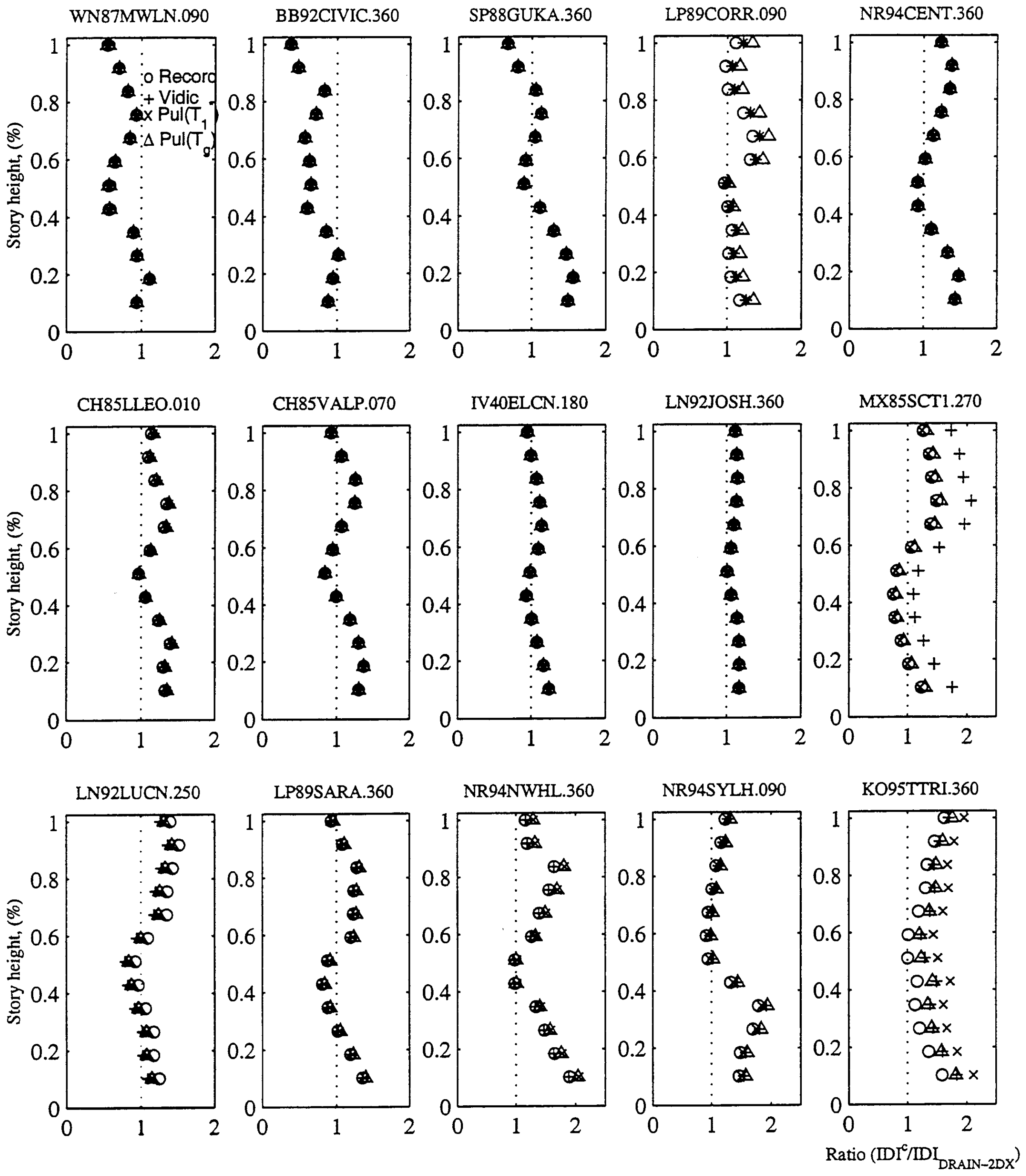

Figure B.11: Ratio $IDI^c/IDI_{DRAIN-2DX}$ for Flexible-12 building subjected to each ground motion using Eq. 6.11

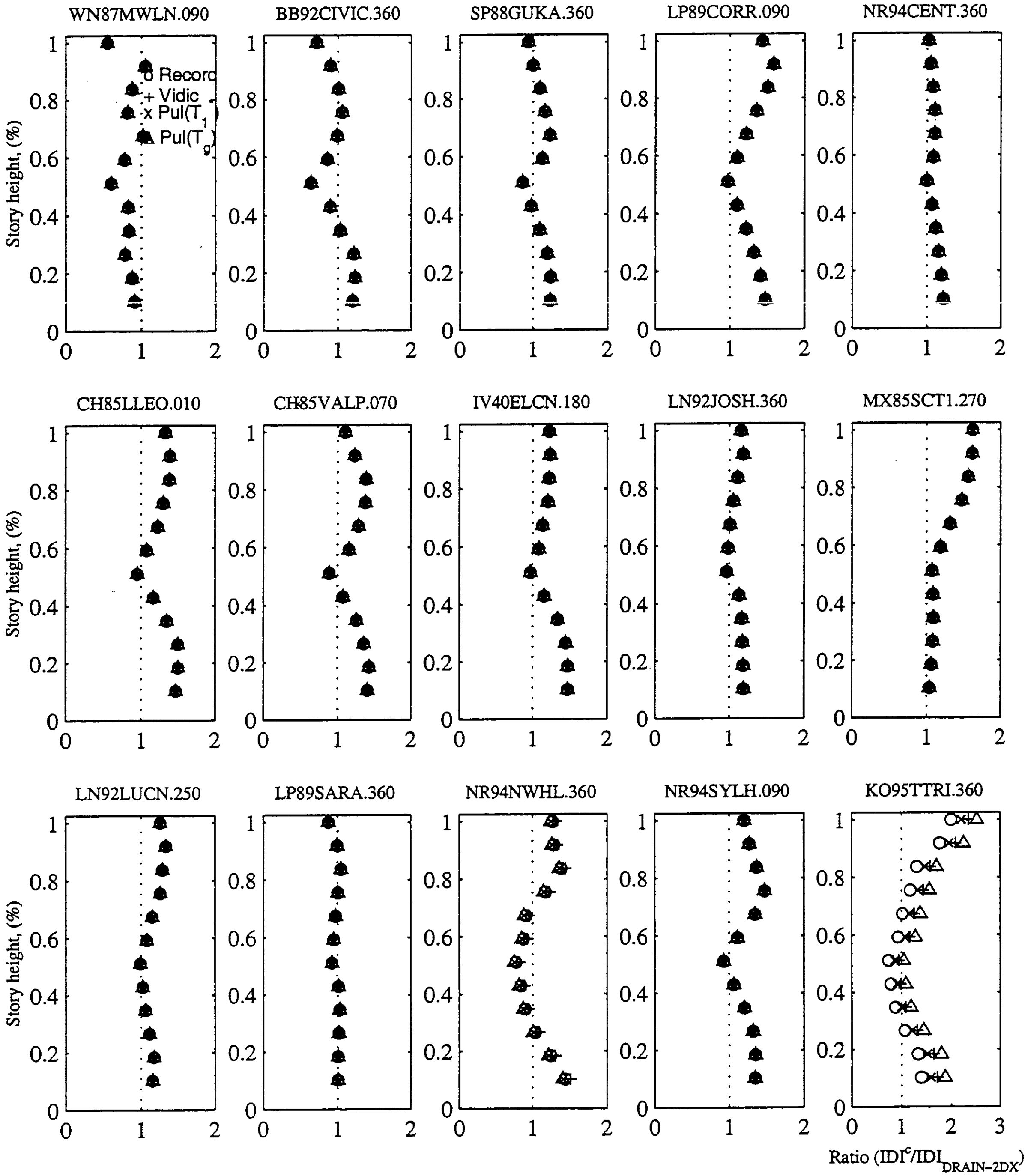

Figure B.12: Ratio $IDI^c/IDI_{DRAIN-2DX}$ for Rigid-12 building subjected to each ground motion using Eq. 6.11

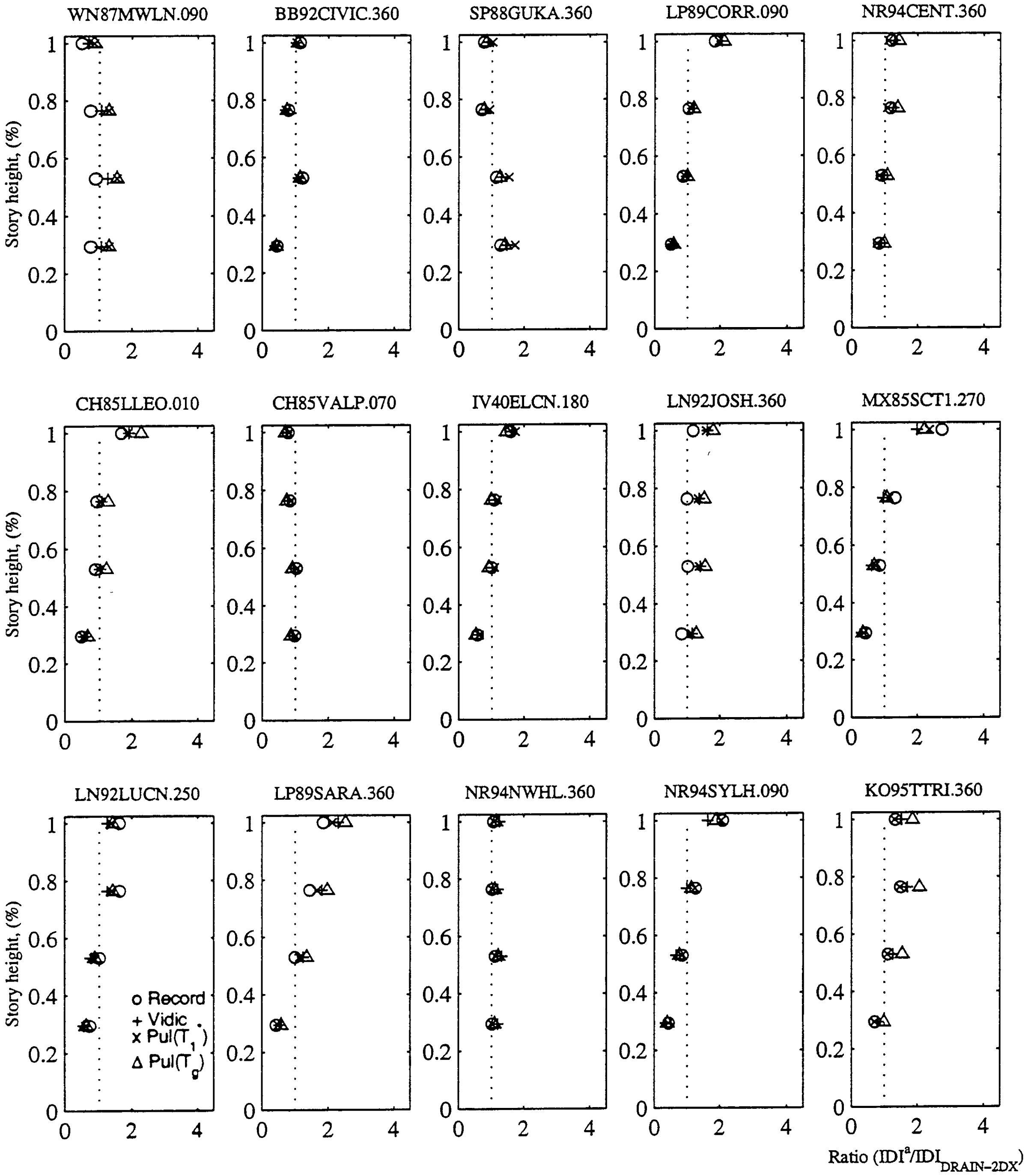

Figure B.13: Ratio $IDI^a/IDI_{DRAIN-2DX}$ for Flexible-4 building subjected to each ground motion scaled to get $\mu \sim 2$, using Eq. 6.9

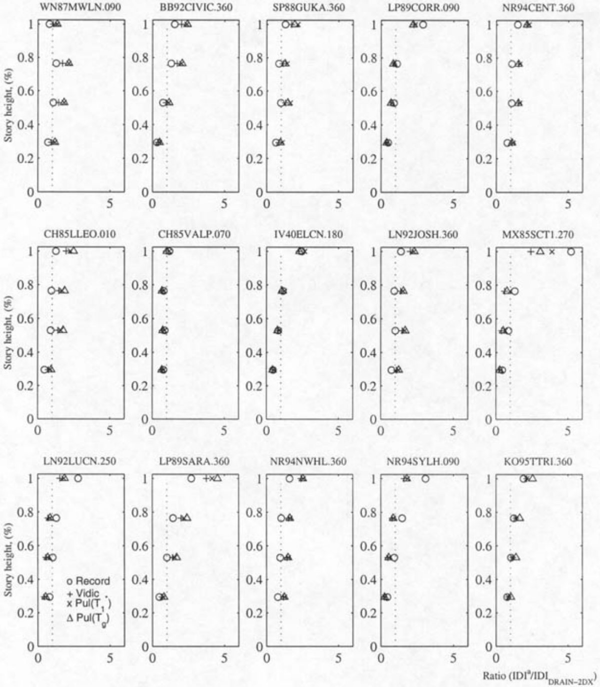

Figure B.14: Ratio $IDI^a/IDI_{DRAIN-2DX}$ for Flexible-4 building subjected to each ground motion scaled to get $\mu \sim 4$, using Eq. 6.9

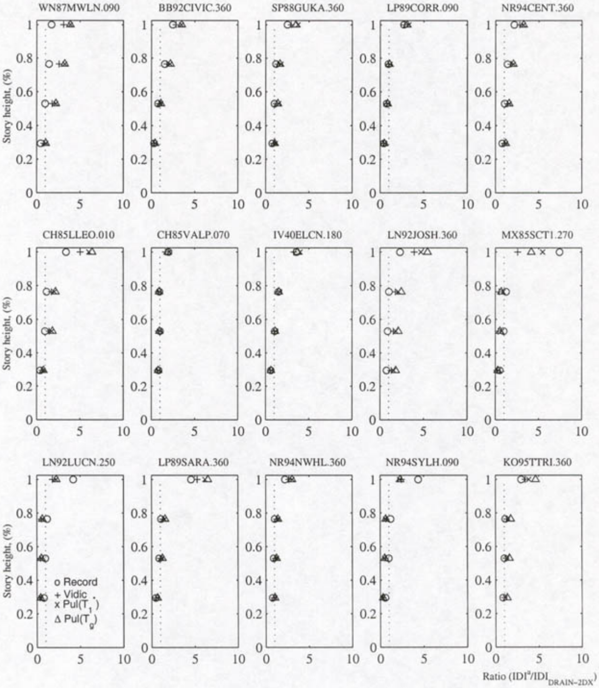

Figure B.15: Ratio $IDI^a/IDI_{DRAIN-2DX}$ for Flexible-4 building subjected to each ground motion scaled to get $\mu \sim 8$, using Eq. 6.9

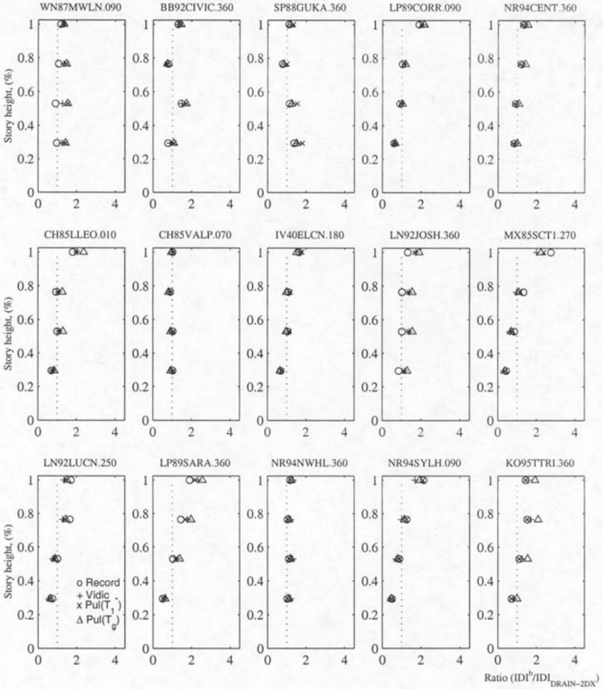

Figure B.16: Ratio $IDI^b/IDI_{DRAIN-2DX}$ for Flexible-4 building subjected to each ground motion scaled to get $\mu \sim 2$ using Eq. 6.10

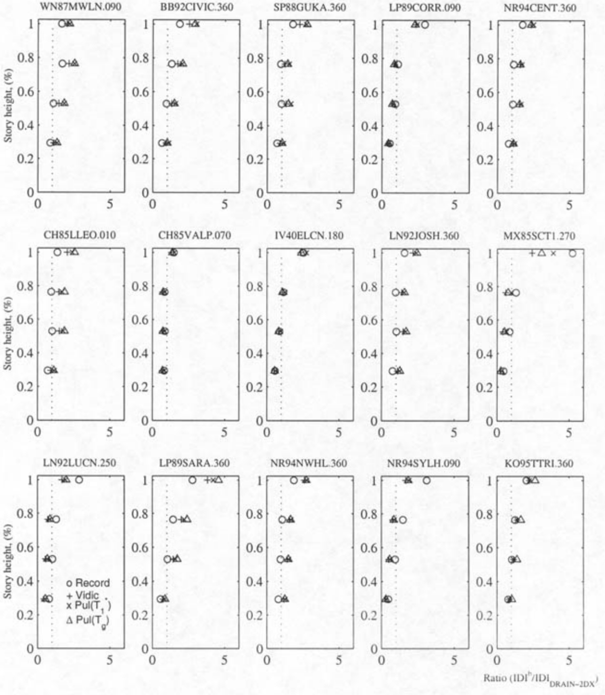

Figure B.17: Ratio $IDI^b/IDI_{DRAIN-2DX}$ for Flexible-4 building subjected to each ground motion scaled to get $\mu \sim 4$ using Eq. 6.10

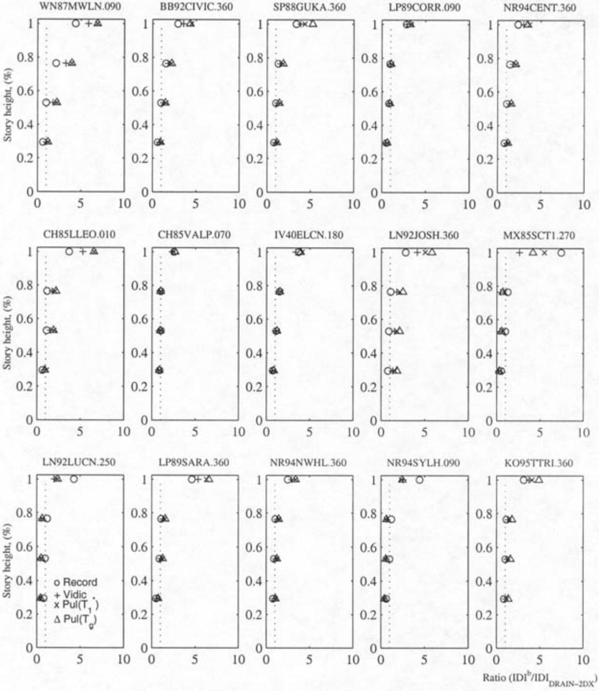

Figure B.18: Ratio $IDI^b/IDI_{DRAIN-2DX}$ for Flexible-4 building subjected to each ground motion scaled to get $\mu \sim 8$ using Eq. 6.10

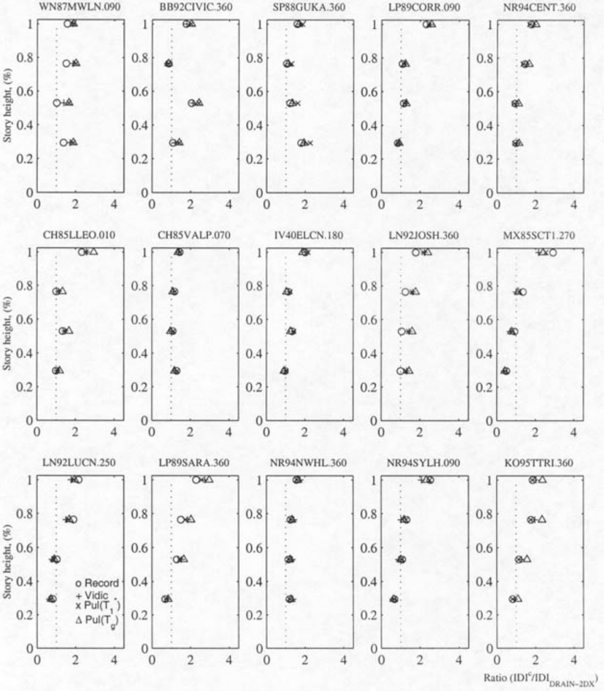

Figure B.19: Ratio $IDI^c/IDI_{DRAIN-2DX}$ for Flexible-4 building subjected to each ground motion scaled to get $\mu \sim 2$ using Eq. 6.11

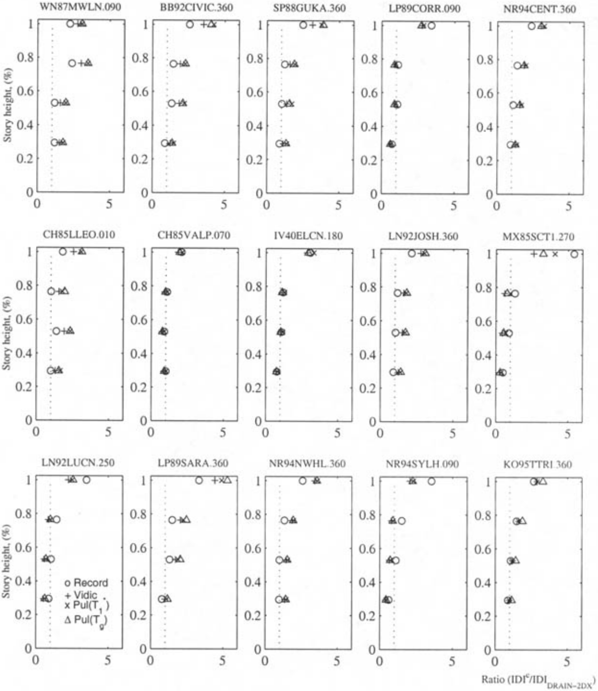

Figure B.20: Ratio $IDI^c/IDI_{DRAIN-2DX}$ for Flexible-4 building subjected to each ground motion scaled to get $\mu \sim 4$ using Eq. 6.11

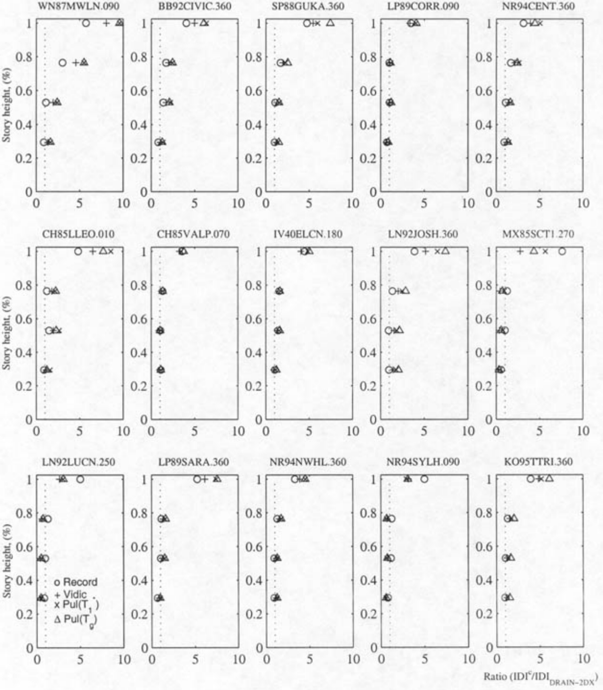

Figure B.21: Ratio $IDI^c/IDI_{DRAIN-2DX}$ for Flexible-4 building subjected to each ground motion scaled to get $\mu \sim 8$ using Eq. 6.11

Bibliography

[1] "Recommended Lateral Force Requirements and Commentary," Tech. Rep. SEAOC 1959, Seismology Committeee, Structural Engineers Association of California, Sacramento, California, 1959.

[2] FEMA-302, "NEHRP Recommendations Provisions for Seismic Regulations for New Buildings and Other Structures, Part 1 - Provisions," Tech. Rep. FEMA-302, Federal Emergency Management Agency, Washington, D.C., February 1998.

[3] "Structures in Seismic Regions - Design - Part 1," Tech. Rep. Eurocode No. 8, Commission of the European Communities, Luxembourg, 1988.

[4] "Structural Response Modification Factors," Tech. Rep. ATC-19, Applied Technology Council, Redwood City, California, 1995.

[5] L. S. Jacobsen and R. S. Ayre, *Engineering Vibrations.* New York: McGraw-Hill, 1958.

[6] A. K. Chopra, *Dynamics of Structures.* Berkeley, California: Prentice-Hall, 1995.

[7] R. W. Clough and J. Penzien, *Dynamics of Structures.* McGraw Hill, 2nd ed., 1993.

[8] "Tentative Provisions for the Development of Seismic Regulations for Buildings," Tech. Rep. ATC-3-06, Applied Technology Council, Redwood City, California, 1978.

[9] "Seismic Design Guidelines for Highway Bridges," Tech. Rep. ATC-6, Applied Technology Council, Redwood City, California, 1982.

[10] California Department of Transportation, Division of Structures, Sacramento, California, *Bridge Design Specifications Manual*, 1990.

[11] E. Miranda and V. V. Bertero, "Evaluation of Strength Reduction Factors for Earthquake-Resistant Design," *Earthquake Spectra*, vol. 10, no. 2, pp. 357–379, 1994.

[12] J. D. Osteraas and H. Krawinkler, "Strength and Ductility Considerations in Seismic Design," Tech. Rep. 90, The John A. Blume Earthquake Engineering Center, Stanford, California, 1991.

[13] C. M. Uang, "Establishing R (or Rw) and Cd Factors for Building Seismic Provisions," *Journal of Structural Engineering*, vol. 117, no. 1, pp. 19–28, 1991.

[14] "A Critical Review of Current Approaches to Earthquake Resistant Design," Tech. Rep. ATC-34, Applied Technology Council, Redwood City, California, 1995.

[15] C. M. Uang and V. V. Bertero, "Earthquake Simulation Tests and Associated Studies of a 0.3-Scale Model of a Six-Story Concentrically Braced Steel Structure," Tech. Rep. UCB/EERC-86/10, Earthquake Engineering Research Center, University of California, Berkeley, California, 1986.

[16] A. S. Whittaker, C. M. Uang, and V. V. Bertero, "An Experimental Study of the Behavior of Dual Steel Systems," Tech. Rep. UCB/EERC-88/14, Earthquake Engineering Research Center, University of California, Berkeley, California, 1990.

[17] S. A. Freeman, "On the Correlation of Codes Forces to Earthquake Demands," Tech. Rep. ATC-15-3, Applied Technology Council, Redwood City, California, 1990.

[18] F. Moses, "Reliability of Structural Systems," *J. of the Structural Division*, vol. 100, pp. 1813–1820, Sept. 1974.

[19] "Recommended Lateral Force Requirements and Commentary," Tech. Rep. SEAOC 1988, Seismology Committeee, Structural Engineers Association of California, Sacramento, California, 1988.

[20] A. S. Veletsos and N. M. Newmark, "Design Procedures for Shock Isolation Systems of Underground Protective Structures," Tech. Rep. RTD TDR-63-3096, Vol. III, Air Force Weapons Laboratory, New Mexico, 1964.

[21] N. M. Newmark and W. J. Hall, "Seismic Design Criteria for Nuclear Reactor Facilities," Tech. Rep. 46, Building Practices for Disaster Mitigation, National Bureau of Standards, U.S. Department of Commerce, 1973.

[22] R. Riddell, P. Hidalgo, and E. Cruz, "Response Modification Factors for Earthquake Resistant Design of Short Period Structures," *Earthquake Spectra*, vol. 5, no. 3, pp. 571–590, 1989.

[23] A. A. Nassar and H. Krawinkler, "Seismic Demands for SDOF and MDOF Systems," Tech. Rep. 95, The John A. Blume Earthquake Engineering Center, Stanford University, California, 1991.

[24] E. Miranda, "Site-Dependent Strength Reduction Factors," *Journal of Structural Engineering*, vol. 119, no. 12, 1993.

[25] T. Vidic, P. Fajfar, and M. Fischinger, "Consistent Inelastic Design Spectra: Strength and Displacement," *Earthquake Engineering and Structural Dynamics*, vol. 23, pp. 507–521, 1994.

[26] M. Ordaz and L. E. Perez-Rocha, "Estimation of Strength-Reduction Factors for Elastoplastic Systems: A New Approach," *Earthquake Engineering and Structural Dynamics*, vol. 27, pp. 889–901, 1998.

[27] N. M. Newmark and W. J. Hall, *Earthquake Spectra and Design*. Oakland, California: Earthquake Engineering Research Institute, EERI Monograph Series, 1982.

[28] T. Vidic, *Inelastic Seismic Response of SDOF Systems*. PhD thesis, Department of Civil Engineering, University of Ljubljana, Slovenia, 1993.

[29] S. P. Lai and J. M. Biggs, "Inelastic Response Spectra for Aseismic Building Design," *Journal Structural Division*, vol. 106, no. ST6, pp. 1295–1310, 1980.

[30] A. S. Veletsos, "Maximum Deformations of Certain Nonlinear Systems," in *4th World Conference Earthquake Engineering*, (Santiago, Chile), pp. 155–170, 1969.

[31] A. S. Veletsos, N. M. Newmark, and C. V. Chelapati, "Deformation Spectra for Elastic and Elastoplastic Systems Subjected to Ground Shock and Earthquake Motions," in *3rd World Conference Earthquake Engineering*, vol. 2, (Wellington, New Zealand), pp. 663–680, 1965.

[32] A. S. Veletsos and W. P. Vann, "Response of Ground-Excited Elasto-plastic Systems," *Journal Structural Division*, vol. 97, no. ST4, pp. 1257–1281, 1971.

[33] J. M. Biggs, *Introduction to Structural Dynamics.* New York: McGraw-Hill, 1964.

[34] A. S. Veletsos and N. M. Newmark, "Effect of Inelastic Behavior on the Response of Simple Systems to Earthquake Motions," in *2nd World Conference Earthquake Engineering*, vol. 2, (Tokyo, Japan), pp. 895–912, 1960.

[35] B. Alavi and H. Krawinkler, "Structural Design Implications of Near-Field Ground Motion-Year 2 Research Report," Tech. Rep. 1998.11, Kajima-CUREe, Kajima Corporation, Tokyo, Japan, 1998.

[36] B. Alavi and H. Krawinkler, "Consideration of Near-Fault Ground Motion Effects in Seismic Design," in *12th World Conference Earthquake Engineering*, no. 2665, (Auckland, New Zealand), 2000.

[37] Y. Bozorgnia and S. A. Mahin, "Ductility and Strength Demands of Near-Fault Ground Motions of the Northridge Earthquake," in *6th World Conference Earthquake Engineering*, (Seattle), Earthquake Engineering Research Institute, 1998.

[38] J. F. Hall, T. H. Heaton, M. W. Halling, and D. J. Wald, "Near-Source Ground Motion and its Effects on Flexible Buildings," *Earthquake Spectra*, vol. 11, no. 4, pp. 569–606, 1995.

[39] H. Krawinkler and B. Alavi, "Development of Improved Design Procedures for Near-Fault Ground Motions," in *SMIP98 Seminar on Utilization of Strong-Motions Data*, (Oakland, California), Earthquake Engineering Research Institute, 1998.

[40] P. G. Somerville, "Development of an Improved Ground Motion Representation for Near-Fault Ground Motions," in *SMIP98 Seminar on Utilization of Strong-Motions Data*, (Oakland, California), Earthquake Engineering Research Institute, 1998.

[41] J. A. Blume, "A Reserve Energy Technique for the Earthquake Design and Rating of Structures in the Inelastic Range," in *2nd World Conference Earthquake Engineering*, vol. II, (Tokyo), pp. 1061–1083, 1960.

[42] P. Bonelli, "Long Seismic Velocity Pulse Effect and Damage," in *Structural Engineering World Congress* (N. K. Srivastava, ed.), no. T227-3, (San Francisco, California), 1998.

[43] I. Cuesta and M. A. Aschheim, "Isoductile Strengths and Strength Reduction Factors of Elasto-plastic SDOF Systems Subjected to Simple Waveforms," *Earthquake Engineering and Structural Dynamics*, 2000. Accepted October 2000.

[44] I. Cuesta and M. A. Aschheim, "Waveform Independence of R-Factors," in *12th World Conference Earthquake Engineering*, no. 1246, (New Zealand), 2000.

[45] R. T. Sewell, *Damage Effectiveness of Earthquake Ground Motion: Characterization Based on the Performance of Structures and Equipment*. PhD thesis, Stanford University, California, 1989.

[46] FEMA-307, "Evaluation of Earthquake Damaged Concrete and Masonry Wall Buildings-Technical Resources," Tech. Rep. FEMA-307, Federal Emergency Management Agency, May 1999.

[47] S. A. Mahin and J. Lin, "Construction of Inelastic Response Spectra for SDOF Systems," Tech. Rep. UCB-EERC-83/17, Earthquake Engineering Research Center, University of California, Berkeley, 1983.

[48] R. L. Borsoschek, *PCNSPEC Manual, A Modified Version of NONSPEC*, 1991. Unpublished.

[49] G. W. Housner, "Limit Design of Structures to Resist Earthquakes," in *World Conference Earthquake Engineering*, 1956.

[50] E. Miranda, "Inelastic Displacement Ratios for Displacement-Based Earthquake Resistant Design," in *12th World Conference Earthquake Engineering*, no. 1096, (New Zealand), 2000.

[51] I. Cuesta and M. A. Aschheim, "Estimating Inelastic Response Spectra Using Pulse R-Factors," *Earthquake Engineering and Structural Dynamics*, 2001. Submitted January 2001.

[52] I. Cuesta, *Using Pulse R-Factors to Estimate Structural Response to Earthquake Ground Motions.* PhD thesis, Department of Civil and Environmental Engineering, University of Illinois, Urbana, Illinois, 2001.

[53] K. Shimazaki and M. A. Sozen, "Seismic Drift of Reinforced Concrete Structures," Tech. Rep. in Japanese, draft in English,, Hasama-Gumi Ltd., Tokyo, 1984.

[54] X. Qi and J. P. Moehle, "Displacement Design Approach for Reinforced Concrete Structures Subjected to Earthquakes," Tech. Rep. UCB/EERC 91/02, Earthquake Engineering Research Center, University of California, Berkeley, California, January 1991.

[55] A. Lepage, *A Method for Drift Control in Earthquake-Resistant Design of RC Building Structures.* PhD thesis, Department of Civil and Environmental Engineering, University of Illinois, Urbana, Illinois, 1997.

[56] W. H. Freeman and Company, *Nuclear Explosions and Earthquakes.* 1976.

[57] W. D. Iwan, "Near-Field Considerations in Specification of Seismic Design Motions for Structures," in *10th European Conferenceon Earthquake Engineering*, (Vienna, Austria), 1994.

[58] W. D. Iwan and X. Chen, "Important Near-Field Ground Motion Data from the Landers Earthquake," in *10th European Conferenceon Earthquake Engineering*, (Vienna, Austria), 1994.

[59] J. I. Baez and E. Miranda, "Amplification Factors to Estimate Inelastic Displacement Demands for the Design of Structures in the Near-Field," in *12th World Conference Earthquake Engineering*, no. 1561, (New Zealand), 2000.

[60] I. Cuesta and M. A. Aschheim, "Inelastic Response Spectra Using Conventional and Pulse R-Factors," *Journal of Structural Engineering*, 2001. Accepted January 2001.

[61] V. Prakash, G. H. Powell, and S. Campbell, "DRAIN-2DX Base Program Description and User Guide - Element Description and User Guide for Elements TYPE01, TYPE02, TYPE04, TYPE06, TYPE09, TYPE15 - Version 1.10," Tech. Rep. UCB/SEMM-93/18, Structural Engineering Mechanics and Materials, University of California, Berkeley, California, December 1993.

[62] "Seismic Evaluation and Retrofit of Concrete Buildings," Tech. Rep. SSC 96-01, ATC-40, Applied Technology Council, Prepared for the California Seismic Safety Commission, Redwood City, CA, November 1996.

[63] FEMA-273, "NEHRP Guidelines for the Seismic Rehabilitation of Buildings," Tech. Rep. FEMA-273, Federal Emergency Management Agency, Washington, D.C., October 1997.

[64] E. Black, *Seismic Design and Evaluation of Multistory Buildings Using Yield Point Spectra.* PhD thesis, Department of Civil and Environmental Engineering, University of Illinois, Urbana, Illinois, 2000.

[65] K. R. Collins, Y. K. Wen, and D. A. Foutch, "Investigation of Alternative Seismic Design Procedures for Standard Buildings," Tech. Rep. 600, Civil Engineering Studies, Structural Research Series, University of Illinois, Urbana, Illinois, May 1995.

[66] V. 2000, *Performance Based Seismic Engineering of Buildings.* prepared by Vision 2000 Committee, Structural Engineers Association of California, Sacramento, California, April 1995.

[67] "Uniform Building Code," Tech. Rep. UBC 1997, International Conference of Building Officials, Whittier, California, 1997.

[68] FEMA-303, "NEHRP Recommended Provisions for Seismic Regulations for New Buildings and Other Structures, Part 2 - Commentary," Tech. Rep. FEMA-303, Federal Emergency Management Agency, Washington, D.C., February 1998.